THE QUANTITATIVE ASSESSMENT OF PHOTODENSITY OF THE THIRD CARPAL BONE IN THE HORSE.

A thesis presented in partial fulfilment of the requirements for the degree of
Master of Veterinary Science
at Massey University, Palmerston North
New Zealand

Cristy Jane Secombe

2000

CONTENTS

LIST OF ILLUSTRATIONS

LIST OF TABLES

ACKNOWLEDGEMENTS

Thank-you to my supervisors, **Elwyn Firth, Nigel Perkins, Donald Bailey** and **Brian Anderson** for their time and effort in assisting me through the journey of my masters project. I am particularly thankful for the enthusiasm and time Elwyn spent helping me with all aspects of this research. Many thanks to Donald, without whom the transition into the world of image analysis would have been far more turbulent. I especially wish to thank Nigel for his continuous support, invaluable statistical assistance and wisdom, particularly regarding manuscript preparation. Thank-you to **Nicki Moffat, Sue Jenkins** and **Julie Warnock** for their help, both practical and theoretical with the radiographic component of the project. My appreciation also goes to **Russell Watson** and **Jim Hargreaves**, without whom the cube, wedge and circle would still be a figment of my imagination. I wish to thank Nigel, **Chris Rogers** and **Jason Shaw** for their assistance with computer related challenges that I faced along the way. Finally a special thank-you to my husband **Mark Secombe**, whose unyielding support, commitment and enthusiasm enabled me to lock myself in front of the computer and complete this project.

The work in this project was supported financially by a grant from the **New Zealand Equine Research Foundation**, of which I am grateful.

ABSTRACT

The purpose of this study was to determine if a method of non-invasive bone mineral analysis could be adapted to quantitatively assess photodensity in the third carpal bone of the horse. The technique chosen was radiographic absorptiometry, which determines bone mineral density from a radiograph that includes a control (usually a wedge) of known photodensity. When taken correctly the tangential view of the distal row of carpal bones allows visualisation of the dorsal aspect of the third carpal bone, without superimposition of overlying structures. The method is technically demanding, because the angle at which the x-ray beam penetrates the third carpal bone can not be exactly replicated in a clinical situation, as it is affected by the x-ray beam angle and the limb flexion angle. To utilise radioabsorptiometry in the tangential view, assessment of the effect of variation in x-ray beam angle was required.

Fourteen isolated distal rows of carpal bones were radiographed varying the x-ray beam angle in 5° increments over 15° from the base angles of 60° and 90°. The radiographs were digitised and processed to determine the photodensity of specific regions of interest in terms of millimetres of aluminium, using the wedge as reference. The results indicated that small variations in x-ray beam angle significantly affect photodensity.

Quantitative assessment of the photodensity of the fourth carpal bone showed changes associated with exercise, similar to those in the third carpal bone. Changing the size of the region of interest when x-ray beam angle was varied by 30° did not affect photodensity of the region of interest. Although conversion from photodensity to bone mineral density was not possible within this project, the findings supported other authors who have studied bone mineral density of the third carpal bone.

There are two tangential views of the distal row of carpal bones. The two methods affect the radiographic image differently because the magnification and distortion changes are different in each, and this precluded accurate comparison. Therefore, it was impossible to determine which method would more accurately assess the photodensity of the third carpal bone.

The study concluded that quantitative assessment of photodensity of the third carpal bone using either tangential view was clinically inapplicable at this time, because of the significant effect of very small changes in angle on photodensity. This is unfortunate, because the current practice of visual subjective assessment of photodensity of the third carpal bone remains unsatisfactory, in particular the differentiation between grades of sclerosis.

INTRODUCTION

Scientific knowledge regarding the diagnosis, treatments and prognosis of osseous disease has greatly increased over the last 30 years. In contrast, research aimed at providing information to prevent osseous disease has lagged behind. An exception has been the development of a variety of non-invasive bone mineral analysis methods used in the prevention of osteoporosis in humans. One technique, radioabsorptiometry (RA), has been found to be a relatively simple and accurate technique for assessment of bone mineral density, and is used by human physicians for the detection and monitoring of osteoporosis.

There are few studies investigating the use of non-invasive bone mineral analysis in horses. Such methods would be useful for the detection of physiological and pathological alterations in the skeleton of horses trained for athletic pursuits. The purpose of this investigation is to evaluate one method of non-invasive bone mineral analysis (RA), using the third carpal bone (C3), in order to try and provide a technique to aid the early detection of pathological alterations in C3. C3 disease and non-invasive bone mineral analysis is reviewed below.

1.1 Prevalence of carpal bone fractures

Retrospective studies performed in a number of countries have shown that lameness appears to be the most common cause of interference with a horse's training schedule, resulting in lost days in work, a prolonged spell, or retirement from racing.[1-3] The carpus is a relatively common site of lameness with fractures of the carpal bones during training or racing accounting for 1-8% of all injuries in some populations.[4-6]

Table 1.1: Prevalence of carpal fractures in Thoroughbreds and Quarterhorses.

Retrospective study	Distal radius	Radial carpal bone	Third carpal bone	Intermediate carpal bone
Mizuno[6]	35.3%	29.5%	35.2%	Not recorded
Park [7]	14.8%	46.4%	19.4%	15.4%
McIlwraith [8]	19.5%	35%	4.4%	27.7%

Table 1.2: Prevalence of carpal fractures in Standardbreds.

Retrospective study	Distal radius	Radial carpal bone	Third carpal bone	Intermediate carpal bone
Lucas[9]	0%	49.6%	49.2%	1.2%
Palmer [10]	2%	35.3%	61.6%	1%

The distribution of fractures within the carpus of Standardbreds (SB's) and Thoroughbreds (TB's) varies (Tables 1.1 and 1.2). In one study of 1852 carpal fractures, 48% involved fractures of the third carpal bone (C3), but the distribution of breeds was not documented.[11] C3 fractures were classified as osteochondral ("chip") or slab fractures and were not differentiated by size or location. Schneider *et al* [11] developed a classification system of C3 fractures based on their size and location.

- Type 1: incomplete fractures of the radial facet. These are often difficult to diagnose as the fracture line is often present in only one projection.
- Type 2: large proximal chip fractures of the radial facet. Almost all have a similar appearance and are on the medial aspect of the ridge that separates the radial and intermediate facet.
- Type 3: small chip fractures in various sites of the radial facet: there is often another fracture in the same joint or in the other carpus.
- Type 4: medial corner fractures, these are large and the fracture line always propagates medially into the second carpal bone (C2-C3) articulation. Often other fractures, associated with C3 or the radiocarpal bone (Cr) are present.
- Type 5: frontal plane slab fractures of the radial facet. These are reasonably uniform in location and appearance. A small number of these fractures are comminuted and 33% are displaced.
- Type 6: frontal slab fractures involving both the intermediate and radial facet. Configuration is to either fracture in the middle of the radial facet (propagating laterally into the C3- fourth carpal bone (C4) articulation) or to break medially from C2 and advance laterally to C4.

Slightly less than 50% of these fractures were comminuted and greater than 65% were displaced, often leading to an unstable carpus.

- Type 7: slab and osteochondral fractures of the intermediate facet.
- Type 8: sagittal slab fractures on the medial side of the radial facet. Nearly 50% are associated with an osteochondral fracture within the same carpus.

Using the above classification scheme the term slab fracture includes Types 5,6, and 8. The total frequency of slab fractures, when taken as a ratio of C3 fractures, is 41%.[11] Type 4 fractures are also considered to be partial sagittal slab fractures.[8] Palmer[10] investigated the frequency of slab fractures and found the prevalence to be 22% of carpal fractures. When classified by breed, 29% of SB's sustained slab fractures of C3 and these were distributed equally between both legs; 19% of TB's sustained slab fractures of the C3, most commonly in the right foreleg. Variation between breed and limb distribution is supported by other studies.[12 13]

Table 1.3: Racing performance following surgical treatment of osteochondral (chip) and slab fractures.

Fracture Type	At least 1 race	Returning to previous level of function
Osteochondral (chip)	85-90%[14 15]	68.1%[14]
Slab	60-70%[12 13 16]	43%[12]

The diagnosis, treatment and prognosis of horses that have sustained slab fractures of C3 is well reported in the literature.[12 13] The overwhelming finding is that the prognosis for return to function is dramatically reduced when compared to osteochondral fractures within the carpus (Table 1.3). Slab fractures are likely to be the end result of C3 disease. Another clinical entity that has recently been described may involve the same pathophysiological process, and perhaps precede slab fractures. Lesions included incomplete frontal fractures of C3, crush fractures of the subchondral trabecular bone, and full thickness or partial thickness cartilage damage of the radial facet. However, clinical signs occur at an earlier stage, before radiographic changes can be detected subjectively.[17] The majority of these fractures were in SB's, and the lesion distribution was equal between both forelimbs. The crush fractures were similar to those reported by Ross[18], however within that case series radiographic lucency was detected in the tangential projection, perhaps due to increased severity of lesions. Surgical treatment is recommended and the prognosis for return to athletic function is similar to that of osteochondral fractures within the carpus.[17,18]

1.2 Normal structure and function of synovial joints

Synovial joints consist of 2 or more articulating bones, joint capsule, synovium, extra and intra-articular ligaments, synovial fluid, joint cavity and articular cartilage.

The joint capsule consists of a thick fibrous portion that inserts a variable distance from the articular surface and is lined by thin subsynovium and synovium. The fibrous section is composed of connective tissue that has a low cellularity; the extracellular matrix is made up of fascicles of collagen bundles (type III and I), proteoglycan, noncollagenous proteins and water.[19] The fascicles are separated by loose connective tissue and have a random organisation allowing them to move independently; this reduces joint friction, resists multidirectional forces, protects the synovial membrane from trauma, and allows maximal range of joint motion. [20] The proteoglycan- glycosaminoglycan component gives the matrix a gel-like quality that supports the collagen, and alterations of these proteins can change the mechanical capability of the capsule.

Collateral ligaments are intracapsular ligaments that aid in stabilisation of the joint. Biochemical composition and biomechanical nature are similar to the joint capsule and they appear to act in accordance with Wolff's law.[19] Extra-articular ligaments originate outside the insertion of the fibrous joint capsule, and are subjected to lower loads than those which cause abrupt failure. Injury usually results in a cumulative failure of individual collagen fibers.[21] Intra-articular ligaments are those within the joint, the most familiar being the intercarpal ligaments and the cruciate ligaments of the stifle joint. Their properties are similar to those of extra- articular ligaments.

Synovium is composed of modified mesenchyme; approximately 1-4 synoviocytes thick and cells have both secretory and phagocytic functions. [19] The synovial membrane serves no biomechanical purpose but like all soft tissues can respond to stress by an increase in collagen production, alterations in trans-synovial diffusion, or changes in synoviocyte metabolism. The lack of basement membrane and gaps between the synoviocytes allow the movement of capillary filtrate through the interstitial fluid into the synovial space, thus forming synovial fluid. This is governed by Starling's forces (hydrostatic and colloid pressure difference between plasma and synovial fluid) and excessive fluid is drained from the joint by lymphatic vessels.[20] Normal synovial fluid pressure is subatmospheric which may assist in stabilizing the joint. [19]

Synovial cells produce proteins (hyaluron) that contribute to the unique nature of synovial fluid and have the potential for direct release of lysosomal enzymes (particularly neutral metalloproteinase), prostaglandins, free radicals and cytokines. [22] Synovial fluid is the medium through which nutrients reach articular cartilage. The endothelium prevents large molecules from leaving the joint while small molecules depart via diffusion. This is controlled by the presence of large proteins (e.g. hyaluronan) which function as a barrier to small molecule exchange.[23] There are a number of proposed mechanisms of joint lubrication that function under different loads and stresses, and all are reliant on synovial fluid and its viscous nature. [21] Viscosity is associated with hyaluron amount and characteristics, and allows the synovial fluid to tolerate transient shear stresses and absorb some of the energy generated by movement. [19]

Articular (hyaline) cartilage derives its translucent appearance from a high water content and collagen structure. Microscopically it is divided into 3 unmineralised zones that are delineated from the calcified zone by the tidemark.

- Zone 1: the most superficial with the highest number of cells, which are small, flat and parallel to the surface. Collagen fibrils are tangential to the articular surface.
- Zone 2: the cells are larger and more rounded than those in zone 1 and the collagen fibrils are arranged in a complex three-dimensional pattern.
- Zone 3: the cells are as large as zone 2, organised with their long axis perpendicular to the surface. The collagen fibrils are larger with a perpendicular orientation, forming a relatively inflexible mesh.

It has been suggested that the variation of zones represents a functional adaptation to differing mechanical requirements: Zone 1 has an abundance of collagen and forms a wear resistant protective layer, whereas the deeper zones contain large amounts of proteoglycans and are organised to withstand compressive loading.[19]

The extracellular matrix of equine articular cartilage is predominantly composed of type II collagen which provides tensile strength, proteoglycans and noncollagenous extracellular matrix molecules, and includes fibronectin and growth factors. Chondrocytes are the cellular component of articular cartilage. Although they make up a small percentage of the cartilage they are responsible for the production and turnover of extracellular matrix. They receive nutrients and excrete wastes via the synovial fluid and are sensitive to changes in the matrix caused by physical stimuli and catabolism. It is not known how the chondrocytes co-ordinate matrix turnover, but, dynamic loading and cytokines are thought to play a substantial role. High and continually compressive loads are pathological to the articular cartilage whereas moderate cyclic compressive loads are beneficial to the matrix.[21] These factors influence the production and activation of the chondrocytic enzymes that can degrade the extracellular matrix. this degradative process is balanced by enzyme inhibitors and growth factor synthesis.[19]

Articular cartilage and subchondral bone are 2 dissimilar tissues. Calcified cartilage. with its intermediate properties acts as an interface between these tissues to reduce shear stresses.[21] Calcified cartilage undergoes remodelling throughout life. as numerous segments contain osteoclastic fibrovascular tissue and new bone. The cause of this may be due to micro-injury as a result of loading a relatively brittle structure when compared to articular cartilage.[24] The tidemark (the junction between calcified and non-calcified cartilage) also reduplicates in response to micro-injury and physiological ageing at the expense of articular cartilage. resulting in cartilage thinning.[25 26]

Subchondral bone provides structural support to overlying articular cartilage allowing high loads to be sustained without significant deformation. The stiffness of subchondral bone is due to its high mineral content (hydroxyapatite). This inorganic matrix accounts for 65% of total bone matrix. The organic matrix (osteoid) is made up of water. collagen and other proteins and is responsible for the elasticity and pliability of subchondral bone. Heterogeneity of trabecular bone in the area of the subchondral bone plate makes it histologically difficult to distinguish between trabecular bone and cortical bone.[19]

Trabecular bone has a distinct architecture: the basic cellular structure consists of individual trabeculae of varying thickness that are interconnected with spaces between them. Wolff's law controls trabecular orientation. which is parallel to the deeper zones of cartilage and perpendicular to the articular surface.[19 27] Trabecular bone is heterogeneous and thus its material properties vary with age and anatomic location. The bone is able to regulate strength and stiffness by changing apparent density. this is governed by a squared power law relationship. meaning small changes in apparent density relate to large changes in strength.[27] Increases in apparent density are due to increasing thickness of the individual trabeculae and decreasing the size of the intra-trabecular spaces. with the reverse being true for decreasing apparent density. Remodeling of trabecular bone occurs on the endosteal surface (the interface between the trabeculae and the marrow) and involves the filling in of a defect created by osteoclasts with bone produced by osteoblasts. [28] The resistance for fatigue failure appears to be greater for trabecular bone than it is for cortical bone as the mechanism for failure is fracture and buckling of individual trabeculae rather that an accumulation of cracks in the bone matrix as in cortical bone. [29]

Osteonic or cortical bone differs from trabecular bone in its porosity (thus apparent density) and architecture. [30] Cortical bone is a solid material that contains a series of voids (Haversian canals), and its porosity, usually around 10%, is related to the number of these voids. Cortical bone is a poorly compliant but relatively tough tissue that becomes stiffer and stronger, absorbing more energy as the loading rate increases. Once a threshold is reached these properties reduce. Remodeling of this tissue involves the formation of a bone-remodeling unit consisting of a cutting cone that resorbs bone. When resorption is complete osteoblasts fill the canal with concentric lamellar bone and the canal becomes progressively smaller until it is only large enough to contain blood vessels.[28]

Relative density and architecture determine the properties of subchondral bone, and as bone is an adaptive tissue these properties are not constant. [31] This is reflected by the changes that occur with increasing age. Young[31] found a significant increase in subchondral bone stiffness and density between yearlings and untrained 2 year olds.

1.3 Functional anatomy of the carpus

In most horses the carpus consists of 7 carpal bones arranged in 2 rows between the radius and the metacarpal bones. In a mid-frontal section, the bones of the carpus, except the accessory carpal bone, are approximately rectangular, leading to the term cuboidal bones. The dorsal and palmar surfaces are convex. The palmar surface is very irregular and with the accessory carpal bone forms part of the carpal canal. Figures 1.1 illustrates the proximal aspects of the proximal row and Figure 1.2 illustrates the articulation of the proximal row with the radius. Cr articulates with the medial styloid process of the radius and C2 and C3. The intermediate carpal bone (Ci) articulates with the interprocess area of the radius and C3 and C4. The ulnar carpal bone (Cu) is the smallest of the proximal row and articulates with the lateral styloid process of the radius and with C4. The accessory carpal bone's dorsal border articulates with the caudal aspect of the lateral radius and the Cu. Figure 1.3 illustrates the proximal aspect of the distal row. The second carpal bone is the smallest constant bone, the proximal surface of which articulates with the Cr, distally with the second metacarpus (MCII) and palmar aspect of the third metacarpus (MCIII). The proximal surface of C4 articulates with the intermediate and the Cu, the distal surface with the MCIII and the fourth metacarpal (MCIV). [32]

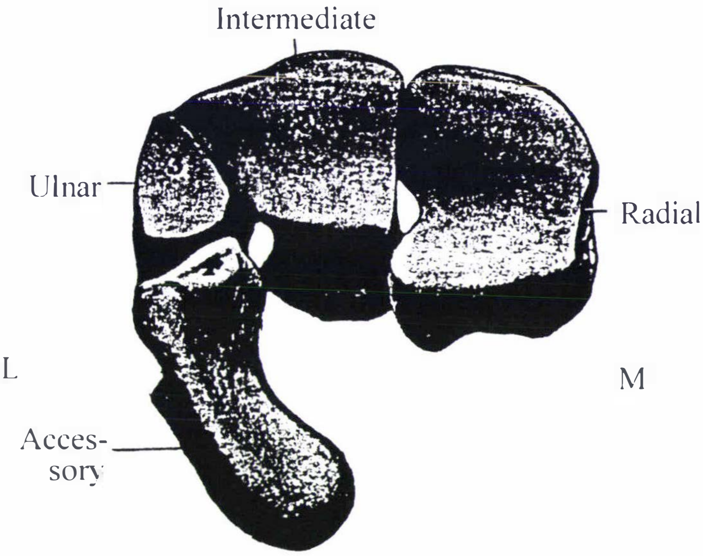

Figure 1.1: Diagrammatic representation of the isolated proximal row of carpal bones. M = medial, L = lateral. (*modified from Getty*[32])

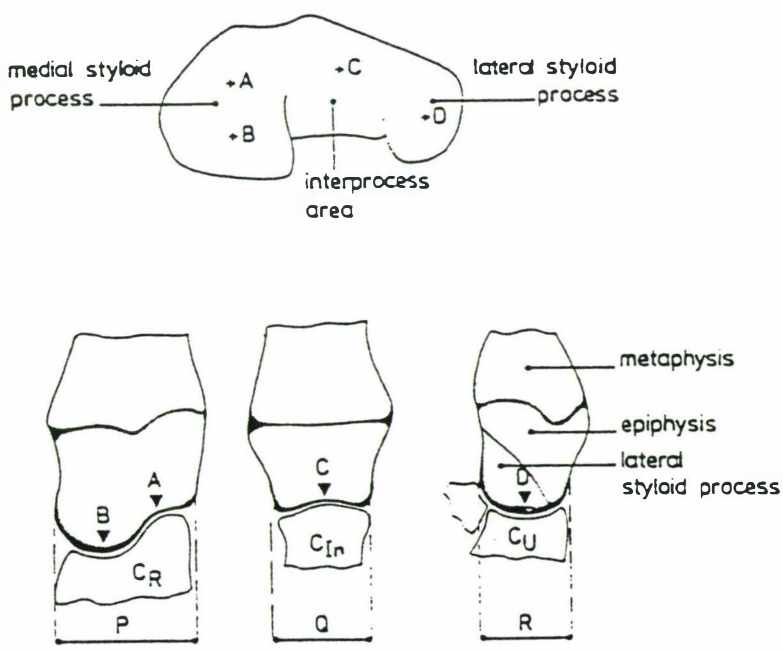

Figure1.2: Diagrammatic representation of the articulation of the proximal row with the radius. (*modified from E.C.Firth and W.Hartman*[33])

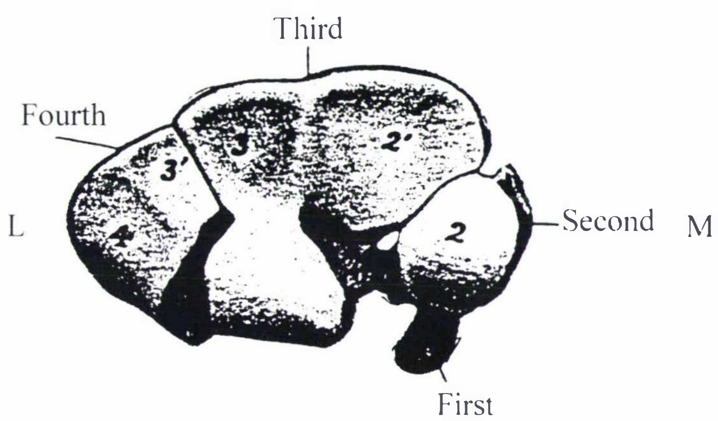

Figure 1.3: Diagrammatic representation of the isolated distal row of carpal bones. M = medial, L = lateral. ***(modified from Getty[32])***

The third carpal bone is the largest bone of the distal row, contributing to 2/3rds of the medial to lateral dimension, and is twice as wide dorsally as palmarly. The 2 facets of the proximal surface are separated by a dorsopalmar ridge. The medial facet (concave) is known as the radial facet and articulates with the distal surface of the Cr. The lateral facet (concave dorsally and convex palmarly) is known as the intermediate facet and articulates with the distal surface of Ci. The distal surface of C3 articulates almost entirely with MCIII, and the lateral and medial aspects of the bone articulate with MCIV and MCII respectively. [32]

The radial carpal bone, Ci and C3 receive the majority of the load accepted by the carpus and are most often injured at fast gaits.[34] The other 3 cuboidal bones are smaller, thereby carrying less load and are not as prone to injury. The proximal joints of the carpus are high motion joints of different types. The radiocarpal joint is a rotating joint with the normal range of flexion being limited by the palmar joint capsule and flexor muscles.[35] The intercarpal joint is a hinged joint and capable of only 10°-20° hyperextension due to the palmar location of the collateral ligaments and the shape of the joint surface.[36] The carpometacarpal joint has very little motion and no capacity for flexion or extension.[36,37] The joint capsule is thought to be common to all 3 joints, attaching proximally to the radius and distally to the proximal metacarpus. The synovial membrane forms three pouches corresponding to the 3 joints; the radiocarpal and the intercarpal pouches are voluminous, whereas the carpometacarpal pouch is limited. The distal 2 pouches communicate. [38]

A study by Firth *et al* [36] described the relationship of movement between the joints of the carpus and associated cuboidal bones during passive movement. The radiocarpal joint contributes most of its flexion at the beginning of passive flexion. The differing rotational axes of the radius result in the Cr and Ci sliding past each other in a proximal-distal direction during movement, so that at full flexion the distal border of Cr is several millimeters distal to that of the distal border of Ci. The Cu, Ci and accessory carpal bone move as a single unit and tilt a total of 25° in full flexion, while the Cr achieves a tilt of 5°. The intercarpal joint plays a role in the later stages of carpal flexion. As the degree of flexion increases the distal row of carpal bones pivots about an axis contributing to the later stages of carpal flexion.

The carpus has a number of extra-articular and intra-articular ligaments. The lateral collateral carpal ligament attaches proximally to the lateral styloid process of the radius and distally to the proximal MCIV, with some fibers ending on MCIII. The medial collateral carpal ligament is stronger and wider distally than the lateral with the proximal attachment on the medial styloid process of the distal radius and the distal attachment on the second and third metacarpus.

Numerous ligaments are present dorsally that are essential in the normal functioning of the carpus. Intra-articular ligaments of the carpus occur in the intercarpal and carpometacarpal joints. intercarpal intra-articular ligaments are more prone to injury. There are 3 ligaments. the dorsomedial intercarpal ligament. the medial palmar and the lateral palmar intercarpal ligaments. The dorsomedial intercarpal ligament arises from the lateral border of the Cr and attaches distally to the dorsomedial aspect of C2 and in some cases C3. The lateral palmar intercarpal ligament has a proximal attachment on the distal palmar medial surface of the Cu and palmar lateral surface of the Ci and travels distomedially to predominantly insert on the proximal palmar lateral surface of C3. The medial palmar intercarpal ligament exhibits variation in anatomy between horses. The proximal attachment is usually to the distolateral surface of the Cr and inserts distally on the proximal palmar medial surface of C3 and the proximal palmar lateral surface of C2. This ligament is usually divided into 4 bundles [39]

1.4 Physiology

When undergoing maximal exercise the carpus acts as a stress absorber. When axially loaded most of the carpal articulations allow an interlocking wedge arrangement to be formed. Some of the load is transferred to the intercarpal ligaments. as illustrated in Figure 1.4.[37] It is thought that by this mechanism sudden stress is converted into a longer elastic loading stress and thus the strain rate is decreased.[40] It appears that the carpus requires this mechanism for energy absorption as its elastic ability to overextend is limited (due to the palmar soft tissues) when supraphysiologic loads are applied. Thus it is postulated that the stresses imposed on the carpus during maximal exercise would lead to degenerative changes if there were a reduction in the number of bones in the carpus.[40] This may occur on the medial aspect of the intercarpal joint. as loads from the radius may pass on to the Cr and directly on to the radial facet of the C3 without being dissipated to the intercarpal ligaments. This predisposes the 3 major weight bearing bones to injury. in particular the radial facet of C3.[37]

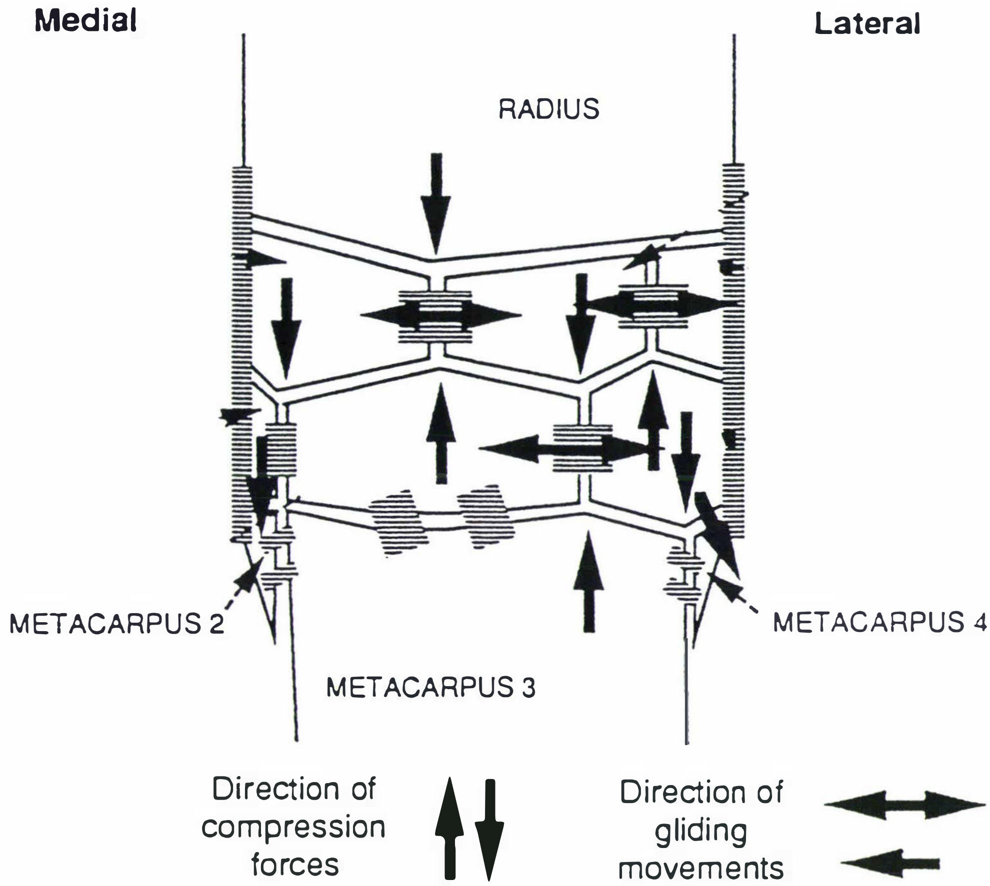

Figure 1.4: Diagrammatic representation of the intercarpal ligaments of the carpus.
(modified from E.C.Firth, N.Deane, K.Gibson et al [36])

When the major weight bearing carpal bones are loaded, the majority of the load is accepted by the fluid component of articular cartilage causing instant deformation. As the load is shifted to the solid component there is slower creep deformation, this continues until equilibrium is reached between the cartilage and the external force applied. This property is true of all viscoelastic materials. [21] It appears that moderate loading enhances cartilage metabolism, however, high continuous loads and complete immobilisation appears to damage cartilage. [21] As mentioned previously there is an abundance of collagen in the superficial zones, which resist tensile forces, consequently small pathologic alterations within this area may weaken the articular surface and its biomechanical resistance to shear, tensile and compressive forces. [41] Compliant subchondral bone acts as a shock absorber between articular cartilage and epiphyseal bone, thereby helping to minimise pathology at the articular surface. The shock absorptive capacity appears to reduce as apparent density increases and thus compliance decreases.

Bone is a constantly adaptive tissue and it is widely accepted that relative density increases with exercise.[31 42 43] It is thought that during exercise the trabecular bone deforms when placed under a mechanical load. Repetitive loading stimulates the osteoblasts lining the spongiosa to upregulate, leading to thickening of the trabeculae at the expense of the intra-trabecular spaces; this is termed modelling.[20] In order to explain the distribution of changes that occur within C3 as a result of exercise, it important to study loading patterns at rest and at varying gaits. At rest the palmar aspect of both the radial and intermediate facets bear the most weight. Application of high loads in this position result in intermittent weight bearing on the dorsal aspect of both facets. When moving at low gaits such as walking and trotting the load is distributed evenly over the radial and intermediate facets excluding the most dorsal aspect. Under load conditions that mimic those of galloping, the load is transferred to include the dorsal rim of the intermediate and radial facets with a shift towards the dorsomedial aspect of the radial facet. [33 43]

Table 1.4: Microradiography studies of excised C3's from horses in different stages of training.

Horses	Microradiography
Untrained	The trabeculae were aligned in a proximodistal direction in an open pattern and the subchondral bone formed a constant width across each section.
Trained but unraced	Inclination to trabecular thickening and decreased intra-trabecular spaces.
Actively racing	A unique pattern of appositional growth, this occurred at the expense of marrow spaces, thus forming a bony bridge between the proximal and distal surfaces of C3. Sclerosis of subchondral bone was greatest at the dorsomedial aspect of the radial facet of the C3 in a band 3mm palmar to the dorsal margin.

Microradiographic examination of C3's from horses that have undergone different levels of exercise show evidence of modelling. This is particularly evident in actively racing horses. In a band 3mm from the dorsal margin an increase in photodensity and change in architecture demonstrate this modelling (Table 1.4). [42, 31] Increasing radiographic photodensity correlates with increasing bone mineral density (BMD). Firth *et al* [44] took sagittal sections in a dorsopalmar direction of the intermediate and radial facets of C3. Radiographs were taken of the sagittal sections and compared with BMD measurements performed by dual x-ray absorptiometry (DXA). Uhlhorn *et al*[45] radiographed isolated C3's in a proximal distal view and compared them with bone volume measurements using morphometry. Both studies found that bone volume density in the dorsal proximal, dorsal central and dorsal distal regions of C3 was significantly greater in trained compared to untrained horses. Both studies demonstrated that the dorsal central regions of interest had the greatest increase in density. Similar findings have been observed in TB's trained on a treadmill. Bone mineral density increases in the distal dorsal region of C3, then the proximal dorsal region and finally the central dorsal region. (Unpublished data Firth 99)

1.5 Changing micromorpholgy of C3

The adaptive response to exercise is a physiological process. However, continued modelling in response to high loads leads to pathological changes demonstrated by microradiography (Table 4).[42] Continued modelling causes sharp gradients in stiffness 5-10mm from the dorsal edge of C3 which may result in incomplete dissipation of forces within articular cartilage during loading, predisposing it to injury.[31] Repetitive micro-trauma to the articular cartilage leads to chondrocyte injury, which in turn responds by producing enzymes that destroy the extracellular matrix. The gross changes that may be seen include yellowish discoloration, dullness, fibrillation and eburnation. Microscopic changes include loss of proteoglycan, disruption of the various zones of articular cartilage, changed chondrocyte morphology, exposure of the calcified cartilage and polishing of the exposed subchondral bone.[20] Uhlhorn *et al* [45] found that bones with cartilage lesions of the radial facet of C3 had a significantly higher bone volume density than those that did not. Pool [20] found that although there does not appear to be a good correlation between the degree of deterioration of the articular cartilage and subchondral bone sclerosis both appear in varying degrees in affected bones.

Remodelling occurs concurrently with modelling. True remodelling occurs when there is no net increase in bone mineral density; repair and damage occur at the same rate. When damage (presumably from the sharp change in stiffness gradient within the subchondral bone, as a result of modelling) exceeds repair it is presumed that the high rate of microfractures disrupts the canalicular system and possibly the capillary bed. The result is a wedge shaped area of ischemic, sclerotic subchondral bone within C3. This secondary lesion usually measures 8-10mm in length, 3-5mm in width and 1-2mm in depth. It is located 2-4mm from the dorsal proximal margin of the radial facet and is composed of acellular fragments of sclerotic bone with the deep surface being separated from viable compacted bone by a line of resorption. A vascular response arises from viable bone to fill the trough with osteogenic granulation tissue that invades and repairs the necrotic subchondral bone.[20]

It is suggested these lesions are associated with development of corner or complete slab fractures. Small areas appear to undergo repair without destabilisation of overlying cartilage. Unsupported articular cartilage either collapses into the cavity or becomes detached. Studies of slab fractures by Pool [20] suggest these fractures occur in pathological bone. All lesions begin at the dorsoproximal surface of C3 in an area of chronic injury and repair. The fracture line extends distally where it either turns obliquely to create a partial slab fracture or continues to create a compete slab fracture. Usually the proximal ¼ of the fracture line appears irregular and contains fibrous tissue, the distal ¾ appears as an acute fracture.[20]

In vivo and *in vitro* studies demonstrate that traumatic loading induces damage to the subchondral bone and calcified cartilage before inducing damage to articular cartilage.[46,47] Therefore it has been proposed that early detection of sclerosis may be helpful in preventing degenerative joint disease and fractures.[48]

1.6 Diagnosis of third carpal bone disease

Radiography is the main diagnostic tool used in the assessment of carpal injuries. As with all radiographic evaluations a number of views are taken to ensure adequate assessment, since superimposition is a problem in the radiographic evaluation of joints. Lesions may be missed due to x-ray beam obliquity in relation to the lesion or by masking of overlying structures. Carpal views taken are the lateromedial, flexed lateromedial, dorsolateral-palmaromedial at 30° and 60°, dorsomedial-palmarolateral at 45° and the flexed dorsoproximal-dorsodistal oblique, the latter is commonly known as the tangential view of the distal carpal row. Most lesions can be detected in some but not all radiographic views, and a proportion of lesions are detected only on the tangential view.[11,48]

There are 2 tangential views used to assess the distal carpal row. View A (Figure 1.5) involves flexing the leg at 60° with MCIII parallel to the floor, the x-ray beam is angled 30° from horizontal, the plate placed distal to the carpus and angled towards the beam as close to 90° as possible. This view results in little distortion of C3, however, some magnification does occur. View B (Figure 1.7) involves flexing the carpus and placing the plate on the dorsal aspect of MCIII, with the centre of the plate at the level of C3 and the x-ray beam angled at 30° from horizontal. This view causes little magnification but a significant amount of distortion, as the beam angle is not perpendicular to the plate. The x-ray beam angle, leg angle and C3 beam angle are similar between both views, however, the plate angle significantly differs.

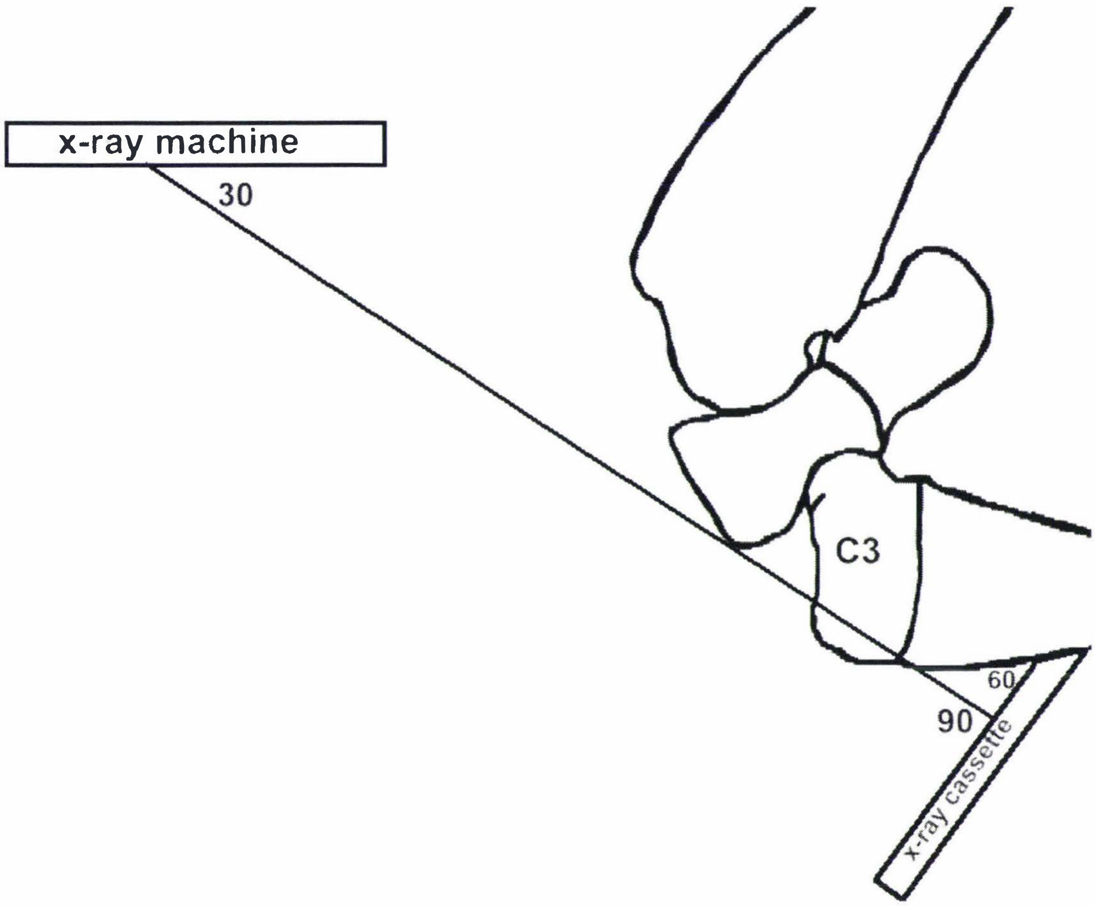

Figure 1.5: Line drawing of view A

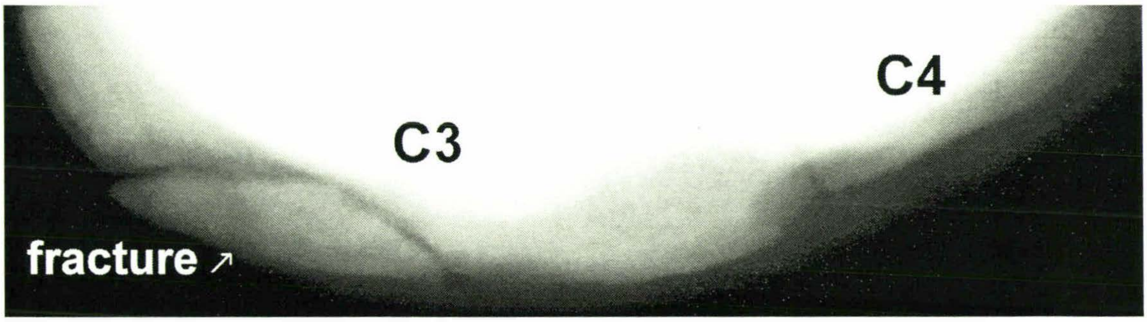

Figure 1.6: Radiograph of the distal row of carpal bones using View A. A fracture is present within the radial facet of C3.

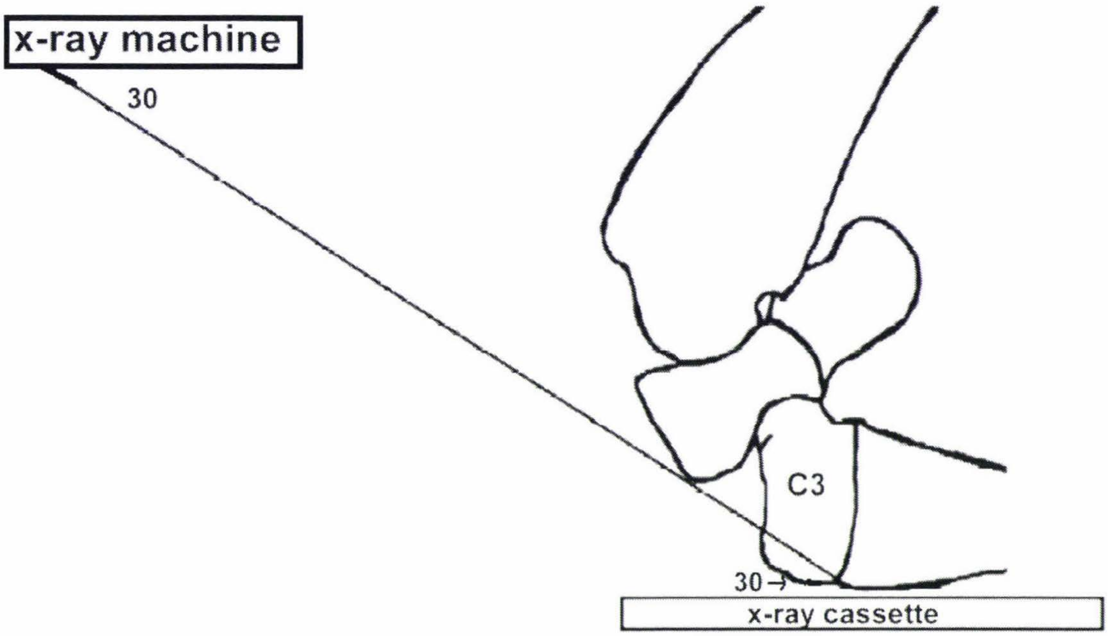

Figure 1.7: Line drawing of View B

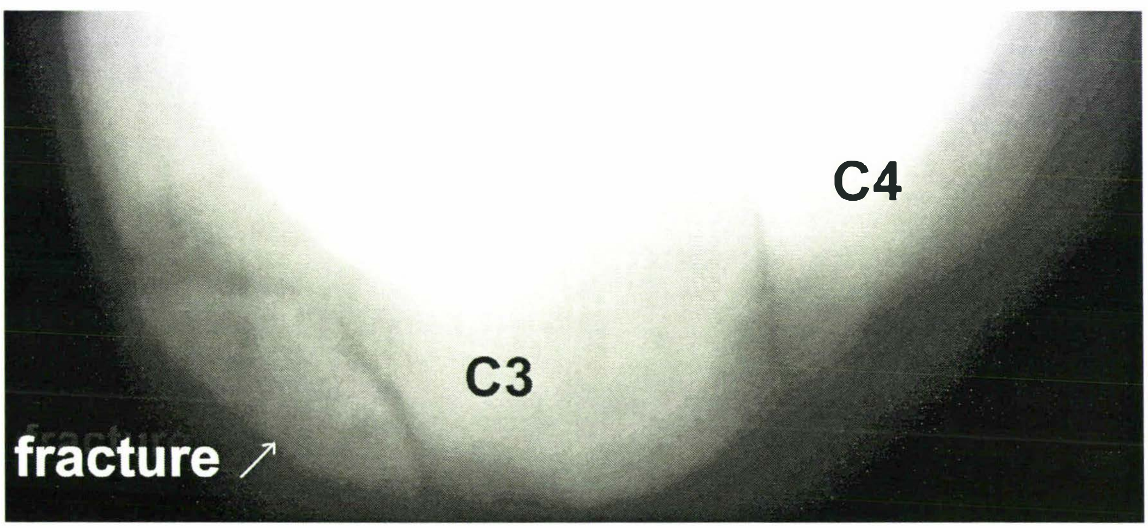

Figure 1.8: Radiograph of the same distal row of carpal bones as in Figure 1.6 using View B. A fracture is present within the radial facet of C3.

Subtle lesions are likely to be detected with advanced radiographic equipment and film/cassette combinations, predominantly due to improvement in intensifying screens and radiographic film. Intensifying screens contain a range of materials which convert a few photons of high energy (x-rays) into many photons of low energy (blue light). In the production of these screens 2 qualities are important, namely speed (the smallest possible exposure to produce an image) and optimum definition of the image. Those factors that contribute to one quality are detrimental to the other, and a compromise must be reached. In most circumstances the advantage of reducing the exposure time is of more importance than optimum detail. In equine radiography speed of exposure may contribute to greater detail as movement blur is reduced.[49]

X-ray film is an emulsion, which is a coating containing finely dispersed grains of silver halide. When exposed to low energy photons, the halide is converted to metallic silver, which on developing and fixing results in the blackening of the exposed area. Most films are double emulsion, with emulsion on both sides of the film. Various emulsions enable fine or standard detail. Single emulsion films are coated on one side only, and are designed for use with cassettes with single intensifying screens and produce very fine detail, at the expense of increased exposure time.[49]

The majority of carpal radiographs taken in the field use medium or standard double emulsion film and cassettes with double standard intensifying screens. This allows minimum exposure time and adequate detail for the subjective analysis of the tangential view of C3. Exposure times vary with film focal distance and equipment used, and each machine should have an exposure chart developed for each film type. Recent improvement in screen and film detail has lead to the use of single emulsion film and screens, and may improve trabecular detail of C3 without much increase in exposure time.

The occurrence of C3 sclerosis without the presence of other radiographic changes has led to the development of a grading scale (Table 1.5).[50] The radiographic views used to assess this are Views A and B. The radiographic quality must be such that the trabecular pattern can be recognised, not only in C3 but also in C4 as the latter is used as a "control". Grade 1 and 2 are believed to represent physiological adaptation.[50]

Table 1.5: Scoring of the trabecular pattern of C3 seen on the skyline projection.[50]

Grade I - trabeculation clearly evident, no areas of focal thickening.
Grade II - trabeculae clearly evident, with evidence of thickening in focal areas.
Grade III - trabeculation lost in focal areas
Grade IV - almost complete loss of trabeculation in the radial and/or the intermediate facet of C3.

C4 sclerosis is rarely seen and if present is more likely to be due to a radiographic artefact. [50] Investigation of subchondral bone changes of C4 do not appear in the literature. There are a small number of reports on slab fractures of C4, these are usually sagittal fractures and are often accompanied by a slab fracture of the intermediate bone. It is speculated that the cause of these fractures is abnormal force acting on normal bones, although this has not been proven. [51 52]

The validity of subjectively grading sclerosis of the third carpal bone has recently been examined.[45] In this study View B was used and only radiographs that showed C4 and C2 were included. The radiographs were graded using a grading system similar to that of O'Brien.[50] Once the horses were euthanased the distal row of carpal bones was disarticualted and radiographed in a proximodistal direction. C3 was then assessed for bone volume density using bone morphometry. The authors found that subjective assessment of the tangential radiographic view allowed differentiation between sclerotic and non-sclerotic C3's, however, the grade of sclerosis could not be determined. Although this is a significant finding some degree of sclerosis is believed to be a physiological response to exercise,[44] thus it appears that subjective analysis of radiographs may not differentiate between physiological and pathological sclerosis.

Subjective analysis of changes in BMD is not without problems. It has been generally believed that that changes in bone mineral density of less than 30% can not be detected subjectively. Although this was based on experiments performed 40 years ago,[53] a more recent study by Finsen[54] agrees with this hypothesis when dealing with the peripheral skeleton. Other studies have shown that although this was true for cortical bone sites, a change of only 8-14% is required for bones with a high trabecular content.[55] It must be stated that all of the work in regard to subjectively assessing BMD has been conducted in humans, in situations where BMD is decreasing rather than increasing as is the usual case in the young working horse.

1.7 Methods of analysing bone mineral density

The prevalence of osteoporosis in humans has resulted in the development of many methods of non-invasive bone mineral analysis in order to detect early disease and monitor its progression and response to therapy. Despite the number of methods, agreement has not been reached over the most effective for the diagnosis and serial assessment of osteoporosis, either for the single patient or when large populations are examined.

The pattern and rate of bone loss varies between the appendicular and axial skeleton, cortical and trabecular bone, and various disease states and therapeutic interventions. Thus variation in measurements using different techniques is not only a function of accuracy, precision and sensitivity, but also physiologic variation. Therefore, many methods of non-invasive bone mineral analysis are complementary rather than exclusive[56], and the following will be discussed.

- Subjective evaluation of radiographs and radiogrammetry
- Objective evaluation of radiographs - radioabsorptiometry
- Photon absorptiometry - single and dual
- Computed tomography
- Ultrasonography
- Neutron activation analysis
- Compton scattering technique

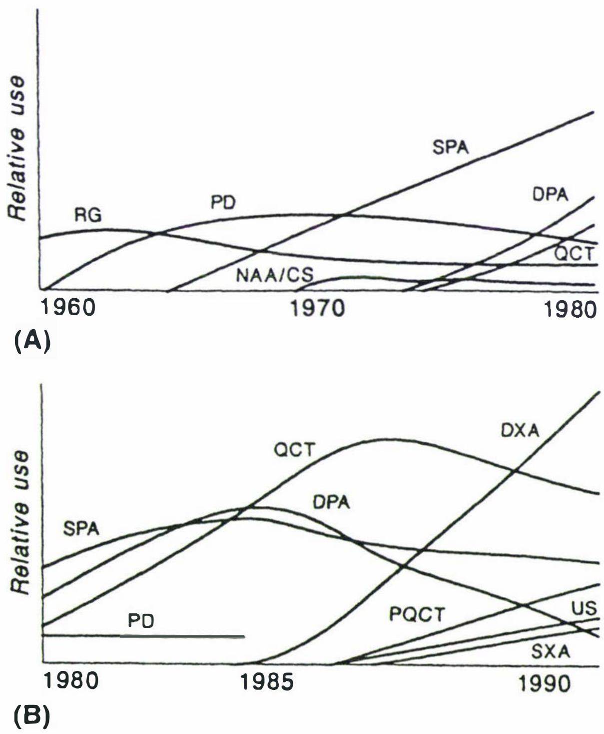

Figure 1.9: The relative use of methods of non-invasive bone mineral density methods from 1960-1990. Abbreviations: RG = radiogrammetry; PD = photodensitometry(RA); NAA/CS = neutron activation analysis and Compton scattering; SPA = single-photon absortiometry; DPA = dual-photon absortiometry; QCT = quantitative computed tomography; pQCT = peripheral quantitative computed tomography; DXA = dual x-ray absortiometry; SXA = single x-ray absorptiometry; US = ultrasound. ***(reprinted from Sartorius[49]. P 234 by courtesy of Marcel Dekker.Inc)***

Most of the above methods measure only bone mineral content (BMC) or BMD. The measurement should be interpreted in light of clinical symptoms, because although BMC and BMD are closely linked with bone strength, it is not the only factor associated with a high fracture risk. Others include bone geometry, architecture, point defects, neuromuscular coordination and frequency of falls. Thus these methods only partially detect an increased risk for fracture.[57]

1.7.1 Subjective evaluation of radiographs

Subjective evaluation of radiographs is the simplest non-invasive method of BMD assessment. Parameters used to indirectly assess change in bone mass include reduced or increased photodensity, or changes in bone morphology. Based on experiments conducted in the 1940's, it was believed that changes in BMD of less than 30% could not be detected subjectively.[58] A more recent study[54] agrees with this hypothesis when assessing the peripheral skeleton. Other studies have shown that although this is true for cortical bone sites, change of just 8-14% is required for detection of subjective BMD differences in trabecular bones.[55] Although subjective assessment is a relatively insensitive method for BMD analysis it is an imperative part of the standard routine of reading radiographs, and is currently the most commonly employed method of estimation of BMD in the horse.

1.7.2 Radiogrammetry

Radiogrammetry a more objective method, is inexpensive and simple to perform. It involves morphometric measurements of cortical bone from radiographs, primarily using the ratio of cortical thickness to the overall thickness of tubular bones. This requires direct caliper measurements of the inner and outer diameters of the cortices from which bone mass indices are then calculated. It is best performed with cortical bone from the appendicular skeleton, most commonly the metacarpal thickness due to their accessibility by x-ray imaging and the low radiation exposure to the patient.[58]

Originally it was thought that radiogrammetry allowed accurate measurement of cortical bone volume and thickness, and as bone remodeling was low in the appendicular skeleton, this reflected changes in total bone mass.[59] Further studies have revealed that the test results of this procedure are relatively inaccurate because of the irregularities in the shape of the metacarpal cortical regions and intracortical resorption.[60] This technique was extensively used in the 1960's and 1970's to assess BMD, but is now thought to be inadequate for the diagnosis of osteoporosis and its progression. However, it appears sufficient for epidemiological studies of large populations.[58]

1.7.3 Objective evaluation of radiographs -radioabsorptiometry

Radioabsorptiometry (RA) measures BMD objectively by measuring radiographic photodensity achieved by comparing a material of known photodensity with bone. The technique has been available for over 50 years, but prior to the development and application of computers and image analysis it was inaccurate, imprecise and time consuming.[61 62]

The technique involves taking a conventional radiographic image, of either the right or left hand. The hand is placed on a template and a reference standard is placed in a predetermined place. Two radiographs are taken at different exposures using single x-ray film. The radiograph is captured, converted into a digital image and an image analysis program is used manage the data. Data are collected on phalanges 2,3 and 4 and the computer calculates the average values for BMD and bone area. The data is collected in arbitrary units rather than g/cm^2 or g/cm^3, however these units do have dimensions of mass and volume.[61 63]

The material of known photodensity to which bone is compared to is often in the form of a wedge, however there are other reference standards. The reference standard is included in the radiographic image to correct between film differences, due to film quality, exposure and processing. Nearly all wedges are in ramp form and the ideal reference wedge has the same absorption coefficient as the material being measured as shown by Figure 1.10. The most common metallic wedge to be used is aluminium or an aluminium alloy. The wedge dimensions are comparable to the thickness of the phalangeal bone.[63]

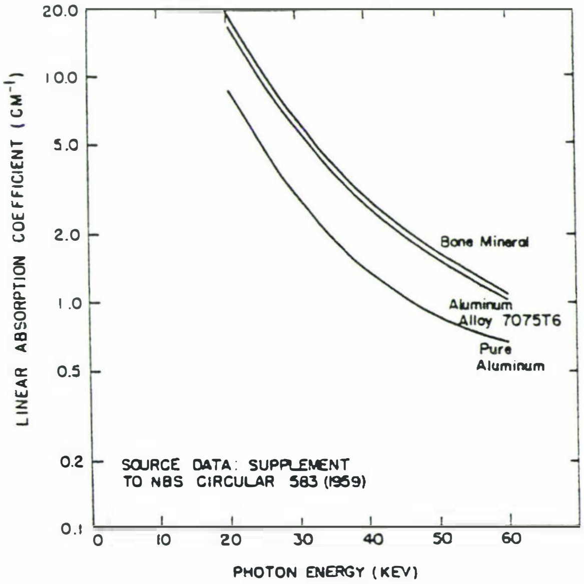

Figure 1.10: Linear absorption coefficient as a function of photon energy.
(modified from Colbert[63])

Two radiographs are taken in order to verify the results. Between film disparities are usually less than 2%. If the discrepancy is more than 3% from the mean then the radiographs are checked for defects, which can be produced by processing or exposure faults. If there is a discrepancy the procedure is repeated.[63] Accuracy error is very low as RA is highly correlated with ash weight of measured bones. This may be because the trabecular and cortical bone of the phalanx is roughly equivalent to the central skeleton.[64] Precision error is also very low as reproducibility of this technique is 99% or greater.[62]

The consistency with which RA studies measure bone mass is high, even when skeletal sites measured and populations studied vary. RA is thought to be as good as, or in some cases better than, other bone mass measurement techniques and its predictive association of fracture risk is high.[61] The main application for this technique is to detect and monitor osteoporosis. It also has been used to assess osseous changes associated with lead poisoning and renal disease, and in the treatment of osteogenesis imperfecta.[63]

The technique has several advantages, it is readily available to the non-specialist physician and no large capital expenditure is required. The radiographs are taken and then submitted to an image analysis laboratory for interpretation, so the technique is of significant use in remote areas where access to other bone mass analysis methods is limited. The use of this technique to assess the efficiency of therapy in individual patients has not been studied in a controlled clinical trail.[61] Recent improvements of RA reduce the disadvantages associated with this technique. A valid concern, as with other techniques utilising the appendicular skeleton, is that the BMD values of the phalanges may not predict BMD of the axial skeleton.[49]

RA has been used in the dog and the horse.[65,66] Both of these studies were performed on isolated bones that had all soft tissue removed, as its presence results in a high accuracy error. The calcaneus was used in the horse because there is a high amount of trabecular bone which is more sensitive to changes in bone mass, however it appeared that the optical density was influenced by the mass of the bone rather than the actual mineral density. The study concluded that RA using the calcaneus was not a reliable indicator of BMC.

1.7.4 Single photon absorptiometry

Single photon absorptiometry (SPA) assesses BMC by a single source of low energy photons (from a highly collimated source) that penetrates the bone of interest, and was one of the most widely accepted and clinically applied devices in the 1970's and 1980's. The degree of attenuation of the beam by the bone is measured by a scintillation detector system, and there is a direct relationship between the number of photons absorbed and BMC.[67]

The main components required for an absorptiometry unit are a single energy source photon unit, most commonly iodine and americuium isotopes, and a detector. As SPA uses only one energy source, the bone site must be encased in a constant thickness of soft tissue or equivalent (e.g. water), as soft tissue critically contributes to the attenuation profile. The photons travel from the source (usually under the patient), pass through the patient and continue upward to enter a detector where the intensity of the beam is determined. The source and the detector are aligned and connected so they move in unison.[68] The forearm is placed in a water bath and a base line measurement obtained in the region of the interosseous membrane. The average attenuation of the beam by the bone is calculated and compared with data in a standard curve derived from a reference, from this information BMC can be calculated.[56 49]

Precision error associated with SPA is as low as 0.3%, however there can be considerable inter-unit variability and miscalibration. Other sources of variation are interosseous and subcutaneous fat.[69] SPA measurements do not reflect axial bone density accurately and there appears to be an accuracy error of up to 12-15% in estimating spine or femoral density.[69] This method does not take into account bone volume and thus only BMC can be measured. In order to assess BMD, cross sectional area (CSA) is required, this can be achieved by using combined ultrasound velocity to detect cortical CSA and thus bone mineral content divided by CSA is equal to bone mineral density.[70]

SPA at peripheral sites has been less successful for the diagnosis and monitoring of osteoporosis than believed possible when the method was first developed, and the development of DPA and DXA have led to dwindling usage of this modality.[69]

SPA has been used in horses in combination with ultrasonic transmission velocity to determine the BMD of MCIII and changes that occur to BMD in response to immobilization.[71 72]Although this is a relatively precise method, the disadvantages include expense, lack of portability of equipment, and the requirement of bandages to provide a constant soft tissue covering. The patient is required to stand completely still for at least 90 seconds.[73] A disadvantage of this process in the horse is that it provides the mineral content per unit length of bone and takes no account of differences in bone size, thus it is only useful in comparing changes in the individuals with negligible CSA alterations.[72]

SPA has been modified to x-ray absorptiometry. This uses a radiographic source as opposed to a radionuclide. The advantages of this are that the radioactive source does not need to be replaced and the waste eliminated. Additionally, extensive control measures required to compensate for isotope decay are not required. The limitations associated with SPA are also apparent when using single energy x-ray absorptiometry.[68] SPA has provided the experience necessary to adapt the DPA and DXA to non-invasive bone mineral analysis.

1.7.5 Dual photon absorptiometry

Dual photon absorptiometry (DPA) involves using 2 photon sources that emit at 2 discrete energies and can more accurately assess BMC when there is variable soft tissue covering.[57] The principle of DPA is that 2 different sources of radiation are attenuated by tissues in differing amounts. Entering the results of the attenuation through soft tissue and bone into a mathematical equation allows an attenuation profile of bone to be determined and eliminates the need for a constant soft tissue covering.[56] This technique is useful in the axial skeleton, as it is not surrounded by a constant soft tissue covering.[68] The most commonly used isotope is gadolinium, as it is a dual energy source.

DPA is superior for measurement of cortical BMC than for trabecular BMC.[57] Sources of precision and accuracy error are greater in DPA than SPA, and thus exactness is compromised, as demonstrated in both human and equine studies.[74]

Although DPA has bought about improvement in measurement of axial BMC disadvantages include an increased scanning time to 20-40 minutes, patient movement causing inaccuracy and decreased resolution. The patient is exposed to a greater amount of radiation. Source energy strength decreases as it passes through the patient, requiring complicated corrections to be made, making the procedure less accurate. The isotope is costly, difficult to obtain and restricted in its use.[49] Additional limitations are most evident in elderly and severely osteoporotic patients. Extraosseous calcification in arteries and degenerative deformities or fractures of the vertebrae can reduce the reproducibility and the accuracy of DPA.[49]

Dual x-ray absorptiometry (DXA), based on SXA was introduced commercially in the late 1980's. The source is an x-ray tube and 2 distinct energy levels are generated. The system is more versatile than SPA and superior to DPA, as it can carry out the functions of DPA at a lower operating cost, scanning time and total radiation dose.[49 68] Lack of radionuclide decay and a large difference between the energy levels emitted result in improved image resolution meaning that the accuracy and precision error are improved.[75 49] These additional advantages have made DXA the most widely used method to assess BMD in clinical and population medicine as well as the primary research tool for BMD assessment. Sources of error apparent to DXA are similar to those of DPA, and are related to calcification seen in the elderly patient.[49]

DPA or DXA have only been used in excised bones in the horse, as the time taken to scan is prohibitively long.[44 76]

1.7.6 Computed tomography

Computed tomography (CT) involves obtaining cross sectional images using narrow beam x-rays and computer processing of the images, integration and analysis. There is advanced soft tissue differentiation and no superimposition of overlying structures, as the third dimension is known which gives CT major benefits over conventional radiography and allows the quantification of tissue densities.[77]

There are a number of components that are involved in the development of an image; these are collection of data from the patient, computer processing of data, image display, and storage of data. The information is collected from the patient in the form of x-ray photons; the patient lies on a table and moves into a gantry. The gantry contains a x-ray tube, collimators and detectors. The x-ray tube emits a beam of photons, and may be stationary or rotating depending on the type of CT scanner. The operator determines the thickness of the slice by altering the collimators. The x-ray detectors convert the photons into an electronic signal of which the relative intensity reflects a number of photons emitted from the patient. Using a number of complex mathematical equations the computer converts the electrical signal into a gray scale, this can be achieved because the number of photons leaving the x-ray tube is known, and the number emerging from the patient is detected.[77]

The image is made up of many rows and columns of pixels; and each pixel represents a small piece of tissue. Each pixel is assigned a number that reflects the intensity of photons that emerged from the patient, known as Hounsfield units. Looking at a matrix of numbers is difficult to interpret, thus the numbers are assigned to a gray scale and an image formed.[77] Image storage is achieved using magnetic tape, or hard copies can be formed with radiographic film.

There are numerous applications of CT in the living animal, including a myriad of uses in the musculoskeletal system. Some of the more important applications in the musculoskeletal system are the assessment of trauma, infection, neoplasia, articular disease, vascular disease and metabolic bone disease. It has recently become a popular method of assessing BMD due to some advantages over other methods of assessment. Firstly, it can directly measure trabecular bone, which has a high turnover rate when compared to cortical bone and reflects rapid, subtle changes in BMD. Secondly, osseous architecture as well as BMD can be studied giving a better indication of bone strength. Finally, CT can exclude heterotrophic calcification such as vascular calcification or heterotrophic ossification e.g. degenerative joint disease. [49]

The disadvantages of this method are: exposure of the patient to the highest radiation dose, considerably longer scan time and although this technique is precise and accurate, reproducibility is a problem due to inaccuracies in positioning patients, leading to high accuracy errors.[49 78]

Given its apparent advantages over other methods of non-invasive BMD analysis, CT has been used in the assessment and prevention of osteoporosis. Site selection is not uniformly agreed on, however, the 2 most common areas are the spine and the appendicular skeleton.[78] Although information derived from one site does not necessarily relate to other sites, peripheral CT analysis appears to be becoming more popular as it offers short examination times, small precision error and a small radiation dose.[56] It appears that like other forms of analysis of BMD, analysis by CT can distinguish patients with osteoporosis but can not predict those patients who are likely to develop fractures, as BMD is only one quality associated with fracture risk.[78]

CT has been used in both small and large animals for a variety of disorders, however there is little work relating to the assessment of BMD. Markel [79] performed a study assessing the BMD of osteotomies of the tibia of the dog, with the view that CT may be useful for prediction of delayed and non-union of fractures.

1.7.8 Quantitative ultrasound

Quantitative ultrasound (QU) is used to assess the BMD via the measurement of the speed of sound through a bone of known diameter. The speed of sound may be influenced by bone mass, distribution of cortical and trabecular bone and architecture of the bone.[58] Absorption and reflection of the ultrasound beam are the factors that are important in attenuation, however, frequency is also important. QU uses low frequencies (200-600 kHz) to measure BMD, as the attenuation of the sound waves is almost linear. Numerous *in vitro* studies substantiate a high correlation between trabecular bone volume and ultrasound attenuation. [58] Other measurements that are performed are velocity, speed of sound and stiffness.[80]

QU provides information on bone quantity and quality.[80] Ultrasound beam attenuation is thought to depend on bone structure and relates to trabecular orientation and size. The more complex the structure, the more the ultrasound beam is attenuated or blocked. As beam attenuation is closely correlated with bone volume, osteoporotic bone has a lower attenuation than normal bone.[80] Velocity assesses the speed of sound from one surface to the other and the greater the complexity of the structure the greater the velocity, thus osteoporotic bone has a lower velocity.

There are relatively few studies assessing bone mass in women using QU, however they have been shown to predict fracture risk in both retrospective and prospective studies.[80] Advantages over other methods are no radiation and lower cost of equipment. As the relationship between bone mass, elastic properties of bone and ultrasound has been established but is uncertain, the influence of surrounding soft tissue, the path of the ultrasound waves and the effect of physical activity have not been adequately determined. QU is primarily a research tool. However it is expected to be used clinically in areas where more expensive forms of BMD analysis are not available and for pregnant women in the near future.[58,80]

Ultrasound velocity measurements have been used in combination with SPA in the horse in order to monitor the effects of treadmill exercise on the MCIII. This study found that ultrasound velocity altered with training, however there was no change in BMC or BMD when assessed by SPA.[81] This may be due to a change in the apparent architecture of the bone without a change in BMD.

1.7.9 Neutron activation analysis

Both neutron activation analysis and Compton scattering techniques are among the earlier methods of noninvasive BMD. They now have negligible clinical influence and their inclusion in this review is for completeness.

The basis of neutron activation analysis is to use neutrons to assail a small fraction of the total calcium contained in the body, producing a radioactive form of calcium which results in gamma photon emission that can be quantified with external detectors.[58] This technique estimates BMC as in the skeleton the calcium makes up a constant fraction of the mineralized tissue. Measurement sites can either be total body or selected areas. The total calcium measured primarily reflects cortical bone. Precision and accuracy error are higher than other methods of BMD analysis and errors can be caused by heterotrophic calcification such as vascular calcification or heterotrophic ossification e.g. degenerative joint disease.[58]

This technique could be applied to horse, but there is a requirement for immobilization for several minutes, which may be difficult to achieve, and as high doses of radiation are required human safety issues are raised.[76]

1.7.10 Compton scattering technique

The Compton scattering technique uses an x-ray source to irradiate a small amount of bone and interprets information from the scattered beam rather than the transmitted beam. This method measures the BMD in cortical or trabecular bone. Precision error is higher than other forms of analysis due to photon attenuation outside the region of interest and using high photon energies and an increased radiation dose counteracts this. [58]

The relative accuracy and inexpensive nature of the method may mean that it could be applicable to horses, however, immobilization is required for around 10 minutes and thus its use is likely to be limited.[76]

1.8 Summary

As BMD is a major determinant of fracture risk associated with osteoporosis there are numerous techniques that measure this parameter. Limitations of older techniques have been overcome however even the most recent methods have advantages and disadvantages and applications in animals are limited.

1.9 Research hypothesis and objectives

Slab fractures of C3 contribute to wastage within the equine industry. As sclerosis of this bone occurs prior to fracture and possibly prior to cartilage changes, an objective method of detection of sclerosis would be useful. RA is a form of quantitative non-invasive bone mineral analysis that may be clinically applicable to C3 in the horse. As RA requires C3 to be isolated from other superimposing structures the tangential view is the only radiographic view that may be used. A standardised procedure is followed when using RA in humans to ensure that changes in photodensity can be attributed to changes in BMD. There is no variation in x-ray beam angle, positioning of the bone or the angle at which the x-ray beam hits the x-ray plate. The procedure involved with achieving a tangential view of C3 is variable. It is difficult to accurately reproduce x-ray beam angle, position of C3 and the angle at which the x-ray hits the plate when taking this view. In order to determine if RA could used to assess BMD of C3 it must be established if variation in the angle that the x-ray beam penetrates C3 (C3-beam angle) significantly affects measured photodensity. On this premise the following null hypothesis was proposed:

Photodensity is not affected by small variations in C3-beam angle.

The objectives of this part of the study are to:

- Radiograph isolated C3's at an x-ray beam angle of 90° as is done in human RA studies and vary the angle in a proximopalmar- distodorsal direction in 5° increments and determine the photodensity of specific regions of interest (ROI's) in millimetres of aluminium.
- Radiograph isolated C3's at the x-ray beam angle suggested in the literature (60°) and vary the angle in proximodorsal- distopalmar direction in 5°increments and determine the photodensity of specific regions of interest (ROI's) in millimetres of aluminium.

During the above experiments the C3 beam angle is to vary over 30°, and the effect of ROI size on the mean photodensity is unknown. This led to the null hypothesis:

ROI size does not significantly affect mean photodensity over a 30° variation in x-ray beam angle (from 90° to 60°).

The objective for this part of the study is to increase and decrease the radius of the ROI by 0.5mm and determine the mean photodensity for each size of ROI at 5 different sites at an x-ray beam angle of 90° and 60°.

As discussed the tangential view can be achieved using 1 of 2 methods, which in this project have been labelled View A and View B. The final part of the project is to determine the inherent differences between View A and View B. This will be achieved by understanding the:

1. Differences in radiographic technique between the 2 views and therefore the differences in image formation.
2. Area of C3 examined by these views and the effect this has on the objective assessment of photodensity of C3.

MATERIALS AND METHODS

2.1 Definitions

- Radiograph - the exposed radiographic film.
- Image - the digitised radiograph.
- X-ray beam angle - the angle between the tube head and the horizontal axis. Horizontal is termed 0°, vertical is 90°. Vertical x-ray beam angle is the angle the tube head deviates in a vertical plane. Horizontal x-ray beam angle is the angle the tube head deviates in a horizontal plane.
- Plate-beam angle - the angle at which the x-ray beam strikes the "plate", i.e. the surface of the cassette containing radiographic film. Horizontal is termed 0°, vertical is 90°. Vertical plate-beam angle is the angle at which the x-ray beam strikes the plate in a vertical plane. Horizontal plate-beam angle is the angle the x-ray beam strikes the plate in a horizontal plane.
- C3-beam angle - the angle between the x-ray beam and a transverse plane through C3, parallel to the distal articular surface of C3.
- Leg angle - the angle between the dorsal surface of the radius and MCIII, full extension of the limb is 180°.
- Plate angle - the angle between the cassette surface and the dorsal surface of MCIII.
- View A - the tangential view of C3 with the cassette at 90° to the x-ray beam. The leg angle is 60°, the x-ray beam angle 30° and the plate angle is 60° (so the plate-beam angle is as close to 90 degrees as possible) (Figure 2.1).
- View B - the tangential view of C3 with the cassette parallel to, and placed against the dorsal surface of MCIII. The leg angle is 60°, the x-ray beam angle 30°, and the plate angle is 0° (Figure 2.2).

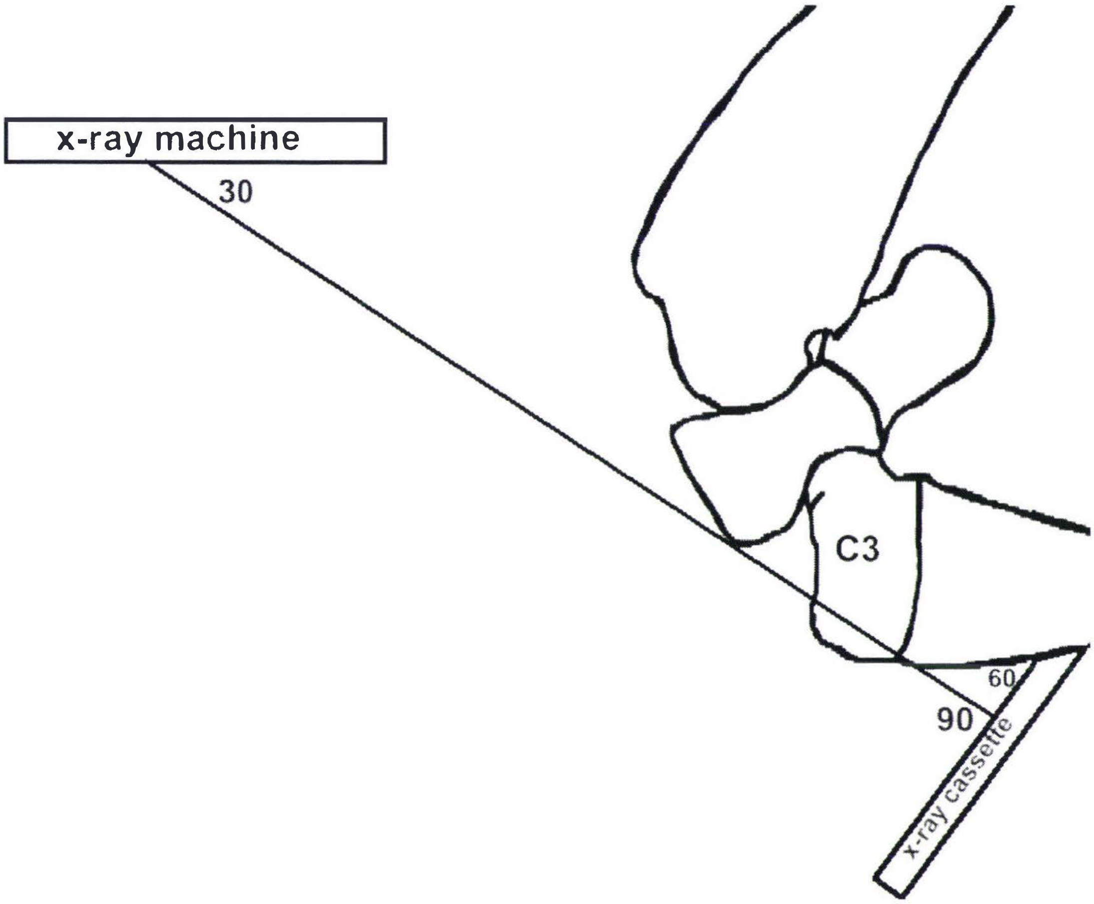

Figure 2.1: Line drawing of View A

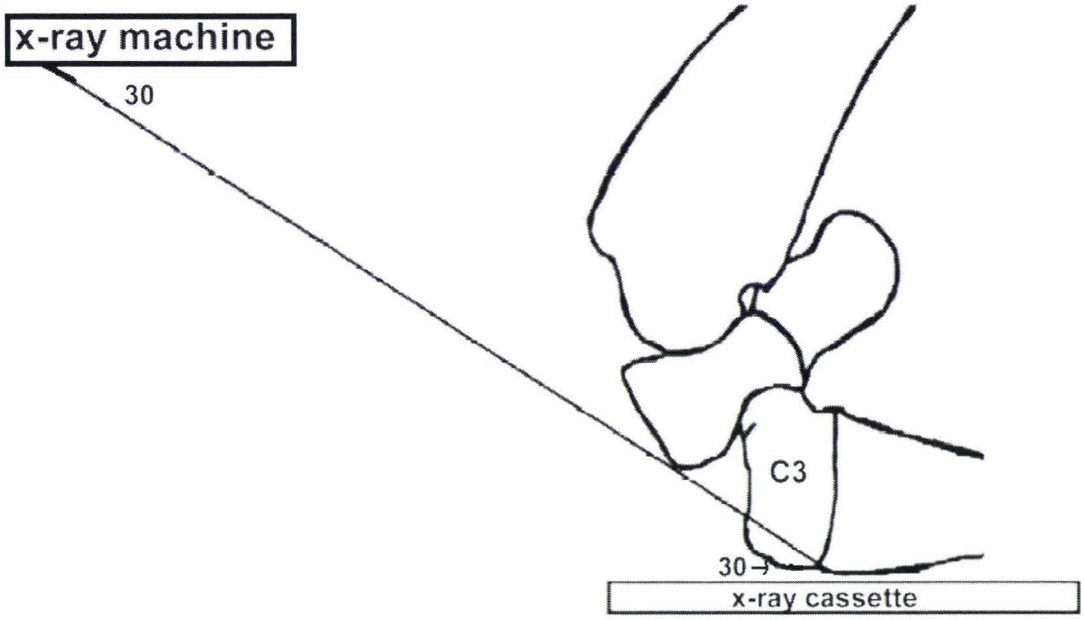

Figure 2.2: Line drawing of View B

2.2 Animals

Bones from fourteen 2-year-old female Thoroughbreds were used. The treatment group consisted of seven fillies broken in over a 6 week period, the control group (the other 7) were confined to pasture pens (25m x 8 m). The horses were fed lucerne chaff, oats, commercially formulated pelleted ration (sweet feed), and clover hay; the control (non-exercised) animals were fed 75% of the ration of the exercised horses. All horses were weighed weekly, and observed daily for any clinical abnormality. The 7 exercised horses were boxed overnight and in small pens during the day. They followed a standard commercial training regimen under the direction of a licensed professional trainer. The exercise regimen consisted of 4 weeks slow cantering, 4 weeks fast cantering, followed by 4 weeks fast cantering with fast gallops superimposed twice weekly. Horses in the exercised group were ready to trial or race at the conclusion of the training period. These horses were euthanased for other purposes, and the left carpal bones were available.

2.3 Disarticulation of the distal row of carpal bones

The left distal carpal row was isolated by sectioning the collateral ligaments, intercarpal ligaments, palmar carpal fascia and carpometacarpal ligaments. Once disarticulated as much soft tissue as possible was removed, and the distal row was immersed in 98% alcohol.

2.4 Determination of the extent of variation in x-ray beam angle required before C3 becomes obscured in the tangential views.

Clinically, within both View A and B small changes in x-ray beam angle appeared to result in variation of the amount of dorsal C3 visualised. In both tangential views the x-ray beam angle travels in a palmaroproximal to dorsodistal direction as shown in figure 2.1. To determine how much to vary the x-ray beam angle in the main study a pilot study was performed. The goal was to ascertain the variation in angle required before C3 was completely obscured. This was determined by radiographing 2 legs disarticulated at the radiohumeral joint and frozen at a leg angle of 60°; the x-ray beam angle was varied in 5° increments from the x-ray beam angle suggested in the literature.[82] In either tangential view, the x-ray beam angle can be varied by up to 15° before the dorsal aspect of C3 becomes completely concealed by either distal radius or proximal MCIII.

2.5 Film type

The film type used was medical grade HR G-30 film (Fugi Photo Film Company Limited, 26-30 Nishiazabu 2-chome, Minato-ku, Tokyo 106, Japan.)

2.6 Digitising the radiographs

The radiographs were scanned using an AGFA DUOSCAN (Agfa-Gevaert N.V. Septestraat 27, B-2640 Mortsel) desktop, flatbed scanner that has a built in scanning bed for transparencies. Transparencies were scanned directly, there was no intervening glass plate between the lens and the film, preventing diffraction and distortion. AGFA FOTOLOOK (Agfa-Gevaert N.V. Septestraat 27, B-2640 Mortsel) was the software scanning interface. The glass slide that holds the radiograph was cleaned prior to each set of 14 radiographs being scanned. The radiographs were scanned using the transmission option, grey scale, at 250 lines per inch and 20%, which reduced the image to 20% of the original radiograph size. The images were then labelled and saved in a bitmap format to a hard drive. Figure 2.3 shows an example image of one bone taken at an x-ray beam angle of 90°.

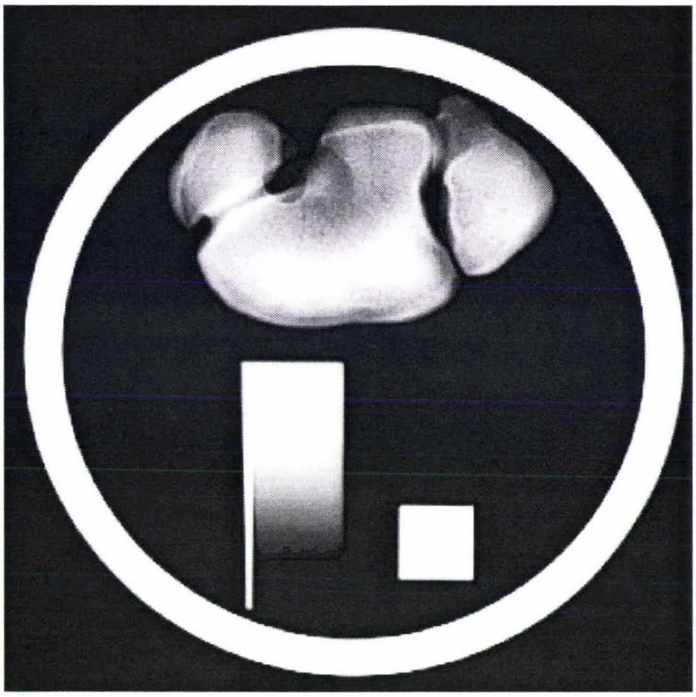

Figure 2.3: Image of isolated distal row taken at 90 degrees.

2.7 Determining photodensity of the distal row when the x-ray beam angle is varied from 90°

2.7.1 Radiographing the distal row

A Picker-Explorer mobile machine was used to expose film in cassettes with medium intensifying screens, which were cleaned prior to taking radiographs. A template was designed so that the metal cube, wedge, circle (used for calibration- see below) and distal row of carpal bones would be in a similar position for every radiograph. The thickest part of the wedge was placed closest to the dorsal edge of C3. The template was the same size as the plate used (18cm x 24cm) and the beam was collimated to the edge of the template and centred between the wedge and the dorsal aspect of the distal row. (Figure 2.4)

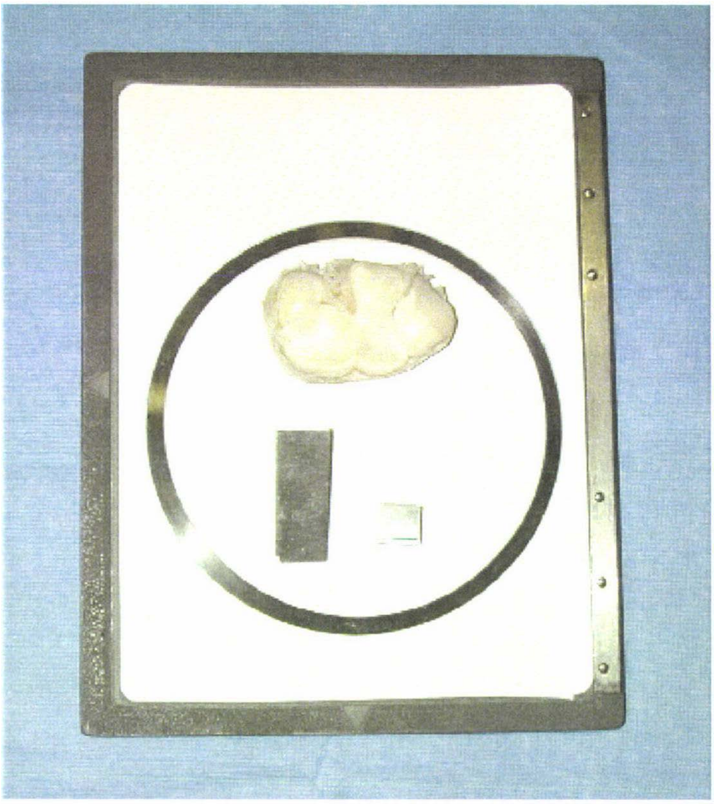

Figure 2.4: The distal row of carpal bones, together with circle, cube and wedge on a radiographic cassette, ready for exposure.

The distal row of carpal bones was removed from alcohol, washed with tap water for 2-3 minutes, towel dried and then placed on the template. On the basis of the findings in section 2.4, the isolated carpal bones were placed on a cassette and radiographed at 90°(control). Further radiographs were taken at 5° increments to a total of 15° from 90°, thus with the x-ray beam travelling in a palmaroproximal to dorsodistal direction the x-ray beam angles were 85°, 80° and 75°. The x-ray head was set for the angle required and a radiograph taken using 45kV and 6.3MAS. The radiograph was processed using an automatic processor (Kodak RP X-Omat Processor, Model M6B). The first radiograph taken was immediately digitally captured and calibrated to determine the exact plate beam angle, which is the same as the x-ray beam angle because the distal row was lying horizontally on the cassette (Figure 2.5). This process was repeated until the x-ray beam angle was as close to the predetermined angles as possible. Once the x-ray head was set to the correct angle, all 14 C3's were radiographed and immediately scanned and digitised to prevent accumulation of particles on the film that may result in subsequent artefactual problems.

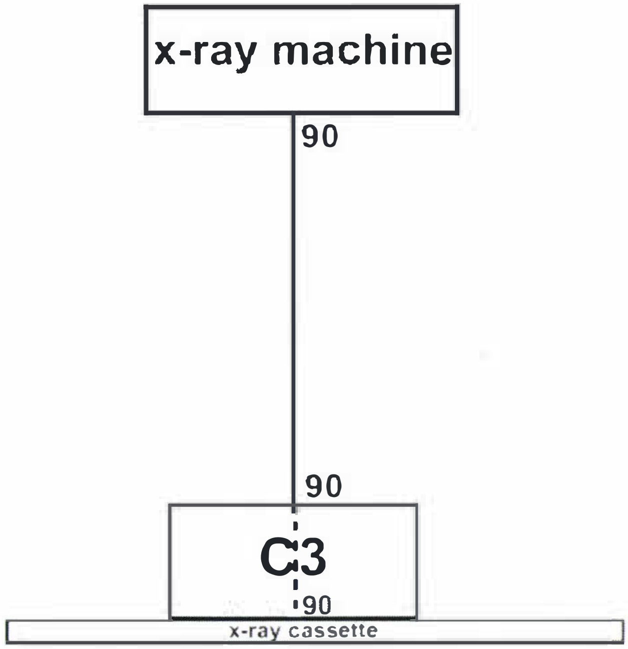

Figure 2.5: Line drawing demonstrating that if the distal row of carpal bones is lying horizontal on the cassette the x-ray beam angle is equal to both the C3-beam angle and the plate-beam angle.

2.7.2 Image analysis

All image analyses were performed using the Vision Image Processing System (VIPS).[83] Two macro programs were specifically written for this project, to define the analytical steps performed inside the VIPS program: the calibration program and the region of interest program.

2.7.2.1 Calibration program

The role of this program was to calibrate the image, to determine the plate-beam angle and allow the photodensity of C3 to be measured in units of millimetres of aluminium. There are three essential components in each image for the program to function: namely the circle, the cube and the wedge.

A stainless steel circle with a 130mm external diameter was made. The outer edge was bevelled in order to provide a sharp edge on the radiograph and digitised image, regardless of beam angle. The aim of the circle was to calibrate the size (in mm) of each pixel and determine the aspect ratio, which gives a ratio between the height and the width of each pixel, thereby allowing accurate reproduction of the radiograph in the form of a digitised image. The calibration was completed using a circle-based measurement, identifying the horizontal and vertical diameter of the circle, and using the known diameter of the circle to calculate the aspect ratio. The circle was as large as possible, to allow more accurate calibration, by reducing the relative error inherent in the measuring process.[84]

A 15 mm x 15 mm stainless steel cube was used to determine the angle at which the radiograph was taken. This was achieved by knowing the dimensions of the cube in an image where the plate-beam angle was 90° (perpendicular to the plate). The cube's image on the radiograph when the plate-beam angle varies allowed subsequent determination of 90°- x°. Both the vertical and horizontal beam plate angles were determined from the cube using the following equation (Figure 2.6).

$$\theta = \tan^{-1} x \left(\frac{C}{L - C} \right)$$

C = actual cube length, width and height.

L = image cube length.

θ = x-ray beam angle, vertical or horizontal.

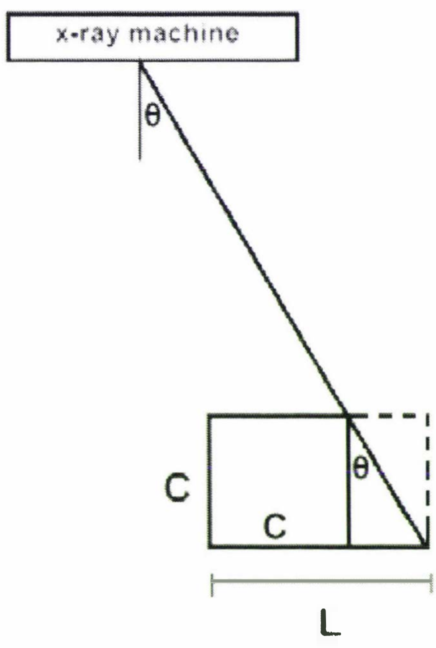

Figure 2.6: Line drawing of determination of θ.

The x-ray beam angle and C3 beam angle could be determined once the beam plate angle was determined, as the distal carpal row was laying horizontal on the plate (Figure 2.5). The dimensions of the cube allowed a change in angle of 2° to be detected.

The smooth surface (i.e. non-graduated) wedge was aluminium, and measured 23.7 mm x 48.5 mm x 20 mm (height x length x width). Its purpose was to provide a scale of densities for comparison with the photodensity of each region of interest (ROI) within C3 and C4. Aluminium was chosen because its atomic number, specific gravity and attenuation coefficient is similar to that of bone mineral. Within an excised bone radiographed in air the specific mixture of mineral, bone matrix and fat is unknown, thus the bone mass determinations made with the wedge are only approximate. The required height of the wedge was determined by radiographing several different aluminium wedges with C3's and subjectively deciding the height that encompassed the range of photodensities likely to be encountered. As aluminium has a similar specific gravity and atomic number to bone, the maximum height of the wedge was very similar to the thickness of C3.

By knowing the plate angle and the distance from one end of the wedge (detectable by the presence of a piece of stainless steel along the length of the wedge) to the density of interest, the average photodensity of each ROI could be calibrated to millimetres of aluminium. This was achieved by determining the thickest part of the wedge at the plate-beam angle according to the following equation

$$T = \frac{(H \times L) \div \sin \theta_h}{(L \times \sin \theta_v) - (H \times \cos\theta_v)}$$

T = maximum thickness of wedge at the specified x-ray beam angle.

H = actual height of the wedge.

L = actual length of the wedge.

θ_h = horizontal angle.

θ_v = vertical angle.

Once the thickness was determined the relative photodensity in terms of millimetres of aluminium of the wedge could be determined. The height of each pixel is ascertained by the following equation:

$$\text{Pixel height} = \frac{\text{aspect ratio x pixel width}}{\text{Cos}\,\theta\text{w}}$$

θ_w = angle of the wedge in the image from vertical.

The photodensity of each pixel is determined by the following equation:

$$\text{Pixel thickness (PT)} = \frac{\text{pixel height x T}}{\text{L}}$$

Thus at the thin end of the wedge the first pixel is Xmm of aluminium, the second pixel from the thin end is (X x 2)mm, the third is (X x 3)mm and so on until the thickest part of the wedge is reached. An intensity curve is then matched to the thickness curve and the photodensity for a particular point on the wedge can be established. This process allows the wedge to be corrected for changes in plate-beam angle, thereby acting as a standard regardless of angle changes. The wedge linearly increased in photodensity until a certain height, where a plateau was reached. In order to accurately assess photodensity in terms of mm of aluminium the photodensity of the ROI must be within the linear range of the wedge (Figure 2.7).

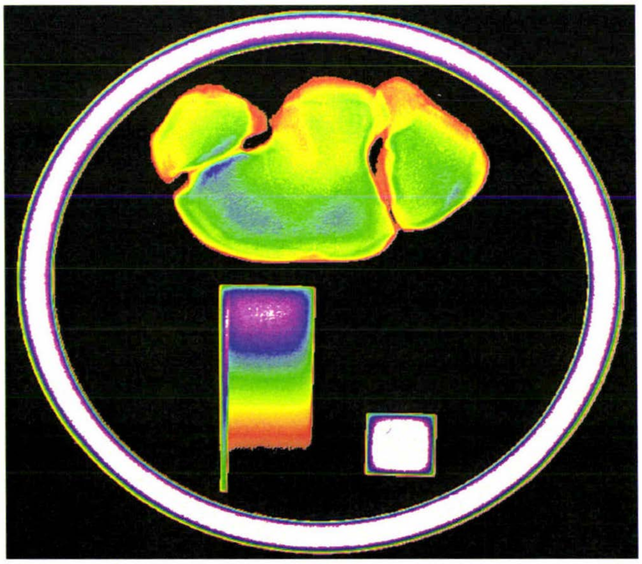

Figure 2.7: A calibrated image taken at 90°.

2.7.2.2 Region of interest program

The ROI program was used to determine the site of 5 ROI's, 4 within C3 and 1 within C4. The ROI's were circles (so orientation is not important), with a radius of 3mm and thus an area of 28mm^2. Radiographs were taken of 5 bones where a 6mm x 6mm marker was placed 2mm from the dorsoproximal edge of the C3. The most dorsal aspect of C3 is at the dorsocentral aspect of the bone, not the dorsoproximal aspect. Therefore in the 90° image the marker appears to be 6mm from the most dorsal edge of the C3, at 85° it is 5.3mm from the dorsal edge, at 80° it is 4.7mm from the dorsal edge and at 75° it appears to be 4mm from the most dorsal edge of the C3. The ROI's move dorsally as the angle reduces, the degree of displacement is dependant on vertical plate-beam angle, and development of the required equation was based on the findings from marker placement as described above.

A consistent width of C3 was difficult to determine as corners are smooth rather than sharp, thus 9mm was removed from all borders of the digitised image of the distal row of carpal bones, resulting in sharp points at which to delineate the line across the widest aspect of the C3. ROI's 1 and 4 were determined from these points, the distance from each point depended on the x-ray-beam angle (at 90° the centre of the ROI's was at 6mm from the dorsal edge). Once ROI's 1 and 4 were determined a line was drawn between them and ROI 2 and 3 were evenly spaced between 1 and 4. The exact position of ROI's 2 and 3 was determined based on the same relationship as ROI 1 and 4, and was also dependent on x-ray beam angle. ROI's 2 and 3 were adjusted slightly to place them at the required distance from the dorsal aspect of the bone, as the dorsal aspect of C3 is not a straight line. ROI 1 was placed on the abaxial aspect of the radial facet, ROI 2 was placed on the axial aspect of the radial facet. ROI 3 was placed on the axial aspect of the intermediate facet and ROI 4 on the abaxial aspect. ROI 5 was placed in the C4. The centre of ROI 5 was determined by extending the line drawn between ROI's 1 and 4 and was dependent on the width of C4 (Figure 2.8).

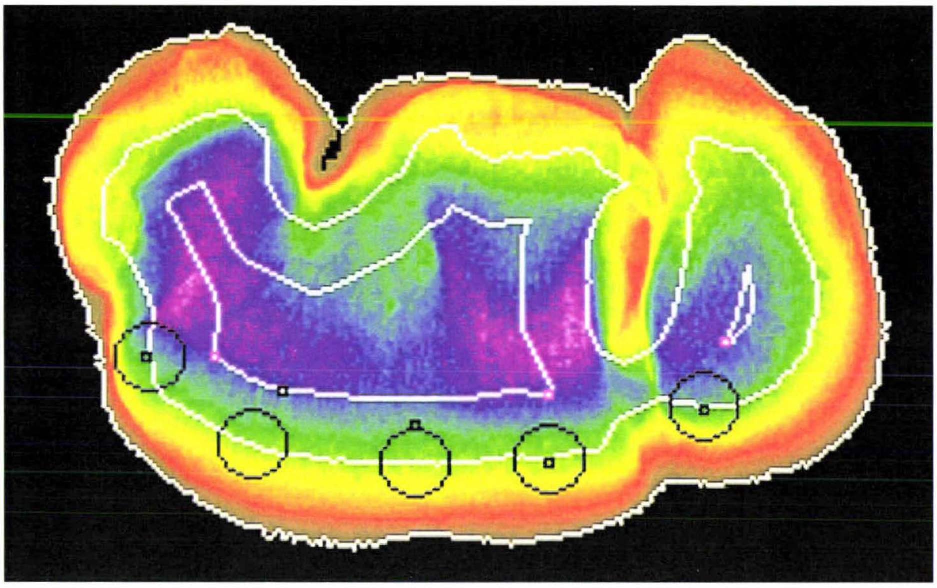

Figure 2.8: Image of isolated distal row of carpal bones with lines determining the position of the ROI's. The inner line is achieved by removing 9mm from outer edge of the distal row. The outer line is dependent of the vertical x-ray beam angle the radiograph was taken at, in this case 60°. The squares within the image are the points that are used to determine the position of the ROI's as described in 2.7.2.2.

Once the ROI program was developed all images were processed with ROI placement in a dorsal position. The dorsal position meant that at a 90° x-ray beam angle the centre of each ROI was 6mm from the dorsal edge. The images were also processed in a more palmar position, which involved the ROI's at 90° being placed 9mm from the dorsal edge. At both dorsal and palmar ROI placements, when the x-ray beam angle was reduced the ROI's moved dorsally as described above (Figure 2.9 and 2.10).

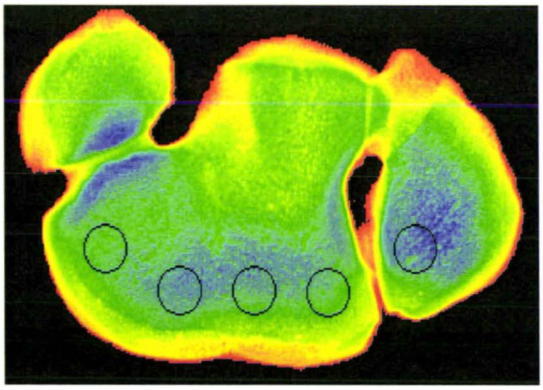

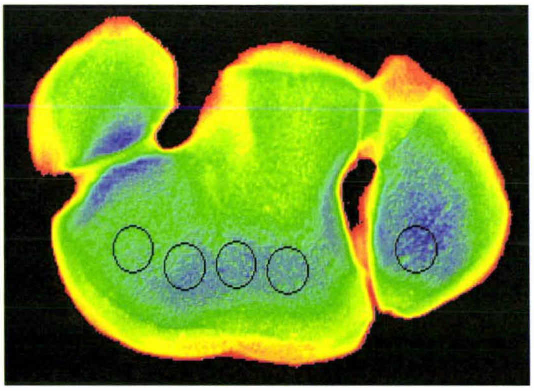

Figure 2.9: ROI's placed in a dorsal position. Figure 2.10: ROI's placed in a palmar postion.

2.8 Determining photodensity of the distal row of carpal bones when x-ray beam angle is varied from 60°.

2.8.1 Radiographing the distal row

The distal row of carpal bones was radiographed in the same manner as per 3.1 with the exception being the x-ray tube was set for the angles 70°, 65° or 60° and radiographs were taken at 44kV and 6.3MAS. Radiographs taken at 75° in section 7 were also included.

2.8.2 Image analysis

2.8.2.1. Calibration program

The calibration program was the same as used in 3.2.1. with the exception that for the radiographs at 60°, 65° and 70° the calibration circle was modified to 160mm in diameter which prevented superimposition of the distal row of carpal bones on the circle when the angle was reduced.

2.8.2.2 Region of interest program

The region of interest program from 7.2.2 was used. The ROI positions were located in both dorsal and palmar positions as in 7.2.2.

2.9 Changing ROI size

2.9.1 ROI program

The region of interest program from 7.2.2 was used and the calibrated digitised images of 90° and 60° were processed. The program was then manually modified to alter the radii sizes to 2.5mm and 3.5mm. The ROI's were placed in the palmar position as for 7.2.2. (Figure's 2.11 and 2.12).

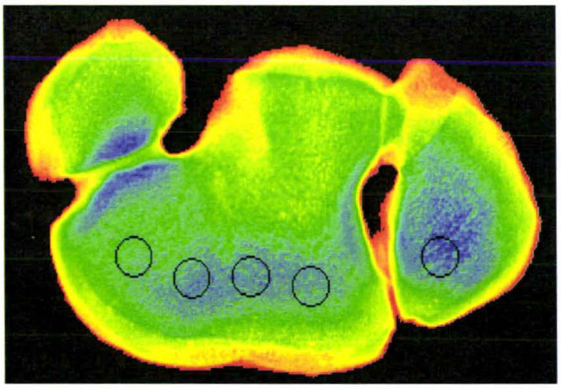

Figure 2.11: ROI's with a radius of 2.5mm.

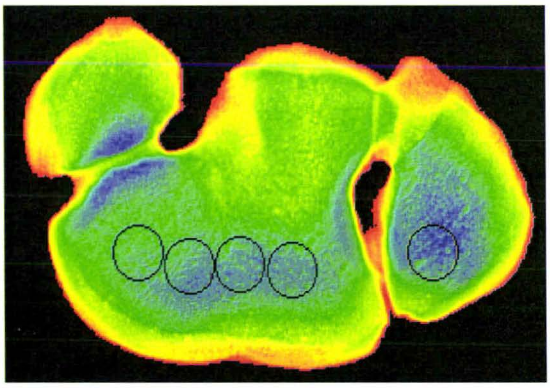

Figure 2.12: ROI's with a radius of 3.5mm.

2.10 Determination of the inherent differences between View A and B

2.10.1 Leg angle

Leg angle was difficult to establish as a result of cranial soft tissue coverage of the radius. To determine if leg angle could be accurately estimated by a goniometer, 3 legs were disarticulated at the radiohumeral joint and frozen at angles, 55°, 45°, 37.5° and leg 4 was chilled so the angle could be varied. The frozen legs were radiographed in a lateral to medial direction with a focal distance of 140cm and exposure of 68kV and 5MAS. Cassettes (24cm x 30cm) with medium intensifying screens were used, and MCIII was placed parallel to the edge of the cassette. The x-ray beam was collimated and centred on the palmar aspect of the flexed carpus, and the radiograph checked to ensure the cranial surface of the radius formed a straight line, if not the radiograph was taken again. Measurements determined from the image were, bone-MCIII angle (the angle between the cranial aspect of the radius and MCIII), skin-MCIII angle (the angle between the cranial surface of the forearm [above the carpus] and MCIII) and C3 beam angle (the angle allowing maximum visualisation of C3) (Figure 2.13)

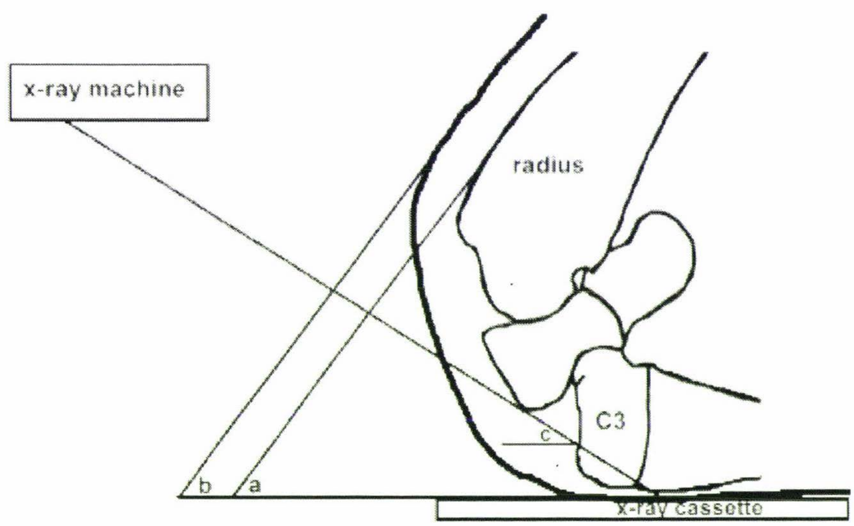

Figure 2.13: Line drawing illustrating bone-MCIII angle(a), skin-MCIII angle(b) and C3 beam angle(c)

From the measurements taken it was determined that limb flexion angle measurement with the goniometer, was the same as the skin-MCIII angle estimated from the radiographs, but less than the bone-MCIII angle. Therefore it appears that flexing the limb with the aid of a goniometer is a relatively accurate method of determining leg angle.

2.10.2 Plate angle

Plate angle is significantly different between View A and B. The cassette is placed parallel (0°) to MCIII with the centre at the level of C3 in View B and as a result plate-beam angle is 30° from horizontal (Figure 2.2). In View A, the cassette is placed in the middle third of MCIII at an angle of 60°, the plate-beam angle is approximately 90° (Figure 2.1). The plate angle difference between View A and B results in radiographic image disparities.

2.10.3 X-ray beam angle

X-ray beam angle should be about 30° to maximise the amount of C3 seen in both tangential views, the exact angle is dependent on leg angle. When the forelimb is flexed the distal row of carpal bones is almost perpendicular to horizontal. Thus the C3-beam angle in both tangential views is 60° when the x-ray beam angle is 30° (Figure 2.1 and 2.2).

2.10.4 Modifying images A and B to form hypothetical image C

Images of View A and B appear different, but to identify the same ROI the images must appear similar. Images of View A and B were manipulated using VIPS to form hypothetical View C (Figure 2.14). Leg angle, x-ray beam angle and C3 beam angle remain unchanged in View C, however the plate angle was 60° and the plate position was at the level of the distal row of carpal bones. To accomplish this, magnification of View A, distortion of View B and difference in x-ray beam intensity were accounted for.

The image of View A was modified to form View C by multiplying the length-based dimensions, by the following equation:

$$\frac{X}{(X+A)}$$

X= the distance from the point source to C3

X+A = the total focal distance

The inherent behaviour of the x-ray beam meant a different intensity of x-rays reached the plate in View A compared to View C, which alters photodensity of the image. In View C the photodensity of each pixel will be greater than in View A. Therefore, pixel thickness (photodensity) in View A, was divided by the following equation to form pixel thickness in View C:

$$\frac{X^2}{(X+A)^2}$$

View B was modified to View C by correcting for the distortion that occurs in View B by a multiplying the vertical dimension by:

$$\sin \theta_v$$

In View B the area over which the x-ray beam was distributed was increased, thus decreasing x-ray beam intensity and pixel thickness (photodensity) when compared to View C. Therefore, pixel thickness (photodensity) in View B, was divided by the following equation to form pixel thickness in View C:

$$\sin \theta_v$$

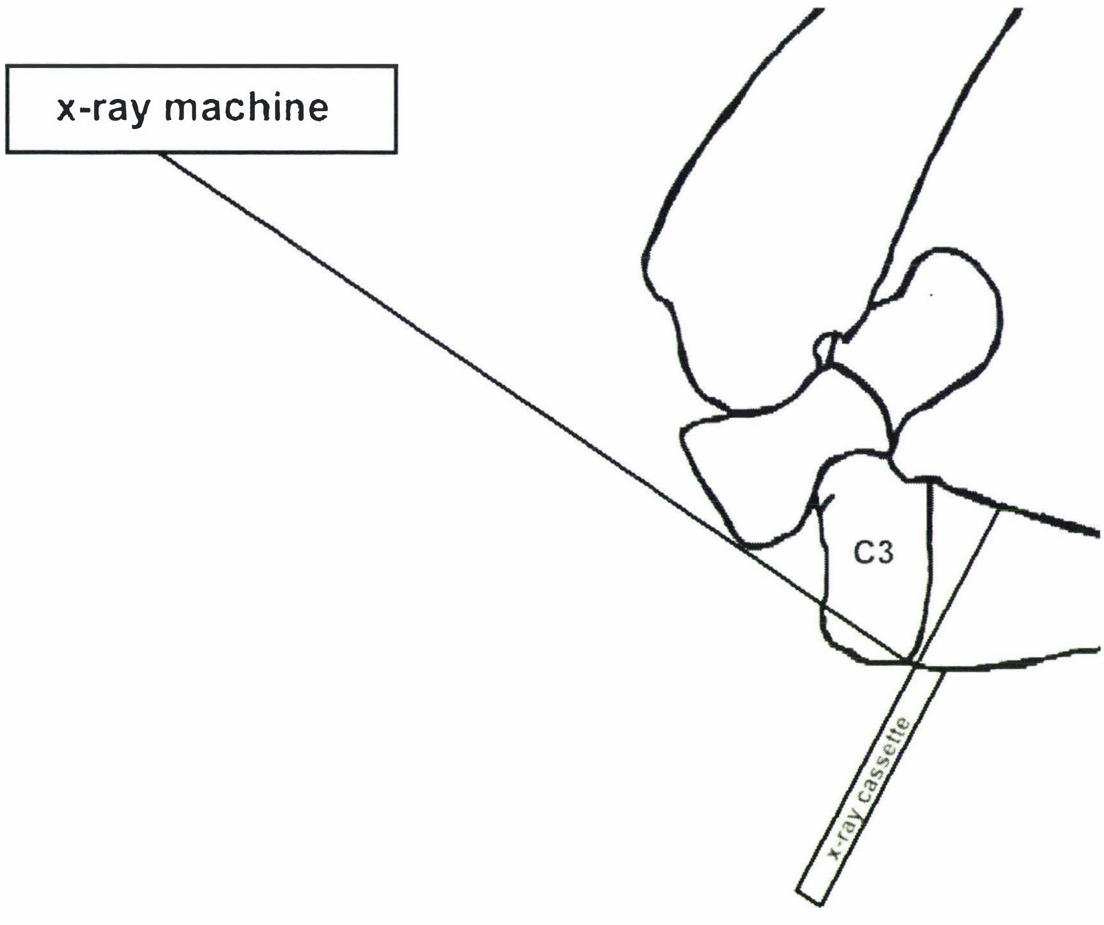

Figure 2.14: Line drawing illustrating hypothetical View C.

2.10.5 Image analysis

2.10.5.1 Calibration

The images were then calibrated using the program as in 3.2.1. The circle was of the same design, however the external diameter was 160mm. The cube was unchanged and the wedge increased in height to cover the range of photodensities required. In View A the cube, wedge and circle were placed as in 3.1. In View B the wedge was placed in the opposite direction, because although C3 is radiographed in a palmaroproximal to dorsodistal direction, the x-ray beam strikes the rest of the plate from a dorsoproximal to palmarodistal direction.

2.10.5.2 Determining the region of interest in image C

The ROI program was used to determine 4 ROI's within C3 and 1 within C4. The ROI's were circles with a radius of 1mm, and thus an area of $3.14mm^2$. The most lateral and medial point of C3 was located by the program, and a line drawn between them. The line was divided by 5 and the outer margins of the divisions became the centre of each ROI. The ROI in C4 was placed 2/5 of the distance from the most axial edge. Once the position was determined the actual ROI's were placed 4mm from the dorsal edge of C3.

2. 11 Statistical analysis

All analyses were performed on the images obtained for each distal row of excised carpal bones (14). The effect of variation of angle and exercise on photodensity as well as ROI size and placement were analysed using analysis of variance (ANOVA) using type III sums of squares. All analyses were performed with SPSS (version 9.0 for Windows).

Three separate analyses were conducted:

1. Analysis of the data generated from the dorsal placement of the ROI's at 60°, 65°, 70°, 75°, 80° and 90°.
2. Analysis of the data generated from the palmar placement of the ROI's at 60°, 65°, 70°, 75°, 80° and 90°.
3. Analysis of the data generated from the palmar placement of ROI's of radius size 2.5mm, 3mm and 3.5mm at 90° and 60°.

Variables in the data sets included horse, ROI (1,2,3,4,5), angle, group (exercised and control) and ROI diameter. Horse was coded as a random effect and nested within group for the purpose of analysis. All other variables were coded as fixed effects. Bonferoni adjusted t-tests were used to follow up significant effects from the ANOVA and α was set at 0.05.

2.11.1 Dorsal analysis

The main effect of ROI, angle and group was determined and pairwise comparisons were performed on both ROI and angle to establish difference between individual means. As there were only 2 treatment groups no follow up analysis was performed on group. Pairwise comparisons were also performed between:

- Angle at each ROI
- Angle at each group
- ROI at each angle
- ROI at each group
- Group at each angle
- Group at each ROI

2.11.2 Palmar analysis

The main effect of ROI, angle and group was determined and pairwise comparisons were performed on both ROI and angle to establish difference between individual means. As there were only 2 treatment groups no follow up analysis was performed on group. Pairwise comparisons were performed between:

- Angle at each ROI
- Angle at each group
- ROI at each angle
- ROI at each group
- Group at each angle
- Group at each ROI

2.11.3 Region of interest size analysis

The main effect of diameter was determined, and pairwise comparisons between angle at a constant diameter size as well as between different diameter sizes at either 60° or 90° were performed.

THE RELIABILITY OF THE QUANTITATIVE MEASUREMENT OF PHOTODENSITY IN ISOLATED DISTAL ROWS OF CARPAL BONES

3.1 Introduction

Radioabsorptiometry (RA) is a sensitive non-invasive quantitative method to assess bone mineral density.[63] This technique has had a resurgence in recent years and been extensively used in humans, resulting in a number of precision and accuracy studies.[62,63] Radioabsorptiometry in its more primitive form has been applied to the horse and the dog with little success.[65,66] There are no known studies of the radioabsorptiometry technique in horses assessing reliability, that is the repeatability or reproducibility of the technique. The purpose of this chapter is to assess the reliability of RA when applied to C3.

3.2 Materials and Methods

To test reliability of this technique 2 investigations were performed. Three statistical methods were used to determine reliability; these were coefficient of variation, coefficient of variation (within) and intra-class correlation coefficient.

3.2.1 Study 1

A single radiograph was taken of an isolated distal row of carpal bones, circle, cube and wedge as described in 2.7.1 and the radiograph was scanned 10 times using the AGFA DUO Scanner as described in 2.6. This resulted in 10 images of the same radiograph that were calibrated as per 2.7.2.1 and had regions of interest (ROI) identified as in 2.7.2.2. The data obtained were the horizontal and vertical plate-beam angle (defined in materials and methods) and 5 ROI's measured in mm of aluminium.

The data were entered into SPSS (version 9.0 for Windows) and separate analyses were performed on the ROI data. Mean estimates of photodensity (expressed as millimetres of aluminium), standard deviation and coefficient of variation were estimated on the ROI data. A one way analysis of variance (ANOVA) was performed using ROI as the between subjects factor. The pooled standard deviation was calculated from the ANOVA table and the within subject coefficient of variation was determined for each ROI. The intra-class correlation coefficient (ICC), an alternative method of measuring reliability, was estimated. A one way, random effects ANOVA was used to estimate between and within ROI mean square terms and ICC calculated for absolute agreement.[85]

The horizontal and vertical x-ray beam angle (see definitions in chapter 2) data were entered into SPSS (version 9.0 for Windows) and similar reliability analyses were performed.

3.2.2 Study 2

In order to determine the repeatability over different radiographs using the same bone at the same angle (bone/angle), 6 bones were radiographed 4 times at exactly the same bone/angle combination, using 4 different exposures as described in 2.7.1. The radiographs were digitised, and specific ROI's identified as in study 1.

The data were organised by ROI for analysis. Mean estimates of photodensity (expressed as millimetres of aluminium), standard deviation and coefficient of variation were calculated for each bone/angle combination within each ROI. A 2-way random effects ANOVA was performed on each level of ROI, and was used to generate within bone/angle coefficients of variation.

A 2-way random effects ANOVA was performed with random factors being bone/angle combination and radiograph. This was used to produce an estimate of the intra-class correlation coefficient for model ICC (2,1) as defined by Shrout and Fleiss.[86]

Estimates of the vertical angle of the x-ray beam were made at different bone/angle combinations in 24 radiographs. In a similar manner estimates of the horizontal angle were made in 12 radiographs. The data were used to assess reliability of angle determination by the VIPS macro. Estimations of the mean angle, standard deviation and coefficient of variation were made for each bone/angle combination. A 2-way random effects ANOVA was used to generate a single estimate of pooled standard deviation for the vertical and horizontal data respectively. These were used to estimate within bone/angle coefficient of variation. A 2-way random effects ANOVA was also used to generate intra-class correlation coefficient estimates for the data using the model ICC (2,1) following the notation of Shrout and Fleiss.[86]

3.3 Results

3.3.1 Study 1

A total of 50 measurements from 10 images of the same radiographs were used in the ROI data analysis. The mean, standard error and the coefficient of variation is presented in table 3.1.

Table 3.1: Results of raw data and descriptive statistics for ROI after digitisation of a radiograph 10 times.

Replicate	ROI 1	ROI 2	ROI 3	ROI 4	ROI 5
1	165.28	135.34	129.54	128.62	124.10
2	162.72	134.49	128.27	127.53	124.93
3	162.49	134.08	127.78	126.60	123.74
4	160.64	134.14	126.30	126.15	124.29
5	162.87	134.49	129.77	128.04	124.86
6	161.04	134.10	127.80	126.80	123.62
7	162.35	136.40	128.56	128.60	125.03
8	163.61	134.78	128.22	128.50	124.70
9	162.33	135.68	127.65	128.29	124.44
10	163.73	135.48	129.05	128.31	125.74
Mean	162.11	134.90	128.26	127.75	124.55
Standard Deviation	1.33	0.79	1.04	0.91	0.64
Coefficient of variation	0.82%	0.58%	0.81%	0.72%	0.51%

Table 3.2: Results of one-way ANOVA for ROI after digitisation of a radiograph 10 times

	Sum of Squares	**Degrees of freedom**	**Mean square**	**F value**	**Significance**
Between ROI's	9729.39	4	2432.348	2584.76	0.000
Within ROI's	42.35	45	0941		
Total	9771.74	49			

The standard deviation of the overall population is calculated to be 0.97. The coefficient of variation (within) is presented in table 3.3.

Table 3.3: The coefficient of variation (within) for each ROI after digitisation of a radiograph 10 times.

ROI	Mean	Standard deviation (population)	Coefficient of variation (within)
1	162.7072	0.97	0.60%
2	134.8995	0.97	0.72%
3	128.2635	0.97	0.76%
4	127.7457	0.97	0.76%
5	124.5471	0.97	0.78%

The CV is consistently less than 1%, indicating that the amount of variation is very small relative to the value of the mean.

The ICC was 0.9961 (95% CI 0.9882, 0.9995), indicating that 99.61% of variation in mean photodensity was due to variation between ROI's and not from differences between the replications.

The statistical processes described above were performed on the angle data of the 10 images and are presented in tables 3.4, 3.5 and 3.6.

Table 3.4: Results of raw data and descriptive statistics for variation of horizontal and vertical angle after digitisation of a radiograph 10 times.

Replicate	Horizontal angle	Vertical angle
1	90.30	89.77
2	90.30	89.91
3	90.26	89.54
4	90.76	90.47
5	90.78	89.50
6	90.30	89.75
7	90.35	89.70
8	90.33	89.72
9	90.31	89.56
10	90.27	89.78
Mean	90.40	89.77
Standard Deviation	0.20	0.28
Coefficient of variation	0.22%	0.31%

Table 3.5: Results of one-way ANOVA for angle after digitisation of radiograph 10 times.

	Sum of Squares	Degrees of freedom	Mean square	F value	Significance
Between angles	1.97	1	1.967	34.221	0.00
Within angles	1.03	18	5.74×10^{-2}		
total	3.00	19			

From this analysis the standard deviation of the overall population is calculated to be 0.24. The coefficient of variation (within) is presented in table 6.

Table 3.6: The coefficient of variation (within) for both horizontal and vertical angle after digitisation of a radiograph 10 times.

Angle	Mean	Standard deviation (population)	Coefficient of variation within
Horizontal	90.40	0.24	0.26%
vertical	89.77	0.24	0.27%

These results indicate that, for the vertical and horizontal angle as the CV is less than 0.3%, the amount of variation is very small relative to the mean. The ICC was 0.7686 (95% CI 0.321 to 0.9997). This means that 76.9% of the total variation is due to differences between the 2 angle methods and 23.1% of the variance is due to the differences between replications.

3.3.2 Study 2

A total of 120 ROI measurements were made from 24 images of 6 bones taken at varying bone/angle combinations. The following table shows values organised by regions of interest. The mean is the average photodensity of ROI values from 4 images for each bone/angle combination. Standard deviation, coefficient of variation, pooled standard deviation and within coefficient of variation are presented in table 3.7.

Table 3.7: Descriptive statistics of varying bone/angle combinations including coefficient of variation and coefficient of variation (within).

Angle	Bone	ROI	X-ray 1	X-ray 2	X-ray 3	X-ray 4	Mean	SD	CV %	CV (within) %	SD (pooled)
90	1	1	156.6	161.4	162	161.6	160.4	2.55	1.59	1.19	1.912
90	2	1	159.1	157.5	156.1	159.6	158.1	1.59	1.01	1.21	1.912
90	3	1	87.8	89.3	87.5	90.7	88.8	1.48	1.67	2.15	1.912
85	4	1	163.3	162.8	161.8	163.4	162.8	0.73	0.45	1.17	1.912
85	5	1	154.6	155.5	154.0	156.9	155.2	1.26	0.81	1.23	1.912
80	6	1	154.3	148.1	148.8	152.3	150.9	2.93	1.94	1.27	1.912
90	1	2	130.9	130.5	130.7	132	131.0	0.67	0.51	2.23	2.916
90	2	2	178.9	172.4	172.3	172.4	174.0	3.27	1.88	1.68	2.916
90	3	2	86.7	88.2	86.2	89.2	87.6	1.38	1.57	3.33	2.916
85	4	2	130.9	131.5	130	131.9	131.1	0.83	0.63	2.22	2.916
85	5	2	170.5	168.3	169.6	172.9	170.3	1.94	1.14	1.71	2.916
80	6	2	174.7	162.2	162.7	165.7	166.3	5.79	3.48	1.75	2.916
90	1	3	126.2	125.4	125.4	125.4	125.4	0.57	0.46	1.93	2.418
90	2	3	164.3	162.6	161.2	162.8	162.8	1.28	0.79	1.48	2.418
90	3	3	80.8	82.1	80.9	81.8	81.8	1.31	1.60	2.95	2.418
85	4	3	129.1	127.7	124.8	127.7	127.7	2.03	1.59	1.89	2.418
85	5	3	161.9	161.8	161.2	162.1	162.1	0.94	0.58	1.49	2.418
80	6	3	169.5	158	159.5	162.6	162.6	5.14	3.16	1.49	2.418
90	1	4	126.5	126.3	124.3	125.9	125.9	1.05	0.84	1.51	1.896
90	2	4	151.9	149.2	148	149.7	149.7	1.63	1.09	1.27	1.896
90	3	4	81.6	83.5	81.7	82.8	82.8	1.38	1.66	2.29	1.896
85	4	4	127.7	128	125.7	127.2	127.2	1.02	0.81	1.49	1.896
85	5	4	149.4	150	149.5	150.1	150.1	0.92	0.61	1.26	1.896
80	6	4	155.9	147.9	148.1	150.8	150.1	3.74	2.48	1.26	1.896
90	1	5	121.4	121.5	120.5	121.5	121.5	0.82	0.67	1.26	1.534
90	2	5	132.7	131	129.9	131.3	131.3	1.16	0.88	1.17	1.534
90	3	5	110.3	114.4	110.6	111.2	111.2	1.07	0.96	1.38	1.534
85	4	5	123.5	122.7	121.6	123.0	123.0	1.12	0.91	1.25	1.534
85	5	5	131.2	130.3	128.2	130.4	130.4	1.61	1.23	1.18	1.534
80	6	5	132.9	129.1	126.4	129.5	129.5	2.67	2.06	1.18	1.534

The ICC from each region was calculated and is shown in table 3.8

Table 3.8: The intra-class coefficient for each ROI at varying bone/angle combinations

ROI	ICC	95% Confidence Interval
1	0.9955	0.9844 to 0.9993
2	0.9925	0.9737 to 0.9988
3	0.9944	0.9799 to 0.9991
4	0.9948	0.9811 to 0.9992
5	0.9612	0.8312 to 0.9941

These results indicate that for ROI's 1-4 more than 99%, and for ROI 5 more than 96%, of the total variation observed in the data collected from different bone/angle combinations is due to difference in bone/angle combinations. Conversely the proportion of variation in the data which can be attributed to the imaging and calibration processes is estimated for each ROI by ICC. For ROI 1-4 this is less than 1% and for ROI 5 is less than 4%.

The statistical processes described in the materials and methods were performed on the vertical and horizontal angle data and are presented in tables 3.9 and 3.10.

Table 3.9: Results of descriptive statistics and the coefficient of variation (within) for vertical angle when the bone/angle combination is varied.

bone	angle	X-ray 1	X-ray 2	X-ray 3	X-ray 4	Mean	SD	CV%	CV% (within)	SD (pooled)
1	90	89.66	90.10	89.68	90.44	89.97	0.37	0.41	0.53	0.478
2	90	89.18	89.77	89.68	90.44	89.77	0.52	0.58	0.53	0.478
3	90	90.56	90.48	90.46	90.44	90.48	0.05	0.06	0.53	0.478
4	85	84.30	84.80	85.00	84.9	84.75	0.31	0.37	0.56	0.478
5	85	84.60	84.80	84.90	84.6	84.73	0.15	0.18	0.56	0.478
6	80	78.8	79.4	80.80	80.20	79.78	0.92	1.15	0.6	0.478

The ICC for the vertical angle was 0.9874 (95% CI 0.9542 to 0.998), indicating that 98.74% of the variation is due to variation between bones rather than variation between radiographs.

Table 3.10: Results of descriptive statistics and the coefficient of variation (within) for horizontal angle when the bone/angle combination is varied.

bone	angle	X-ray 1	X-ray 2	X-ray 3	X-ray 4	Mean	SD	CV%	CV% (within)	SD (pooled)
1	90	90.16	90.38	90.55	90.67	90.44	0.23	0.25	0.26	0.234
2	90	90.02	90.33	90.63	90.67	90.42	0.3	0.34	0.26	0.243
3	90	90.80	90.47	90.72	90.72	90.68	0.15	0.16	0.26	0.234

The ICC for the horizontal angle was 0.1831(95% CI 0.00 to 0.9366), indicating that 18.31% of the variation is due to variation between bones rather than variation between radiographs.

3.4 Discussion

Once processed each image provides information on the plate-beam angle at which the radiograph was taken, in both vertical and horizontal directions, and the mean photodensity in terms of mm of aluminium of 4 ROI's within C3 and 1 within C4. The transformation of a radiograph into a digitised image is a highly precise event as evidenced by very low coefficient of variation and coefficient of variation (within) of each ROI in study 1. Although the coefficient of variation and coefficient of variation (within) assess the amount of variation within the data, they do not indicate how much of the variation results from the measuring process. The ICC seeks to determine the percentage of variation due to the measuring process, compared to inherent differences between the scanned images. The ICC in study 1 indicates only 0.39% of total variation between the ROI's is due to the measurement technique. The excellent reproducibility is likely to be as a result of calculating the aspect ratio using a large circle. It appears that the method of calculating the aspect ratio greatly facilitates the reproducibility of the image when a large calibration circle is used, which may not be true when smaller calibration circles are used. The other factor involved in a high reproducibility is the ROI program's ability to detect the same ROI between images. The variation that did occur is likely to have arisen for 2 reasons: firstly there is always random noise when digitising an image that is uncorrelated between images. Secondly, even when digitising the same radiograph several times there are small variations in pixel placement, which affect edges and areas of fine detail and affect all aspects of image calibration and detection of ROI's.

Digitisation of the radiograph results in minimal total variation of the horizontal and vertical angles between replications as shown by the coefficient of variation and the coefficient of variation (within). The ICC indicates that 23.1% of the variation is due to measuring error between replications. This appears to be high, but is only a percentage of the total variation, which itself is very small as determined by the coefficient of variation.

Study 2 revealed when the same bone was radiographed 4 times at exactly the same x-ray beam angle using varying exposures the CV between radiographs taken at the same bone/angle combination was less than 4%. The reliability was excellent as evidenced by the ICC for each ROI. For all ROI's within C3 the CV was less than 1%, indicating very little difference in radiographs resulting from measuring errors, within C4 the CV was increased to just under 4%. The high repeatability of this technique is due to calibration of the images and the ability of the ROI program to detect the same ROI's between images. The difference between C3 and C4 may be the way the ROI's were positioned. A consistent width of C3 was difficult to determine as corners are smooth rather than sharp, and a specified distance was removed from all borders of the distal row of carpal bones, resulting in sharp points at which to delineate the line across the widest aspect of the C3. ROI's 1 and 4 were extrapolated, based on a linear relationship from these points, and ROI's 2 and 3 were placed between them. The centre of ROI 5 was determined drawing a line from ROI 4 and was dependent on the width of C4. The fact that the ROI's within C3 were positioned between 2 points, whereas the ROI within C4 was positioned based on one point may have resulted in C4 having a higher measuring error.

The second part of study 2 was to determine if plate-beam angle accurately reflected x-ray beam angle. Vertical plate-beam angle varied less than 1% from the x-ray beam angle, and the horizontal plate-beam angle varied less than 0.3% from the x-ray beam angle as demonstrated by the coefficient of variation (within). The ICC of the vertical angle suggests that of the total variation, 1.26% is due to differences between successive radiographs that occurs as a result of the measuring process. The ICC of the horizontal angle suggests that 81% of the total variation was due to difference between successive radiographs as a result of measuring errors. This appears to be high, but is only a percentage of the total variation, which is very small as determined by the coefficient of variation (within). The reason for variability of angle between successive radiographs is due to the dimensions of the cube. The size of the cube chosen was such that a change in 2° could be detected, had the cube been larger the variation is likely to have been even smaller.

In vivo precision errors of radiographic methods of bone mineral density analysis have been employed by a number of investigators and the precision error varies between 1% and 15% (using coefficient of variation) [63] The methods employed in this research appear to have less than 1% precision error (based on coefficient of variation and intra-class coefficient) when determining the photodensity of ROI's. This is less than in some previously reported studies,[63] however similar to the study by Yang *et al.* In both Yang *et al*'s investigation as well as this study the same x-ray machine was used, by the same operator and the radiographs were processed at the same time using the same machine. In the study by Colbert [63] a number of different x-ray machines were used, with varying techniques by differing operators and at varying times, thereby more accurately simulating clinical application.

From this study it can be concluded that the reliability of the method of radiographic absorptiometry used in this project is very high in the circumstances in which it was used.

RESULTS

The outcome of interest is a measurement of bone density expressed in terms of millimetres of aluminium. The experimental method and design has been described in materials and methods.

Three separate analyses were run on:

1. Data generated with ROI's placed dorsally with x-ray beam angles of 60°, 65°, 70°, 75°, 80° and 90°.
2. Data generated with ROI's placed dorsally with x-ray beam angles of 60°, 65°, 70°, 75°, 80° and 90°.
3. Data generated from the palmar placement of ROI's of radius size 2.5mm, 3mm and 3.5mm at 90° and 60°.

The most complex interaction, namely angle/group/ROI interaction, was not significant. Therefore no follow up statistical tests were performed on 3-way interactions. Many of the two-way interactions were significant and a number of follow-up tests were performed.

All raw data is in appendix 1, while the statistical analyses are in tabulated form within appendix 2. The results are presented graphically. In the column graphs, columns that are the same colours are not statistically different from each other when α is set at 0.05. Values represented by columns containing 2 colours are not significantly different from any column containing either one of those 2 colours. For example

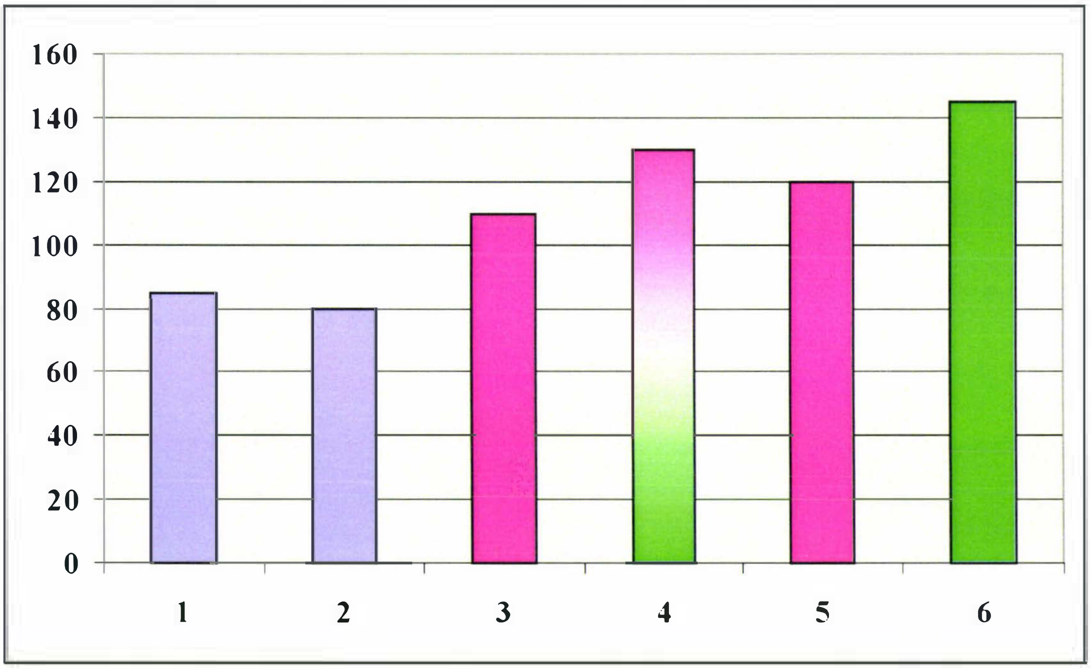

Figure 4.1: Graph illustrating the effect of colour in reading the graph.

Numbers 1 and 2 are significantly different from numbers 3, 4, 5 and 6. Numbers 3, and 5 are significantly different from 1, 2 and 6. Number 6 is significantly different from 1, 2, 3 and 5. Number 4 is significantly different from numbers 1 and 2.

4.1 Dorsal analysis

The raw data is presented in appendix 1 under the heading Dorsal analysis. The mean data is presented in appendix 2 under the heading of Dorsal analysis.

Source		TypeIII Sum of Squares	Degrees of Freedom	Mean Square	F Value	Significance
Intercept	Hypothesis Error	6821166.03 96666.20	1 12	6821166.03 805.52[a]	8468.06	0.000
Angle	Hypothesis Error	23784.02 22930.41	6 408	3964.00 56.202[b]	70.531	0.000
Group	Hypothesis Error	26718.24 9666.20	1 12	26718.24 805.52[a]	33.17	0.000
ROI	Hypothesis Error	11877.05 22930.41	4 408	2969.26 56.20[b]	52.83	0.000
Horse (group)	Hypothesis Error	9666.20 22930.41	12 408	805.517 56.20[b]	14.33	0.000
Angle/ Group	Hypothesis Error	746.7 22930.41	6 408	124.45 56.20[b]	2.21	0.041
Angle/ ROI	Hypothesis Error	3995.00 22930.41	24 408	166.46 56.20[b]	2.96	0.000
Group/ ROI	Hypothesis Error	2229.99 22930.41	4 408	557.50 56.20[b]	9.92	0.000
Angle/ Group/ ROI	Hypothesis Error	749.06 22930.41	24 408	31.21 56.20[b]	.55	0.958

a. MS(Horse(Group))

b. MS(error)

Table 4.1: A table of the overall ANOVA results for the dorsal analysis.

4.1.1 Main effect of angle

Pairwise comparisons were performed to compare the main effect of x-ray beam angle when ROI's were in a dorsal position. The tabulated data and actual significance values are within appendix 2 under the heading of 1.1

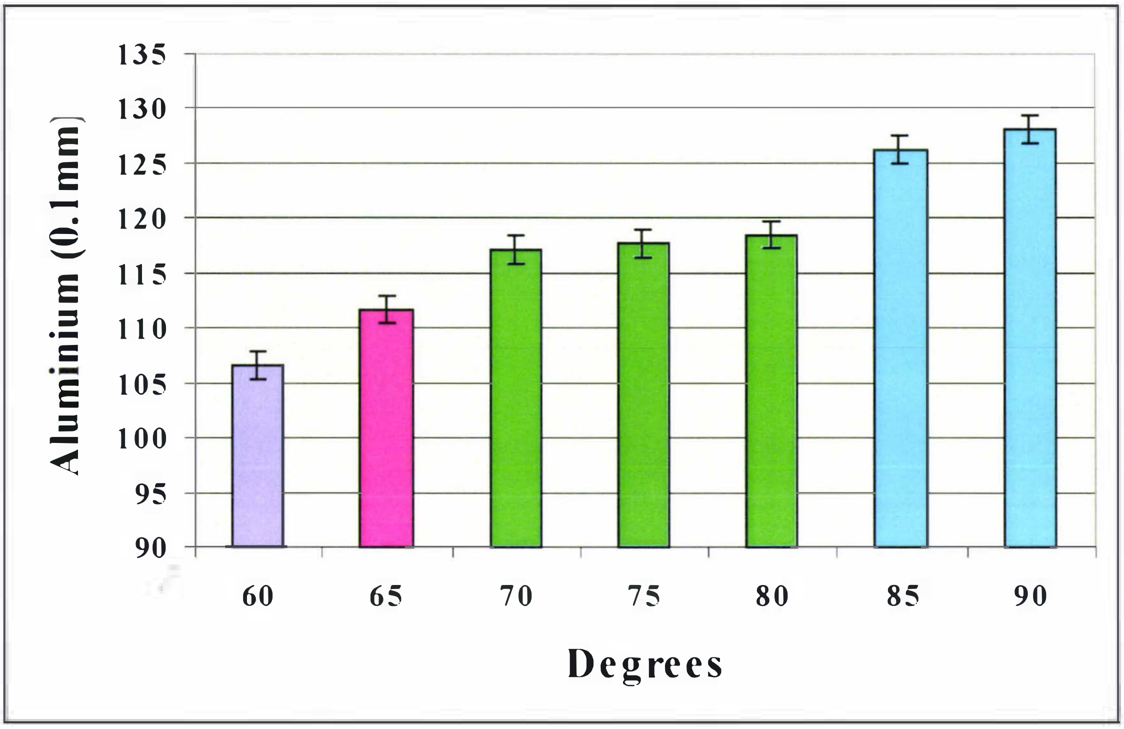

Figure 4.2: Column graph of the main effect of x-ray beam angle on the photodensity of ROI's when in a dorsal position. Error bars represent +/- 1 standard error (s.e.m.).

The photodensity at 60° was significantly different to 65°(p value 0.002), 70° (p value <0.001), 75° (p value <0.001), 80° (p value <0.001), 85° (p value <0.001) and 90° (p value <0.001). The photodensity at 65° was significantly different to70° (p value <0.001), 75°(p value <0.001) and 80° (p value <0.001), 85° (p value <0.001) and 90° (p value <0.001). The photodensity at 70° was significantly different to of 85°(p value <0.001) and 90°(p value <0.001). The photodensity at 75° was significantly different to 85°(p value <0.001) and 90° (p value <0.001). The photodensity at 80° was significantly different to 85° (p value <0.001) and 90° (p value <0.001).

These results show that when the ROI's were in a dorsal position there was significant variation in photodensity when angle was varied less than 5° from 60°(the x-ray beam angle recommended in the literature when taking the tangential view of C3), or less than 10° from 90°(the x-ray beam angle at which the majority of radiographs of excised bones are taken).

4.1.1.1 Angle at one level of ROI

Pairwise comparisons were performed to compare angle means at each level of ROI, when ROI's were in a dorsal position. The tabulated data and actual significance values are within appendix 2 under the heading of 1.1.1.

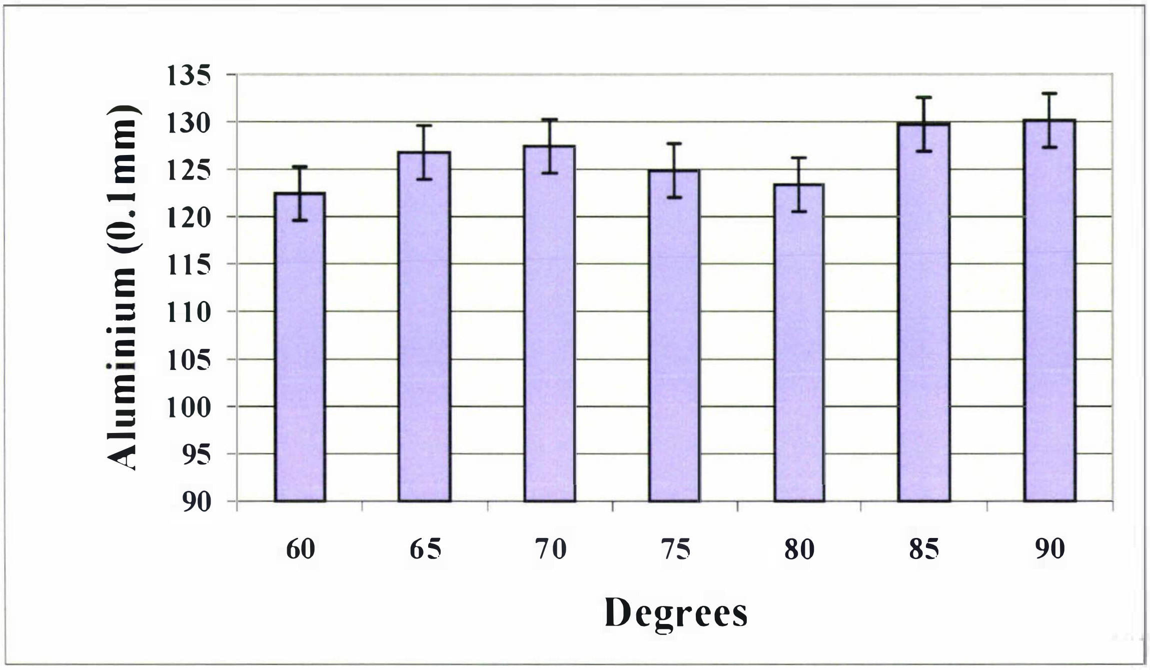

Figure 4.3: Column graph of the effect of angle on photodensity of ROI 1 in a dorsal position. Error bars represent +/- 1 s.e.m.

Variation in angle does not significantly affect the photodensity of ROI 1.

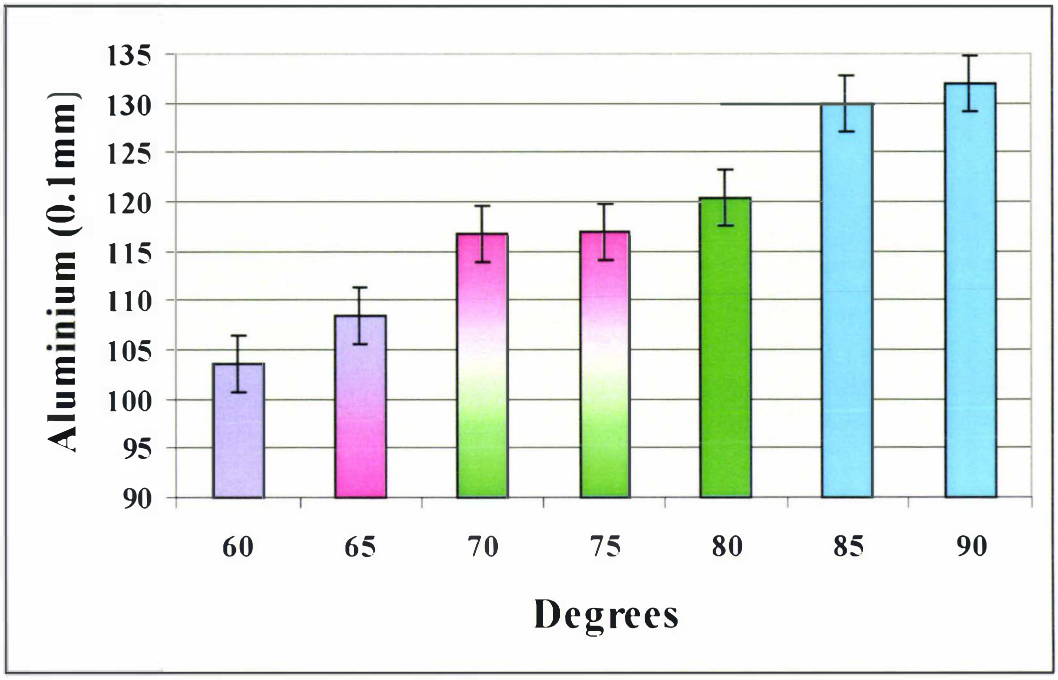

Figure 4.4: Column graph of the effect of angle on photodensity of ROI 2 in a dorsal position. Error bars represent +/- 1 s.e.m.

At ROI 2 the photodensity at 60° was significantly different to 70° (P value <0.001), 75°(p value <0.001), 80°(p value <0.001), 85°(p value <0.001) and 90°(p value <0.001). The photodensity at 65° was significantly different to 80°(P value 0.001), 85°(p value <0.001) and 90°(p value <0.001). The photodensity at 70° was significantly different to 85°(p value <0.001) and 90°(p value <0.001). The photodensity at 75° was significantly different to 85°(p value <0.001) and 90°(p value <0.001). The photodensity at 80° was significantly different to 85°(p value 0.021) and 90°(p value 0.001).

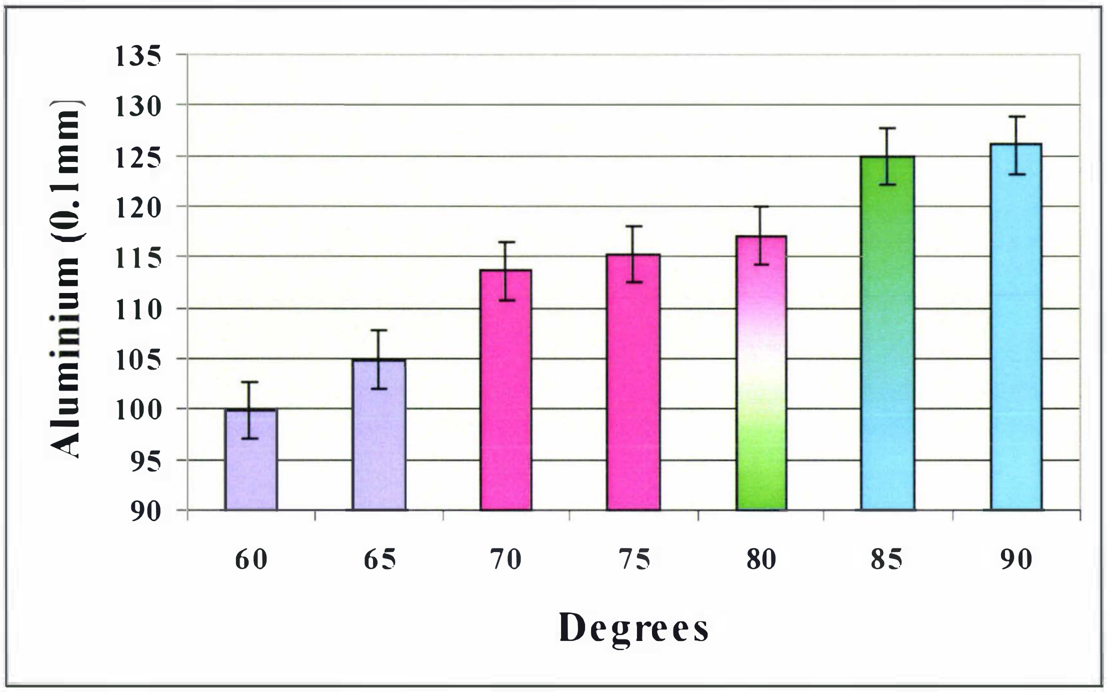

Figure 4.5:Column graph of the effect of angle on photodensity of ROI 3 in a dorsal position. Error bars represent +/- 1 s.e.m.

At ROI 3 the photodensity at 60° was significantly different to 70°(p value <0.001), 75°(p value <0.001), 80°(p value <0.001), 85°(p value <0.001) and 90°(p value <0.001). The photodensity at 65° was significantly different to 70°(p value 0.044), 75°(p value 0.006), 80°(p value <0.001), 85°(p value <0.001) and 90°(p value <0.001). The photodensity at 70° was significantly different to 85°(p value 0.002) and 90°(p value <0.001). The photodensity at 75° was significantly different to 85°(p value 0.016) and 90°(p value 0.003). The photodensity at 80° was significantly different 90°(p value 0.036).

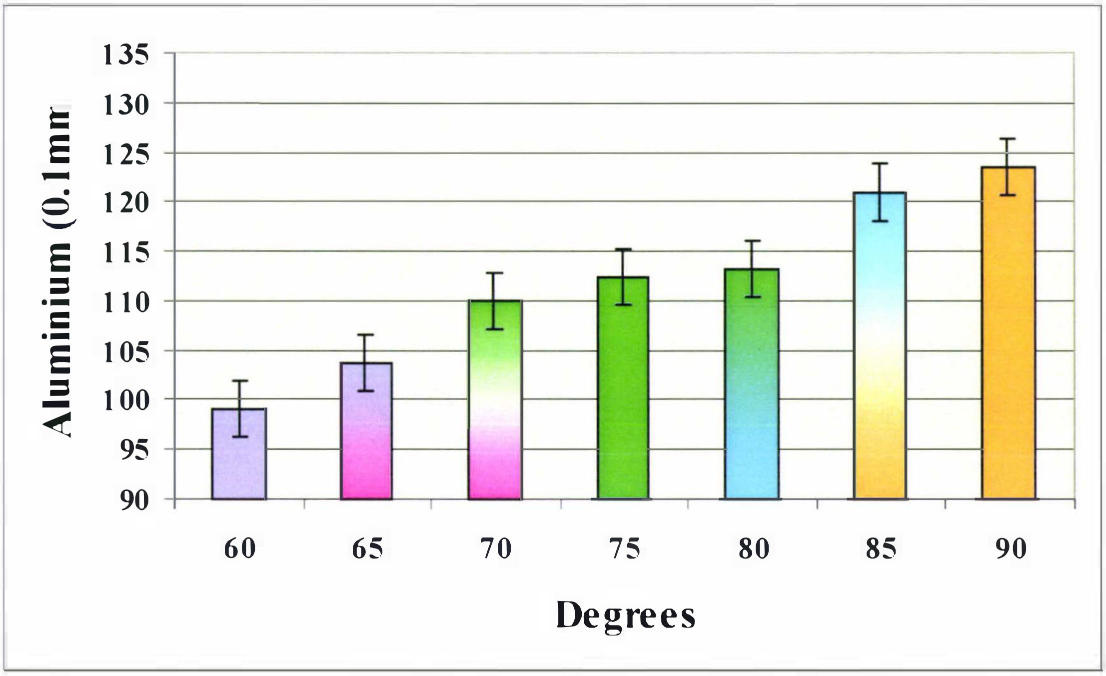

Figure 4.6: Column graph of the effect of angle on photodensity of ROI 4 in a dorsal position. Error bars represent +/- 1 s.e.m.

At ROI 4 the photodensity at 60° was significantly different from 70° (p value 0.003), 75°(p value <0.001), 80° (p value <0.001), 85°(p value <0.001) and 90°(p value <0.001). The photodensity at 65° was significantly different to 75° (p value 0.042), 80° (p value 0.017), 85° (p value <0.001) and 90° (p value <0.001). The photodensity at 70° was significantly different to 85° (p value 0.003) and 90° (p value <0.001). The photodensity at 75° was significantly different to 90° (p value 0.003). The photodensity at 80° was significantly different to 90°(p value 0.008).

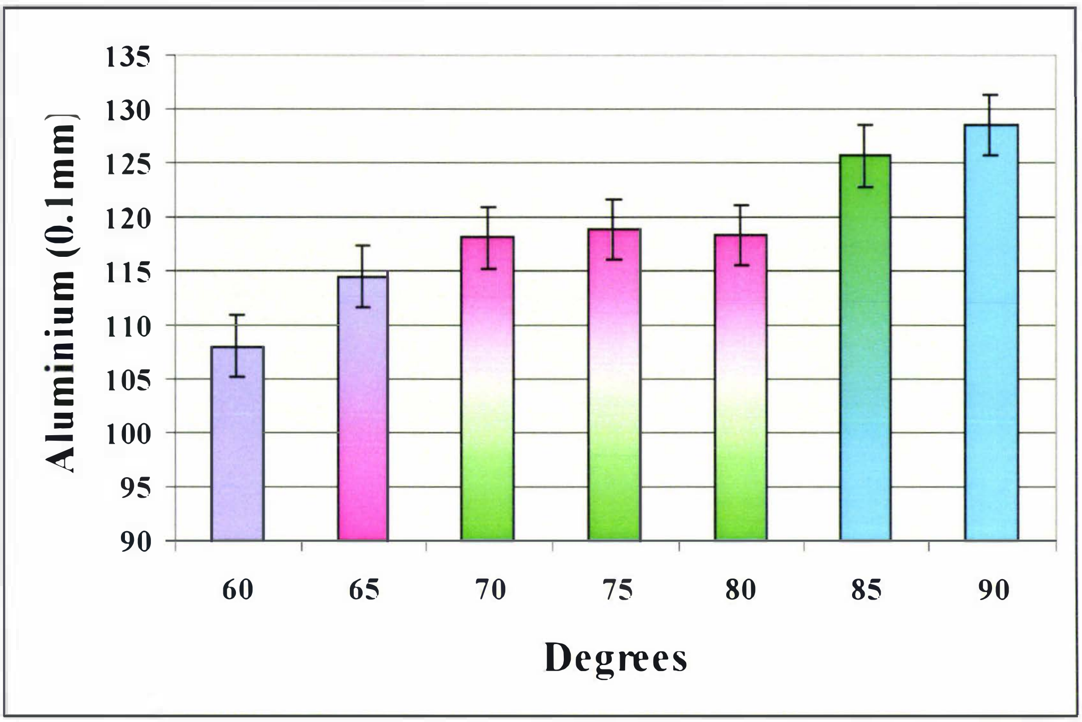

Figure 4.7: Column graph of the effect of angle on the photodensity of ROI 5 in a dorsal position. Error bars represent +/- 1 s.e.m.

At ROI 5 the photodensity at 60° was significantly different to 70° (p value 0.009), 75°(p value 0.003), 80° (p value 0.007), 85°(p value <0.001) and 90°(p value <0.001). The photodensity at 65° was significantly different to 85° (p value 0.002) and 90° (p value <0.001). The photodensity at 70° was significantly different to 90° (p value 0.005). The photodensity at 75° was significantly different to 90° (p value 0.015). The photodensity at 80° was significantly different to 90°(p value 0.007).

4.1.1.2 Angle at one level of group

Pairwise comparisons were performed to compare angle means while holding group (non-exercise or exercise) constant when ROI's were in a dorsal position. The tabulated data and actual significance values are within appendix 2 under the heading of 1.1.2.

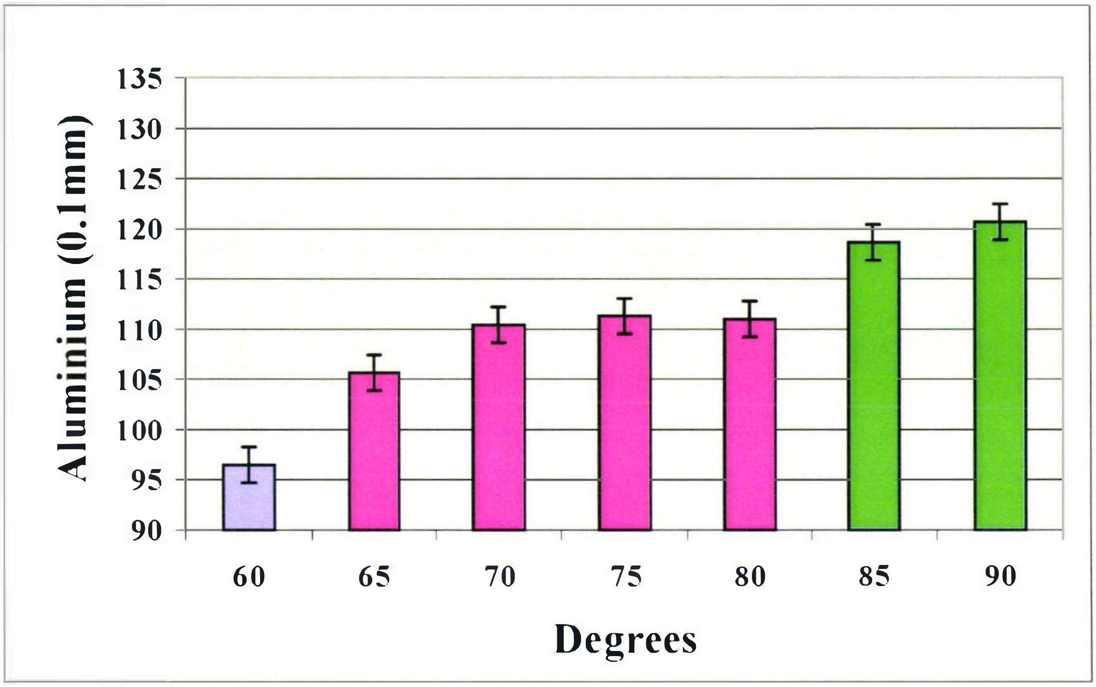

Figure 4.8: Column graph of the effect of angle on the photodensity of the non-exercised group when ROI's were in a dorsal position. Error bars represent +/- 1 s.e.m.

In the non-exercised group the photodensity at 60° was significantly different to 65° (p value <0.001), 70°(p value <0.001), 75°(p value <0.001), 80°(p value <0.001), 85°(p value <0.001) and 90°(p value <0.001). The photodensity at 65° was significantly different to 85°(p value <0.001) and 90°(p value <0.001). The photodensity at 70° was significantly different to 85°(p value <0.001) and 90°(p value <0.001). The photodensity at 75° was significantly different to 85°(p value 0.001) and 90°(p value <0.001). The photodensity at 80° was significantly different to 85°(p value <0.001) and 90°(p value <0.001).

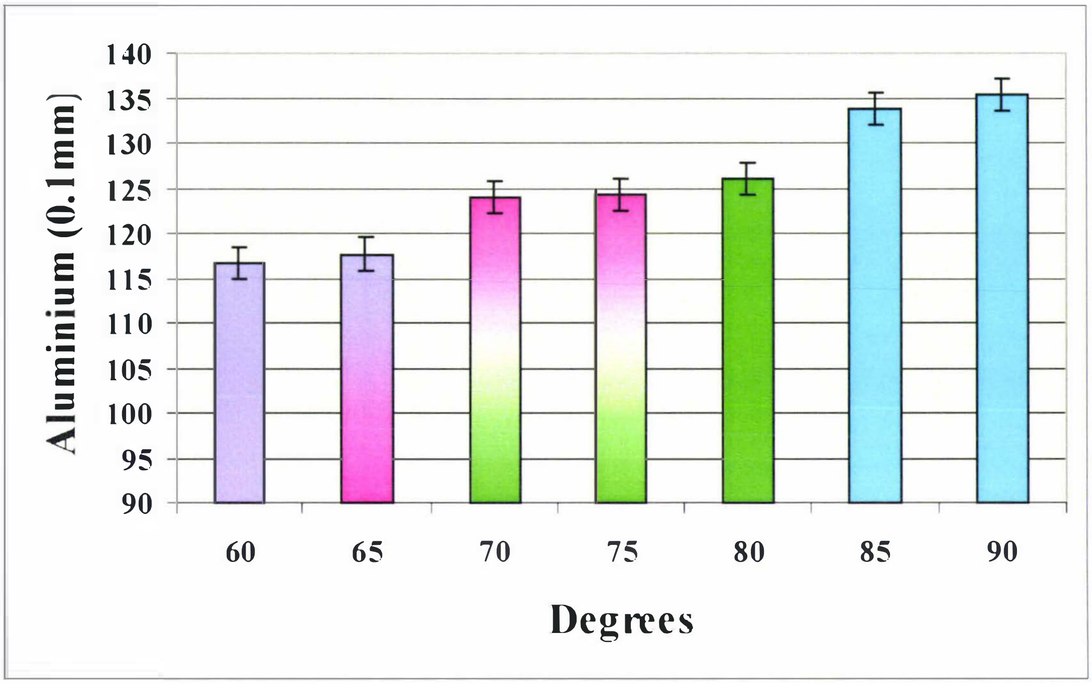

Figure 4.9: Column graph of the effect of angle on the photodensity of the exercised group when ROI's were in a dorsal position. Error bars represent +/- 1 s.e.m.

In the exercised group photodensity at 60° was significantly different to 70°(p value 0.001), 75°(p value 0.001), 80°(p value <0.001), 85°(p value <0.001) and 90°(p value <0.001). The photodensity at 65° is significantly different to 70°(p value 0.01), 75°(p value 0.007), 80°(p value <0.001), 85°(p value <0.001) and 90°(p value <0.001). The photodensity at 70° was significantly different to 85°(p value <0.001) and 90°(p value <0.001). The photodensity at 75° was significantly different to 85°(p value 0.001) and 90°(p value <0.001). The photodensity at 80° was significantly different to 85°(p value <0.001) and 90°(p value <0.001).

These results suggest that a variation of greater than 5° from 90° and an even smaller variation from 60° results in a significant variation in photodensity. When radiographing the excised distal row of carpal bones between 80°and 65° variation in angle does not significantly affect photodensity.

4.1.2 Main effect of ROI

Pairwise comparisons were performed to compare the main effect of ROI when ROI's were in a dorsal position. The tabulated data and actual significance values are within appendix 2 under the heading of 1.2.

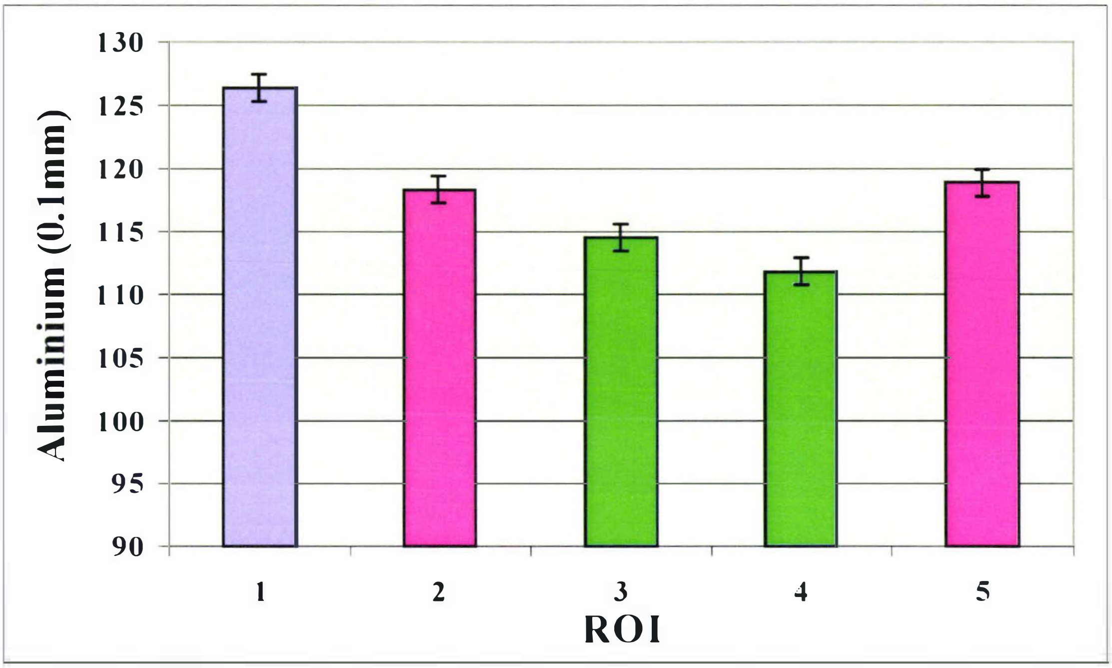

Figure 4.10: Column graph demonstrating the main effect of ROI site on photodensity when ROI's were in a dorsal postion. Error bars represent +/- 1 s.e.m.

Photodensity of ROI 1 was significantly different from ROI 2 (p value <0.001), ROI 3 (p value <0.001), ROI 4 (p value <0.001), ROI 5 (p value <0.001). Photodensity of ROI 2 was significantly different from ROI 3 (p value 0.005) and ROI 4 (p value <0.001). Photodensity of ROI 3 was significantly different from ROI 5 (p value 0.001). Photodensity of ROI 4 was significantly different from ROI 5 (p value <0.001).

4.1.2.1 ROI at one level of group

Pairwise comparisons were performed comparing ROI means, holding group (non-exercise or exercise) constant when ROI's were in a dorsal position. The tabulated data and actual significance values are within appendix 2 under the heading of 1.2.1.

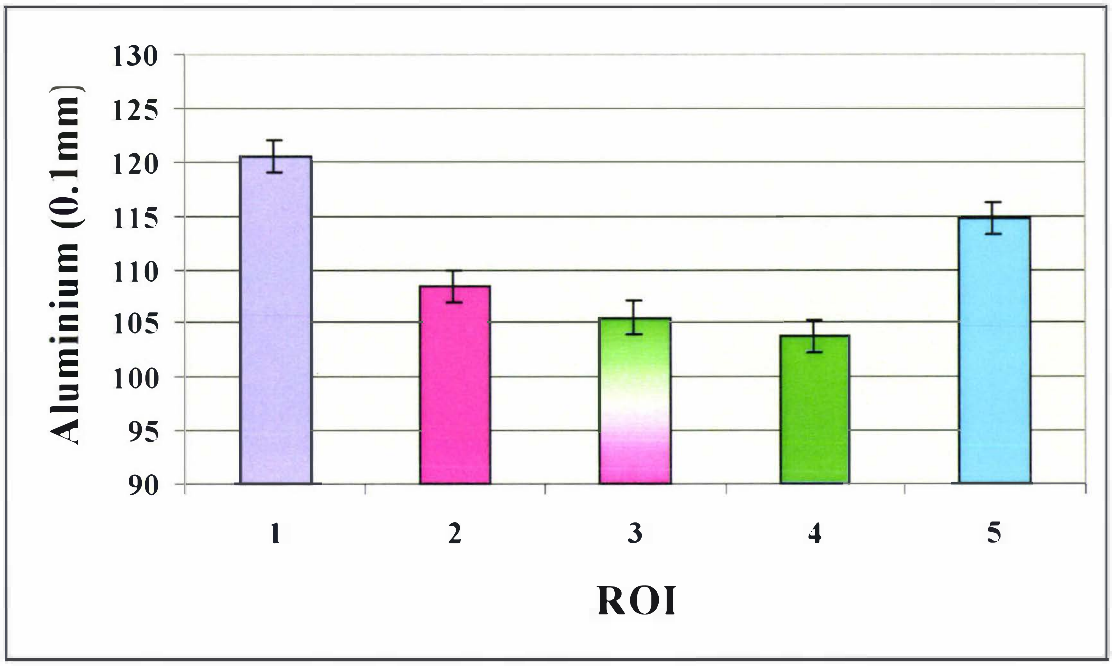

Figure 4.11: Column graph of the effect non-exercise on the photodensity of ROI's in a dorsal position. Error bars represent +/- 1 s.e.m.

In the non-exercised group photodensity of ROI 1 was significantly different from ROI 2 (p value <0.001), ROI 3 (p value <0.001), ROI 4 (p value <0.001), ROI 5 (p value 0.002). The photodensity of ROI 2 was significantly different from ROI 4 (p value 0.023) and ROI 5 (p value <0.001). The photodensity of ROI 3 was significantly different from ROI 5 (p value <0.001). The photodensity of ROI 4 was significantly different from ROI 5 (p value <0.001).

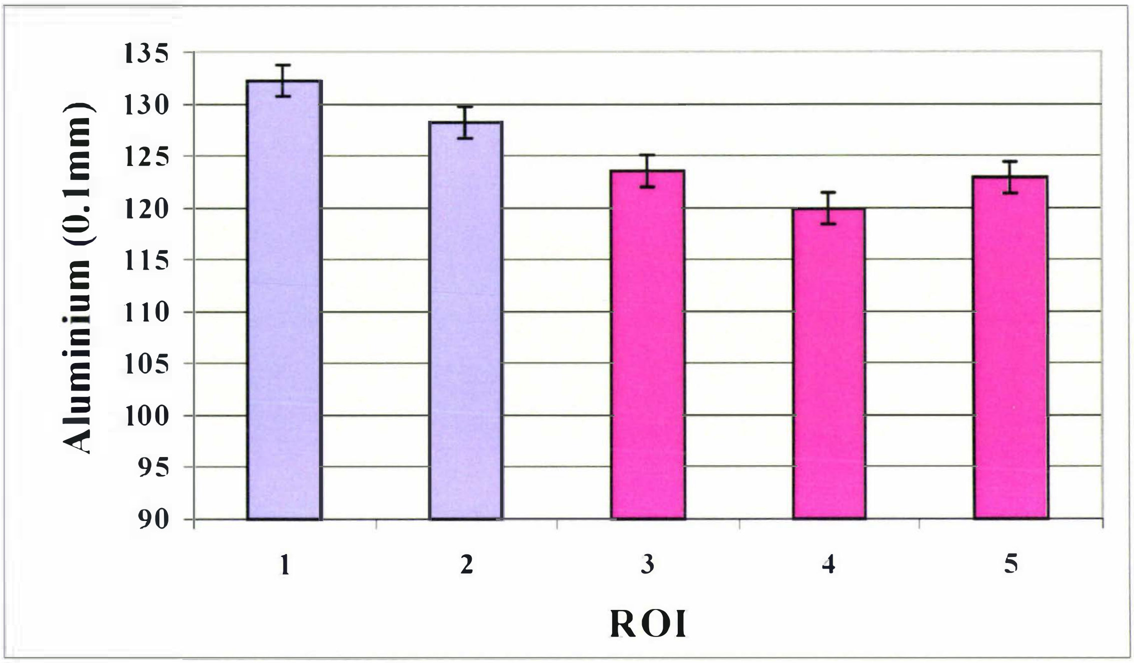

Figure 4.12: Column graph of the effect of exercise on the photodensity of ROI's in a dorsal position. Error bars represent +/- 1 s.e.m.

In the exercised group photodensity of ROI 1 was significantly different from ROI 3 (p value <0.001), ROI 4 (p value <0.001), ROI 5 (p value 0.002). The photodensity of ROI 2 was significantly different from ROI 3 (p value 0.021), ROI 4 (p value 0.023) and ROI 5 (p value 0.005).

4.1.2.2 ROI at one level of angle

Pairwise comparisons were performed to compare ROI means, holding angle constant when ROI's were in a dorsal position. The tabulated data and actual significance values are within appendix 2 under the heading of 1.2.2.

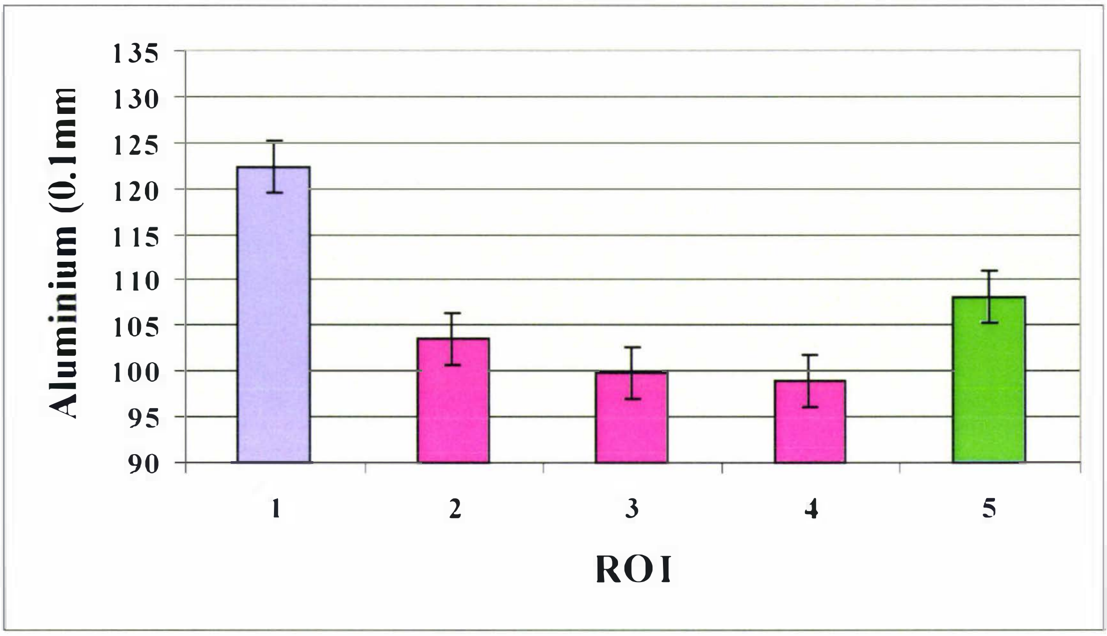

Figure 4.13: Column graph of the photodensity of ROI's in a dorsal position when x-ray beam angle was 60 degrees. Error bars represent +/- 1 s.e.m.

At 60° the photodensity of ROI 1 was significantly different from ROI 2 (p value <0.001), ROI 3 (p value <0.001), ROI 4 (p value <0.001), ROI 5 (p value 0.002). The photodensity of ROI 3 was significantly different from ROI 5 (p value 0.04). The photodensity of ROI 4 was significantly different from ROI 5 (p value 0.016).

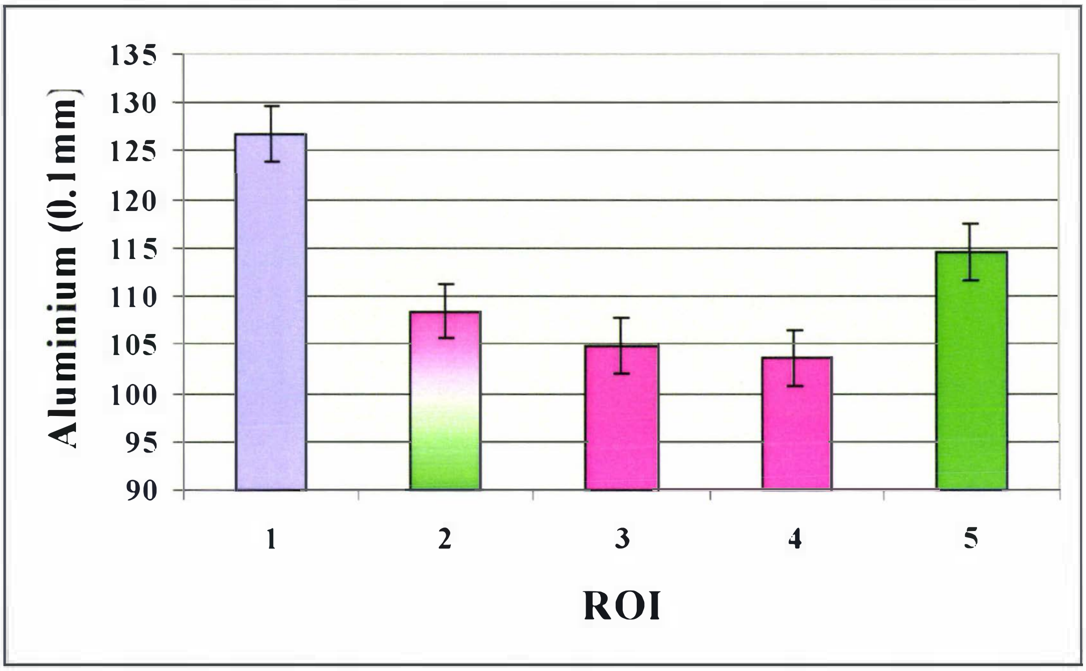

Figure 4.14: Column graph of photodensity of ROI's in a dorsal position when x-ray beam angle was 65 degrees. Error bars represent +/- 1 s.e.m.

At 65° the photodensity of ROI 1 was significantly different from ROI 2 (p value <0.001), ROI 3 (p value <0.001), ROI 4 (p value <0.001) and ROI 5 (p value 0.002). The photodensity of ROI 3 was significantly different from ROI 5 (p value 0.007). The photodensity of ROI 4 was significantly different from ROI 5 (p value 0.001).

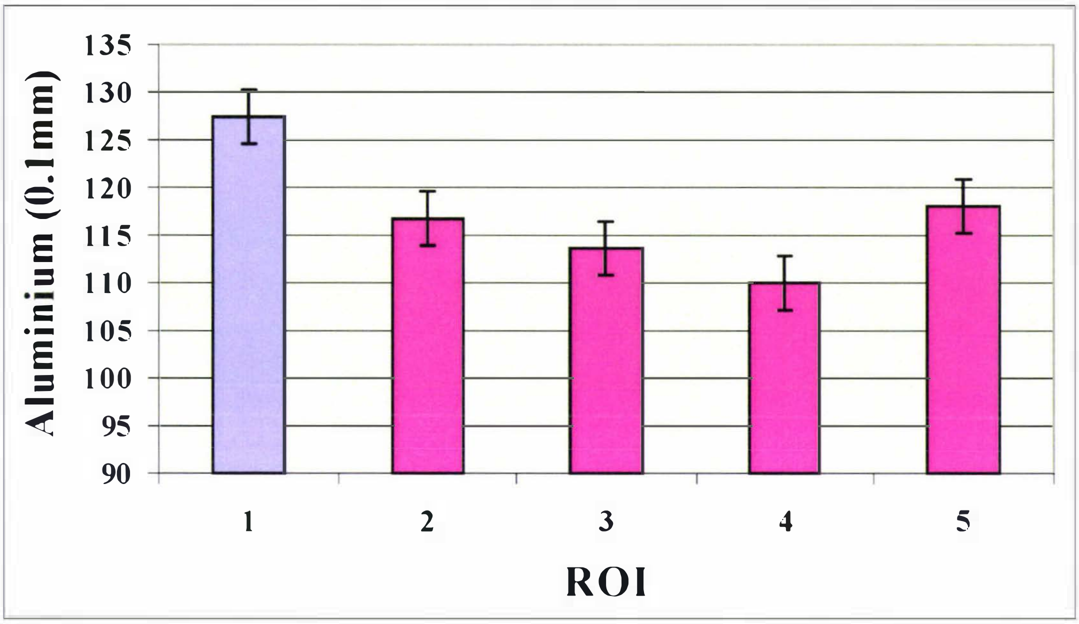

Figure 4.15: Column graph of photodensity of ROI's in a dorsal position when x-ray beam angle was at 70 degrees. Error bars represent +/- 1 s.e.m.

At 70° the photodensity of ROI 1 was significantly different from ROI 2 (p value 0.002), ROI 3 (p value <0.001), ROI 4 (p value <0.001) and ROI 5 (p value 0.011).

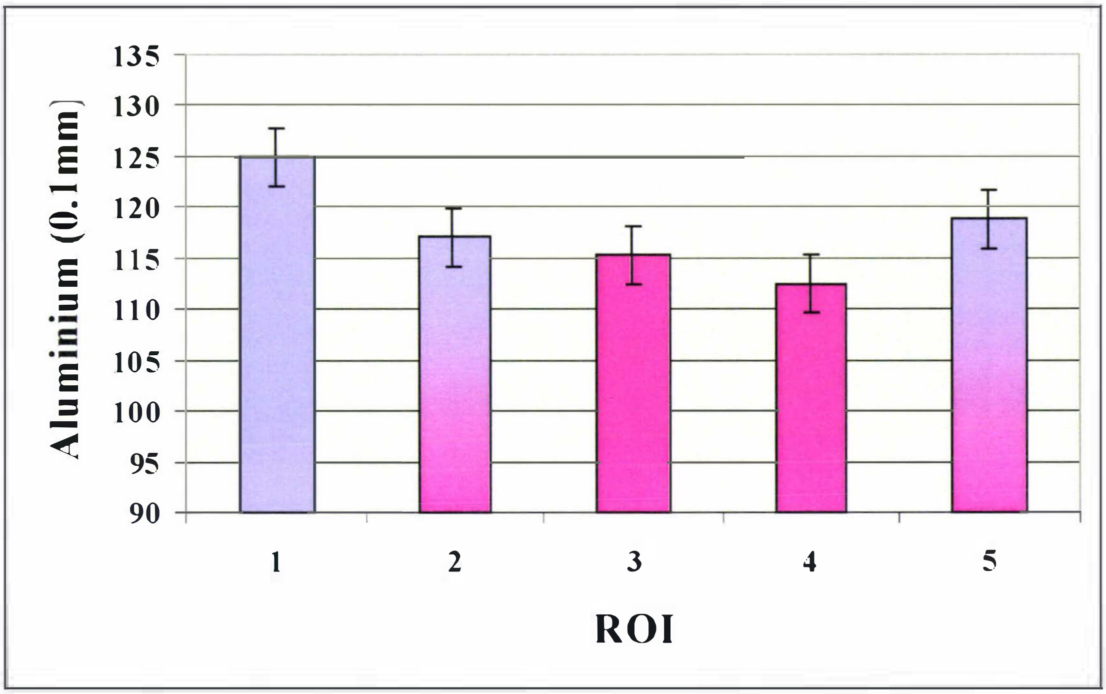

Figure 4.16: Column graph of photodensity of ROI's in a dorsal postion when x-ray beam angle was 75 degrees. Error bars represent +/- 1 s.e.m.

At 75° the photodensity of ROI 1 was significantly different from ROI 3 (p value 0.008) and ROI 4 (p value <0.001).

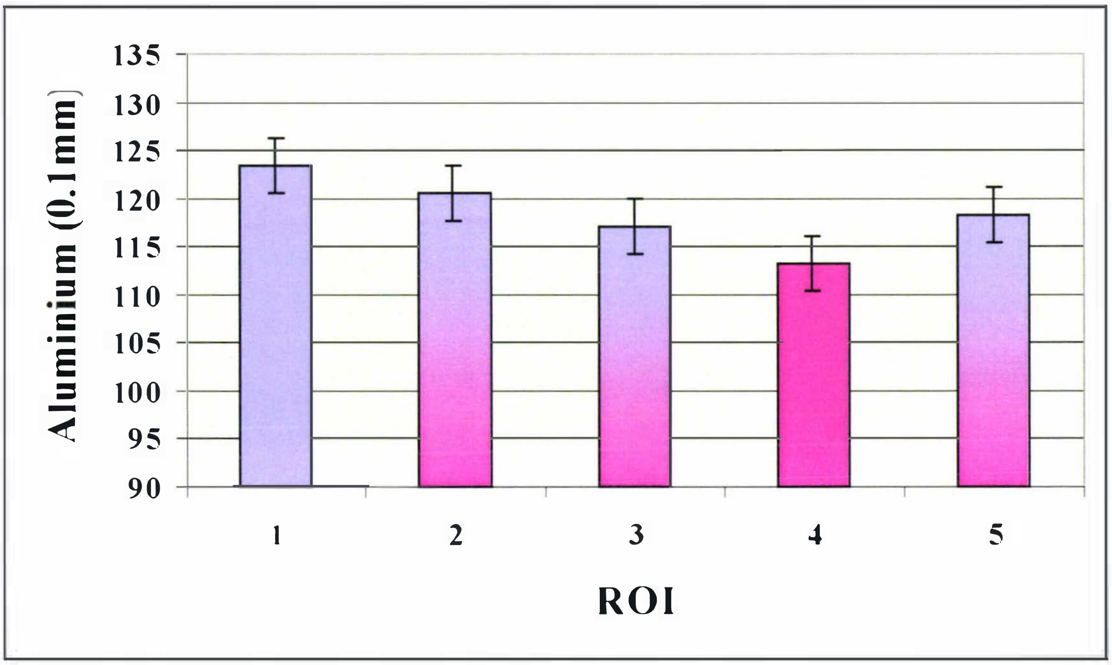

Figure 4.17: Column graph of photodensity of ROI's in a dorsal position when x-ray beam angle was 80 degrees. Error bars represent +/- 1 s.e.m.

At 80° the photodensity of ROI 1 was significantly different from ROI 4 (p value 0.004).

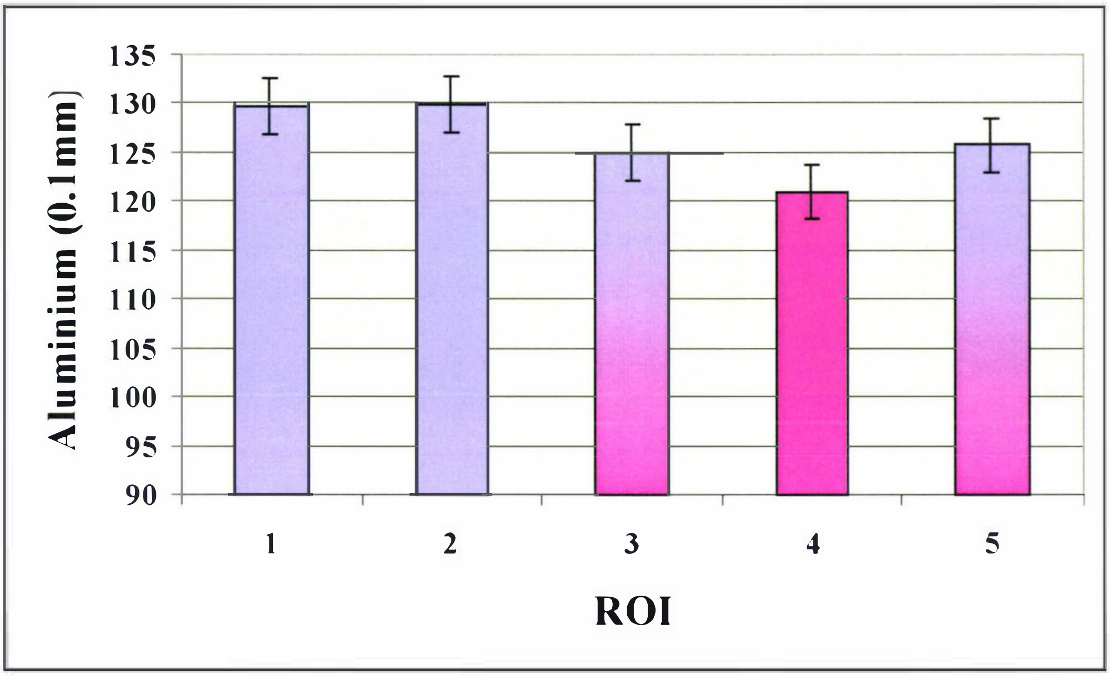

Figure 4.18: Column graph of photodensity of ROI's in a dorsal position when x-ray beam angle was 85 degrees. Error bars represent +/- 1 s.e.m.

At 85° the photodensity of ROI 2 was significantly different from ROI 4 (p value 0.018).

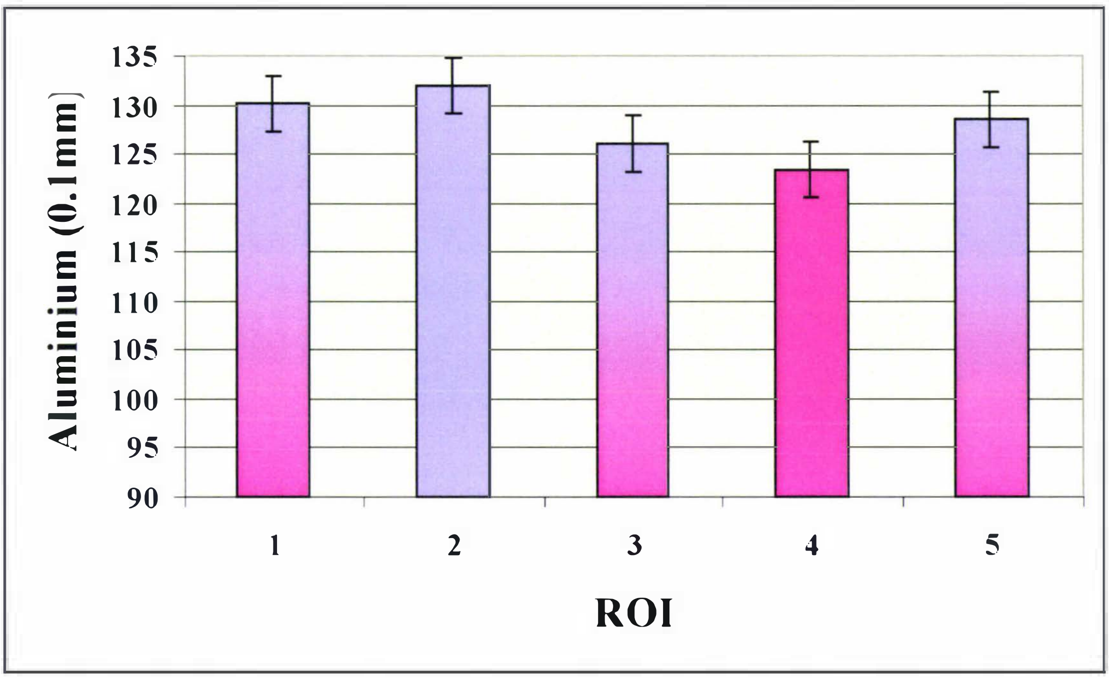

Figure 4.19: Column graph of photodensity of ROI's in a dorsal position when x-ray beam angle was 90 degrees. Error bars represent +/- 1 s.e.m.

At 90° the photodensity of ROI 2 was significantly different form ROI 4 (p value 0.026).

Variation in angle appears to affect ROI photodensity. As the angle reduces from 90° to 60° the photodensity of each ROI decreases however the relationship between ROI's 1 to 5 appears similar at all angles. The change in actual value means that at some angles some ROI's is not significantly different to others while at others they are.

4.1.3 Main effect of group

Pairwise comparisons were performed on the main effect of group when ROI were in a dorsal position. The tabulated data and actual significance values are within appendix 2 under the heading of 1.3.

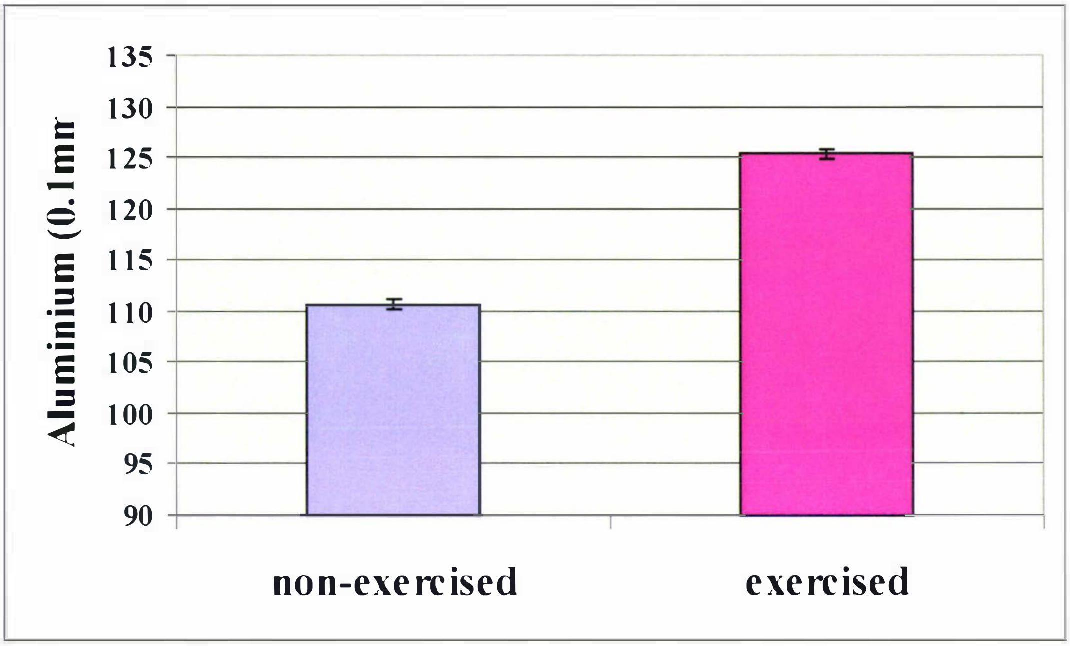

Figure 4.20: Column graph of the effect of group on photodensity when ROI's were in a dorsal position. Error bars represent +/- 1 s.e.m.

Photodensity of the non-exercised group was significantly less than the exercised group (p value <0.001).

4.1.3.1 Group at one level of angle

Pairwise comparisons were performed to compare group means when ROI's were in a dorsal position. The tabulated data and actual significance values are within appendix 2 under the heading of 1.3.1.

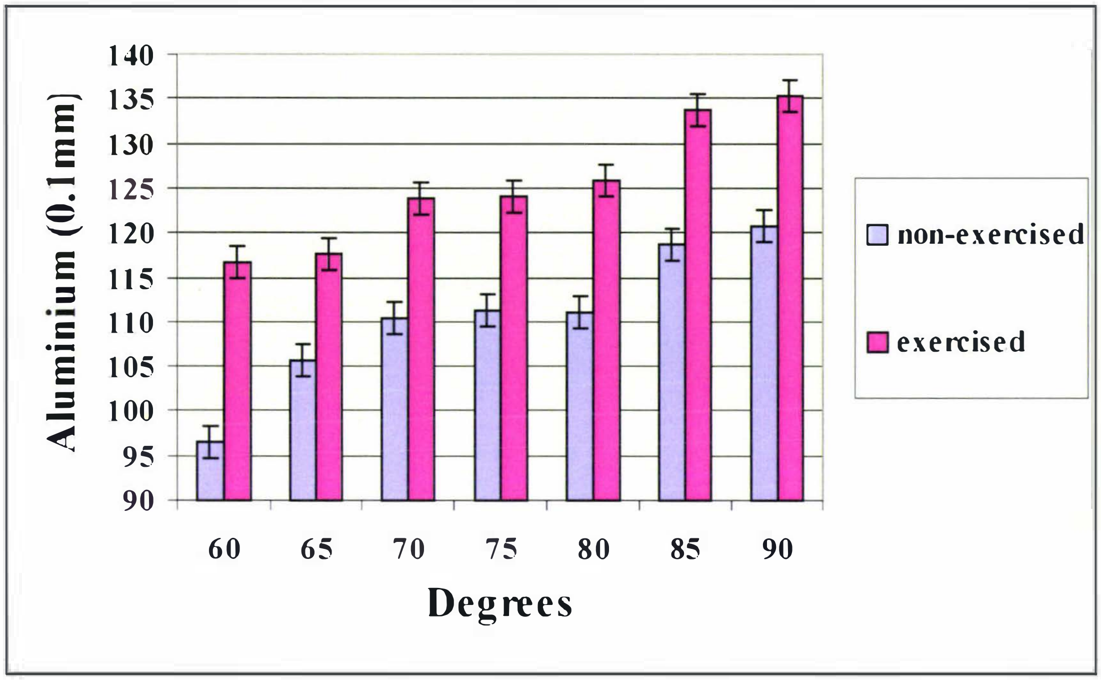

Figure 4.21: Column graph of the effect of group on angle when ROI's were in a dorsal position. Error bars represent +/- 1 s.e.m.

Photodensity of the exercised group was significantly greater than the non-exercised group at 60° (p value <0.001), 65° (p value <0.001), 70° (p value <0.001), 75° (p value <0.001), 80° (p value <0.001), 85° (p value <0.001) and 90° (p value <0.001).

4.1.3.2 Group at one level of ROI

Pairwise comparisons were performed to compare group means, holding ROI constant when ROI's were in a dorsal position. The tabulated data and actual significance values are within appendix 2 under the heading of 1.3.2.

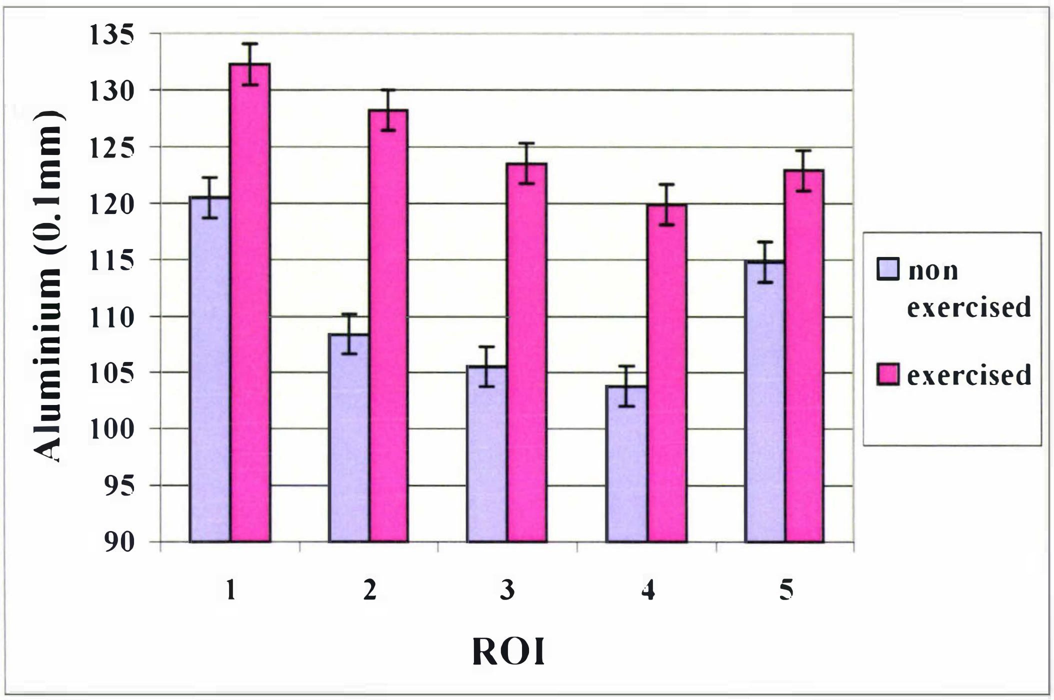

Figure 4.22: Column graph of the effect of group on photodensity of ROI's when in a dorsal position. Error bars represent +/- 1 s.e.m.

Photodensity significantly increased from the non-exercised to the exercised group at ROI 1 (p value <0.001), ROI 2(p value <0.001), ROI 3(p value <0.001), ROI 4(p value <0.001) and ROI 5(p value <0.001). ROI 2 had the greatest increase in photodensity between groups (15.5%). ROI 3 had the next largest increase in photodensity (14.6%), followed by ROI 4 (13.4 %), ROI 1(9%) and ROI 5(6.5%).

4.2 Palmar analysis

The raw data is presented in appendix 1 under the heading Palmar analysis. The mean data is presented in appendix 2 under the heading of Palmar analysis.

Source		TypeIII Sum of Squares	Degrees of freedom	Mean Square	F Value	Significance
Intercept	Hypothesis Error	8184751.40 16884.38	1 12	8184751 1407.03[a]	5817.03	0.000
Angle	Hypothesis Error	6997.88 22618.20	6 408	1166.31 55.44[b]	21.04	0.000
Group	Hypothesis Error	40938.81 16884.38	1 12	40938.81 1407.03[a]	29.09	0.000
ROI	Hypothesis Error	4848.33 22618.2	4 408	1212.08 55.44[b]	21.86	0.000
Horse(group)	Hypothesis Error	16884.38 22618.20	12 408	1407.03 55.44[b]	25.38	0.000
Angle/Group	Hypothesis Error	474.83 22618.20	6 408	79.14 55.44[b]	1.43	0.203
Angle/ROI	Hypothesis Error	1196.07 22618.20	24 408	49.83 55.44[b]	0.899	0.604
Group/ROI	Hypothesis Error	5090.84 22618.20	4 408	1272.71 55.44[b]	22.96	0.000
Angle/Group /ROI	Hypothesis Error	1913.5 22618.200	24 408	7.97 55.44[b]	0.144	1.000

a. MS(Horse(Group))
b. MS(Error)

Table 4.2: A table of the overall ANOVA results for the palmar analysis.

4.2.1 Main effect of angle

Pairwise comparisons were performed on the main effect of angle when ROI's were in a palmar position. The tabulated data and actual significance values are within appendix 2 under the heading of 2.1

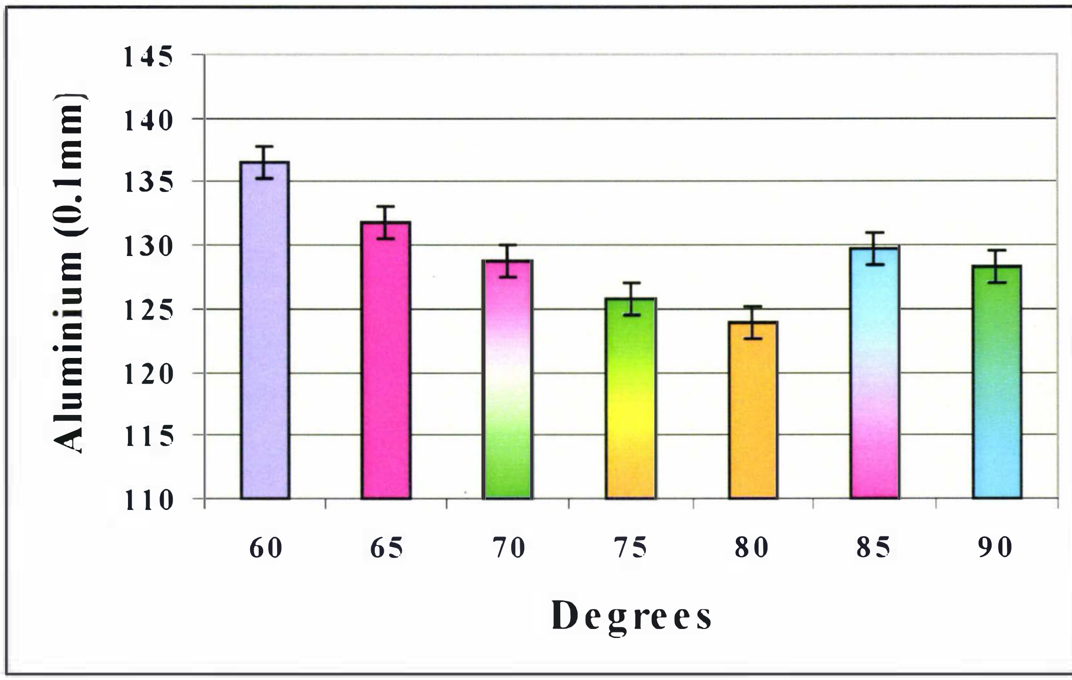

Figure 4.23: Column graph of the main effect of x-ray beam angle on photodensity when ROI's were in the palmar postion. Error bars represent +/- 1 standard error (s.e.m.).

The photodensity at 60° was significantly different to 65° (p value <0.001), 70° (p value <0.001), 75° (p value <0.001), 80° (p value <0.001), 85° (p value <0.001) and 90° (p value <0.001). The photodensity at 65° was significantly different to 70°(p value 0.019), 75°(p value <0.001), 80°(p value <0.001) and 90°(p value 0.007). The photodensity at 70° was significantly different to 75° (p value 0.019) and 80° (p value <0.001). The photodensity at 75° was significantly different to 85°(p value 0.002) and 90°(p value 0.046). The photodensity at 80° was significantly different from 85°(p value <0.001) and 90°(p value 0.001).

These results show that when the ROI's were in a palmar position there was significant variation in photodensity when angle was varied less than 5° from 60°(the x-ray beam angle recommended in the literature when taking the tangential view of C3), or less than 10° from 90°(the x-ray beam angle at which the majority of radiographs of excised bones are taken).

4.2.1.1 Angle at one level of ROI

Pairwise comparisons were performed to compare x-ray beam angle means at one level of ROI when ROI's were in a palmar position. The tabulated data and actual significance values are within appendix 2 under the heading of 2.1.1

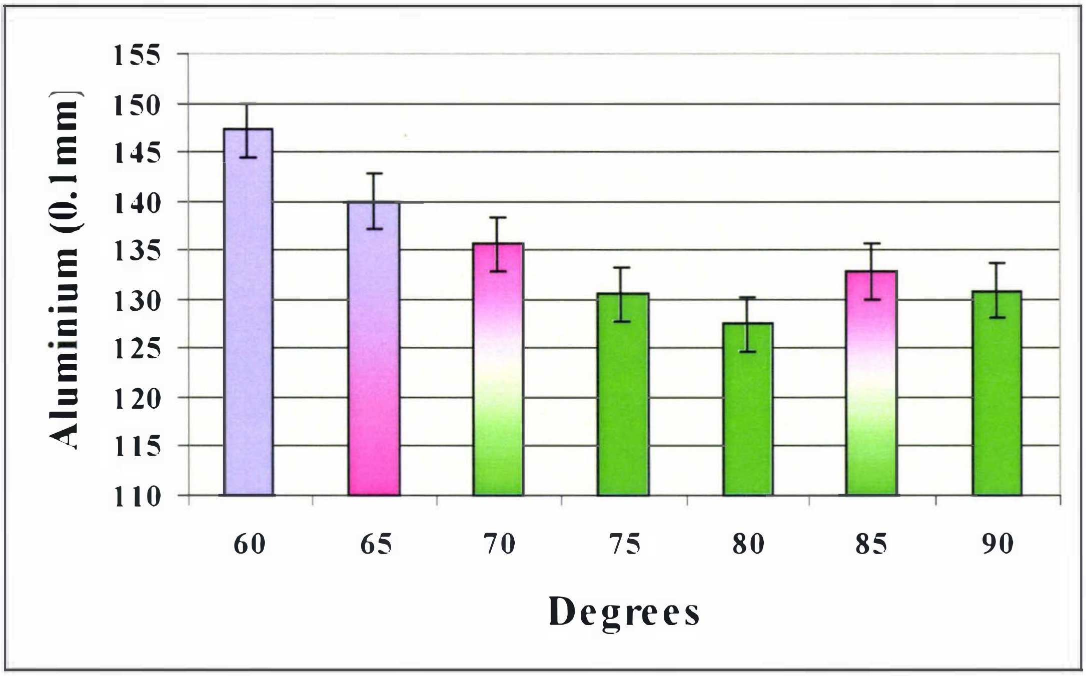

Figure 4.24: Column graph of the effect of x-ray beam angle on photodensity of ROI 1 when ROI's were in a palmar position. Error bars represent +/- 1 s.e.m.

At ROI 1 the photodensity of 60° was significantly different to 70° (p value 0.001), 75° (p value <0.001), 80° (p value <0.001), 85° (p value <0.001) and 90° (p value <0.001). Photodensity at 65° was significantly different to 75° (p value 0.019), 80° (p value <0.001) and 90° (p value 0.029).

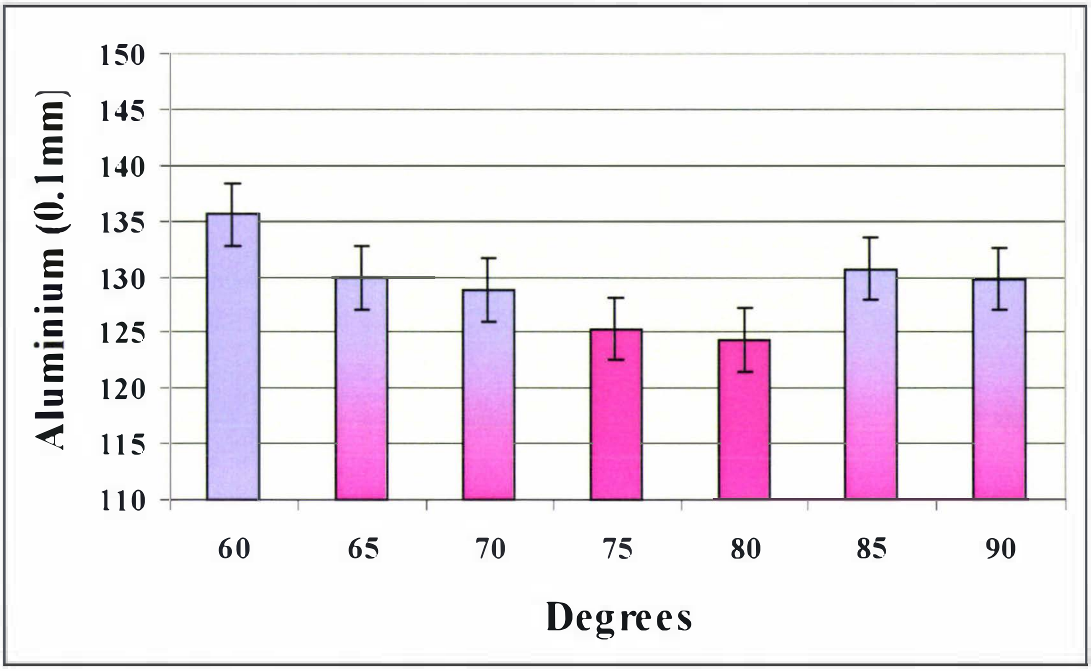

Figure 4.25: Column graph of the effect of x-ray beam angle on photodensity of ROI 2 when ROI's were in a palmar position. Error bars represent +/- 1 s.e.m.

At ROI 2 the photodensity of 60° was significantly different to 75° (p value 0.006) and 80° (p value 0.002).

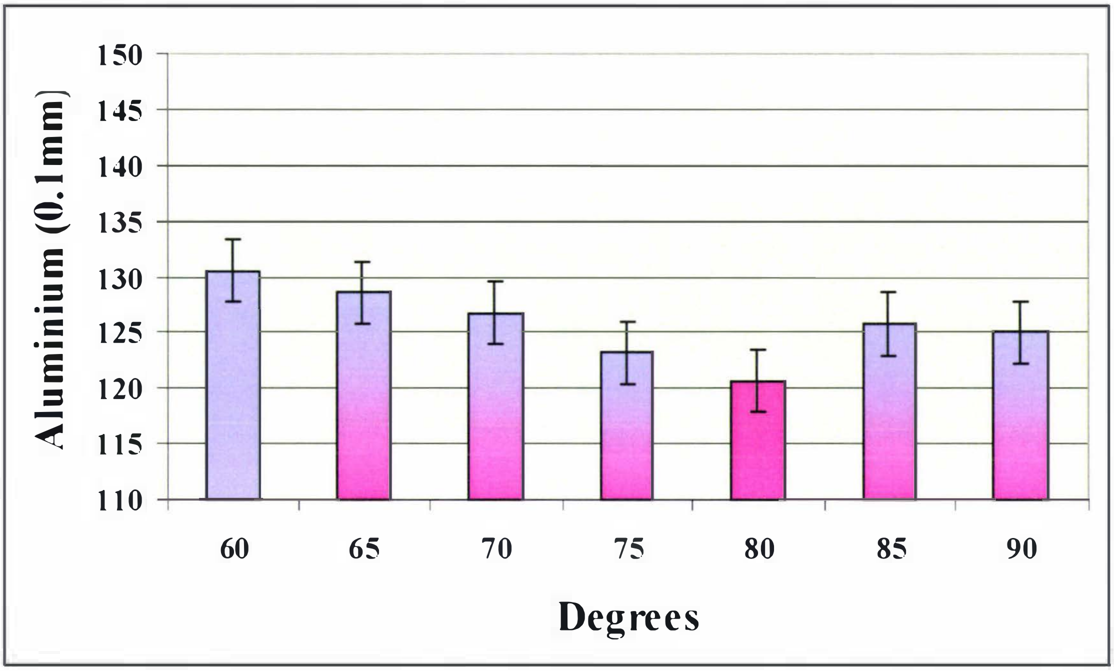

Figure 4.26: Column graph of the effect of x-ray beam angle on the photodensity of ROI 3 when ROI's were in a palmar position. Error bars represent +/- 1 s.e.m.

At ROI 3 the photodensity at 60° was significantly different to 80° (p value 0.011).

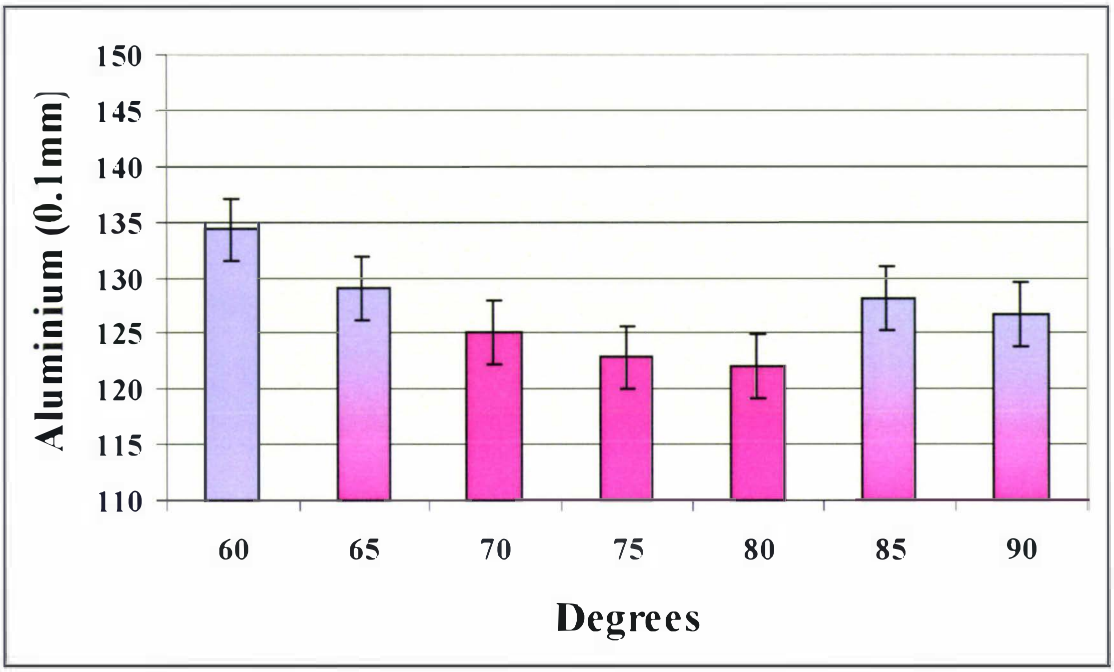

Figure 4.27: Column graph of the effect of x-ray beam angle on ROI 4 when ROI's were in a palmar position. Error bars represent +/- 1 s.e.m.

At ROI 4 the photodensity at 60° was significantly different to 70° (p value 0.022), 75° (p value 0.001) and 80° (p value <0.001).

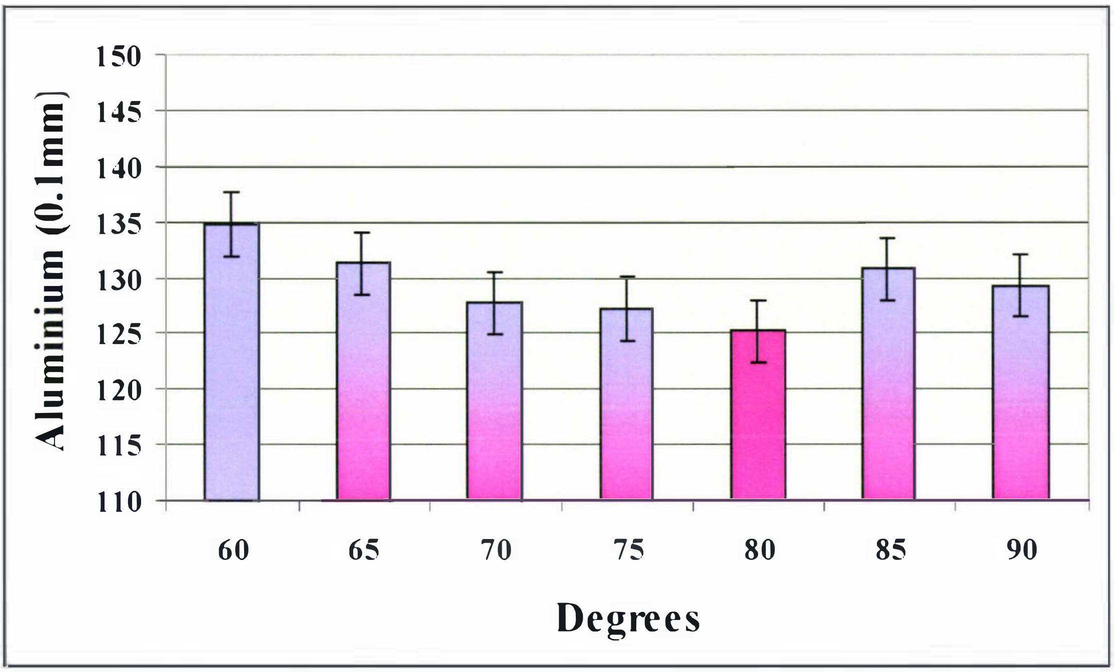

Figure 4.28: Column graph of the effect of x-ray beam angle at ROI 5 when ROI's were in a palmar position. Error bars represent +/- 1 s.e.m.

At ROI 5 the photodensity at 60° was significantly different from 80° (p value 0.015).

4.2.1.2 Angle at one level of group

Pairwise comparisons were performed to compare x-ray beam angle means while holding group (non-exercise or exercise) constant when ROI's were in a palmar position. The tabulated data and actual significance values are within appendix 2 under the heading of 2.1.2.

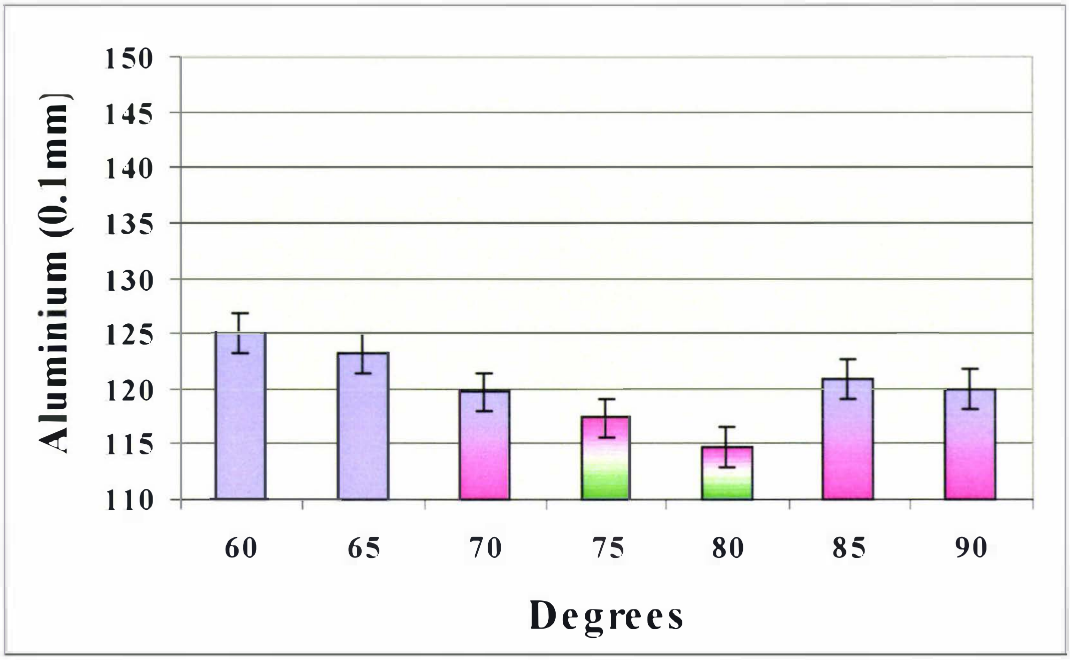

Figure 4.29: Column graph of the effect of x-ray beam angle on photodensity of the non-exercised group when ROI's were in a palmar position. Error bars represent +/- 1 s.e.m.

In the non-exercised group the photodensity at 60° was significantly different from 75°(p value <0.001) and 80°(p value <0.001). The photodensity at 65° was significantly different from 75°(p value 0.024) and 80°(p value <0.001). The photodensity at 80° was significantly different from 85°(p value 0.013).

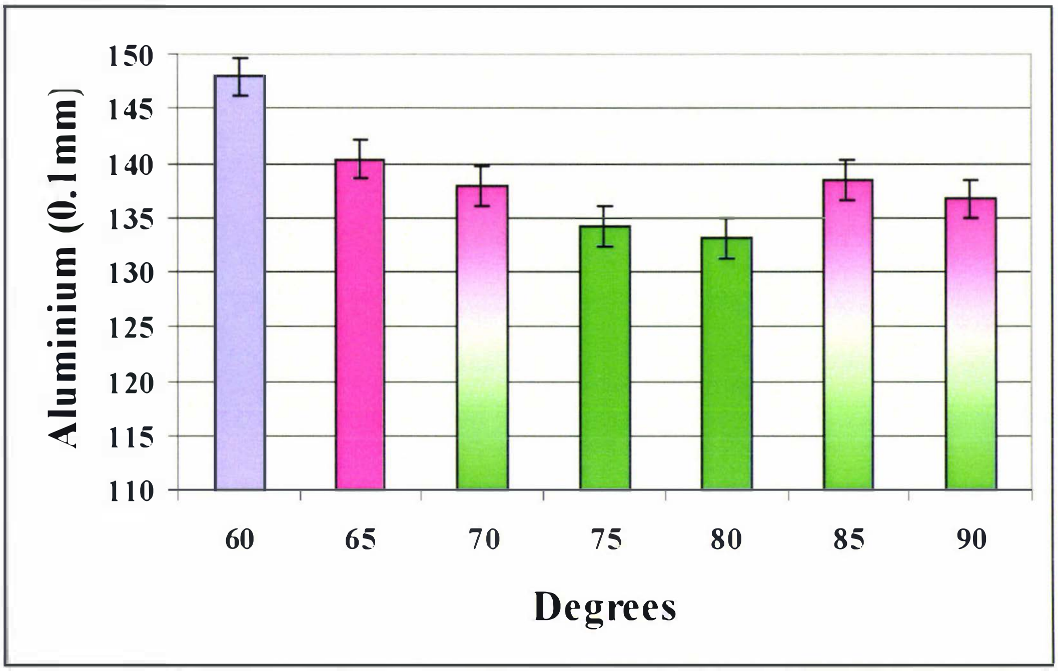

Figure 4.30: Column graph of the effect of x-ray beam angle on photodensity of the exercised group when ROI's were in a palmar position. Error bars represent +/- 1 s.e.m.

In the exercised group the photodensity at 60° was significantly different to 65° (p value <0.001), 70° (p value <0.001), 75° (p value <0.001), 80° (p value <0.001), 85° (p value <0.001) and 90° (p value <0.001). The photodensity at 65° was significantly different to 75°(p value 0.015) and 80°(p value 0.001).

4.2.2 Main effect of ROI

Pairwise comparisons were performed to compare the main effect of ROI when ROI's were in a palmar position. The tabulated data and actual significance values are within appendix 2 under the heading of 2.2

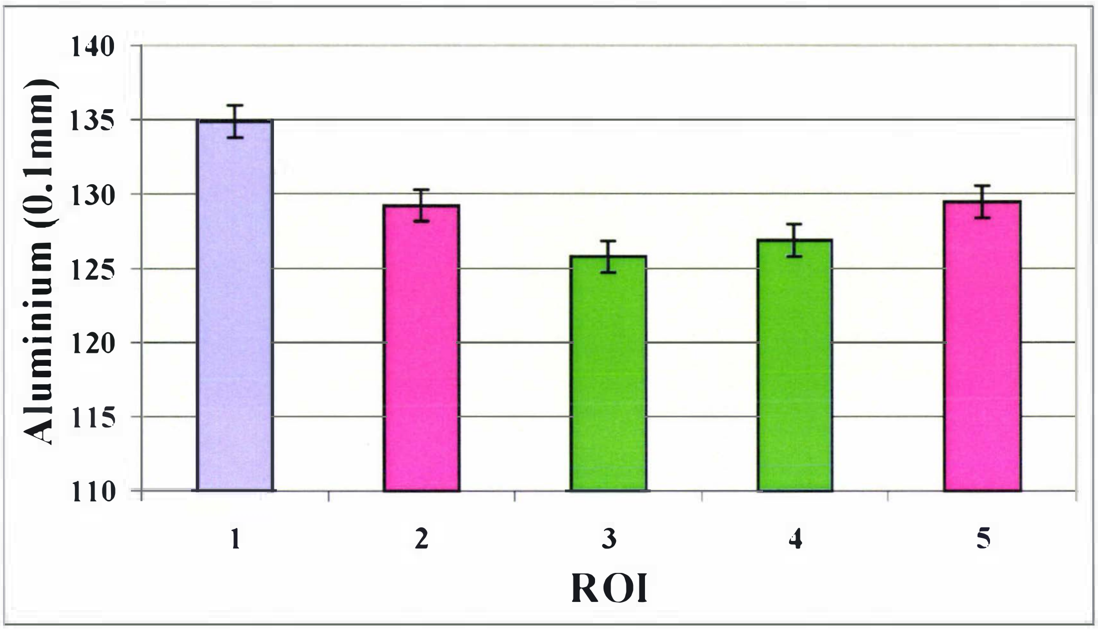

Figure 4.31: Column graph of the main effect of ROI site on photodensity when ROI's were in a palmar position. Error bars represent +/- 1 s.e.m.

Photodensity of ROI 1 was significantly different from ROI 2 (p value <0.001), ROI 3 (p value <0.001), ROI 4 (p value <0.001), ROI 5 (p value <0.001). Photodensity of ROI 2 was significantly different from ROI 3 (p value 0.005) and ROI 4 (p value <0.001). The photodensity of ROI 3 was significantly different from ROI 5 (p value 0.001). The photodensity of ROI 4 was significantly different from ROI 5 (p value <0.001).

4.2.2.1 ROI at one level of group

Pairwise comparisons were performed to compare ROI means, holding group (non-exercise) constant when ROI's were in a dorsal position. The tabulated data and actual significance values are within appendix 2 under the heading of 2.2.1.

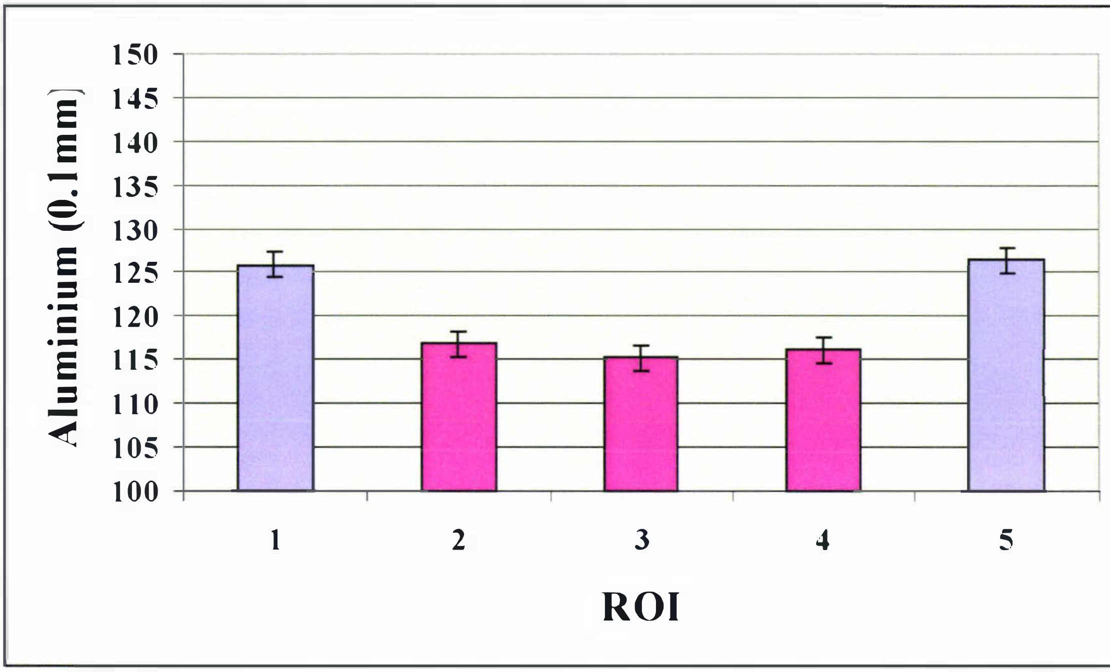

Figure 4.32: Column graph of the effect of the non-exercise group on photodensity of ROI's in a palmar position. Error bars represent +/- 1 s.e.m.

In the non-exercised group the photodensity of ROI 1 was significantly different from ROI 2 (p value <0.001), ROI 3 (p value <0.001) and ROI 4 (p value <0.001). The photodensity of ROI 2 was significantly different from ROI 5 (p value <0.001). The photodensity of ROI 3 was significantly different from ROI 5 (p value <0.001). The photodensity of ROI 4 was significantly different from ROI 5 (p value <0.001).

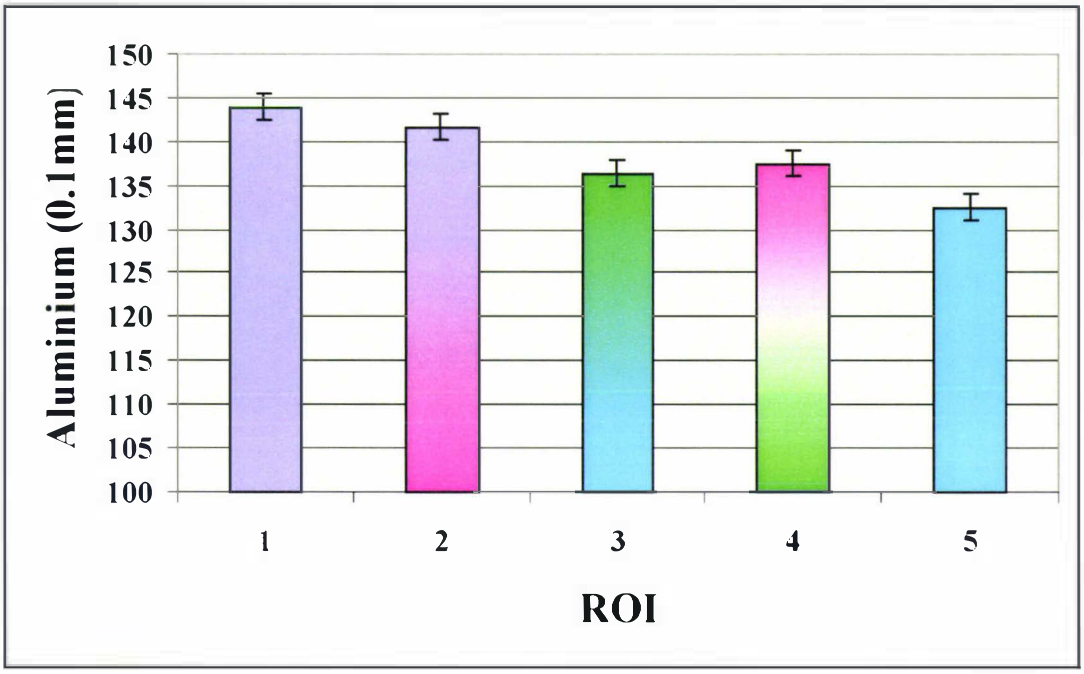

Figure 4.33: Column graph of the effect of exercise on the photodensity of ROI's in a palmar position. Error bars represent +/- 1 s.e.m.

In the exercised group the photodensity of ROI 1 was significantly different from ROI 3 (p value <0.001), ROI 4 (p value <0.001) and ROI 5 (p value <0.001). The photodensity of ROI 2 was significantly different from ROI 3 (p value 0.006) and ROI 5 (p value <0.001). The photodensity of ROI 4 was significantly different from ROI 5 (p value 0.009).

4.2.2.2 ROI at one level of angle

Pairwise comparisons were performed to compare ROI means, holding angle constant when ROI's were in a palmar position. The tabulated data and actual significance values are within appendix 2 under the heading of 2.2.2 .

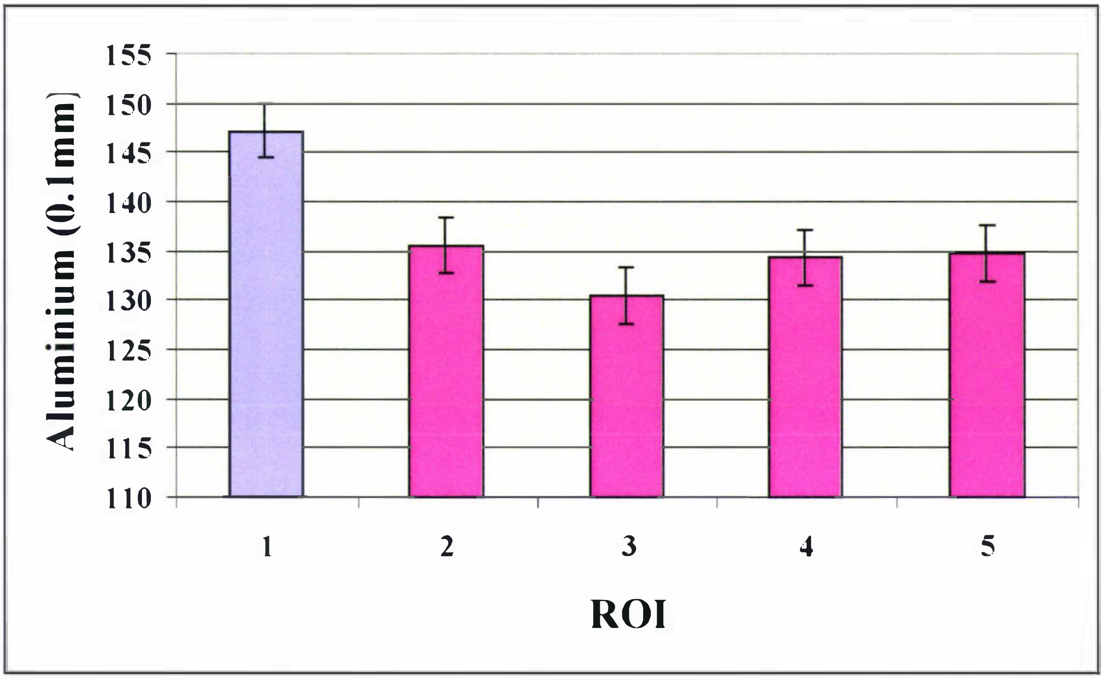

Figure 4.34: Column graph of the photodensity of ROI's in a palmar position when x-ray beam angle was 60 degrees. Error bars represent +/- 1 s.e.m.

At 60° the photodensity of ROI 1 was significantly different from ROI 2 (p value <0.001), ROI 3 (p value <0.001), ROI 4 (p value <0.001) and ROI 5 (p value <0.001).

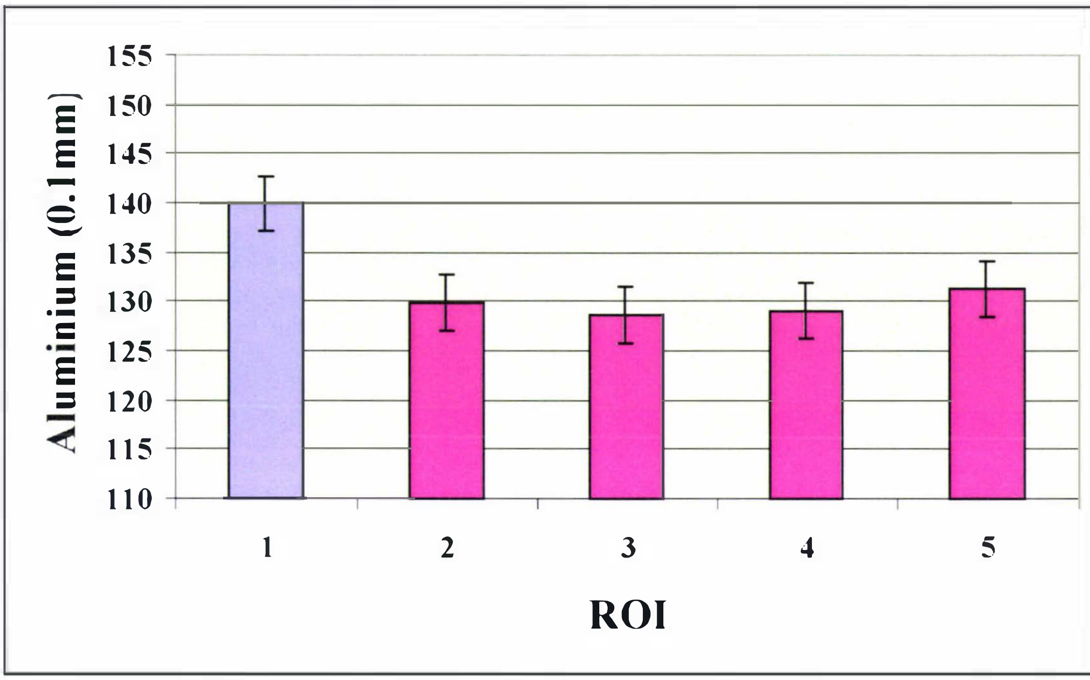

Figure 4.35: Column graph of the photodensity of ROI's in a palmar position when x-ray beam angle was 65 degrees. Error bars represent +/- 1 s.e.m.

At 65° the photodensity of ROI 1 was significantly different from ROI 2 (p value 0.004), ROI 3 (p value 0.001), ROI 4 (p value 0.001) and ROI 5 (p value 0.024).

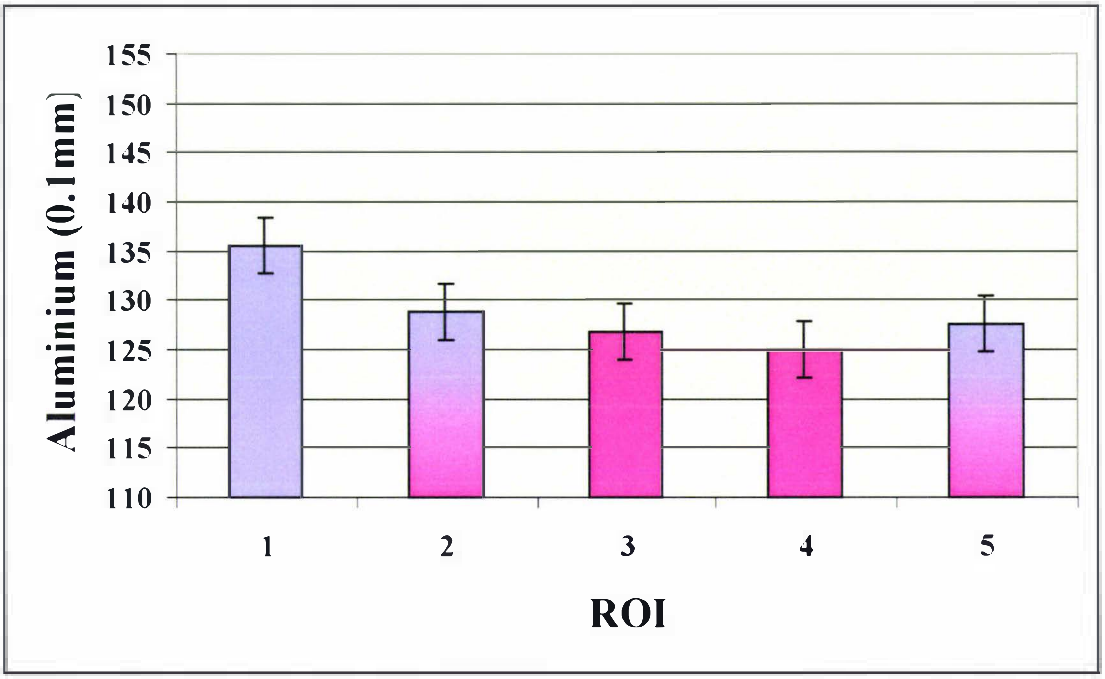

Figure 4.36: Column graph of the photodensity of ROI's in a palmar position when the angle was 70 degrees. Error bars represent +/- 1 s.e.m.

At 70° the photodensity of ROI 1 was significantly different from ROI 3 (p value 0.019) and ROI 4 (p value 0.002).

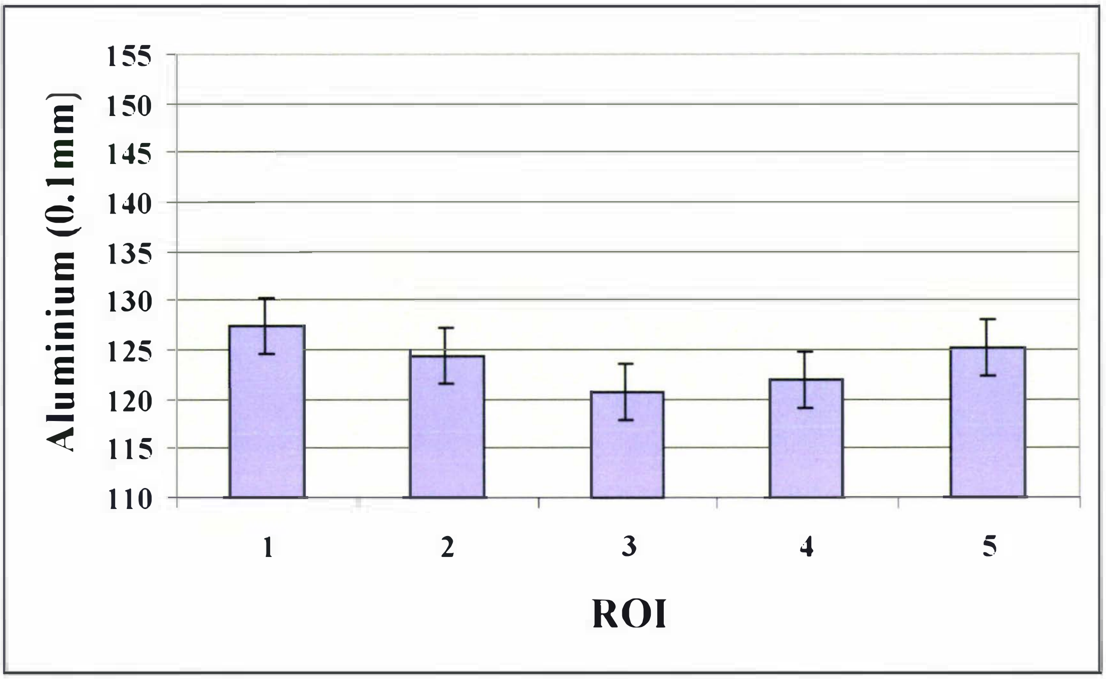

Figure 4.37: Column graph of the photodensity of ROI's in a palmar position when x-ray beam angle was 75 degrees. Error bars represent +/- 1 s.e.m.

When angle is 75° photodensity of each ROI was not significantly different from each other.

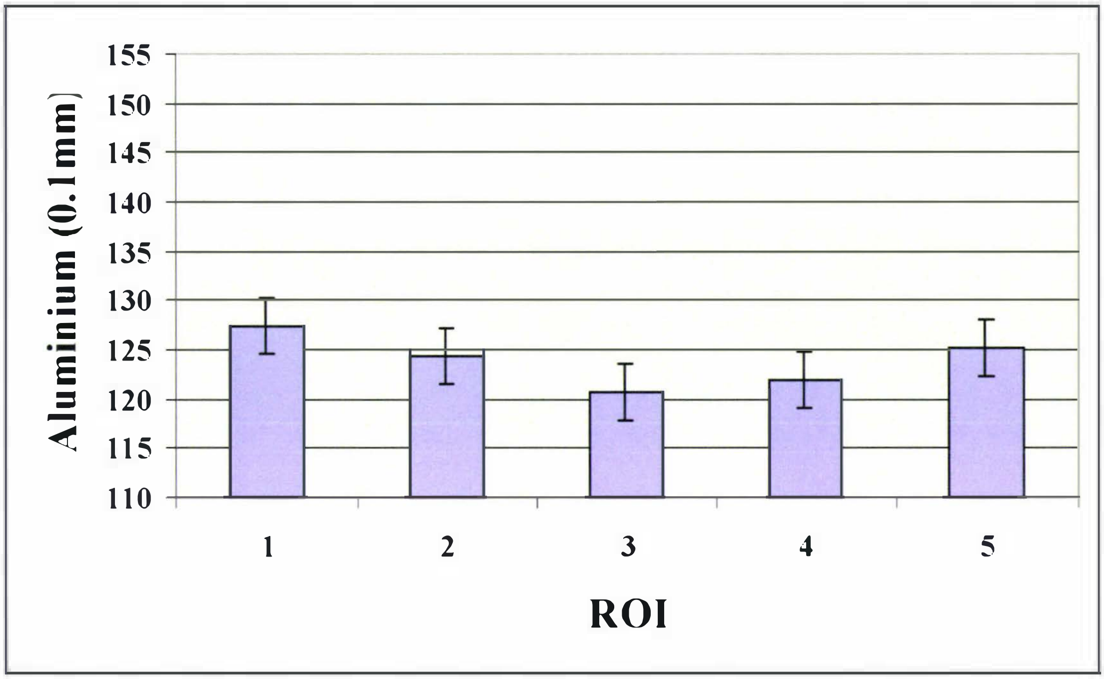

Figure 4.38: Column graph of the photodensity of ROI's in a palmar position when the angle was 80 degrees. Error bars represent +/- 1 s.e.m.

When angle is 80° photodensity of each ROI was not significantly different from each other.

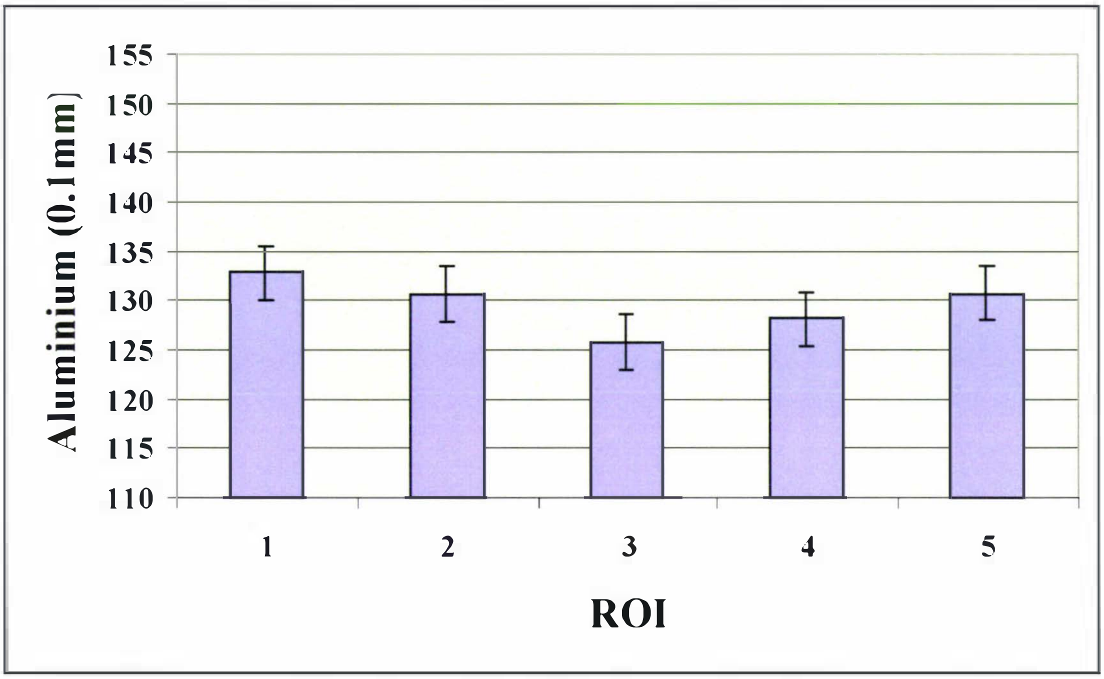

Figure 4.39: Column graph of photodensity of ROI's in a palmar position when angle was 85 degrees. Error bars represent +/- 1 s.e.m.

When angle is 85° photodensity of each ROI was not significantly different from each other.

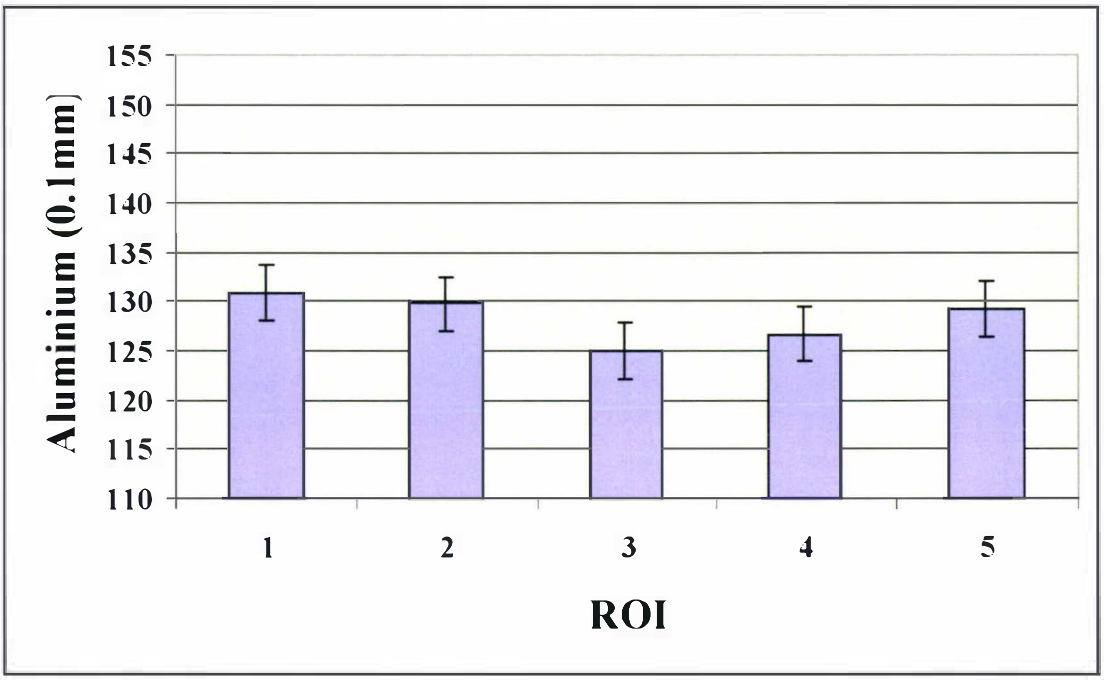

Figure 4.40: Column graph of photodensity of ROI's in a palmar position when angle was 90 degrees.

When angle was 90° photodensity of each ROI was not significantly different from each other.

Variation in angle appears to affect ROI photodensity, however the relationship between ROI's 1 to 5 appears similar at all angles. At all angles ROI 2, 3, 4 and 5 did not have significantly different photodensities. ROI 1's photodensity may significantly vary from the other ROI's depending on the angle.

4.2.3 Main effect of group

Pairwise comparisons were performed on the main effect of group when ROI were in a palmar position. The tabulated data and actual significance values are within appendix 2 under the heading of 2.3

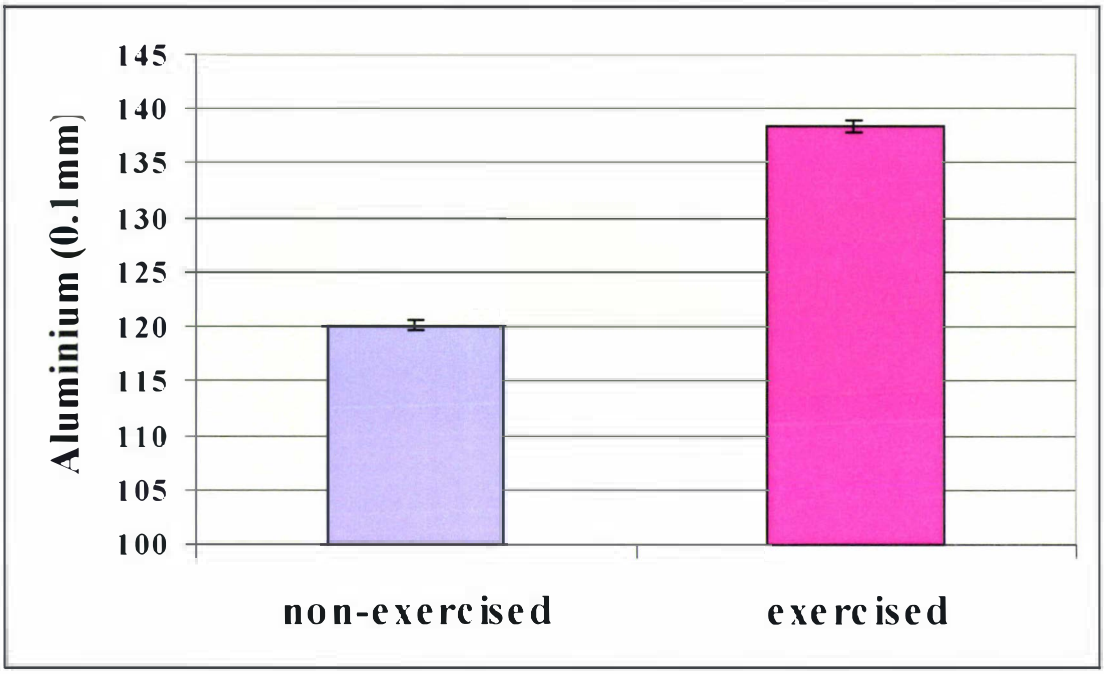

Figure 4.41: Column graph of the main effect of group on photodensity when ROI's were in a palmar position.

Photodensity of the non-exercised group was significantly different from the exercised group (p value <0.001).

4.2.3.1 Group at one level of angle

Pairwise comparisons were performed to compare group means, at varying angles when ROI's were in a palmar position. The tabulated data and actual significance values are within appendix 2 under the heading of 2.3.1.

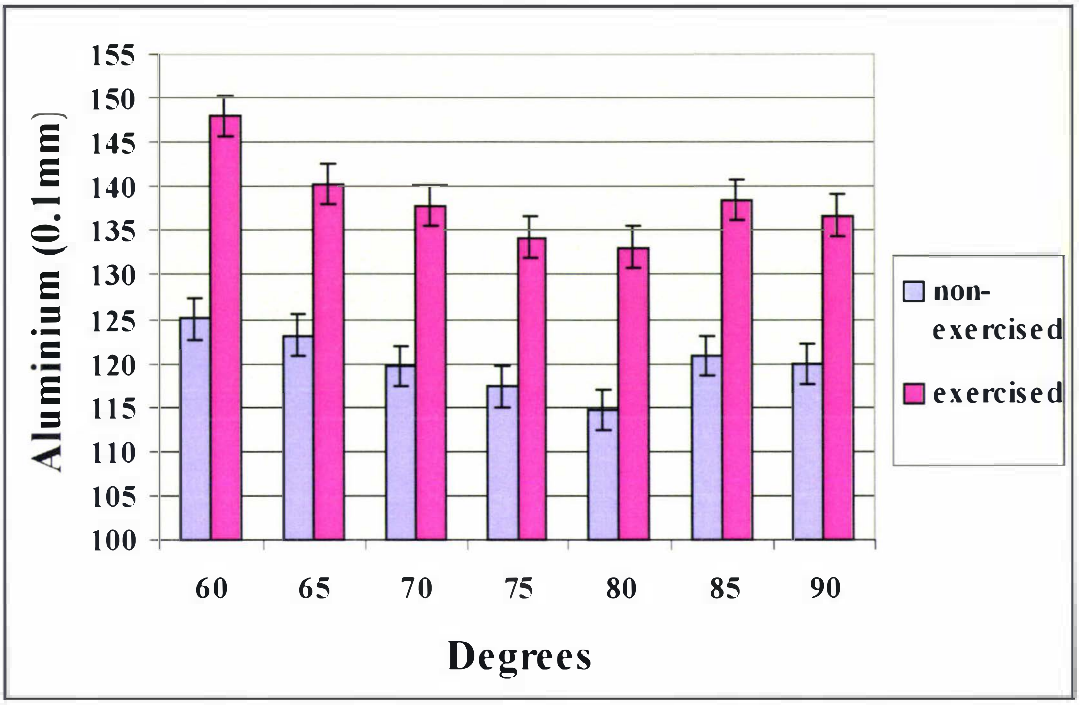

Figure 4.42: Column graph of the effect of x-ray beam angle on the photodensity of the exercised and non-exercised group.

Photodensity significantly increased between the non-exercised and the exercised group at 60° (p value <0.001), 65° (p value <0.001), 70° (p value <0.001), 75° (p value <0.001), 80° (p value <0.001), 85° (p value <0.001) and 90° (p value <0.001).

4.2.3.2 Group at one level of ROI

Pairwise comparisons were performed to compare group means, at varying ROI's when ROI's were in a palmar position. The tabulated data and actual significance values are within appendix 2 under the heading of 2.3.2.

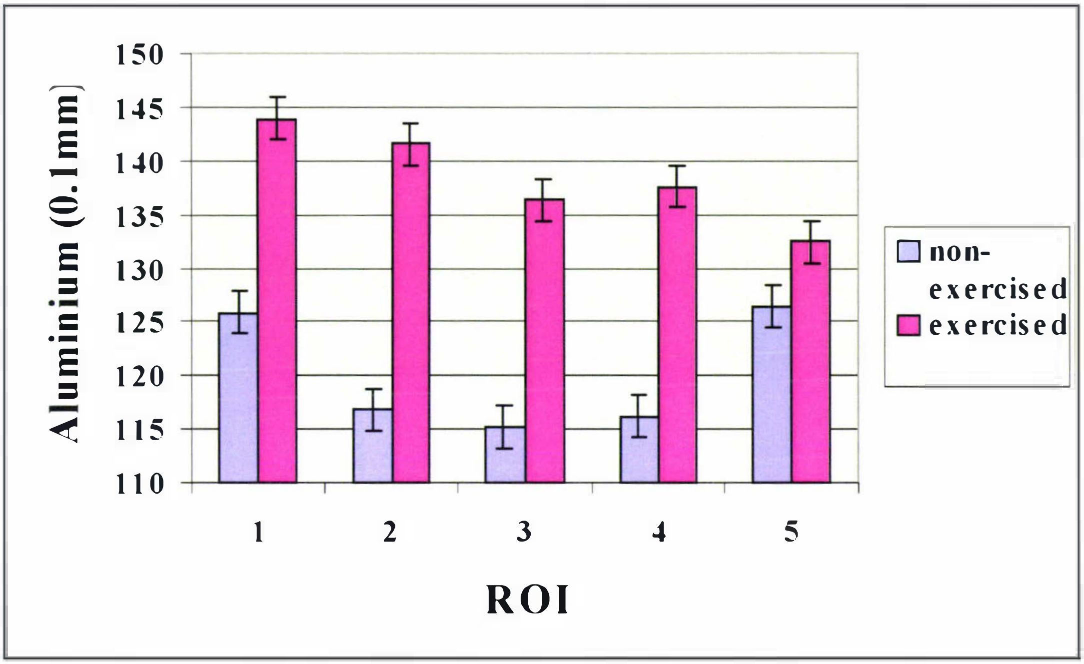

Figure 4.43: Column graph of the effect of group on the photodensity of ROI's in a palmar position.

Photodensity significantly increased from the non-exercised to the exercised group at ROI 1 (p value <0.001), ROI 2(p value <0.001), ROI 3(p value <0.001), ROI 4(p value <0.001) and ROI 5(p value 0.003). ROI 2 had the greatest increase in photodensity (17.5%) as a result of exercise. This was followed by ROI 4 (15%) and ROI 3 (15%), then ROI 1 (12.5%) and finally ROI 5 (4.5%).

4.3 Region of interest size analysis

The raw data is presented in appendix 1 under the heading ROI size analysis. The mean data is presented in appendix 2 under the heading of ROI size analysis.

Source		TypeIII Sum Of Squares	Degrees of Freedom	Mean Square	F Value	Significance
Intercept	Hypothesis Error	7341341.83 16296.99	1 12	7341341.83 1358.08[a]	5405.69	0.000
Angle	Hypothesis Error	7130.2 19801.50	1 348	7130.20 56.90[b]	125.31	0.000
Group	Hypothesis Error	43966.59 16296.91	1 12	43966.59 1358.08[a]	32.37	0.000
ROI	Hypothesis Error	505.19 19801.50	4 348	1258.80 56.80[b]	22.12	0.000
Radius	Hypothesis Error	22.67 19801.50	2 348	11.33 56.90[b]	0.19	0.819
Horse (Group)	Hypothesis Error	16296.91 19801.50	12 348	1358.08 56.90[b]	23.87	0.000
Angle /Group	Hypothesis Error	626.37 19801.50	1 348	626.37 56.90[b]	11.01	0.001
Angle/ROI	Hypothesis Error	2078.201 19801.50	4 348	519.55 56.90[b]	9.13	0.000
Angle /Radius	Hypothesis Error	492.22 19801.50	2 348	246.11 56.90[b]	4.32	0.014
Group/ROI	Hypothesis Error	3292.92 19801.50	4 348	823.23 56.90[b]	14.47	0.000
Group /Radius	Hypothesis Error	96.39 19801.50	2 348	48.19 56.90[b]	0.85	0.430
ROI/Radius	Hypothesis Error	290.46 19801.50	8 348	36.31 56.90[b]	0.64	0.746
Angle /Group/ROI	Hypothesis Error	62.59 19801.50	4 348	15.65 56.90[b]	0.27	0.894
Group/ROI/ Radius	Hypothesis Error	430.88 19801.50	8 348	56.86 56.90[b]	0.95	0.478
Angle/ROI/ Radius	Hypothesis Error	150.87 19801.50	8 348	18.86 56.90[b]	0.33	0.954
Angle/Group /Radius	Hypothesis Error	91.42 19801.50	2 348	45.71 56.90[b]	0.80	0.449
Angle/Group /ROI/Radius	Hypothesis Error	385.45 199801.50	2 348	48.18 56.90[b]	0.85	0.562

a. MS(Horse(Group))

b. MS(Error)

Table 4.3: A table of the overall ANOVA results for the ROI size analysis.

4.3.1 Main effect of radius size.

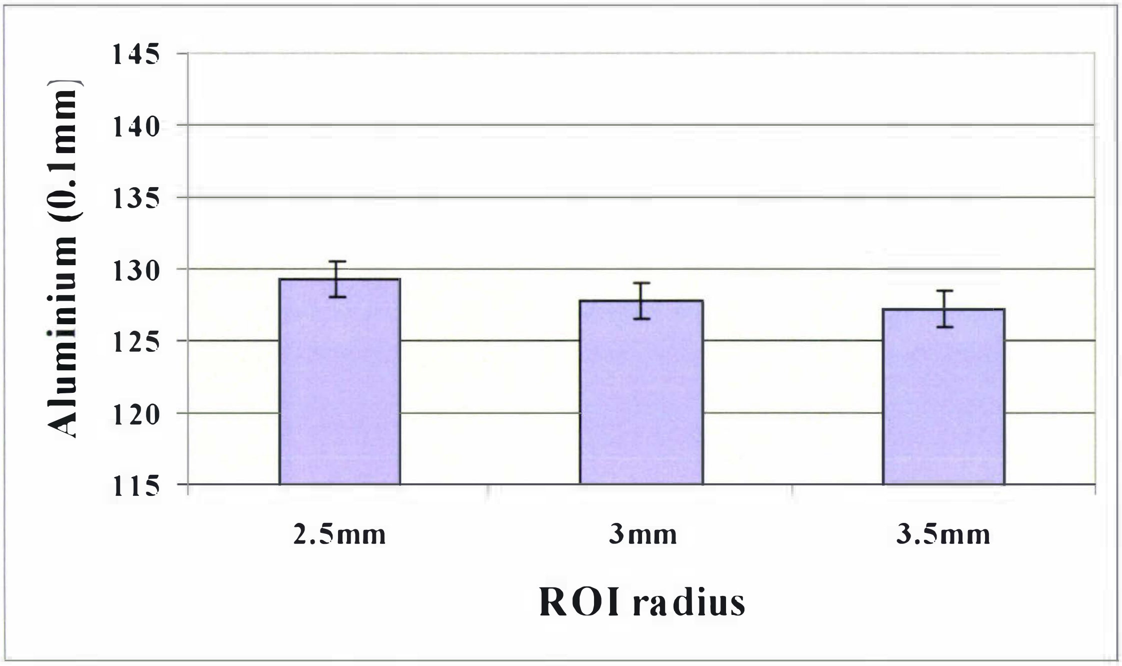

Figure 4.44: Column graph of the effect of ROI size when ROI's were in a palmar position.

ROI size did not significantly affect photodensity.

4.3.1.1 Different angles at one level of radius

Pairwise comparison were performed to compare between angle means while holding size of ROI constant The tabulated data and actual significance values are within appendix 2 under the heading of 3.1.1.

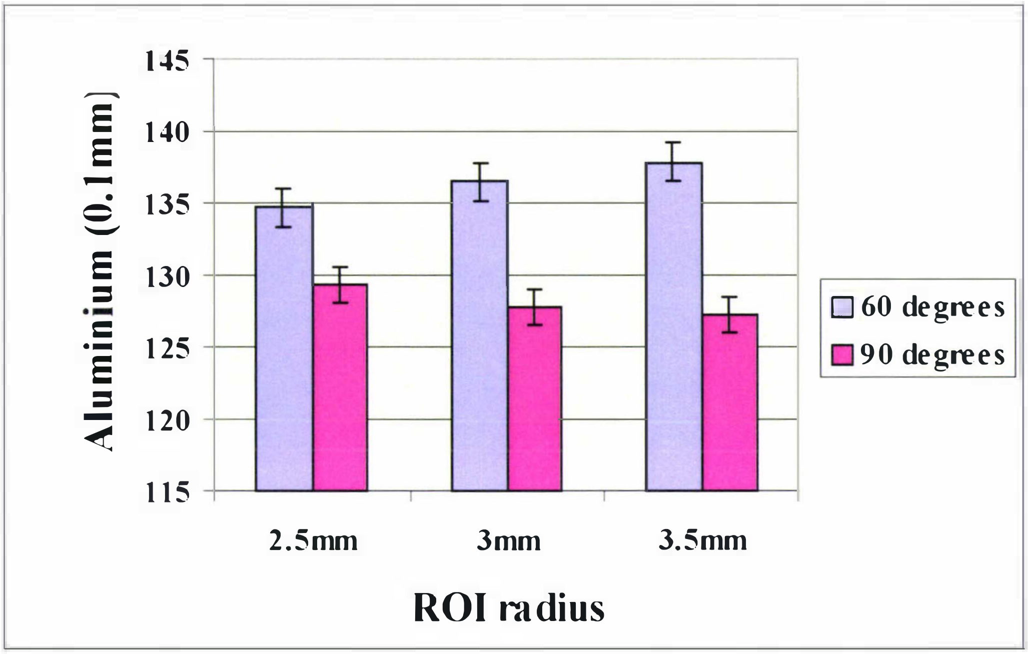

Figure 4.45: Column graph of the effect of x-ray beam angle on photodensity of ROI's at varying radius sizes.

The significant change in photodensity between 60° and 90° is similar between the 3 different ROI sizes.

4.3.1.2 Different radius size at one level of angle.

Pairwise comparisons were performed to compare ROI size while holding x-ray beam angle constant. The tabulated data and actual significance values are within appendix 2 under the heading of 3.1.2.

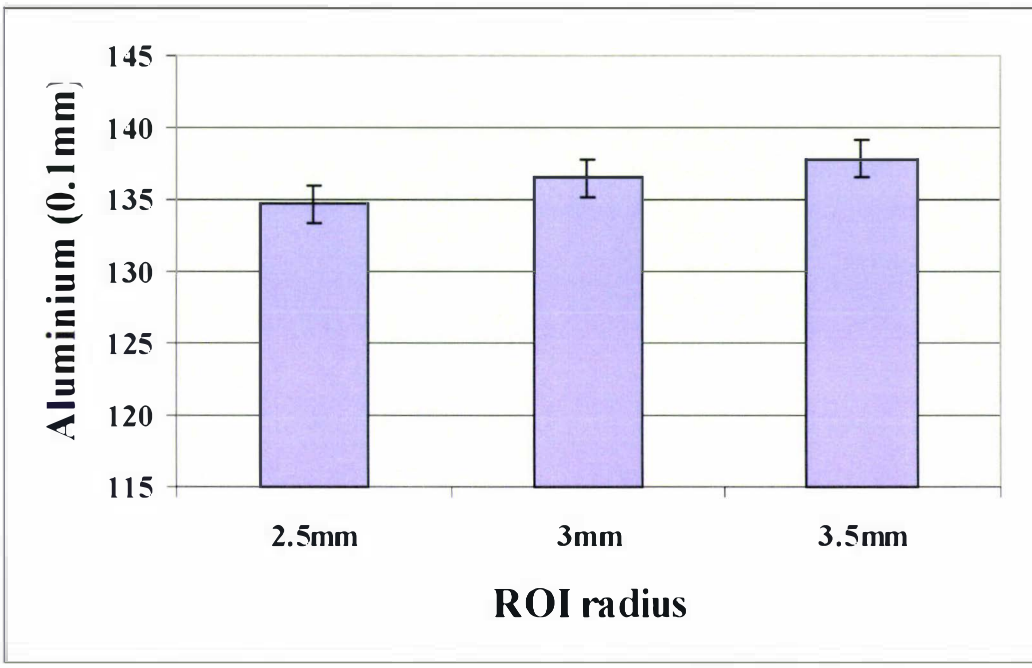

Figure 4.46: Column graph of the effect of ROI size on photodensity while holding the angle at 60 degrees.

There was no significant change in photodensity between ROI size at an x-ray beam angle of 60°.

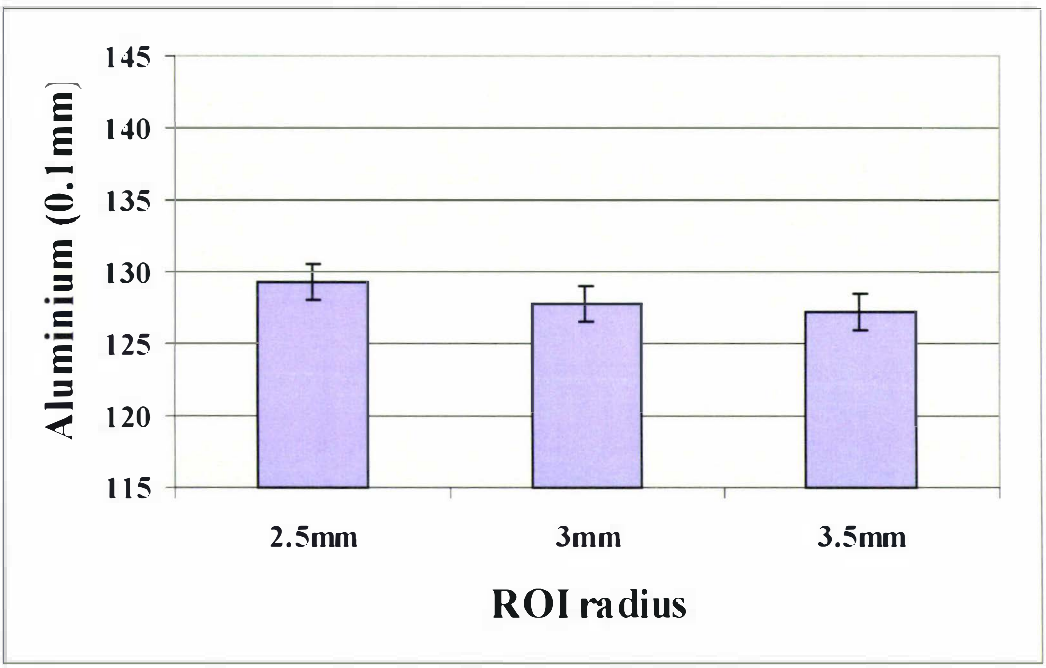

Figure 4.47: Column graph of the effect of ROI size while holding x-ray beam angle at 90 degrees.

There was no significant change in photodensity between ROI size when x-ray beam angle was 90°.

DISCUSSION

The object of this study was to determine if radioabsorptiometry (RA) could be used to objectively assess the variation in BMD of the dorsal part of C3. When using RA, BMD is characterised in computer units, which are calculated from photodensity. The difficulties associated with this conversion are discussed. Clarifying the effect of variation in angle on photodensity formed the basis of the first hypothesis. A discussion of these results is presented below. In attempting to confirm the hypothesis, additional information regarding ROI position and the effect of exercise on photodensity was considered. ROI size formed the basis of the second hypothesis and the results are analysed and discussed.

Radiographic assessment of C3 is best achieved using the tangential view. The tangential view of the distal row of carpal bones may be taken by 1 of 2 radiographic methods, each of which is reviewed, as well as the difficulties in determining which view more accurately assesses photodensity. The relevance of this study and the clinical application of RA in detecting changes in C3 are contemplated, as is the accuracy of the subjective assessment of photodensity of C3.

5.1 Photodensity in relation to BMD

Photodensity of bone can be accurately determined in terms of aluminium equivalents, because the atomic number and specific gravity of aluminium is similar to that of bone. Aluminium is homogeneous, pure and relatively stable, and therefore it has been used extensively in RA.[61 63 64]

Although photodensity of bone mineral can be accurately measured by aluminium, conversion to bone mineral concentration is more complex.[63] Additional factors that are involved are attenuation of photons by the bone and aluminium, the role of scatter and photon/film interactions. The predominant photon interactions that occur at the kilovoltage level used in this study are photoelectric. This type of interaction is dependent on atomic number and results in total absorption of photons. A small number of interactions, likely to be less than 10% at the kilovoltage used in this study result from Compton interactions, which cause scatter, and reduction in the quality of the image. Therefore, in order to accurately convert photodensity into bone mineral density the effect of these interactions must be taken into consideration. The advent of computer assisted RA has enabled these interactions to be accounted for by using a series of complex equations.[63] However, in doing so an assumption is made that the x-ray beam is effectively homogeneous, which is unlikely to be true.

Within this study the effect of scatter and the absorption coefficient at the kilovoltage used could not been accounted for. It is suspected that Compton interactions were a constant between views, as these interactions are not affected by atomic number, rather by kilovoltage used, and in this experiment the same kilovoltage was used each time. Therefore the results of this study are discussed in terms of photodensity, using a scale of aluminium thickness, and not as BMD, using a scale of computer units. Because a measure of BMD is not being used, comparison to studies using other methods of non-invasive bone mineral analysis is based on the assumption that photodensity in terms of millimetres of aluminium is directly proportional to BMD.

5.2 Effect of angle on photodensity

When performing peripheral skeletal radiography in humans the relationship between x-ray beam and object can be kept constant. However when imaging C3 using the tangential view of the carpus in horses, the object (C3)-beam angle is difficult to accurately replicate, especially in equine clinical practice conditions. Therefore, it was necessary to establish if small variations in C3 beam angle significantly affected photodensity. Isolated distal rows of carpal bones lying flat on an x-ray cassette were used, and thus the plate-beam angle, C3-beam angle and x-ray beam angles were identical. The significance of variation in angle was determined at 90°, the recommended x-ray beam angle used in RA studies of human small bones[63,64], as well as at 60°, which is the C3-beam angle recommended in the literature for the tangential view of the distal row of carpal bones in the horse.[82]

In this study the ROI's were initially placed in a dorsal position (6mm from the dorsal edge at 90°), which is in the zone visualised by the tangential view. Variations in angle less than 10° from 90° significantly affected photodensity in these ROI's. This was supported by the significant main effect of angle and the angle/ ROI interaction. ROI's 2, 3, 4 and 5 all followed the same pattern, the exception being ROI 1 where no significant difference in photodensity with variation in angle was observed.

Variation in angle of less than 10° from 60° appeared to significantly affect photodensity. This was supported by analysis of the angle/ ROI interaction. The results demonstrated that photodensity is minimally affected when C3 beam angle is varied between the angle 70° and 80°. However, clinically this is not useful, because when the tangential view is taken at these angles superimposition of the proximal row of carpal bones prevents adequate visualisation of the dorsal aspect of the distal row of carpal bones.

The analysis of the dorsal ROI's demonstrated that as x-ray beam angle was reduced, photodensity decreased. It was postulated that as the x-ray beam angle decreased from 90° the distance travelled through the bone increased. As the ROI's were placed in such a dorsal position, once the angle was less than 85° the dorsodistal aspect of C3 was not penetrated by the x-ray beam. This effect increased as the angle continued to decrease. Thus it was proposed that if ROI's were placed in a more palmar site, a stepwise reduction of C3 beam angle would result in a stepwise increase in photodensity as the distance the x-ray beam travelled though the bone increased. As discussed in the materials and methods, the calibrated images were reprocessed with the ROI's placed in a more palmar site. The results were statistically analysed and photodensity did increase as angle reduced. This was supported by the main effect of angle and angle/ROI comparisons.

Photodensity significantly changes when the angle is varied by more than 5° from 90° and less than 5° from 60°. In both the dorsal and palmar ROI placements this is likely to be due to increased travelling distance of the radiographic beam through bone: at 10° from 90° the beam traverses 1.5% further and at 10° from 60° it traverses a further 7.8% through C3. The increase in distance travelled through the bone appears to be inversely proportional to Sin (x-ray beam angle). Therefore a small deviation from an x-ray beam angle of 90°, only slightly increases the distance travelled though the bone. However the same small deviation from an x-ray beam angle of 60° results in a substantially greater distance travelled through the bone. This form of variation may explain why a change of less than 5° from 60° is required before photodensity significantly changes whereas a change of less than 10° is required from 90° before photodensity significantly changes.

Loading within C3 is predominately uniaxial, which results in the trabeculae developing a columnar structure with cylindrical symmetry. The columns of bone are orientated in a vertical direction, and thus the bone has a high stiffness and strength in the direction when loaded in a sagittal direction and reduced strength and stiffness if loaded in a transverse direction.[87] The orientation of the columns results in a honeycomb like morphology. When the x-ray beam traverses through the bone at 90° and most likely at 85° it is reasonable to suggest the x-ray beam travels through the columns, resulting in a lower photodensity. At greater beam angles, it traverses the trabecular columns obliquely and therefore passing through a greater volume of bone relative to the more vertical angles. This results in a higher photodensity. The morphology of C3 may explain why a variation of 10° from 90° results in a significant change in photodensity when the distance traversed through the bone compared to a variation of 10° from 60°, is relatively small.

To the author's knowledge the effect of variation in angle on photodensity when applied to RA has not been documented. The findings of this study indicate that due care must be taken in application of object-beam angle (in this case C3-beam angle) when radiographing areas for analysis using RA. The findings also suggest that care should be taken when comparing tangential views of C3 (taken at a C3-beam angle of 65°) to radiographs of isolated C3's taken at 90°. Our results indicate that variation in angle of 25° significantly affects photodensity, and objectively there is unlikely to be a good correlation between the 2 views. These results are in direct contrast to the study by Ulhorn.[45] in which there was a significant relationship between the photodensity taken at a C3-beam angle of 65° and those taken at 90°. The likely reason for this is that the radiographs were compared subjectively rather than quantitatively.

5.3 Effect of ROI on photodensity

Five ROI's were chosen within the distal carpal row. ROI 1 and 2 were within the radial facet of C3 and ROI 3 and 4 were within the intermediate facet of C3. ROI 5 was within C4. The photodensity of the ROI's varied within C3, when the ROI's were positioned dorsally. Within this study, at 60° (C3-beam angle of the tangential view) dorsal ROI placement resulted in photodensity of the abaxial aspect of the radial facet being significantly higher than the rest of C3. The photodensity of the axial aspect of the radial facet, and both aspects of the intermediate facet were not significantly different. When the radiographs were taken at a C3-beam angle of 90° with ROI's placed dorsally, the photodensities of the radial facet and the axial aspect of the intermediate facet were not significantly different. The abaxial aspect of the intermediate facet had a significantly different photodensity to the axial aspect of the radial facet but not the other ROI's. The discrepancy of photodensity of the abaxial aspect of the radial facet between the 2 angles is thought to be due to the prominent transverse ridge that is present on the medial dorsocentral aspect of C3. When the C3-beam angle is at 60° the amount of bone travelled through is significantly higher at the abaxial aspect of the radial facet when compared to the rest of C3, whereas when the C3-beam angle is 90° the x-ray beam does not travel through the bone on the dorsocentral aspect of the radial facet.

In all microradiographic and BMD studies, C3 has been assessed in a proximodorsal or lateromedial direction, and comparison with the present study can be made only with data collected at a C3-beam angle of 90°. A study assessing subchondral bone stiffness and bone density of C3 found no change in stiffness between the intermediate and radial facets in trained horses.[31] This has also been found when objectively assessing the BMD of C3 using DXA.[44] In both studies there was only 1 area of interest in the radial facet and 1 in the intermediate facet of C3. In the study by Young [31] the area of interest in the radial facet was between ROI 1 and 2, and between ROI 3 and 4 in the intermediate facet. In the study by Firth [44] the area of interest in the radial facet was in a similar position to ROI 2 and in the intermediate facet it was in a similar position to ROI3. The results from the present study support those reported by Young[31] and Firth[44].

ROI 5 was within C4 and the mean photodensity as well as photodensities of individual horses was always within the range of photodensities present in C3. To the author's knowledge there have been no studies objectively assessing photodensity of C4. C4 has been suggested as a control when subjectively assessing the photodensity of C3 from the tangential radiographic view,[48,50] which means that C3 is classified as not sclerotic if the subjective photodensity and trabeculation is the same as that of C4. The objective assessment of photodensity at a C3-beam angle of 60° in this study indicates that the photodensity of C4 is similar to that of the axial aspect of the radial facet, is significantly less than the abaxial aspect of the radial facet, and is significantly more than the axial aspect of the intermediate facet. When C3-beam angle is 90° the photodensity of C4 is not significantly different from any ROI in C3 in this study. These findings suggest that radiographing C3 using the tangential view causes the abaxial radial facet to be more photodense than C4, perhaps resulting in false positive diagnoses of sclerosis in the radial facet.

5.4 Effect of exercise on photodensity

The bones used in this experiment came from horses used in an exercise study: one group was exercised in a training programme typical of that used to condition horses for racing in New Zealand. The other group remained in small yards for the duration of the study. The results indicate that exercise significantly affects the photodensity of all ROI's in the dorsal aspect of C3. In the exercised group of horses it appears that the axial aspect of the radial facet had the greatest increase in photodensity, followed by the intermediate facet and then the abaxial aspect of the radial facet. Therefore the 2 ROI's within the radial facet, and the 2 ROI's within the intermediate facet were not significantly different from each other, however the radial and intermediate facets were significantly different from each other. These results support those of Firth [44, 88] who found that exercise resulted in increased BMD of C3.

Exercise significantly affected photodensity of C4 and as a result C4 post exercise had a photodensity not significantly different from the intermediate facet in this group of horses. As these horses did not appear to have pathological changes in their C3's no comment can be made as to whether C4 continues to model or if it reaches a particular BMD and remodels only. This study indicates that C4 responds to the same stresses as C3 and models accordingly, which may place doubt on whether C4 should be used as a radiographic control.

5.5 Effect of ROI size on photodensity

It was unknown if ROI size significantly would affect photodensity when x-ray beam angles were varied. The ROI size was changed by 19mm^2, increasing from 2.5mm to 3.5mm radii, and this change in size did not significantly affect photodensity. The relationship between photodensity at 60° and 90° did not change with ROI size. To the author's knowledge, the effect of ROI size has not been examined when the angle of examination is 90° or if object -beam angle is varied. These results suggest that in bones of the size and morphology of C3 with a relatively uniform photodensity, ROI size can be altered to suit the study.

5.6 View A Compared to View B - Which is the more accurate view?

View A and B both assess the dorsal margin of the distal row of carpal bones. However, it is likely that only the proximo-dorsal and centro-dorsal aspect of this row of carpal bones is imaged. Although the two views assess the same area of interest, the radiographic image of each differs markedly. This difference is due solely to plate angle, as x-ray beam angle, C3 beam angle and leg angle are the same. When using View B the plate-beam angle is not at 90° to the x-ray beam as in View A and the geometry of image formation is disrupted, leading to distortion of the radiographic image and an inaccurate image of the distal row of carpal bone. Distortion results in loss of definition and blurring of the image and this affects subjective interpretation.[89] When using View A the plate is at 90° to the x-ray beam and minimal distortion of the image occurs. However the object film-focal distance is a relatively large distance when compared to View B and this results in magnification of the radiographic image that increases marginal blurring.[90] Subjectively, View A appears to be less blurred than View B, although when compared to radiographs of isolated distal rows of carpal bones taken at the same C3 beam angle, both views are obviously blurred.

Although both View A and B are used to assess the dorsal aspect of C3, the radiographic images produced are different. In order to determine if one view more accurately assesses photodensity the exact same ROI's must be identified. Once the radiographs were digitised the images were manipulated to appear as if they were taken at the same plate-beam angle and object-film distance. The distortion of View B and the magnification of View A were thus corrected for in the digitised image. Even when the images were manipulated identical placement of ROI's was difficult to achieve and any small variation in placement resulted in error. The reason for this was that in the manipulated images the dorsal aspect of C3 had a linear increase in photodensity rather than the relatively uniform density quantified in the isolated C3's. The ROI size used had a radius of 1mm, which is significantly smaller than those used in the rest of the study. Such a small size was required in order to measure the photodensity of the area of interest without including the superimposition of either MCIII or the proximal row of carpal bones. The small size of the ROI's may have resulted in a higher error associated with ROI placement than if larger ROI's had been used. In determining which view more accurately assessed photodensity, an additional proven accurate method of non-invasive bone mineral analysis was required to establish the true BMD of the area of C3 visualised in each tangential view. This was not possible within the present study. Considering all the above-mentioned problems it was not possible to determine which view more accurately assesses photodensity.

5.7 Relevance of this study

This study has provided important information on the effect of variation of angle when assessing the photodensity of a bone at an object-beam angle of 90°. In many articles discussing the technique of RA the angle at which the radiograph was taken was not specified but assumed by this author to be 90°.[62-64] As this study indicates that variation in x-ray beam angle of between 5° and 10° significantly affects photodensity it is recommended to take due care in determining x-ray beam angle. Difficulties may arise when different machines are used, and the inclusion of a cube in the radiograph to determine plate-beam angle may be useful to ensure x-ray beam angles are similar between operators and machines.

The clinical usefulness of this technique appears to be limited because it is imperative to ensure that C3-beam angle can be replicated within 5° every time the tangential view is taken, which involves ensuring that x-ray beam angle and leg angle can be accurately replicated each time. X-ray beam angle is challenging to replicate in a clinical situation when taking the tangential view. However, leg angle, which directly affects C3-beam angle, is even more difficult to accurately replicate in a clinical situation, and natural variation of C3 position within the carpus between horses may result in a differing C3-beam angle despite leg angle remaining constant. This study indicates that because small variation in C3-beam angle significantly affects photodensity and C3-beam angle is difficult to reproduce accurately, RA may not be clinically applicable in assessment of BMD of C3 under current practical constraints involved in taking radiographs in the live animal.

5.8 Sources of error

A number of accuracy studies have been performed on RA in humans and the technique has been determined to be accurate.[62 63] In this study accuracy validation has not been performed because identification of ROI's with an alternate method of non-invasive bone mineral analysis was not possible. However the study has assumed a directly proportional relationship between photodensity and BMD and the results are comparable to other BMD studies performed on C3.

5.9 Critique of the subjective assessment of photodensity of C3

A complete radiographic series of the carpus includes the tangential view,[48 50] which is useful in detecting the presence of fractures and possibly the presence of lucent areas other than vascular channels.[91] In the past it has been thought that the tangential view was useful for the detection of pathological changes in BMD of C3 likely to precede fracture.[48] This evaluation has been purely subjective and a number of studies have demonstrated that the subjective assessment of radiographs is relatively inaccurate method,[54] but may provide a broad guide to BMD assessment.[55] One study has specifically considered the accuracy of assessment of bone density using the tangential view and found it to be an accurate method to detect radiographic sclerosis.[45] The visual assessment of C3 sclerosis in that study was based on a subjective grading system modified from O'Brien.[50] Using a uniform point count procedure to determine bone density, the authors concluded that sclerotic C3's could be differentiated from non-sclerotic C3's. However, differentiation between mild, moderate and severe sclerosis was problematical, and it was not stated if the little variation in bone density measurements present was statistically significant. The study also found that subjectively there was good agreement between the tangential view (C3-beam angle 60°) and the proximodistal view (C3-beam angle 90°), in direct contrast to the present study in which photodensities at a C3 beam angle of 60° and at 90° were significantly different. However it is possible that subjectively this difference in photodensity may not be detectable.

The aim of this study was to apply the technique of RA to the tangential view of C3. As small variation in angle significantly affects photodensity and C3-beam angle can not be accurately reproduced between horses, or on repeated radiographs of the same horse (under practice or even hospital conditions), the accurate objective assessment of photodensity of C3 is thought not to be clinically applicable at this time. Given that objective assessment of photodensity is considered to be a more accurate assessment of BMD than subjective assessment,[63,61] the indirect conclusion of this study is that the current method of subjective evaluation of photodensity of C3 using the tangential view is relatively inaccurate. Although not apparent when differentiating between radiographically sclerotic and non-sclerotic C3's, the inaccuracies of subjective assessment become obvious when distinguishing between the varying grades of sclerosis. This is an important point as some degree of radiographic sclerosis is considered physiological and it is currently unknown when sclerosis becomes pathological. A recent retrospective study evaluating sclerosis of C3 supports this, as no significant relationship between C3 sclerosis, lameness or prognosis was found.[91]

5.10 Further research

Although this technique does not appear to be clinically applicable for assessment of C3, it may have other applications when object-beam angle can be accurately reproduced. In order for this to occur, accuracy studies comparing the technique to another method of non-invasive bone mineral analysis would be important.

5.11 Conclusion

RA does not appear to be clinically applicable in the determination of photodensity of C3 as the first null hypothesis: "photodensity is not affected by small variations in C3-beam angle" was disproved. This result also has connotations for the use of the RA in humans. This study substantiates work by other authors regarding regional differences in BMD of C3 as well as the effect of exercise on C3, and it is believed to be the first study to objectively assess C4. The second hypothesis of the study, "ROI size does not significantly affect mean photodensity over a 30° variation in x-ray beam angle (from 90° to 60°)", was sustained.

The tangential view of C3 can be taken by 1 of 2 methods, each of which has disadvantages. At this time, it remains unclear which view more accurately assesses photodensity of C3. Because of the effect of x-ray beam angle on photodensity, objective assessment of photodensity is likely to be inaccurate in the clinical situation. Therefore, current methods of subjective assessment[50] are also likely to be inaccurate and should be used cautiously.

REFERENCE LIST

1. L.Jeffcott. P.Rossdale. J.Freestone. C.J.Frank. P.F.Towers-Clark. An assessment of wastage in Thoroughbred racing from conception to 4 years of age. *Equine Veterinary Journal* 1982;14:185-98.

2. P. Rossdale. R.Hopes. N.Winfield Digby. K.Offord. Epidemiological study of wastage among racehorses 1982 and 1983. *Veterinary Record* 1985;116:66-9.

3. A.Lindner. P.von Wittke. A.Dingerkus. M.Temme. H.Sommer. Causes and rates of training failure in Thoroughbreds. *Equine Athlete* 1992;5:3-7.

4. H.O.Mohammed. T.Hill. J.Lowe. Risk factors associated with injuries in Thoroughbred horses. *Equine Veterinary Journal* 1991;23:445-8.

5. J.H.Wilson. S.B.Howe. R.C.Jensen. R.A.Robinson. Injuries sustained during racing at racetracks in the U.S. in 1992. *Proceedings of the American Association of Equine Practitioners.* 1993; 39:267-268.

6. Y.Mizuno. Fractures of the carpus in racing Thoroughbreds of the Japan racing association: prevalence. location and current modes of surgical therapy. *Journal of Equine Vetereinary Science* 1996;16:25-31.

7. R.D.Park. J.P.Morgan. T.O'Brien. Chip fractures in the carpus of the horse: a radiographic study of their incidence and location. *Journal of American Veterinary Medical Association* 1970;15:1305-1311.

8. C.W.McIlwraith. Fractures of the carpus. In A.J.Nixon. eds. *Equine Fracture Repair*. W.B.Saunders. United States of America. 1996:208-21.

9. J.M.Lucas. M.W.Ross. D.W.Richardson. Post operative performance of racing Standardbreds treated arthroscopically for carpal chip fractures: 176 cases (1986-1993). *Equine Veterinary Journal* 1999:31:48-52.

10. S.E.Palmer. Prevalence of carpal fractures in Thoroughbred and Standardbred racehorses. *Journal of American Veterinary Association* 1986;188:1171-3.

11. R.K Schneider. L.R.Bramlage. A.A.Gabel. L.M.Barone. B.M.Kantroitz. Incidence. location and classification of 371 third carpal bone fractures in 313 horses. *Equine Veterinary Journal Supplement* 1988;Supplement 6:33-42.

12. P.R.Stephens. D.W.Richardson. P.A.Spencer. Slab fractures of the third carpal bone in Standardbreds and Thoroughbreds: 155 cases (1977-1984). *Journal of American Veterinary Medical Association* 1988;193:353-358.

13. G.S.Martin. P.F.Haynes. J.R.McClure. Effect of third carpal slab fracture and repair on racing performance in Thoroughbred horses:31 cases (1977-1984). *Journal of American Veterinary Medical Association* 1988:193:107-110.

14. C.W.McIlwratih. J.V.Yovich. G.S.Martin. Arthroscopic surgery for the treatment of osteochondral chip fractures in the equine carpus. *Journal of American Veterinary Medical Association* 1987:19:531-40.

15. N.J.Kannegieter. N.Ryan. Racing performance of Thoroughbred horses after arthroscopic surgery of the carpus. *Australian Veterinary Journal* 1991:68:258-60.

16. D.W.Richardson. Technique for the arthroscopic repair of third carpal bone slab fractures in the horse. *Journal of American Veterinary Medical Association* 1986:188:288-91.

17. R.M.Moore. R.K.Schneider. Arthroscopic findings in the carpal joints of lame horses without radiographically visible abnormalities: 41 cases (1986-1991). *Journal of American Veterinary Association* 1995:206:1741-6.

18. M.W.Ross. D.W.Richardson. G.A.Berzoa. Subchondral lucency of the third carpal bone in Standardbred racehorses. *Journal of American Veterinary Medical Association* 1989:195:789-794.

19. R.J.Todhunter. Anatomy and physiology of synovial joints. In C.W.McIlwraith. G.W.Trotter. eds. *Joint Disease in the Horse.* W.B.Saunders. Philadelphia. 1996:9-19.

20. R.R.Pool. Pathologic manifestations of joint disease in the athletic horse. In C.W.McIlwraith. G.W.Trotter. eds. *Joint Disease in the Horse.* W.B.Saunders. Phildelphia. 1996:91-6.

21. J.L.Palmer. A.L.Bertone. Joint biomechanics in the pathogenesis of traumatic arthritis. In C.W.McIlwraith and G.W.Trotter. eds. *Joint Disease in the Horse.* W.B.Saunders. Philidelphia. 1996:110-1.

22. C.W.McIlwraith. General pathobiology of the joint and response to injury. In C.W.McIlwraith. G.W.Trotter. eds. *Joint disease in the Horse.* W.B.Saunders. Philadelphia. 1996:40-70.

23. H.R.Kerr. B.Warbuston. Surface rheological properties of hyaluronic acid solutions. *Biorheology* 1985:22:133-44.

24. E.L.Radin. H.G.Parker. J.W.Pugh. R.S.Steinberg. I.L.Paul. R.M.Rose. Response of joints to impact loading III: relationship between trabecular microfractures and cartilage degeneration. *Journal of Biomechanics* 1973:6:51-7.

25. D.B.Burr. M.B.Schaflet. The involvement of subchondral mineralized tissues in osteoarthrosis: Quantitative microscopic evidence. *Microscopic Research and Technique* 1997:37:343-57.

26. P.G.Bullough. The geometry of diarthrodial joints. its physiological maintenance and the possible significance of age-related changes in the geometry to load distribution and the development of osteoarthritis. *Clinical Orthopedic Related Reseach* 1981:156:61-6.

27. T.M.Keaveny. W.C.Hayes. Mechanical properties of cortical and trabecular bone. In B.K.Hall, eds. *Bone Growth - B.* CRC Press Inc. United States of America. 1993:285-344.

28. D.Resnick, S.C.Mangolagas, G.Niwayama, M.D.Fallon. Histogenesis, anatomy and physiology of bone. In D.Resnick, eds. *Diagnosis of Bone and Joint Disorders.* W.B.Saunders, Philadelphia, 1995:617-24.

29. M.C.Michel, P.K.Zysset, W.C.Hayes. Fatigue behaviour of trabecular bone. *Transactions of the Orthopaedic Research Society.* 1991;16:156 referred to by T.M.Keaveny, W.C.Hayes. Mechanical properties of cortical and trabecular bone. In B.Hall *Bone-Bone Growth-B.* CRC Press, London, 1993;7:335.

30. D.R.Carter, D.M.Spengler. Mechanical properties and composition of cortical bone. *Clinical Orthopedics* 1978;135:192-217.

31. D.R.Young, D.W.Richardson, M.D.Markel, D.M.Nunamaker. Mechanical and morphometric analysis of the third carpal bone in Thoroughbreds. *American Journal of Veterinary Research* 1991;52:402-409.

32. R.Getty. Equine osteology. In R Getty, eds. *Sisson and Grossman's The anatomy of the Domestic Animals.* W.B.Saunders, London, 1975:286-9.

33. E.C.Firth, W.Hartman. An in vitro study on joint fitting and cartilage thickness in the radiocarpal joint of foals. *Research in Veterinary Science* 1983:34:320-6.

34. P.Colahan, T.A.Turner, P.Poulas, G.Piotrowski. Mechanical function and sources of injury in the fetlock and carpus. *Proceedings of the American Association of Equine Practitioners.* 1988;33:689-699.

35. L.R.Bramlage. Surgical diseases of the carpus. *Veterinary Clinics Of North America (Large Animal Practice)* 1983;5:261-74.

36. E.C.Firth, N.Deane, K.Gibson *et al.* Current studies in carpal disease and function in the horse. Nutrition and lameness in horses. New Zealand: Veterinary Continuing Education, Massey University, 1991;135:81-9.

37. L.R.Bramlage, R.K.Schneider, A.A.Gabel. A clinical perspective on lameness originating in the carpus. *Equine Veterinary Journal Supplement* 1988; 6:12-18.

38. S.Sisson. Equine syndesmology. In R.Getty, eds. *Sisson and Grossman's The Anatomy of the Domestic Animals.* W.B.Saunders, London, 1975:355-7.

39. R.C.Whitton, T.H.McCarthy, R.J.Rose. The intercarpal ligaments of the equine midcarpal joint, Part 1: the anatomy of the palmar and the dorsomedial intercarpal ligaments of the midcarpal joint. *Veterinary Surgery* 1997;26:359-66.

40. N.J.Deane, A.S.Davies. The function of the equine carpal joint: A review. *New Zealand Veterinary Journal* 1995:43:45-7.

41. L.A.Setton, W.Zhu, V.C.Mow. The biphasic poro-viscoelastic behaviour of articular cartilage: role of the surface zone in governing the compressive behaviour. *Jorunal of Biomechanics* 1993;26:581-92.

42. A.Young, T.R. O'Brien, R.R.Pool. Exercise-related sclerosis in the third carpal bone of the racing Thoroughbred. *Proceedings of the American Association of Equine Practitioners* 1989:34:339-346.

43. J.L.Palmer, A.L.Bertone, A.S.Litsky. Contact area and pressure distribution changes of the equine third carpal bone during loading. *Equine Veterinary Journal* 1994;26:197-202.

44. E.C.Firth, J.Delahunt, J.W.Wichtel, H.L.Birch, A.E.Goodship. Galloping exercise induces regional changes in bone density within the third and radial carpal bones of Thoroughbred horses. *Equine Veterinary Journal* 1999;31:111-115.

45. H.Uhlhorn, S.Ekman, A.Haglund, J.Carlsten. The accuracy of the dorsoproximal-dorsodistal projection in assessing third carpal bone sclerosis in Standardbred trotters. *Veterinary Radiology and Ultrasound* 1998;39:412-417.

46. M.J.Verner, R.C.Thompson, J.L.Lewis, T.R.Oegema. Subchondral damage after acute transarticular loading: An in vitro model of joint injury. *Journal of Orthopedic Research* 1992;10:759-65.

47. H.Silyn-Roberts, N.D.Broom. Fracture behaviour of cartilage-on-bone in response to repeated impact loading. *Connective Tissue Research* 1990;24:143-56.

48. C.E.DeHaan, T.R.O'Brien, P.D.Koblik. A radiographic investigation of third carpal bone injury in 42 racing Thoroughbreds. *Veterinary Radiology* 1987;28:88-92.

49. D.M.Wong, D.J.Satoris. Noninvasive methods for the assessment of bone density, architecture, and biomechanical properties: fundamental concepts. In D.J.Sartoris, eds. *Osteoporosis Diagnosis and Treatment.* Marcel Dekker Inc, USA, 1996:201-33.

50. T.R.O'Brien, C.E.DeHaan, R.Arthur. Third carpal bone lesions of the racing Thoroughbred. *Proceedings of the American Association of Equine Practitioners.* 1986;31: 515-24.

51. J.R.Field, J.F.Zaruby. Repair of a fracture of the fourth carpal bone in a yearling Standardbred horse. *Candian Veterinary Journal* 1994;35:371-2.

52. J.A.Auer, J.P.Watkins, N.A.White, T.S.Taylor. Slab fractures of the fourth and intermediate carpal bones in five horses. *Journal of American Veterinary Association* 1986;188:595-601.

53. E.Lachmann, M.Whelan. Roentgen diagnosis of osteoporosis and its limitations. *Radiology* 1936;26:165-77.

54. V.Finsen, S.Andra. Accuracy of visually estimated bone mineralization in routine radiographs of the lower extremity. *Skeletal Radiology* 1988;17:270-5.

55. M.J.Garton, E.M.Robertson, F.J.Gilbert, L.Gomersall, D.M.Reid. Can radiologists detect osteopenia on plain radiographs? *Clinical Radiology* 1994;49:118-22.

56. M Jergas, H.K.Genant. Quantitative bone mineral analysis. In D.Resnick, eds. *Diagnosis of Bone and Joint Disorders.* W.B.Saunders, Philadelphia, 1995:1854-85.

57. R.B.Mazess. Photon Absortiometry. In S.H.Cohn, eds. *Non-invasive Measurements of Bone Mass and Their Clinical Application.* CRC Press, Florida, 1981:52-82.

58. S.Grampp, M.Jergas, P.Lang, H.K.Genant, C.C.Gluer. Quantitative assessment of osteoporosis: current and future status. In D.J.Sartoris, eds. *Osteoporosis Diagnosis and Treatment.* Marcel Dekker Inc, U.S.A, 1996:233-65.

59. H.E.Meema, S.Meema. Radiogrammetry. In S.H.Cohn, eds. *Non-invasive Measurements of Bone Mass and Their Clinical Application.* CRC Press Inc, United States, 1981:5-51.

60. T.H.Hughes, J.S.Yu, D.J.Sartoris. Imaging of osteoporosis. *Journal of South Orthopeadic Association* 1993;2:173-84.

61. A.J.Yates, P.D.Ross, R.S.Epstein. Radiographic absorptiometry in the diagnosis of osteoporosis. *The American Journal of Medicine* 1995;98:41-7.

62. S.Yang, S.Hagiwara, K.Engelke *et al*. Radiographic absorptiometry for bone mineral measurement of the phalanges: precision and accuracy study. *Radiology* 1994;192:857-9.

63. C.Colbert, R.S.Bachtell. Radiographic absorptiometry (photodensitometry). In S.H.Cohn, eds. *Non-invasive Measurements of Bone Mass and Their Clinical Application.* CRC Press Inc, United States, 1981:51-85.

64. F.Cosman, B.Herrington, S.Himmelstein, R.Lindsay. Radiographic absorptiometry: a simple method for determination of bone mass. *Osteoporosis International* 1991;2:34-8.

65. E.Scotti, L.B.Jeffcott. The hock as a potential site for non-invasive bone measurement. *Equine Veterinary Journal Supplement* 1988;Supplement 6:93-8.

66. L. Delaquerriere-Richardson, C.Anderson, U.M.Jorch, M.Cook. Radiographic morphometry and radiographic photodensitometry of the femur in the beagle at 13 and 21 months. *American Journal of Veterinary Reseach* 1982:43:2255-8.

67. J.A.Sorenson, J.R.Cameron. A reliable *in vivo* measurement of bone mineral content. *Journal of Bone and Joint Surgery* 1967;49A:481-97.

68. H.W.Walmer, I. Fogelham. The evaluation of osteoporosis: Dual energy X-ray absorptiometry in clinical practice. Cambridge U.K.: Martin Dunitz LTD, 1994.

69. R.B.Mazess, H.M.Walmer. Nuclear medicine and densitometry. In B.L.Riggs, L.J.Melton III, eds. *Osteoporosis Etiology, Diagnosis and Management.* Raven Press, U.S.A, 1988:251-82.

70. M.A.Greenfield, J.D.Cravern, A.Huddleston, D.Wishko, M.L.Kehrer, R.Stern. Measurement of the velocity of ultrasound in human cortical bone *in vivo*. *Radiology* 1981;138:701-10.

71. S.H.W.Buckingham, L.B.Jeffcott. Osteopenic effects of forelimb immobilisation in horses. *Veterinary Record* 1991;128:370-3.

72. L.B.Jeffcott, R.N.McCartney, V.C.Speirs. Single photon absorptiometry for the measurement of bone mineral content in horses. *The Veterinary Record* 1986;118:499-505.

73. L.B.Jeffcott. Photon absorptiometry in the assessment of bone quality: a pilot study. *Proceedings of the Annual Convention of American Association of Equine Practitioners.* 1986;31:227-40.

74. R.N.McCarthy, L.B.Jeffcott. Ultrasonic transmission velocity and single photon absorptiometric measurement of metacarpal bone strength: An *in vitro* study in the horse. *Equine Veterinary Journal Supplement* 1988;Supplement 6:80-87.

75. D.J.Sartoris, D.Resnick. Current and innovative methods for noninvasive bone densitometry. *Radiologic Clinics of North America* 1990;28:257-78.

76. L.B.Jeffcott, S.H.W.Buckingham, R.N.McCarthy, J.C.Cleeland, E.Scotti. Non-invasive measurement of bone: A review of clinical and research applications in the horse. *Equine Veterinary Journal Supplement* 1988;Supplement 6:71-9.

77. J.T.Hathcock, R.L.Stickle. Principles and concepts of computed tomography. *Veterinary Clinics Of North America (Small Animal Practice)* 1993;23:399-415.

78. M.Andre, D.Resnick. Computed tomography. In D.Resnick, eds. *Diagnosis of Bone and Joint Disorders.* W.B.Saunders, Philadelphia, 1995:118-56.

79. M.D.Markel, R.L. Morin, M.A.Wikenheiser, R.A.Robb, SE.Y.S.Chao. Multiplanar quantitative computed tomography for bone mineral analysis in dogs. *American Journal of Veterinary Research* 1991;52:1479-83.

80. D.T.Baran, K.G.Faulkner, H.K.Genant, P.D.Miller, R.Pacifici. Diagnosis and management of osteoporosis: guidelines for the utilization of bone densitometry. *Calcified Tissue International* 1997;61:433-40.

81. R.N.McCarthy, L.B.Jeffcott. Monitoring the effects of treadmill exercise on bone by non-invasive means during a progressive fitness programme. *Equine Veterinary Journal Supplement* 1988;Supplement 6:88-91.

82. A.Mendenhall, H.D.Cantwell. *Equine radiographic procedures.* Lea and Febiger, Philadelphia,1988: 89.

83. D.G.Bailey, R.M.Hodgson. VIPS- a digital image processing algorithm development environment. *Image and Vision Computing* 1988;6:176-84.

84. D.G.Bailey. Pixel calibration techniques. Proceedings of the New Zealand Image and Vision Computing '95 Workshop. Lincon: 1995; 37-42.

85. J.L.Fleiss. *The Design and Analysis of Experiments.* John Wiley and Sons, New York,1986.

86. P.E.Shrout, J.L.Fleiss. Intra-class correlations: Uses in assessing rater reliability. *Psychological Bulletin* 1979;86:420-8.

87. L.J.Gibson. The mechanical behaviour of cancellous bone. *Journal of Biomechanics* 1985;18:317-28.

88. E.C.Firth, P.R.Van Weeren, D.U.Pfeiffer, J.Delahunt, A.Barneveld. Effect of age, exercise and growth rate on bone mineral density (BMD) in third carpal bone and distal radius of Dutch Warmblood foals with osteochondrosis. *Equine Veterinary Journal Supplement* 1999;Supplement 31:74-78.

89. P.Sprawls Jr. *The Physical Principles of Diagnostic Radiology.* University Park Press, Lonndon,1977:196.

90. C.A.Jacobi, D.Q.Paris. *Textbook of Radiologic Technology.* C.V.Mosby Company, St Louis,1972:99.

91. H.Uhlhorn, J.Carlsten. Retrospective study of subchondral sclerosis and lucency in the third carpal bone of Standardbred trotters. *Equine Veterinary Journal* 1999;31:500-5.

APPENDIX 1

Dorsal data

HORSE	ANGLE	GROUP	ROI	MEAN (0.1 mm Aluminium)
25	90	0	1	129.4186
31	90	0	1	118.8062
41	90	0	1	126.6673
42	90	0	1	117.5052
58	90	0	1	122.3113
59	90	0	1	130.833
99	90	0	1	125.2268
25	90	0	2	120.6763
31	90	0	2	111.1423
41	90	0	2	130.4807
42	90	0	2	115.9835
58	90	0	2	114.0186
59	90	0	2	120.2021
99	90	0	2	127.0021
25	90	0	3	120.699
31	90	0	3	108.4577
41	90	0	3	129.5963
42	90	0	3	108.3423
58	90	0	3	113.8454
59	90	0	3	117.3814
99	90	0	3	119.1155
25	90	0	4	117.8
31	90	0	4	111.6557
41	90	0	4	126.4057
42	90	0	4	112.1608
58	90	0	4	113.3485
59	90	0	4	115.167
99	90	0	4	114.2227
25	90	0	5	123.1608
31	90	0	5	117.2639
41	90	0	5	135.1826
42	90	0	5	130.4371
58	90	0	5	117.6021
59	90	0	5	133.7155
99	90	0	5	128.934
13	90	1	1	134.8515
14	90	1	1	132.8062
37	90	1	1	143.9938
50	90	1	1	125.1134
55	90	1	1	138.2474
57	90	1	1	145.0557
60	90	1	1	130.9794
13	90	1	2	156.8124
14	90	1	2	144.901
37	90	1	2	152.3959
50	90	1	2	131.9835

HORSE	ANGLE	GROUP	ROI	MEAN (0.1 mm Aluminium)
55	90	1	2	142.7975
57	90	1	2	148.9381
60	90	1	2	130.8392
13	90	1	3	142.6557
14	90	1	3	140.2577
37	90	1	3	126.5835
50	90	1	3	123.965
55	90	1	3	134.3272
57	90	1	3	159.5711
60	90	1	3	120.0041
13	90	1	4	143.367
14	90	1	4	134.033
37	90	1	4	107.967
50	90	1	4	135.0392
55	90	1	4	139.0798
57	90	1	4	140.7773
60	90	1	4	116.8763
13	90	1	5	128.6433
14	90	1	5	149.9959
37	90	1	5	120.4577
50	90	1	5	136.9175
55	90	1	5	122.5031
57	90	1	5	132.0742
60	90	1	5	122.6
25	85	0	1	131.534
31	85	0	1	116.833
41	85	0	1	121.9856
42	85	0	1	117.2165
58	85	0	1	123.3361
59	85	0	1	128.8619
99	85	0	1	127.7876
25	85	0	2	120.3691
31	85	0	2	109.0742
41	85	0	2	127.2763
42	85	0	2	114.4021
58	85	0	2	115.1876
59	85	0	2	111.2928
99	85	0	2	127.2124
25	85	0	3	116.099
31	85	0	3	107.1814
41	85	0	3	126.6515
42	85	0	3	106.8124
58	85	0	3	115.2598
59	85	0	3	112.9052
99	85	0	3	121.5897
25	85	0	4	110.4186

HORSE	ANGLE	GROUP	ROI	MEAN (0.1 mm Aluminium)
31	85	0	4	110.3629
41	85	0	4	121.8021
42	85	0	4	110.365
58	85	0	4	115.2309
59	85	0	4	108.5897
99	85	0	4	114.7835
25	85	0	5	119.8144
31	85	0	5	116.0825
41	85	0	5	128.6186
42	85	0	5	123.1608
58	85	0	5	118.899
59	85	0	5	127.3773
99	85	0	5	128.5134
13	85	1	1	133.2103
14	85	1	1	133.4783
37	85	1	1	143.7814
50	85	1	1	121.7072
55	85	1	1	138.3052
57	85	1	1	145.4948
60	85	1	1	132.3629
13	85	1	2	151.8722
14	85	1	2	142.5237
37	85	1	2	152.9959
50	85	1	2	128.965
55	85	1	2	141.932
57	85	1	2	145.9835
60	85	1	2	128.9732
13	85	1	3	139.6577
14	85	1	3	137.4351
37	85	1	3	127.7093
50	85	1	3	122.1423
55	85	1	3	135.0763
57	85	1	3	160.4516
60	85	1	3	119.7526
13	85	1	4	139.0577
14	85	1	4	130.0784
37	85	1	4	108.9258
50	85	1	4	129.4598
55	85	1	4	138.9753
57	85	1	4	140.934
60	85	1	4	114.6227
13	85	1	5	125.0763
14	85	1	5	148.3959
37	85	1	5	118.3979
50	85	1	5	132.4907
55	85	1	5	122.8433
57	85	1	5	129.0928
60	85	1	5	121.0309
25	80	0	1	125.4928

HORSE	ANGLE	GROUP	ROI	MEAN (0.1 mm Aluminium)
31	80	0	1	110.8247
41	80	0	1	114.3753
42	80	0	1	113.0062
58	80	0	1	116.6124
59	80	0	1	123.0598
99	80	0	1	118.5299
25	80	0	2	112.701
31	80	0	2	101.7505
41	80	0	2	120.3629
42	80	0	2	105.8433
58	80	0	2	107.3258
59	80	0	2	100.301
99	80	0	2	115.6247
25	80	0	3	108.2124
31	80	0	3	99.2701
41	80	0	3	120.1381
42	80	0	3	99.7629
58	80	0	3	107.9691
59	80	0	3	105.1381
99	80	0	3	112.0784
25	80	0	4	105.7361
31	80	0	4	104.2619
41	80	0	4	113.5835
42	80	0	4	101.666
58	80	0	4	105.9794
59	80	0	4	100.3113
99	80	0	4	109.0433
25	80	0	5	112.334
31	80	0	5	109.9732
41	80	0	5	118.1938
42	80	0	5	113.2722
58	80	0	5	111.8227
59	80	0	5	119.7134
99	80	0	5	121.8247
13	80	1	1	128.3093
14	80	1	1	129.9381
37	80	1	1	139.8309
50	80	1	1	115.2021
55	80	1	1	131.4412
57	80	1	1	133.1629
60	80	1	1	127.8289
13	80	1	2	139.6516
14	80	1	2	132.3484
37	80	1	2	144.4907
50	80	1	2	124.3155
55	80	1	2	132.9608
57	80	1	2	129.7072
60	80	1	2	119.0433
13	80	1	3	130.0784

HORSE	ANGLE	GROUP	ROI	MEAN (0.1 mm Aluminium)
14	80	1	3	128.3217
37	80	1	3	122.5856
50	80	1	3	116.9093
55	80	1	3	127.2722
57	80	1	3	151.2392
60	80	1	3	110.5443
13	80	1	4	128.9608
14	80	1	4	124
37	80	1	4	102.2701
50	80	1	4	123.1567
55	80	1	4	129.7959
57	80	1	4	131.2722
60	80	1	4	105.501
13	80	1	5	119.8206
14	80	1	5	142.7526
37	80	1	5	111.9546
50	80	1	5	127.9505
55	80	1	5	117.2103
57	80	1	5	119.6103
60	80	1	5	109.9278
25	75	0	1	130.4165
31	75	0	1	114.2309
41	75	0	1	115.2082
42	75	0	1	113.0763
59	75	0	1	131.1629
58	75	0	1	122.7423
99	75	0	1	119.0742
25	75	0	2	110.7216
31	75	0	2	102.3072
41	75	0	2	119.2289
42	75	0	2	105.0969
59	75	0	2	99.2021
58	75	0	2	109.732
99	75	0	2	110.9464
25	75	0	3	107.1443
31	75	0	3	99.2598
41	75	0	3	117.334
42	75	0	3	100.6247
59	75	0	3	103.7835
58	75	0	3	108.9608
99	75	0	3	110.3835
25	75	0	4	105.4186
31	75	0	4	102.0742
41	75	0	4	110.534
42	75	0	4	103.033
59	75	0	4	99.5361
58	75	0	4	104.6701
99	75	0	4	104.6536
25	75	0	5	113.2268

HORSE	ANGLE	GROUP	ROI	MEAN (0.1 mm Aluminium)
31	75	0	5	114.5278
41	75	0	5	120.3856
42	75	0	5	116.9464
59	75	0	5	120.1299
58	75	0	5	112.2454
99	75	0	5	117.1629
13	75	1	1	132.967
14	75	1	1	125.8474
37	75	1	1	139.5464
50	75	1	1	114.0515
55	75	1	1	132.2969
57	75	1	1	131.2021
60	75	1	1	126.5897
13	75	1	2	133.1485
14	75	1	2	125.8887
37	75	1	2	139.767
50	75	1	2	121.3918
55	75	1	2	127.3691
57	75	1	2	122.5794
60	75	1	2	111.3691
13	75	1	3	134.4701
14	75	1	3	119.1464
37	75	1	3	119.3835
50	75	1	3	117.4866
55	75	1	3	125.5835
57	75	1	3	144.3918
60	75	1	3	105.9155
13	75	1	4	141.9485
14	75	1	4	115.9196
37	75	1	4	102.134
50	75	1	4	124.268
55	75	1	4	131.499
57	75	1	4	126.6454
60	75	1	4	102.3361
13	75	1	5	148.0083
14	75	1	5	113.468
37	75	1	5	113.3485
50	75	1	5	126.8804
55	75	1	5	117.8062
57	75	1	5	119.0247
60	75	1	5	110.9381
25	70	0	1	130.5302
31	70	0	1	115.7722
41	70	0	1	119.9964
42	70	0	1	116.605
58	70	0	1	121.4377
59	70	0	1	132.0854
99	70	0	1	121.032
25	70	0	2	104.8221

HORSE	ANGLE	GROUP	ROI	MEAN (0.1 mm Aluminium)
31	70	0	2	101.9537
41	70	0	2	123.4875
42	70	0	2	107.3879
58	70	0	2	111.7936
59	70	0	2	97.9146
99	70	0	2	108.8541
25	70	0	3	102.968
31	70	0	3	97.6406
41	70	0	3	123.21
42	70	0	3	101.4662
58	70	0	3	107.7224
59	70	0	3	97.2171
99	70	0	3	108.7971
25	70	0	4	97.9893
31	70	0	4	97.3203
41	70	0	4	112
42	70	0	4	104.8399
58	70	0	4	101.669
59	70	0	4	97.0214
99	70	0	4	102.6939
25	70	0	5	109.9786
31	70	0	5	110.9537
41	70	0	5	121.5267
42	70	0	5	116.6762
58	70	0	5	109.2029
59	70	0	5	116.8256
99	70	0	5	112.7651
13	70	1	1	130.9146
14	70	1	1	138.4164
37	70	1	1	140.7402
50	70	1	1	119.6192
55	70	1	1	135.2206
57	70	1	1	130.8221
60	70	1	1	130.5552
13	70	1	2	126.3025
14	70	1	2	124.1032
37	70	1	2	139.0391
50	70	1	2	127.3808
55	70	1	2	125.4057
57	70	1	2	123.7829
60	70	1	2	112.4769
13	70	1	3	117.9858
14	70	1	3	121.5765
37	70	1	3	117.7971
50	70	1	3	122.9146
55	70	1	3	120.6655
57	70	1	3	143.1139
60	70	1	3	107.9609
13	70	1	4	119.9004

HORSE	ANGLE	GROUP	ROI	MEAN (0.1 mm Aluminium)
14	70	1	4	123.5552
37	70	1	4	103.3594
50	70	1	4	125.79
55	70	1	4	125.8541
57	70	1	4	125.0569
60	70	1	4	102.8149
13	70	1	5	119.968
14	70	1	5	143.8541
37	70	1	5	115.0854
50	70	1	5	127.3559
55	70	1	5	116.1566
57	70	1	5	120.1851
60	70	1	5	112.5587
25	65	0	1	123.242
31	65	0	1	112.1103
41	65	0	1	118.2527
42	65	0	1	117.0961
58	65	0	1	124.7789
59	65	0	1	128.395
99	65	0	1	130.3488
25	65	0	2	96.2669
31	65	0	2	90.6406
41	65	0	2	114.4093
42	65	0	2	102.0783
58	65	0	2	107.7053
59	65	0	2	93.1566
99	65	0	2	110.6904
25	65	0	3	95.7331
31	65	0	3	86.0036
41	65	0	3	107.3986
42	65	0	3	99.6584
58	65	0	3	98.6456
59	65	0	3	89.8897
99	65	0	3	105.3452
25	65	0	4	89.032
31	65	0	4	87.8363
41	65	0	4	99.7865
42	65	0	4	102.3701
58	65	0	4	100.8175
59	65	0	4	90.089
99	65	0	4	106.3167
25	65	0	5	101.5623
31	65	0	5	99.8292
41	65	0	5	113.6584
42	65	0	5	113.7687
58	65	0	5	111.993
59	65	0	5	109.0641
99	65	0	5	119.5765
13	65	1	1	129.6014

HORSE	ANGLE	GROUP	ROI	MEAN (0.1 mm Aluminium)
14	65	1	1	127.7295
37	65	1	1	136.3123
50	65	1	1	131.9822
55	65	1	1	135.758
57	65	1	1	125.8185
60	65	1	1	133.014
13	65	1	2	113.427
14	65	1	2	105.605
37	65	1	2	122.3439
50	65	1	2	125.6228
55	65	1	2	116.9039
57	65	1	2	111.9822
60	65	1	2	107.5228
13	65	1	3	109.5623
14	65	1	3	104.573
37	65	1	3	109.5158
50	65	1	3	123.8043
55	65	1	3	113.153
57	65	1	3	124.2242
60	65	1	3	100.8316
13	65	1	4	113.5018
14	65	1	4	106.8861
37	65	1	4	97.1368
50	65	1	4	127.0107
55	65	1	4	121.4413
57	65	1	4	112.3559
60	65	1	4	96.7895
13	65	1	5	119.1886
14	65	1	5	126.2918
37	65	1	5	113.9439
50	65	1	5	126.7367
55	65	1	5	117.6263
57	65	1	5	117.2206
60	65	1	5	112.9053
25	60	0	1	105.3607
31	60	0	1	110.3808
41	60	0	1	106.2349
42	60	0	1	108.6157
58	60	0	1	106.7971
59	60	0	1	124.4484
99	60	0	1	124.4667
25	60	0	2	82.8861
31	60	0	2	91.2029
41	60	0	2	98.0641
42	60	0	2	86.0249
58	60	0	2	90.4448
59	60	0	2	100.6477
99	60	0	2	106.186
25	60	0	3	85.7402

HORSE	ANGLE	GROUP	ROI	MEAN (0.1 mm Aluminium)
31	60	0	3	87.7402
41	60	0	3	89.6085
42	60	0	3	85.1281
58	60	0	3	82.4235
59	60	0	3	97.1566
99	60	0	3	97.5614
25	60	0	4	74.0534
31	60	0	4	87.4342
41	60	0	4	85.2598
42	60	0	4	89.0534
58	60	0	4	85.0712
59	60	0	4	99.0142
99	60	0	4	102.0351
25	60	0	5	80.7153
31	60	0	5	102.331
41	60	0	5	89.0641
42	60	0	5	94.6121
58	60	0	5	94.7722
59	60	0	5	112.9573
99	60	0	5	113.3579
13	60	1	1	127.1068
14	60	1	1	135.4057
37	60	1	1	133.4413
50	60	1	1	134.1139
55	60	1	1	143.6192
57	60	1	1	125.6477
60	60	1	1	128.0534
13	60	1	2	107.0747
14	60	1	2	114.2989
37	60	1	2	108.8932
50	60	1	2	117.9466
55	60	1	2	129.8434
57	60	1	2	111.5267
60	60	1	2	105.5196
13	60	1	3	104.9146
14	60	1	3	112.5196
37	60	1	3	97.4377
50	60	1	3	116.0214
55	60	1	3	124.9324
57	60	1	3	116.4591
60	60	1	3	100.2349
13	60	1	4	105.4413
14	60	1	4	112.21
37	60	1	4	91.5587
50	60	1	4	120.3523
55	60	1	4	129.6192
57	60	1	4	109.3238
60	60	1	4	96.2527
13	60	1	5	107.2954

HORSE	ANGLE	GROUP	ROI	MEAN (0.1 mm Aluminium)
14	60	1	5	129.605
37	60	1	5	102.1779
50	60	1	5	123.484
55	60	1	5	135.7117
57	60	1	5	115.9893
60	60	1	5	110.5338

Palmar data

HORSE	GROUP	ANGLE	ROI	MEAN (0.1 mm Aluminium)
41	0	90	1	127.284
42	0	90	1	116.2948
59	0	90	1	121.5057
25	0	90	1	127.3567
58	0	90	1	120.701
31	0	90	1	115.5248
99	0	90	1	125.468
57	1	90	1	152.8742
14	1	90	1	134.4866
13	1	90	1	142.1876
37	1	90	1	147.8557
50	1	90	1	126.9072
55	1	90	1	141.5184
60	1	90	1	131.9052
41	0	85	1	123.6722
42	0	85	1	116.8062
59	0	85	1	128.8577
25	0	85	1	130.1505
58	0	85	1	122.4
31	0	85	1	118.1381
99	0	85	1	128.5876
57	1	85	1	156.4948
14	1	85	1	137.5484
13	1	85	1	141.9072
37	1	85	1	149.7031
50	1	85	1	126.7361
55	1	85	1	144.9753
60	1	85	1	133.4598
41	0	80	1	117.0701
42	0	80	1	112.8825
59	0	80	1	123.2062
25	0	80	1	125.4433
58	0	80	1	116.4062
31	0	80	1	112.6598
99	0	80	1	119.2619
57	1	80	1	148.8845
14	1	80	1	132.866
13	1	80	1	137.0948
37	1	80	1	145.2392
50	1	80	1	122.5175

HORSE	ANGLE	GROUP	ROI	MEAN (0.1 mm Aluminium)
55	1	80	1	140.4412
60	1	80	1	129.7959
41	0	75	1	117.4845
42	0	75	1	114.4124
59	0	75	1	129.7443
25	0	75	1	130.1814
58	0	75	1	124.0742
31	0	75	1	116.8351
99	0	75	1	121.6887
57	1	75	1	149.7485
14	1	75	1	136.5299
13	1	75	1	137.6371
37	1	75	1	149.2784
50	1	75	1	123.934
55	1	75	1	144.266
60	1	75	1	131.0928
41	0	90	2	122.7809
42	0	90	2	113.567
59	0	90	2	121.5057
25	0	90	2	116.3443
58	0	90	2	113.3546
31	0	90	2	115.5248
99	0	90	2	126.8351
57	1	90	2	150.2144
14	1	90	2	143.3567
13	1	90	2	152.0227
37	1	90	2	146.167
50	1	90	2	123.3443
55	1	90	2	141.5184
60	1	90	2	130.2845
41	0	85	2	122.6247
42	0	85	2	112.9093
59	0	85	2	120.0124
25	0	85	2	119.0784
58	0	85	2	114.3567
31	0	85	2	110.2268
99	0	85	2	128.9402
57	1	85	2	153.9423
14	1	85	2	145.8845
13	1	85	2	154.8247

HORSE	ANGLE	GROUP	ROI	MEAN (0.1 mm Aluminium)
37	1	85	2	148.6804
50	1	85	2	125.4948
55	1	85	2	141.0866
60	1	85	2	131.9753
41	0	80	2	117.8392
42	0	80	2	106.501
59	0	80	2	112.0639
25	0	80	2	112.701
58	0	80	2	107.332
31	0	80	2	103.7588
99	0	80	2	119.6309
57	1	80	2	145.132
14	1	80	2	139.5753
13	1	80	2	149.1588
37	1	80	2	144.4371
50	1	80	2	122.6289
55	1	80	2	135.5423
60	1	80	2	124.8928
41	0	75	2	121.1711
42	0	75	2	108.8062
59	0	75	2	110.3216
25	0	75	2	113.3526
58	0	75	2	112.4887
31	0	75	2	105.7381
99	0	75	2	118.7526
57	1	75	2	141.8928
14	1	75	2	142.0412
13	1	75	2	146.1649
37	1	75	2	148.3526
50	1	75	2	123.2619
55	1	75	2	137.7155
60	1	75	2	124.1649
41	0	90	3	126.6
42	0	90	3	104.8557
59	0	90	3	121.5057
25	0	90	3	117.2165
58	0	90	3	112.0825
31	0	90	3	109.4588
99	0	90	3	117.0041
57	1	90	3	156.4371
14	1	90	3	144.8206
13	1	90	3	142.9917
37	1	90	3	129.7464
50	1	90	3	120.8742
55	1	90	3	128.2372
60	1	90	3	118.4804
41	0	85	3	125.299
42	0	85	3	105.3402
59	0	85	3	112.534

HORSE	ANGLE	GROUP	ROI	MEAN (0.1 mm Aluminium)
25	0	85	3	120.8536
58	0	85	3	114.4227
31	0	85	3	106.8515
99	0	85	3	120.8124
57	1	85	3	162.8949
14	1	85	3	145.8557
13	1	85	3	143.3608
37	1	85	3	128.5134
50	1	85	3	122.1196
55	1	85	3	130.8742
60	1	85	3	120.9835
41	0	80	3	122.9773
42	0	80	3	101.4371
59	0	80	3	108.9629
25	0	80	3	115.2371
58	0	80	3	107.868
31	0	80	3	100.5918
99	0	80	3	111.6412
57	1	80	3	157.299
14	1	80	3	139.7814
13	1	80	3	137.8474
37	1	80	3	122.8
50	1	80	3	118.0742
55	1	80	3	128.167
60	1	80	3	116.7258
41	0	75	3	125.1485
42	0	75	3	104.2227
59	0	75	3	112.8515
25	0	75	3	116.4701
58	0	75	3	114.0825
31	0	75	3	103.2103
99	0	75	3	115.7443
57	1	75	3	156.9629
14	1	75	3	144.1402
13	1	75	3	137.5918
37	1	75	3	122.7175
50	1	75	3	120.7567
55	1	75	3	132.7423
60	1	75	3	117.9773
41	0	90	4	126.6
42	0	90	4	104.035
59	0	90	4	121.5057
25	0	90	4	120.6247
58	0	90	4	112.767
31	0	90	4	109.4588
99	0	90	4	114.6928
57	1	90	4	151.8
14	1	90	4	143.8247
13	1	90	4	156.1505

HORSE	ANGLE	GROUP	ROI	MEAN (0.1 mm Aluminium)
37	1	90	4	114.233
50	1	90	4	138.3237
55	1	90	4	138.6749
60	1	90	4	121.2536
41	0	85	4	126.3732
42	0	85	4	109.8021
59	0	85	4	115
25	0	85	4	122.0021
58	0	85	4	116.5773
31	0	85	4	112.1794
99	0	85	4	120.9546
57	1	85	4	152.5381
14	1	85	4	143.1299
13	1	85	4	154.1402
37	1	85	4	113.7691
50	1	85	4	139.5629
55	1	85	4	144.1216
60	1	85	4	123.8536
41	0	80	4	121.1917
42	0	80	4	105.1113
59	0	80	4	110.666
25	0	80	4	116.5753
58	0	80	4	111.0103
31	0	80	4	106.3216
99	0	80	4	112.4866
57	1	80	4	143.132
14	1	80	4	138.1072
13	1	80	4	146.2619
37	1	80	4	107.2742
50	1	80	4	134.5876
55	1	80	4	140.1608
60	1	80	4	114.9505
41	0	75	4	120.5464
42	0	75	4	108.9505
59	0	75	4	110.6598
25	0	75	4	117.068
58	0	75	4	116.7443
31	0	75	4	110.0433
99	0	75	4	111.8083
57	1	75	4	141.7979
14	1	75	4	147.0495
13	1	75	4	131.7753
37	1	75	4	107.501
50	1	75	4	138.4103
55	1	75	4	144.6165
60	1	75	4	112.6206
41	0	90	5	139.6511
42	0	90	5	130.4165
59	0	90	5	133.7155

HORSE	ANGLE	GROUP	ROI	MEAN (0.1 mm Aluminium)
25	0	90	5	123.2206
58	0	90	5	118.1856
31	0	90	5	122.1629
99	0	90	5	126.8701
57	1	90	5	132.8784
14	1	90	5	151.1402
13	1	90	5	128.6433
37	1	90	5	121.2742
50	1	90	5	136.2309
55	1	90	5	122.9632
60	1	90	5	122.5072
41	0	85	5	137.1299
42	0	85	5	130.033
59	0	85	5	129.9052
25	0	85	5	122.4165
58	0	85	5	120.4124
31	0	85	5	128.7485
99	0	85	5	135.7588
57	1	85	5	137.1485
14	1	85	5	153.3938
13	1	85	5	128.765
37	1	85	5	126.7629
50	1	85	5	132.3588
55	1	85	5	124.8845
60	1	85	5	123.1031
41	0	80	5	129.9588
42	0	80	5	122.5753
59	0	80	5	123.9278
25	0	80	5	117.3155
58	0	80	5	114.3134
31	0	80	5	122.4948
99	0	80	5	125.3134
57	1	80	5	132.4227
14	1	80	5	148.7917
13	1	80	5	123.4619
37	1	80	5	117.7031
50	1	80	5	132.9629
55	1	80	5	123.035
60	1	80	5	118.2866
41	0	75	5	127.6
42	0	75	5	127.2227
59	0	75	5	129.3876
25	0	75	5	119.6742
58	0	75	5	120.1629
31	0	75	5	125.3402
99	0	75	5	125.2103
57	1	75	5	132.2206
14	1	75	5	148.967
13	1	75	5	125.466

HORSE	ANGLE	GROUP	ROI	MEAN (0.1 mm Aluminium)
37	1	75	5	122.0619
50	1	75	5	135.1588
55	1	75	5	123.7959
60	1	75	5	118.4804
41	0	70	1	122.8114
42	0	70	1	119.6014
59	0	70	1	133.8363
25	0	70	1	135.6192
58	0	70	1	127.4626
31	0	70	1	121.637
99	0	70	1	125.9573
57	1	70	1	149.3701
14	1	70	1	144.6584
13	1	70	1	142.7651
37	1	70	1	154.3203
50	1	70	1	131.8149
55	1	70	1	151.6726
60	1	70	1	136.2954
41	0	70	2	128.6335
42	0	70	2	115.3416
59	0	70	2	110.879
25	0	70	2	115.9431
58	0	70	2	114.242
31	0	70	2	107.5552
99	0	70	2	121.8826
57	1	70	2	1431174
14	1	70	2	145.1637
13	1	70	2	153.8363
37	1	70	2	151.4021
50	1	70	2	127.3986
55	1	70	2	140.1708
60	1	70	2	128.0249
41	0	70	3	132.8505
42	0	70	3	108.0996
59	0	70	3	112.8541
25	0	70	3	115.3452
58	0	70	3	115.4626
31	0	70	3	108.0854
99	0	70	3	118.6655
57	1	70	3	161.2918
14	1	70	3	144.4021
13	1	70	3	142.726
37	1	70	3	126.5623
50	1	70	3	128.7794
55	1	70	3	137.0605
60	1	70	3	122.5089
41	0	70	4	124.8185
42	0	70	4	113.9964
59	0	70	4	112.2456

HORSE	ANGLE	GROUP	ROI	MEAN (0.1 mm Aluminium)
25	0	70	4	113.6228
58	0	70	4	116.4093
31	0	70	4	112.8826
99	0	70	4	113.5587
57	1	70	4	142.8043
14	1	70	4	145.9502
13	1	70	4	142.0107
37	1	70	4	110.0605
50	1	70	4	139.8968
55	1	70	4	145.5267
60	1	70	4	116.8826
41	0	70	5	131.2491
42	0	70	5	126.2206
59	0	70	5	127.3879
25	0	70	5	118.8826
58	0	70	5	118.6797
31	0	70	5	119.9395
99	0	70	5	126.4911
57	1	70	5	133.3203
14	1	70	5	154.0783
13	1	70	5	129.3167
37	1	70	5	122.4982
50	1	70	5	135
55	1	70	5	123.6477
60	1	70	5	120.847
41	0	65	1	122.5267
42	0	65	1	125.7722
59	0	65	1	138.1174
25	0	65	1	134.8648
58	0	65	1	140.3754
31	0	65	1	125.452
99	0	65	1	136.4164
57	1	65	1	150.4199
14	1	65	1	143.7616
13	1	65	1	146.7082
37	1	65	1	156.5263
50	1	65	1	139.1317
55	1	65	1	156.8541
60	1	65	1	14 1.7123
41	0	65	2	129.8683
42	0	65	2	119.0961
59	0	65	2	108.5231
25	0	65	2	115.1673
58	0	65	2	122.4105
31	0	65	2	105.9466
99	0	65	2	129.484
57	1	65	2	143.1139
14	1	65	2	137.4555
13	1	65	2	149.7331

HORSE	ANGLE	GROUP	ROI	MEAN (0.1 mm Aluminium)
37	1	65	2	149.9439
50	1	65	2	133.5516
55	1	65	2	143.0605
60	1	65	2	131.3965
41	0	65	3	131.8185
42	0	65	3	113.3843
59	0	65	3	112.3167
25	0	65	3	115
58	0	65	3	122.3684
31	0	65	3	109.7295
99	0	65	3	125.2883
57	1	65	3	162.0498
14	1	65	3	139.8577
13	1	65	3	138.694
37	1	65	3	127.2351
50	1	65	3	134.452
55	1	65	3	142.7046
60	1	65	3	125.3403
41	0	65	4	122.2883
42	0	65	4	119.452
59	0	65	4	112.2135
25	0	65	4	113.8327
58	0	65	4	126.5649
31	0	65	4	115.8577
99	0	65	4	124.637
57	1	65	4	143.4733
14	1	65	4	143.3381
13	1	65	4	144.8327
37	1	65	4	114.1263
50	1	65	4	151.3986
55	1	65	4	153.3665
60	1	65	4	121.0772
41	0	65	5	127.8648
42	0	65	5	129.2918
59	0	65	5	130.6833
25	0	65	5	119.2527
58	0	65	5	127.2842
31	0	65	5	121.7438
99	0	65	5	136.0854
57	1	65	5	132.8612
14	1	65	5	153.4947
13	1	65	5	135.5196
37	1	65	5	125.4526
50	1	65	5	140.1139
55	1	65	5	132.8114
60	1	65	5	125.6
41	0	60	1	126.21
42	0	60	1	131.0498
59	0	60	1	146.3843

HORSE	ANGLE	GROUP	ROI	MEAN (0.1 mm Aluminium)
25	0	60	1	136.7046
58	0	60	1	139.8577
31	0	60	1	128.5765
99	0	60	1	143.7509
57	1	60	1	157.9822
14	1	60	1	159.6904
13	1	60	1	151.3665
37	1	60	1	166.7722
50	1	60	1	153.9359
55	1	60	1	170.8363
60	1	60	1	147.2954
41	0	60	2	129.3381
42	0	60	2	114.7794
59	0	60	2	128.3025
25	0	60	2	111.8826
58	0	60	2	118.0783
31	0	60	2	114
99	0	60	2	135.8842
57	1	60	2	148.6299
14	1	60	2	154.2527
13	1	60	2	150.7117
37	1	60	2	152.4164
50	1	60	2	139.1957
55	1	60	2	162.4235
60	1	60	2	138.5872
41	0	60	3	124.8754
42	0	60	3	110.8256
59	0	60	3	121.5303
25	0	60	3	115.1922
58	0	60	3	117.7651
31	0	60	3	111.0783
99	0	60	3	127.4351
57	1	60	3	164.7117
14	1	60	3	150.6904
13	1	60	3	137.9324
37	1	60	3	126.2562
50	1	60	3	138.3345
55	1	60	3	150.5338
60	1	60	3	129.8327
41	0	60	4	120.9644
42	0	60	4	117.6797
59	0	60	4	131.4555
25	0	60	4	107.452
58	0	60	4	117.0996
31	0	60	4	117.8719
99	0	60	4	126.4035
57	1	60	4	151.79
14	1	60	4	160.3452
13	1	60	4	150.4804

HORSE	ANGLE	GROUP	ROI	MEAN (0.1 mm Aluminium)
37	1	60	4	117.4733
50	1	60	4	158.6584
55	1	60	4	173.1281
60	1	60	4	130.0463
41	0	60	5	124.4982
42	0	60	5	130.242
59	0	60	5	138.2135
25	0	60	5	120.5267
58	0	60	5	125.1922
31	0	60	5	127.3772
99	0	60	5	137.5614
57	1	60	5	139.0071
14	1	60	5	160.2669
13	1	60	5	138.8221
37	1	60	5	130.8114
50	1	60	5	146.1922
55	1	60	5	136.8648
60	1	60	5	131.2562

ROI size data

HORSE	ANGLE	GROUP	ROI	RADIUS (mm)	MEAN (0.1mm Aluminium)
13	60	1	1	2.5	148.7411
13	60	1	2	2.5	147.6193
13	60	1	3	2.5	132.9594
13	60	1	4	2.5	147.2437
13	60	1	5	2.5	139.0609
13	60	1	1	3	151.3665
13	60	1	2	3	150.7117
13	60	1	3	3	137.9324
13	60	1	4	3	150.4804
13	60	1	5	3	138.8221
13	60	1	1	3.5	152.3483
13	60	1	2	3.5	153.942
13	60	1	3	3.5	143.3773
13	60	1	4	3.5	156.2612
13	60	1	5	3.5	139
13	90	1	1	2.5	140.7449
13	90	1	2	2.5	155.1391
13	90	1	3	2.5	143.8464
13	90	1	4	2.5	156
13	90	1	5	2.5	129.629
13	90	1	1	3	142.1876
13	90	1	2	3	152.0227
13	90	1	3	3	142.9917
13	90	1	4	3	156.1505
13	90	1	5	3	156.1505
13	90	1	1	3.5	141.591
13	90	1	2	3.5	148.7865
13	90	1	3	3.5	141.2887
13	90	1	4	3.5	155.0135
13	90	1	5	3.5	128.3023
14	60	1	1	2.5	158.2437
14	60	1	2	2.5	150.1624
14	60	1	3	2.5	145.7919
14	60	1	4	2.5	154.2843
14	60	1	5	2.5	160.2437
14	60	1	1	3	159.6904
14	60	1	2	3	154.2527
14	60	1	3	3	150.6904
14	60	1	4	3	160.3452
14	60	1	5	3	160.2669
14	60	1	1	3.5	160.2823
14	60	1	2	3.5	155.8549
14	60	1	3	3.5	152.1873
14	60	1	4	3.5	162.9842
14	60	1	5	3.5	158.3404
14	90	1	1	2.5	134.3826
14	90	1	2	2.5	144.7101

HORSE	ANGLE	GROUP	ROI	RADIUS (mm)	MEAN (0.1mm Aluminium)
14	90	1	3	2.5	145.7043
14	90	1	4	2.5	143.1044
14	90	1	5	2.5	151.7449
14	90	1	1	3	134.4866
14	90	1	2	3	143.3567
14	90	1	3	3	144.8206
14	90	1	4	3	143.8247
14	90	1	5	3	143.8247
14	90	1	1	3.5	140.116
14	90	1	2	3.5	140.116
14	90	1	3	3.5	140.116
14	90	1	4	3.5	143.2178
14	90	1	5	3.5	150.1846
25	60	0	1	2.5	135.198
25	60	0	2	2.5	109.0508
25	60	0	3	2.5	112.9442
25	60	0	4	2.5	103.4873
25	60	0	5	2.5	117.9746
25	60	0	1	3	136.7046
25	60	0	2	3	111.8826
25	60	0	3	3	115.1922
25	60	0	4	3	107.452
25	60	0	5	3	120.5267
25	60	0	1	3.5	136.7256
25	60	0	2	3.5	113.3483
25	60	0	3	3.5	116.2639
25	60	0	4	3.5	112.0158
25	60	0	5	3.5	121.3615
25	90	0	1	2.5	128.2493
25	90	0	2	2.5	117.5594
25	90	0	3	2.5	119.1275
25	90	0	4	2.5	122.0841
25	90	0	5	2.5	123.5362
25	90	0	1	3	127.3567
25	90	0	2	3	116.3443
25	90	0	3	3	117.2165
25	90	0	4	3	120.6247
25	90	0	5	3	120.6247
25	90	0	1	3.5	117.6165
25	90	0	2	3.5	117.6165
25	90	0	3	3.5	117.6165
25	90	0	4	3.5	117.6165
25	90	0	5	3.5	122.8105
31	60	0	1	2.5	127.1269
31	60	0	2	2.5	112.7817
31	60	0	3	2.5	110.132
31	60	0	4	2.5	116.7563
31	60	0	5	2.5	126.2589
31	60	0	1	3	128.5765

HORSE	ANGLE	GROUP	ROI	RADIUS (mm)	MEAN (0.1mm Aluminium)
31	60	0	2	3	114
31	60	0	3	3	111.0783
31	60	0	4	3	117.8719
31	60	0	5	3	127.3772
31	60	0	1	3.5	128.7256
31	60	0	2	3.5	115.4776
31	60	0	3	3.5	111.5515
31	60	0	4	3.5	120.3615
31	60	0	5	3.5	127.8232
31	90	0	1	2.5	119.9681
31	90	0	2	2.5	111.6957
31	90	0	3	2.5	108.1333
31	90	0	4	2.5	112.2087
31	90	0	5	2.5	128.3913
31	90	0	1	3	115.5248
31	90	0	2	3	115.5248
31	90	0	3	3	109.4588
31	90	0	4	3	109.4588
31	90	0	5	3	109.4588
31	90	0	1	3.5	111.2148
31	90	0	2	3.5	111.2148
31	90	0	3	3.5	111.2148
31	90	0	4	3.5	111.2148
31	90	0	5	3.5	121.8632
37	60	1	1	2.5	165.25
37	60	1	2	2.5	150.2347
37	60	1	3	2.5	123.1327
37	60	1	4	2.5	115.8469
37	60	1	5	2.5	129.8725
37	60	1	1	3	166.7722
37	60	1	2	3	152.4164
37	60	1	3	3	126.2562
37	60	1	4	3	117.4733
37	60	1	5	3	130.8114
37	60	1	1	3.5	169.3958
37	60	1	2	3.5	154.2401
37	60	1	3	3.5	128.248
37	60	1	4	3.5	120.248
37	60	1	5	3.5	132.058
37	90	1	1	2.5	148.7971
37	90	1	2	2.5	147.7159
37	90	1	3	2.5	128.4087
37	90	1	4	2.5	113.7043
37	90	1	5	2.5	121.3478
37	90	1	1	3	147.8557
37	90	1	2	3	146.167
37	90	1	3	3	129.7464
37	90	1	4	3	114.233
37	90	1	5	3	114.233

HORSE	ANGLE	GROUP	ROI	RADIUS (mm)	MEAN (0.1mm Aluminium)
37	90	1	1	3.5	133.5226
37	90	1	2	3.5	133.5226
37	90	1	3	3.5	133.5226
37	90	1	4	3.5	133.5226
37	90	1	5	3.5	121.1729
41	60	0	1	2.5	125.6599
41	60	0	2	2.5	128.7157
41	60	0	3	2.5	120.7614
41	60	0	4	2.5	118.2284
41	60	0	5	2.5	122.9594
41	60	0	1	3	126.21
41	60	0	2	3	129.3381
41	60	0	3	3	124.8754
41	60	0	4	3	120.9644
41	60	0	5	3	124.4982
41	60	0	1	3.5	127.0185
41	60	0	2	3.5	130.3509
41	60	0	3	3.5	127.314
41	60	0	4	3.5	122.7573
41	60	0	5	3.5	126.905
41	90	0	1	2.5	128.5362
41	90	0	2	2.5	124.742
41	90	0	3	2.5	126.6435
41	90	0	4	2.5	129.7507
41	90	0	5	2.5	140.2232
41	90	0	1	3	127.284
41	90	0	2	3	122.7809
41	90	0	3	3	126.6
41	90	0	4	3	126.6
41	90	0	5	3	126.6
41	90	0	1	3.5	123.2916
41	90	0	2	3.5	123.2916
41	90	0	3	3.5	123.2916
41	90	0	4	3.5	123.2916
41	90	0	5	3.5	139.1158
42	60	0	1	2.5	129.9239
42	60	0	2	2.5	111.3553
42	60	0	3	2.5	108.198
42	60	0	4	2.5	116.2081
42	60	0	5	2.5	129.3858
42	60	0	1	3	131.0498
42	60	0	2	3	114.7794
42	60	0	3	3	110.8256
42	60	0	4	3	117.6797
42	60	0	5	3	130.242
42	60	0	1	3.5	131.715
42	60	0	2	3.5	116.6491
42	60	0	3	3.5	112.0844
42	60	0	4	3.5	119.9631

HORSE	ANGLE	GROUP	ROI	RADIUS (mm)	MEAN (0.1mm Aluminium)
42	60	0	5	3.5	131.4617
42	90	0	1	2.5	116.229
42	90	0	2	2.5	113.8174
42	90	0	3	2.5	106.1072
42	90	0	4	2.5	108.3333
42	90	0	5	2.5	131.0783
42	90	0	1	3	116.2948
42	90	0	2	3	113.567
42	90	0	3	3	104.8557
42	90	0	4	3	104.035
42	90	0	5	3	104.035
42	90	0	1	3.5	110.7817
42	90	0	2	3.5	110.7817
42	90	0	3	3.5	110.7817
42	90	0	4	3.5	101.7098
42	90	0	5	3.5	129.6677
50	60	1	1	2.5	153.8673
50	60	1	2	2.5	138.6275
50	60	1	3	2.5	137.2857
50	60	1	4	2.5	157.2347
50	60	1	5	2.5	147.148
50	60	1	1	3	153.9359
50	60	1	2	3	139.1957
50	60	1	3	3	138.3345
50	60	1	4	3	158.6584
50	60	1	5	3	146.1922
50	60	1	1	3.5	154.0185
50	60	1	2	3.5	139.3377
50	60	1	3	3.5	139.4301
50	60	1	4	3.5	161.438
50	60	1	5	3.5	145.8628
50	90	1	1	2.5	127.3565
50	90	1	2	2.5	125.3362
50	90	1	3	2.5	121.2551
50	90	1	4	2.5	138.9971
50	90	1	5	2.5	136.5565
50	90	1	1	3	126.9072
50	90	1	2	3	123.3443
50	90	1	3	3	120.8742
50	90	1	4	3	138.3237
50	90	1	5	3	138.3237
50	90	1	1	3.5	126.4387
50	90	1	2	3.5	121.3268
50	90	1	3	3.5	120.2905
50	90	1	4	3.5	137.177
50	90	1	5	3.5	135.5688
55	60	1	1	2.5	169.6205
55	60	1	2	2.5	162.9897
55	60	1	3	2.5	151.1385

HORSE	ANGLE	GROUP	ROI	RADIUS (mm)	MEAN (0.1mm Aluminium)
55	60	1	4	2.5	170.8205
55	60	1	5	2.5	136.4821
55	60	1	1	3	170.8363
55	60	1	2	3	162.4235
55	60	1	3	3	150.5338
55	60	1	4	3	173.1281
55	60	1	5	3	136.8648
55	60	1	1	3.5	170.8053
55	60	1	2	3.5	162.5227
55	60	1	3	3.5	152.52
55	60	1	4	3.5	177.5947
55	60	1	5	3.5	136.2053
55	90	1	1	2.5	143.5304
55	90	1	2	2.5	141.171
55	90	1	3	2.5	128.7971
55	90	1	4	2.5	140.9565
55	90	1	5	2.5	122.9536
55	90	1	1	3	141.5184
55	90	1	2	3	141.5184
55	90	1	3	3	128.2372
55	90	1	4	3	138.6749
55	90	1	5	3	138.6749
55	90	1	1	3.5	136.0608
55	90	1	2	3.5	136.0608
55	90	1	3	3.5	136.0608
55	90	1	4	3.5	136.0608
55	90	1	5	3.5	122.9188
57	60	1	1	2.5	154.0769
57	60	1	2	2.5	145.2821
57	60	1	3	2.5	160.559
57	60	1	4	2.5	147.9385
57	60	1	5	2.5	136.8564
57	60	1	1	3	157.9822
57	60	1	2	3	148.6299
57	60	1	3	3	164.7117
57	60	1	4	3	151.79
57	60	1	5	3	139.0071
57	60	1	1	3.5	159.3588
57	60	1	2	3.5	150.8259
57	60	1	3	3.5	165.6385
57	60	1	4	3.5	153.3483
57	60	1	5	3.5	138.6332
57	90	1	1	2.5	153.5275
57	90	1	2	2.5	152.342
57	90	1	3	2.5	158.4116
57	90	1	4	2.5	150.8928
57	90	1	5	2.5	133.3855
57	90	1	1	3	152.8742
57	90	1	2	3	150.2144

HORSE	ANGLE	GROUP	ROI	RADIUS (mm)	MEAN (0.1mm Aluminium)
57	90	1	3	3	156.4371
57	90	1	4	3	151.8
57	90	1	5	3	151.8
57	90	1	1	3.5	152.1128
57	90	1	2	3.5	148.3955
57	90	1	3	3.5	153.8541
57	90	1	4	3.5	152.6075
57	90	1	5	3.5	132.4165
58	60	0	1	2.5	138.8265
58	60	0	2	2.5	118.1173
58	60	0	3	2.5	114.4337
58	60	0	4	2.5	115.1939
58	60	0	5	2.5	125.2653
58	60	0	1	3	139.8577
58	60	0	2	3	118.0783
58	60	0	3	3	117.7651
58	60	0	4	3	117.0996
58	60	0	5	3	125.1922
58	60	0	1	3.5	139.6702
58	60	0	2	3.5	119.5198
58	60	0	3	3.5	118.6385
58	60	0	4	3.5	120.6649
58	60	0	5	3.5	125.0633
58	90	0	1	2.5	121.2841
58	90	0	2	2.5	113.8377
58	90	0	3	2.5	112.8319
58	90	0	4	2.5	115.2348
58	90	0	5	2.5	118.4261
58	90	0	1	3	120.701
58	90	0	2	3	113.3546
58	90	0	3	3	112.0825
58	90	0	4	3	112.767
58	90	0	5	3	112.767
58	90	0	1	3.5	113.9398
58	90	0	2	3.5	113.9398
58	90	0	3	3.5	113.9398
58	90	0	4	3.5	113.9398
58	90	0	5	3.5	117.9489
59	60	0	1	2.5	145.7817
59	60	0	2	2.5	125.7868
59	60	0	3	2.5	119.3299
59	60	0	4	2.5	128.7005
59	60	0	5	2.5	139.665
59	60	0	1	3	146.3843
59	60	0	2	3	128.3025
59	60	0	3	3	121.5303
59	60	0	4	3	131.4555
59	60	0	5	3	138.2135
59	60	0	1	3.5	146.409

HORSE	ANGLE	GROUP	ROI	RADIUS (mm)	MEAN (0.1mm Aluminium)
59	60	0	2	3.5	130.124
59	60	0	3	3.5	121.9921
59	60	0	4	3.5	132.3456
59	60	0	5	3.5	137.7599
59	90	0	1	2.5	131.2899
59	90	0	2	2.5	124.7942
59	90	0	3	2.5	114.8377
59	90	0	4	2.5	117.8319
59	90	0	5	2.5	134.5652
59	90	0	1	3	121.5057
59	90	0	2	3	121.5057
59	90	0	3	3	121.5057
59	90	0	4	3	121.5057
59	90	0	5	3	121.5057
59	90	0	1	3.5	120.2667
59	90	0	2	3.5	120.2667
59	90	0	3	3.5	120.2667
59	90	0	4	3.5	120.2667
59	90	0	5	3.5	132.8539
60	60	1	1	2.5	145.7026
60	60	1	2	2.5	137.1333
60	60	1	3	2.5	128.9231
60	60	1	4	2.5	128.7128
60	60	1	5	2.5	131.3179
60	60	1	1	3	147.2954
60	60	1	2	3	138.5872
60	60	1	3	3	129.8327
60	60	1	4	3	130.0463
60	60	1	5	3	131.2562
60	60	1	1	3.5	147.5937
60	60	1	2	3.5	141.2296
60	60	1	3	3.5	130.1715
60	60	1	4	3.5	132.7942
60	60	1	5	3.5	131.1372
60	90	1	1	2.5	132.0696
60	90	1	2	2.5	131.6754
60	90	1	3	2.5	119.5304
60	90	1	4	2.5	123.113
60	90	1	5	2.5	122.8957
60	90	1	1	3	131.9052
60	90	1	2	3	130.2845
60	90	1	3	3	118.4804
60	90	1	4	3	121.2536
60	90	1	5	3	121.2536
60	90	1	1	3.5	126.0336
60	90	1	2	3.5	126.0336
60	90	1	3	3.5	126.0336
60	90	1	4	3.5	119.2496
60	90	1	5	3.5	122.2752

HORSE	ANGLE	GROUP	ROI	RADIUS (mm)	MEAN (0.1mm Aluminium)
99	60	0	1	2.5	143.2915
99	60	0	2	2.5	134.1457
99	60	0	3	2.5	124.2965
99	60	0	4	2.5	122.7588
99	60	0	5	2.5	137.3015
99	60	0	1	3	143.7509
99	60	0	2	3	135.8842
99	60	0	3	3	127.4351
99	60	0	4	3	126.4035
99	60	0	5	3	137.5614
99	60	0	1	3.5	144.4433
99	60	0	2	3.5	138.4855
99	60	0	3	3.5	129.7678
99	60	0	4	3.5	127.5462
99	60	0	5	3.5	137.7678
99	90	0	1	2.5	125.4116
99	90	0	2	2.5	127.7275
99	90	0	3	2.5	117.7391
99	90	0	4	2.5	116.2493
99	90	0	5	2.5	130.0928
99	90	0	1	3	125.468
99	90	0	2	3	126.8351
99	90	0	3	3	117.0041
99	90	0	4	3	114.6928
99	90	0	5	3	114.6928
99	90	0	1	3.5	120.1827
99	90	0	2	3.5	120.1827
99	90	0	3	3.5	120.1827
99	90	0	4	3.5	120.1827
99	90	0	5	3.5	128.2376

APPENDIX 2

1. Dorsal data

Tabulated data prior to statistical analysis

Average of mean		ROI	ROI	ROI	ROI	ROI
angle	group	1	2	3	4	5
60	0	112.3291857	93.63664286	89.33692857	88.8459	98.25855714
	1	132.484	113.5861571	110.3599571	109.2511429	117.8281571
60 Total		122.4065929	103.6114	99.84844286	99.04852143	108.0433571
65	0	122.0319714	102.1353429	97.52488571	96.60687143	109.9217429
	1	131.4594143	114.7725143	112.2377429	110.7317286	119.1304571
65 Total		126.7456929	108.4539286	104.8813143	103.6693	114.5261
70	0	122.4941286	108.0305	105.5744857	101.9334	113.9898286
	1	132.3269	125.4987286	121.7163286	118.0472714	122.1662571
70 Total		127.4105143	116.7646143	113.6454071	109.9903357	118.0780429
75	0	120.8444714	108.1764429	106.7843714	104.2742286	116.3749714
	1	128.9287143	125.9305143	123.7682	120.6786571	121.3534571
75 Total		124.8865929	117.0534786	115.2762857	112.4764429	118.8642143
80	0	117.4144429	109.1298857	107.5098714	105.7973571	115.3048571
	1	129.3876286	131.7882143	126.7072429	120.7081	121.3181
80 Total		123.4010357	120.45905	117.1085571	113.2527286	118.3114786
85	0	123.9363857	117.8306429	115.2141429	113.0789571	123.2094286
	1	135.4771571	141.8922143	134.6035571	128.8648143	128.1896857
85 Total		129.7067714	129.8614286	124.90885	120.9718857	125.6995571
90	0	124.3954857	119.9293714	116.7768	115.8229143	126.6137143
	1	135.8639143	144.0953714	135.3377571	131.0199429	130.4559571
90 Total		130.1297	132.0123714	126.0572786	123.4214286	128.5348357

1.1 Main effect of angle

Pairwise comparisons comparing the main effect of angle when ROI's are in a dorsal position.

Dependent Variable: MEAN

Angle (I)	Angle (J)	Mean difference (I-J)	Standard error	Significance[a]
60	65	-5.064*	1.267	0.002
	70	-10.586*	1.267	<0.001
	75	-11.120*	1.267	<0.001
	80	-11.915*	1.267	<0.001
	85	-19.638*	1.267	<0.001
	90	-21.439*	1.267	<0.001
65	60	5.064*	1.267	0.002
	70	-5.523*	1.267	<0.001
	75	-6.056*	1.267	<0.001
	80	-6.851*	1.267	<0.001
	85	-14.574*	1.267	<0.001
	90	-16.376*	1.267	<0.001
70	60	10.586*	1.267	<0.001
	65	5.523*	1.267	<0.001
	75	-5.34[b]	1.267	1.000
	80	-1.329[b]	1.267	1.000
	85	-9.052*	1.267	<0.001
	90	-10.853*	1.267	<0.001
75	60	11.120*	1.267	<0.001
	65	6.056*	1.267	<0.001
	70	0.534[b]	1.267	1.000
	80	-0.795[b]	1.267	1.000
	85	-8.518*	1.267	<0.001
	90	-10.320*	1.267	<0.001
80	60	11.195*	1.267	<0.001
	65	6.851*	1.267	<0.001
	70	1.329[b]	1.267	1.000
	75	0.795[b]	1.267	1.000
	85	-7.723*	1.267	<0.001
	90	-9.525*	1.267	<0.001
85	60	19.638*	1.267	<0.001
	65	14.574*	1.267	<0.001
	70	9.052*	1.267	<0.001
	75	8.518*	1.267	<0.001
	80	7.723*	1.267	<0.001
	90	-1.801[b]	1.267	1.000
90	60	21.439*	1.267	<0.001
	65	16.376*	1.267	<0.001
	70	10.853*	1.267	<0.001
	75	10.320*	1.267	<0.001
	80	9.525*	1.267	<0.001
	85	1.801[b]	1.267	1.000

Based on estimated marginal means

*. The mean difference is significant at the 0.5 level

a. Adjustment for multiple comparisons: Bonferroni

b. An estimate of the modified population marginal mean (I)

1.1.1 Angle at one level of ROI

Pairwise comparisons to compare angle means at each level of ROI when ROI's are in a dorsal position.

Dependent Variable: MEAN

ROI	(I) ANGLE	(J) ANGLE	Mean Difference (I-J)	Std. Error	t value	Degrees of freedom	Significance[a]
1	60	65	-4.339	2.834	-1.531	408	0.334
		70	-5.004	2.834	-1.766	408	1.000
		75	-2.480	2.834	-0.875	408	1.000
		80	-0.994	2.834	-0.351	408	1.000
		85	-7.300	2.834	-2.576	408	0.217
		90	-7.723	2.834	-2.726	408	0.141
	65	60	4.339	2.834	1.531	408	1.000
		70	-0.665	2.834	-0.235	408	1.000
		75	1.859	2.834	0.656	408	1.000
		80	3.345	2.834	1.181	408	1.000
		85	-2.961	2.834	-1.045	408	1.000
		90	-3.384	2.834	-1.194	408	1.000
	70	60	5.004	2.834	1.766	408	1.000
		65	0.665	2.834	0.235	408	1.000
		75	2.252	2.834	0.795	408	1.000
		80	4.010	2.834	1.415	408	1.000
		85	-2.296	2.834	-0.810	408	1.000
		90	-2.719	2.834	-0.960	408	1.000
	75	60	2.480	2.834	0.875	408	1.000
		65	-1.859	2.834	-0.656	408	1.000
		70	-2.252	2.834	-0.795	408	1.000
		80	1.486	2.834	0.524	408	1.000
		85	-4.820	2.834	-1.701	408	1.000
		90	-5.243	2.834	-1.850	408	1.000
	80	60	0.994	2.834	0.351	408	1.000
		65	-3.334	2.834	-1.177	408	1.000
		70	-4.010	2.834	-1.415	408	1.000
		75	-1.486	2.834	-0.524	408	1.000
		85	-6.306	2.834	-2.225	408	0.558
		90	-6.729	2.834	-2.375	408	0.378
	85	60	7.300	2.834	2.576	408	0.217
		65	2.961	2.834	1.045	408	1.000
		70	2.296	2.834	0.810	408	1.000
		75	-1.486	2.834	-0.524	408	1.000
		80	6.306	2.834	2.225	408	0.558
		90	-0.423	2.834	-0.149	408	1.000
	90	60	7.723	2.834	2.726	408	0.141
		65	3.384	2.834	1.194	408	1.000
		70	2.719	2.834	0.960	408	1.000
		75	5.243	2.834	1.850	408	1.000
		80	6.729	2.834	2.375	408	0.378
		85	0.423	2.834	0.149	408	1.000
2	60	65	-4.843	2.834	-1.709	408	1.000
		70	-13.154	2.834	-4.642	408	<0.001

		75	-13.442	2.834	-4.744	408	<0.001
		80	-16.848	2.834	-5.946	408	<0.001
		85	-26.250	2.834	-9.264	408	<0.001
		90	-28.401	2.834	-10.023	408	<0.001
	65	60	4.484	2.834	1.582	408	1.000
		70	-8.311	2.834	-2.933	408	0.07
		75	-8.599	2.834	-3.035	408	0.054
		80	-12.005	2.834	-4.237	408	0.001
		85	-21.407	2.834	-7.555	408	<0.001
		90	-23.558	2.834	-8.314	408	<0.001
	70	60	13.154	2.834	4.642	408	<0.001
		65	8.311	2.834	2.933	408	0.074
		75	-0.288	2.834	-0.102	408	1.000
		80	-3.694	2.834	-1.304	408	1.000
		85	-13.096	2.834	-4.622	408	<0.001
		90	-15.247	2.834	-5.381	408	<0.001
	75	60	13.442	2.834	4.744	408	<0.001
		65	8.559	2.834	3.021	408	0.056
		70	0.228	2.834	0.080	408	1.000
		80	-3.406	2.834	-1.202	408	1.000
		85	-12.808	2.834	-4.520	408	<0.001
		90	-14.959	2.834	-5.279	408	<0.001
	80	60	16.848	2.834	5.946	408	<0.001
		65	12.005	2.834	4.237	408	0.001
		70	3.694	2.834	1.304	408	1.000
		75	3.406	2.834	1.202	408	1.000
		85	-9.402	2.834	-3.318	408	0.021
		90	-11.553	2.834	-4.077	408	0.001
	85	60	2.625	2.834	0.926	408	1.000
		65	21.407	2.834	7.555	408	<0.001
		70	13.096	2.834	4.622	408	<0.001
		75	12.808	2.834	4.520	408	<0.001
		80	9.402	2.834	3.318	408	0.021
		90	-2.151	2.834	-0.759	408	1.000
	90	60	28.401	2.834	10.023	408	<0.001
		65	23.558	2.834	8.314	408	<0.001
		70	15.247	2.834	5.381	408	<0.001
		75	14.959	2.834	5.279	408	<0.001
		80	11.553	2.834	4.077	408	0.001
		85	2.151	2.834	0.759	408	1.000
3	60	65	-5.033	2.834	-1.776	408	1.000
		70	-13.797	2.834	-4.869	408	<0.001
		75	-15.428	2.834	-5.445	408	<0.001
		80	-17.261	2.834	-6.092	408	<0.001
		85	-25.061	2.834	-8.844	408	<0.001
		90	-26.209	2.834	-9.250	408	<0.001
	65	60	5.033	2.834	1.776	408	1.000
		70	-8.764	2.834	-3.093	408	0.044
		75	-10.395	2.834	-3.669	408	0.006
		80	-12.228	2.834	-4.315	408	<0.001
		85	-20.028	2.834	-7.068	408	<0.001
		90	-21.176	2.834	-7.473	408	<0.001

	70	60	13.797	2.834	4.869	408	<0.001
		65	8.764	2.834	3.093	408	0.044
		75	-1.622	2.834	-0.572	408	1.000
		80	-3.455	2.834	-1.219	408	1.000
		85	-11.255	2.834	-3.972	408	0.002
		90	-12.403	2.834	-4.377	408	<0.001
	75	60	15.428	2.834	5.445	408	<0.001
		65	10.395	2.834	3.669	408	0.006
		70	1.622	2.834	0.572	408	1.000
		80	-1.833	2.834	-0.647	408	1.000
		85	-9.633	2.834	-3.400	408	0.016
		90	-10.781	2.834	-3.805	408	0.003
	80	60	17.261	2.834	6.092	408	<0.001
		65	12.228	2.834	4.315	408	<0.001
		70	3.455	2.834	1.219	408	1.000
		75	1.833	2.834	0.647	408	1.000
		85	-7.800	2.834	-2.753	408	0.130
		90	-8.948	2.834	-3.158	408	0.036
	85	60	25.061	2.834	8.844	408	<0.001
		65	20.028	2.834	7.068	408	<0.001
		70	11.255	2.834	3.972	408	0.002
		75	9.633	2.834	3.400	408	0.016
		80	7.800	2.834	2.753	408	0.130
		90	-11.480	2.834	-4.051	408	0.001
	90	60	26.209	2.834	9.250	408	<0.001
		65	21.176	2.834	7.473	408	<0.001
		70	12.043	2.834	4.250	408	0.001
		75	10.781	2.834	3.805	408	0.003
		80	8.948	2.834	3.158	408	0.036
		85	11.480	2.834	4.051	408	0.001
4	60	65	-4.620	2.834	-1.630	408	1.000
		70	-10.941	2.834	-3.861	408	0.003
		75	-13.427	2.834	-4.739	408	<0.001
		80	-14.204	2.834	-5.013	408	<0.001
		85	-21.923	2.834	-7.737	408	<0.001
		90	-24.372	2.834	-8.601	408	<0.001
	65	60	4.620	2.834	1.630	408	1.000
		70	-6.321	2.834	-2.231	408	0.551
		75	-8.807	2.834	-3.108	408	0.042
		80	-9.584	2.834	-3.382	408	0.017
		85	-17.303	2.834	-6.107	408	<0.001
		90	-19.752	2.834	-6.971	408	<0.001
	70	60	10.941	2.834	3.861	408	0.003
		65	6.321	2.834	2.231	408	0.551
		75	-2.486	2.834	-0.877	408	1.000
		80	-3.263	2.834	-1.152	408	1.000
		85	-10.982	2.834	-3.876	408	0.003
		90	-13.431	2.834	-4.740	408	<0.001
	75	60	13.427	2.834	4.739	408	<0.001
		65	8.807	2.834	3.108	408	0.042
		70	2.486	2.834	0.877	408	1.000
		80	-0.777	2.834	-0.274	408	1.000

		85	-8.496	2.834	-2.998	408	0.060
		90	-10.945	2.834	-3.863	408	0.003
	80	60	14.204	2.834	5.013	408	<0.001
		65	9.584	2.834	3.382	408	0.017
		70	3.263	2.834	1.152	408	1.000
		75	0.777	2.834	0.274	408	1.000
		85	-7.719	2.834	-2.724	408	0.141
		90	-10.168	2.834	-3.588	408	0.008
	85	60	21.923	2.834	7.737	408	<0.001
		65	17.303	2.834	6.107	408	<0.001
		70	10.982	2.834	3.876	408	0.003
		75	8.496	2.834	2.998	408	0.060
		80	7.719	2.834	2.724	408	0.141
		90	-2.449	2.834	-0.864	408	1.000
	90	60	24.372	2.834	8.601	408	<0.001
		65	19.752	2.834	6.971	408	<0.001
		70	13.431	2.834	4.740	408	<0.001
		75	10.945	2.834	3.863	408	0.003
		80	10.168	2.834	3.588	408	0.008
		85	2.449	2.834	0.864	408	1.000
5	60	65	-6.483	2.834	-2.288	408	0.476
		70	-10.035	2.834	-3.542	408	0.009
		75	-10.821	2.834	-3.819	408	0.003
		80	-10.268	2.834	-3.624	408	0.007
		85	-17.668	2.834	-6.235	408	<0.001
		90	-20.492	2.834	-7.232	408	<0.001
	65	60	6.483	2.834	2.288	408	0.476
		70	-3.552	2.834	-1.254	408	1.000
		75	-4.338	2.834	-1.531	408	1.000
		80	-3.785	2.834	-1.336	408	1.000
		85	-11.184	2.834	-3.947	408	0.002
		90	-14.009	2.834	-4.944	408	<0.001
	70	60	10.035	2.834	3.542	408	0.009
		65	3.552	2.834	1.254	408	1.000
		75	-0.786	2.834	-0.277	408	1.000
		80	-0.233	2.834	-0.082	408	1.000
		85	-7.622	2.834	-2.690	408	0.156
		90	-10.457	2.834	-3.690	408	0.005
	75	60	10.821	2.834	3.819	408	0.003
		65	4.338	2.834	1.531	408	1.000
		70	0.786	2.834	0.277	408	1.000
		80	0.553	2.834	0.195	408	1.000
		85	-6.847	2.834	-2.416	408	0.338
		90	-9.671	2.834	-3.413	408	0.015
	80	60	10.268	2.834	3.624	408	0.007
		65	3.785	2.834	1.336	408	1.000
		70	0.233	2.834	0.082	408	1.000
		75	0.553	2.834	0.195	408	1.000
		85	-7.369	2.834	-2.601	408	0.202
		90	-10.204	2.834	-3.601	408	0.007
	85	60	17.668	2.834	6.235	408	<0.001
		65	11.184	2.834	3.947	408	0.002

		70	7.622	2.834	2.690	408	0.156
		75	6.847	2.834	2.416	408	0.338
		80	7.369	2.834	2.601	408	0.202
		90	-2.835	2.834	-1.001	408	1.000
	90	60	20.492	2.834	7.232	408	<0.001
		65	14.009	2.834	4.944	408	<0.001
		70	10.457	2.834	3.690	408	0.005
		75	9.671	2.834	3.413	408	0.015
		80	10.204	2.834	3.601	408	0.007
		85	2.835	2.834	1.001	408	1.000

Based on estimated marginal means

a. Adjustment for multiple comparisons: Bonferroni
b. An estimate of the modified population marginal mean (I)

1.1.2 Angle at one level of group

Pairwise comparisons to compare angle while holding group (non-exercise) constant.

Dependent Variable: MEAN

Angle(I)	Angle(J)	Mean Difference (I-J)	Std. Error	t value	Degrees of freedom	Significance[a]
60	65	-9.163	1.780	-9.163	408	<0.001
	70	-13.923	1.780	-13.923	408	<0.001
	75	-14.810	1.780	-14.81	408	<0.001
	80	-14.550	1.780	-14.55	408	<0.001
	85	-22.173	1.780	-22.173	408	<0.001
	90	-24.227	1.780	-24.227	408	<0.001
65	60	9.163	1.780	9.163	408	<0.001
	70	-4.760	1.780	-4.76	408	0.164
	75	-5.647	1.780	-5.647	408	0.034
	80	-5.387	1.780	-5.387	408	0.055
	85	-13.010	1.780	-13.01	408	<0.001
	90	-15.064	1.780	-15.064	408	<0.001
70	60	13.923	1.780	13.923	408	<0.001
	65	4.760	1.780	4.76	408	0.164
	75	-0.887	1.780	-0.887	408	1.000
	80	-0.627	1.780	-0.627	408	1.000
	85	-8.250	1.780	-8.25	408	<0.001
	90	-10.304	1.780	-10.304	408	<0.001
75	60	14.810	1.780	14.81	408	<0.001
	65	5.647	1.780	5.647	408	0.034
	70	0.887	1.780	0.887	408	1.000
	80	0.260	1.780	0.26	408	1.000
	85	-7.363	1.780	-7.363	408	0.001
	90	-9.417	1.780	-9.417	408	<0.001
80	60	14.550	1.780	14.55	408	<0.001
	65	5.387	1.780	5.387	408	0.055
	70	0.627	1.780	0.627	408	1.000
	75	-0.260	1.780	-0.26	408	1.000
	85	-7.623	1.780	-7.623	408	<0.001
	90	-9.677	1.780	-9.677	408	<0.001
85	60	22.173	1.780	22.173	408	<0.001
	65	13.010	1.780	13.01	408	<0.001
	70	8.250	1.780	8.25	408	<0.001
	75	7.363	1.780	7.363	408	0.001
	80	7.623	1.780	7.623	408	<0.001
	90	-2.054	1.780	-2.054	408	1.000
90	60	24.227	1.780	24.227	408	<0.001
	65	15.064	1.780	15.064	408	<0.001
	70	10.304	1.780	10.304	408	<0.001
	75	9.417	1.780	9.417	408	<0.001
	80	9.677	1.780	9.677	408	<0.001
	85	2.054	1.780	2.054	408	1.000

Based on estimated marginal means

a. Adjustment for multiple comparisons: Bonferroni

Pairwise comparisons to compare angle while holding group (exercise) constant

Dependent Variable: MEAN

Angle(I)	Angle(J)	Mean Difference(I-J)	Std. Error	t value	Degrees of freedom	Significance[a]
60	65	0.964	1.780	0.964	408	1.000
	70	-7.249	1.780	-7.249	408	0.001
	75	-7.430	1.780	-7.430	408	0.001
	80	-9.280	1.780	-9.280	408	<0.001
	85	-17.103	1.780	-17.103	408	<0.001
	90	-18.653	1.780	-18.653	408	<0.001
65	60	-0.964	1.780	-0.964	408	1.000
	70	-6.285	1.780	-6.285	408	0.010
	75	-6.466	1.780	-6.466	408	0.007
	80	-8.316	1.780	-8.316	408	<0.001
	85	-16.139	1.780	-16.139	408	<0.001
	90	-17.689	1.780	-17.689	408	<0.001
70	60	7.249	1.780	7.249	408	0.001
	65	6.285	1.780	6.285	408	0.010
	75	-0.181	1.780	-0.181	408	1.000
	80	-2.031	1.780	-2.031	408	1.000
	85	-9.854	1.780	-9.854	408	<0.001
	90	-11.404	1.780	-11.404	408	<0.001
75	60	7.430	1.780	7.430	408	0.001
	65	6.466	1.780	6.466	408	0.007
	70	0.181	1.780	0.181	408	1.000
	80	-1.850	1.780	-1.850	408	1.000
	85	-9.673	1.780	-9.673	408	<0.001
	90	-11.223	1.780	-11.223	408	<0.001
80	60	9.280	1.780	9.280	408	<0.001
	65	8.316	1.780	8.316	408	<0.001
	70	2.031	1.780	2.031	408	1.000
	75	1.850	1.780	1.850	408	1.000
	85	-7.823	1.780	-7.823	408	<0.001
	90	-9.373	1.780	-9.373	408	<0.001
85	60	17.103	1.780	17.103	408	<0.001
	65	16.139	1.780	16.139	408	<0.001
	70	9.854	1.780	9.854	408	<0.001
	75	9.673	1.780	9.673	408	<0.001
	80	7.823	1.780	7.823	408	<0.001
	90	-1.550	1.780	-1.550	408	1.000
90	60	18.653	1.780	18.653	408	<0.001
	65	17.689	1.780	17.689	408	<0.001
	70	11.404	1.780	11.404	408	<0.001
	75	11.223	1.780	11.223	408	<0.001
	80	9.373	1.780	9.373	408	<0.001
	85	1.550	1.780	1.550	408	1.000

Based on estimated marginal means2

Adjustment for multiple comparisons: Bonferroni

1.2 Main effect of ROI

Pairwise comparison to compare the main effect of ROI when ROI's are in a dorsal position.

Dependent variable : MEAN

ROI (I)	ROI (J)	Mean difference	Std Error	Significance[a]
1	2	8.037*	1.071	<0.001
	3	11.852*	1.071	<0.001
	4	14.221*	1.071	<0.001
	5	7.518*	1.071	<0.001
2	1	-8.067*	1.071	<0.001
	3	3.784*	1.071	0.005
	4	6.484*	1.071	<0.001
	5	-0.549[b]	1.071	1.000
3	1	-11.852*	1.071	<0.001
	2	-3.784*	1.071	0.005
	4	2.699[b]	1.071	0.121
	5	-4.333*	1.071	0.001
4	1	-14.551*	1.071	<0.001
	2	-6.484*	1.071	<0.001
	3	-2.699[b]	1.071	0.121
	5	-7.032*	1.071	<0.001
5	1	-7.518*	1.071	<0.001
	2	0.549[b]	1.071	1.000
	3	4.333*	1.071	0.001
	4	7.032*	1.071	<0.001

Based on estimated marginal means

*. The mean difference is significant at the 0.5 level

a. Adjustment for multiple comparisons: Bonferroni

b. An estimate of the modified population marginal mean (I)

1.2.1 ROI at one level of group

Pairwise comparisons comparing ROI holding group (non-exercise) constant when ROI's are in a dorsal position.

Dependent Variable :MEAN

ROI (I)	ROI (J)	mean difference (I-J)	Std error	T value	Degrees of freedom	Significance[a]
1	2	12.092	1.515	7.984	408	<0.001
	3	14.973	1.515	9.886	408	<0.001
	4	16.740	1.515	11.053	408	<0.001
	5	5.687	1.515	3.755	408	0.002
2	1	-12.092	1.515	7.984	408	<0.001
	3	2.880	1.515	1.902	408	0.579
	4	4.648	1.515	3.069	408	0.023
	5	-6.405	1.515	-4.229	408	<0.001
3	1	-14.973	1.515	9.886	408	<0.001
	2	-2.880	1.515	1.902	408	0.579
	4	1.768	1.515	1.167	408	1.000
	5	-9.286	1.515	-6.131	408	<0.001
4	1	-16.740	1.515	11.053	408	<0.001
	2	-4.648	1.515	3.069	408	0.023
	3	-1.768	1.515	1.167	408	1.000
	5	-11.053	1.515	-7.298	408	<0.001
5	1	-5.687	1.515	3.755	408	0.002
	2	6.405	1.515	-4.229	408	<0.001
	3	9.286	1.515	-6.131	408	<0.001
	4	11.053	1.515	-7.298	408	<0.001

Based on estimated marginal means

a. Adjustment for multiple comparisons: Bonferroni

Pairwise comparison comparing ROI holding group (exercise) constant when ROI's are in a dorsal position.

Dependent Variable :MEAN

ROI (I)	ROI (J)	Mean Difference (I-J)	Std error	T value	Degrees of freedom	Significance[a]
1	2	4.055	1.515	2.678	408	0.077
	3	8.750	1.515	5.777	408	<0.001
	4	12.386	1.515	8.178	408	<0.001
	5	9.375	1.515	6.190	408	<0.001
2	1	-4.055	1.515	2.678	408	0.077
	3	4.694	1.515	3.099	408	0.021
	4	8.340	1.515	5.507	408	<0.001
	5	5.307	1.515	3.504	408	0.005
3	1	8.750	1.515	5.777	408	<0.001
	2	-4.694	1.515	3.099	408	0.021
	4	3.636	1.515	2.401	408	0.168
	5	0.614	1.515	0.405	408	1.000
4	1	-12.386	1.515	8.178	408	<0.001
	2	-8.340	1.515	5.507	408	<0.001
	3	-3.636	1.515	2.401	408	0.168
	5	-3.023	1.515	-1.996	408	0.466
5	1	-9.375	1.515	6.190	408	<0.001
	2	-5.307	1.515	3.504	408	0.005
	3	-0.614	1.515	0.405	408	1.000
	4	3.023	1.515	-1.996	408	0.466

Based on estimated marginal means

a. Adjustment for multiple comparisons: Bonferroni

1.2.2 ROI at one level of angle

Pairwise comparisons to compare ROI means while holding angle constant when ROI's are in a dorsal position.

Dependent variable:MEANS

ANGLE	(I) ROI	(J) ROI	Mean Difference (I-J)	Std. Error	T value	Degrees of freedom	Significance[a]
60	1	2	18.796	2.834	6.633	408	<0.001
		3	22.559	2.834	7.961	408	<0.001
		4	23.258	2.834	8.208	408	<0.001
		5	14.364	2.834	5.069	408	<0.001
	2	1	-18.796	2.834	-6.633	408	<0.001
		3	3.763	2.834	1.328	408	1.000
		4	4.562	2.834	1.610	408	1.000
		5	-4.432	2.834	-1.564	408	1.000
	3	1	-22.559	2.834	-7.961	408	<0.001
		2	-3.763	2.834	-1.328	408	1.000
		4	0.799	2.834	0.282	408	1.000
		5	-8.195	2.834	-2.892	408	0.040
	4	1	-23.258	2.834	-8.208	408	<0.001
		2	-4.562	2.834	-1.610	408	1.000
		3	-0.799	2.834	-0.282	408	1.000
		5	-8.994	2.834	-3.174	408	0.016
	5	1	-14.364	2.834	-5.069	408	<0.001
		2	4.432	2.834	1.564	408	1.000
		3	8.195	2.834	2.892	408	0.040
		4	8.994	2.834	3.174	408	0.016
65	1	2	18.292	2.834	6.456	408	<0.001
		3	21.865	2.834	7.717	408	<0.001
		4	23.077	2.834	8.144	408	<0.001
		5	12.220	2.834	4.313	408	<0.001
	2	1	-18.292	2.834	-6.456	408	<0.001
		3	3.573	2.834	1.261	408	1.000
		4	4.785	2.834	1.689	408	0.920
		5	-6.072	2.834	-2.143	408	0.327
	3	1	-21.865	2.834	-7.717	408	<0.001
		2	-3.573	2.834	-1.261	408	1.000
		4	1.212	2.834	0.428	408	1.000
		5	-9.645	2.834	-3.404	408	0.007
	4	1	-23.077	2.834	-8.144	408	<0.001
		2	-4.785	2.834	-1.689	408	0.920
		3	-1.212	2.834	-0.428	408	1.000
		5	-10.857	2.834	-3.832	408	0.001
	5	1	-12.220	2.834	-4.313	408	<0.001
		2	6.072	2.834	2.143	408	0.327
		3	-0.645	2.834	-0.228	408	1.000
		4	10.857	2.834	3.832	408	0.001
70	1	2	10.646	2.834	3.757	408	0.002
		3	13.766	2.834	4.858	408	<0.001
		4	17.511	2.834	6.180	408	<0.001
		5	9.333	2.834	3.294	408	0.011

	2	1	-10.646	2.834	-3.757	408	0.002
		3	3.120	2.834	1.101	408	1.000
		4	6.820	2.834	2.407	408	0.165
		5	-1.313	2.834	-0.463	408	1.000
	3	1	-13.766	2.834	-4.858	408	<0.001
		2	-3.120	2.834	-1.101	408	1.000
		4	3.745	2.834	1.322	408	1.000
		5	-4.433	2.834	-1.564	408	1.000
	4	1	-17.511	2.834	-6.180	408	<0.001
		2	-6.820	2.834	-2.407	408	0.165
		3	-3.745	2.834	-1.322	408	1.000
		5	-7.178	2.834	-2.533	408	0.117
	5	1	-9.333	2.834	-3.294	408	0.011
		2	1.313	2.834	0.463	408	1.000
		3	4.433	2.834	1.564	408	1.000
		4	7.178	2.834	2.533	408	0.117
75	1	2	7.834	2.834	2.765	408	0.060
		3	9.611	2.834	3.392	408	0.008
		4	12.411	2.834	4.380	408	<0.001
		5	6.023	2.834	2.126	408	0.341
	2	1	-7.834	2.834	-2.765	408	0.060
		3	1.777	2.834	0.627	408	1.000
		4	4.577	2.834	1.615	408	1.000
		5	-1.811	2.834	-0.639	408	1.000
	3	1	-9.611	2.834	-3.392	408	0.008
		2	-1.777	2.834	-0.627	408	1.000
		4	2.800	2.834	0.988	408	1.000
		5	-3.588	2.834	-1.266	408	1.000
	4	1	-12.411	2.834	-4.380	408	<0.001
		2	-4.577	2.834	-1.615	408	1.000
		3	-2.800	2.834	-0.988	408	1.000
		5	-6.388	2.834	-2.254	408	0.247
	5	1	-6.023	2.834	-2.126	408	0.341
		2	1.811	2.834	0.639	408	1.000
		3	3.588	2.834	1.266	408	1.000
		4	6.388	2.834	2.254	408	0.247
80	1	2	2.942	2.834	1.038	408	1.000
		3	6.292	2.834	2.221	408	0.269
		4	10.148	2.834	3.581	408	0.004
		5	5.090	2.834	1.796	408	0.732
	2	1	-2.942	2.834	-1.038	408	1.000
		3	3.350	2.834	1.182	408	1.000
		4	7.334	2.834	2.588	408	0.100
		5	2.145	2.834	0.757	408	1.000
	3	1	-6.292	2.834	-2.221	408	0.269
		2	-3.350	2.834	-1.182	408	1.000
		4	3.856	2.834	1.361	408	1.000
		5	-1.202	2.834	-0.424	408	1.000
	4	1	-10.148	2.834	-3.581	408	0.004
		2	-7.334	2.834	-2.588	408	0.100
		3	-3.856	2.834	-1.361	408	1.000
		5	-5.058	2.834	-1.785	408	0.750

	5	1	-5.090	2.834	-1.796	408	0.732
		2	-2.145	2.834	-0.757	408	1.000
		3	1.202	2.834	0.424	408	1.000
		4	5.058	2.834	1.785	408	0.750
85	1	2	-0.154	2.834	-0.054	408	1.000
		3	4.798	2.834	1.693	408	0.912
		4	8.735	2.834	3.083	408	0.022
		5	4.007	2.834	1.414	408	1.000
	2	1	0.154	2.834	0.054	408	1.000
		3	4.952	2.834	1.748	408	0.813
		4	8.889	2.834	3.137	408	0.018
		5	4.161	2.834	1.468	408	1.000
	3	1	-4.798	2.834	-1.693	408	0.912
		2	-4.952	2.834	-1.748	408	0.813
		4	3.937	2.834	1.389	408	1.000
		5	-0.863	2.834	-0.305	408	1.000
	4	1	-8.735	2.834	-3.083	408	0.022
		2	-8.889	2.834	-3.137	408	0.018
		3	-3.937	2.834	-1.389	408	1.000
		5	-4.428	2.834	-1.563	408	1.000
	5	1	-4.007	2.834	-1.414	408	1.000
		2	-4.161	2.834	-1.468	408	1.000
		3	0.863	2.834	0.305	408	1.000
		4	4.428	2.834	1.563	408	1.000
90	1	2	-1.882	2.834	-0.664	408	1.000
		3	4.073	2.834	1.437	408	1.000
		4	6.709	2.834	2.368	408	0.184
		5	1.595	2.834	0.563	408	1.000
	2	1	1.882	2.834	0.664	408	1.000
		3	5.955	2.834	2.102	408	0.362
		4	8.591	2.834	3.032	408	0.026
		5	3.477	2.834	1.227	408	1.000
	3	1	-4.073	2.834	-1.437	408	1.000
		2	-5.955	2.834	-2.102	408	0.362
		4	2.636	2.834	0.930	408	1.000
		5	-2.478	2.834	-0.875	408	1.000
	4	1	-6.709	2.834	-2.368	408	0.184
		2	-8.591	2.834	-3.032	408	0.026
		3	-2.636	2.834	-0.930	408	1.000
		5	-5.114	2.834	-1.805	408	0.718
	5	1	-1.595	2.834	-0.563	408	1.000
		2	-3.477	2.834	-1.227	408	1.000
		3	2.478	2.834	0.875	408	1.000
		4	5.114	2.834	1.805	408	0.718

Based on estimated marginal means

a. Adjustment for multiple comparisons: Bonferroni

1.3 Main effect of group

Pairwise comparisons to compare the main effect of group when ROI is in a dorsal and palmar position

position	Exercised (I)	Non exercised (J)	Mean difference (I-J)	Std Error	Sig
Dorsal	125.37	110.60	14.77	0.479	<0.001
palmar	138.38	120.10	18.28	0.476	<0.001

b. An estimate of the modified population marginal mean

1.3.1 Group at one level of angle

Pairwise comparisons to compare group means while holding angle constant when ROI's are in a dorsal position.

Dependent Variable: MEAN

ANGLE	Mean Difference (I-J)	Std. Error	t value	Degrees of freedom	significance
60	20.221	1.792	11.284	408	<0.001
65	12.022	1.792	6.708	408	<0.001
70	13.547	1.792	7.559	408	<0.001
75	12.841	1.792	7.165	408	<0.001
80	14.951	1.792	8.343	408	<0.001
85	15.151	1.792	8.454	408	<0.001
90	14.647	1.792	8.173	408	<0.001

I = exercised
J = nonexercised

1.3.2 group at one level of ROI

Pairwise comparisons to compare group means while holding ROI constant when ROI's are in a dorsal position.

Dependent Variable: MEAN

ROI	Mean Difference (I-J)	Std. Error	t value	Degrees of freedom	significance
1	-11.782	1.773	-6.646	117	<0.001
2	-19.813	1.773	-11.176	117	<0.001
3	-18.001	1.773	-10.154	117	<0.001
4	-16.134	1.773	-9.101	117	<0.001
5	-8.110	1.773	-4.575	117	<0.001

I = exercised
J = nonexercised

2. Palmar data

Tabulated data prior to statistical analysis

Average of mean		ROI	ROI	ROI	ROI	ROI
angle	group	1	2	3	4	5
60	0	136.0762571	121.7521571	118.386	119.8466571	129.0873143
	1	158.2684143	149.4595857	142.6131	148.8459571	140.4601
60 Total		147.1723357	135.6058714	130.49955	134.3463071	134.7737071
65	0	131.9321286	118.6422714	118.5579571	119.2637286	127.458
	1	147.8734429	141.1792857	138.6190714	138.8018143	135.1219143
65 Total		139.9027857	129.9107786	128.5885143	129.0327714	131.2899571
70	0	126.7036	116.3538571	115.9089857	115.3619857	124.1215
	1	144.4138286	141.3019714	137.6187143	134.7331143	131.2440286
70 Total		135.5587143	128.8279143	126.76385	125.04755	127.6827643
75	0	122.0600857	112.9472714	113.1042714	113.6886571	124.9425571
	1	138.9266714	137.6562571	133.2698143	131.9673	129.4500857
75 Total		130.4933786	125.3017643	123.1870429	122.8279786	127.1963214
80	0	118.1328571	111.4038286	109.8164857	111.9089714	122.2712857
	1	136.6913	137.3381714	131.5278286	132.0677429	128.0948429
80 Total		127.4120786	124.371	120.6721571	121.9883571	125.1830643
85	0	124.0874714	118.3069286	115.1590571	117.5555286	129.2006143
	1	141.5463857	143.1269429	136.3717286	138.7307714	132.3452286
85 Total		132.8169286	130.7169357	125.7653929	128.14315	130.7729214
90	0	122.0192857	118.5589143	115.5319	115.6691429	127.7460429
	1	139.6764143	140.9868571	134.5125143	137.7514857	130.8053429
90 Total		130.84785	129.7728857	125.0222071	126.7103143	129.2756929

2.1 Main effect of angle

Pairwise comparisons to compare the main effect of angle when ROI's are in a palmar position.

Dependent variable: MEAN

Angle (I)	Angle (J)	Mean difference (I-J)	Std error	Significance[a]
60	65	4.735*	1.259	<0.001
	70	7.703*	1.259	<0.001
	75	10.678*	1.259	<0.001
	80	12.554*	1.259	<0.001
	85	6.826*	1.259	<0.001
	90	8.154*	1.259	<0.001
65	60	-4.735*	1.259	<0.001
	70	2.969*	1.259	0.019
	75	5.944*	1.259	<0.001
	80	7.820*	1.259	<0.001
	85	2.102[b]	1.259	0.096
	90	3.419*	1.259	0.007
70	60	-7.703*	1.259	<0.001
	65	-2.969*	1.259	0.019
	75	2.975*	1.259	0.019
	80	4.851*	1.259	<0.001
	85	-0.867[b]	1.259	0.491
	90	0.450[b]	1.259	0.721
75	60	-10.678*	1.259	<0.001
	65	-5.944*	1.259	<0.001
	70	-2.957*	1.259	0.019
	80	1.876[b]	1.259	0.137
	85	-3.842*	1.259	0.002
	90	-2.524*	1.259	0.046
80	60	-12.554*	1.259	<0.001
	65	-7.820*	1.259	<0.001
	70	-4.851*	1.259	<0.001
	75	-1.876[b]	1.259	0.137
	85	-5.718*	1.259	<0.001
	90	-4.400*	1.259	0.001
85	60	-6.836*	1.259	<0.001
	65	-2.102[b]	1.259	0.096
	70	0.867[b]	1.259	0.491
	75	3.842*	1.259	0.002
	80	5.718*	1.259	<0.001
	90	1.317[b]	1.259	0.296
90	60	-8.154*	1.259	<0.001
	65	-3.419*	1.259	0.007
	70	-0.450[b]	1.259	0.721
	75	2.524*	1.259	0.046
	80	4.400*	1.259	0.001
	85	-1.317[b]	1.259	0.296

Based on estimated marginal means

*. The mean difference is significant at the 0.5 level

a. Adjustment for multiple comparisons: Bonferroni

b. An estimate of the modified population marginal mean (I)

2.1.1 Angle at one level of ROI

Pairwise comparisons comparing angle means at one level of ROI when ROI's are in a palmar position.

Depedent variable:MEAN

ROI	(I) ANGLE	(J) ANGLE	Mean Difference (I-J)	Std. Error	T value	Degrees of freedom	Significance[a]
1	60	65	7.270	2.814	2.583	408	0.213
		70	11.614	2.814	4.127	408	0.001
		75	16.679	2.814	5.927	408	<0.001
		80	19.760	2.814	7.022	408	<0.001
		85	14.355	2.814	5.101	408	<0.001
		90	16.324	2.814	5.801	408	<0.001
	65	60	-7.270	2.814	-2.583	408	0.213
		70	4.344	2.814	1.544	408	1.000
		75	9.409	2.814	3.344	408	0.019
		80	12.491	2.814	4.439	408	<0.001
		85	7.086	2.814	2.518	408	0.256
		90	9.055	2.814	3.218	408	0.029
	70	60	-11.614	2.814	-4.127	408	0.001
		65	-4.344	2.814	-1.544	408	1.000
		75	5.065	2.814	1.800	408	1.000
		80	8.147	2.814	2.895	408	0.084
		85	2.742	2.814	0.974	408	1.000
		90	4.711	2.814	1.674	408	1.000
	75	60	-16.679	2.814	-5.927	408	<0.001
		65	-9.409	2.814	-3.344	408	0.019
		70	-5.065	2.814	-1.800	408	1.000
		80	3.081	2.814	1.095	408	1.000
		85	-2.324	2.814	-0.826	408	1.000
		90	-0.354	2.814	-0.126	408	1.000
	80	60	-19.760	2.814	-7.022	408	<0.001
		65	-12.491	2.814	-4.439	408	<0.001
		70	-8.147	2.814	-2.895	408	0.084
		75	-3.081	2.814	-1.095	408	1.000
		85	-5.405	2.814	-1.921	408	1.000
		90	-3.436	2.814	-1.221	408	1.000
	85	60	-14.355	2.814	-5.101	408	<0.001
		65	-7.086	2.814	-2.518	408	0.256
		70	-2.742	2.814	-0.974	408	1.000
		75	2.324	2.814	0.826	408	1.000
		80	5.405	2.814	1.921	408	1.000
		90	1.969	2.814	0.700	408	1.000
	90	60	-16.324	2.814	-5.801	408	<0.001
		65	-9.055	2.814	-3.218	408	0.029
		70	-4.711	2.814	-1.674	408	1.000
		75	0.354	2.814	0.126	408	1.000
		80	3.436	2.814	1.221	408	1.000
		85	-1.969	2.814	-0.700	408	1.000
2	60	65	5.695	2.814	2.024	408	0.917
		70	6.778	2.814	2.409	408	0.346
		75	10.304	2.814	3.662	408	0.006
		80	11.235	2.814	3.992	408	0.002

		85	4.889	2.814	1.737	408	1.000
		90	5.833	2.814	2.073	408	0.815
	65	60	-5.695	2.814	-2.024	408	0.917
		70	1.083	2.814	0.385	408	1.000
		75	4.609	2.814	1.638	408	1.000
		80	5.540	2.814	1.969	408	1.000
		85	-0.806	2.814	-0.286	408	1.000
		90	0.138	2.814	0.049	408	1.000
	70	60	-6.778	2.814	-2.409	408	0.346
		65	-1.083	2.814	-0.385	408	1.000
		75	3.526	2.814	1.253	408	1.000
		80	4.457	2.814	1.584	408	1.000
		85	-1.889	2.814	-0.671	408	1.000
		90	-0.945	2.814	-0.336	408	1.000
	75	60	-10.304	2.814	-3.662	408	0.006
		65	-4.609	2.814	-1.638	408	1.000
		70	-3.526	2.814	-1.253	408	1.000
		80	0.931	2.814	0.331	408	1.000
		85	-5.415	2.814	-1.924	408	1.000
		90	-4.471	2.814	-1.589	408	1.000
	80	60	-11.235	2.814	-3.992	408	0.002
		65	-5.540	2.814	-1.969	408	1.000
		70	-4.457	2.814	-1.584	408	1.000
		75	-0.931	2.814	-0.331	408	1.000
		85	-6.346	2.814	-2.255	408	0.518
		90	-5.402	2.814	-1.920	408	1.000
	85	60	-4.889	2.814	-1.737	408	1.000
		65	0.806	2.814	0.286	408	1.000
		70	1.889	2.814	0.671	408	1.000
		75	5.415	2.814	1.924	408	1.000
		80	6.346	2.814	2.255	408	0.518
		90	0.944	2.814	0.335	408	1.000
	90	60	-5.833	2.814	-2.073	408	0.815
		65	-0.138	2.814	-0.049	408	1.000
		70	0.945	2.814	0.336	408	1.000
		75	4.471	2.814	1.589	408	1.000
		80	5.402	2.814	1.920	408	1.000
		85	-0.944	2.814	-0.335	408	1.000
3	60	65	1.911	2.814	0.679	408	1.000
		70	3.736	2.814	1.327	408	1.000
		75	7.313	2.814	2.598	408	0.204
		80	9.827	2.814	3.492	408	0.011
		85	4.734	2.814	1.682	408	1.000
		90	5.477	2.814	1.946	408	1.000
	65	60	-1.911	2.814	-0.679	408	1.000
		70	1.825	2.814	0.648	408	1.000
		75	5.401	2.814	1.919	408	1.000
		80	7.916	2.814	2.813	408	0.108
		85	2.823	2.814	1.003	408	1.000
		90	3.566	2.814	1.267	408	1.000
	70	60	-3.736	2.814	-1.327	408	1.000
		65	-1.825	2.814	-0.648	408	1.000

		75	3.577	2.814	1.271	408	1.000
		80	6.092	2.814	2.165	408	0.651
		85	0.998	2.814	0.355	408	1.000
		90	1.742	2.814	0.619	408	1.000
	75	60	-7.313	2.814	-2.598	408	0.204
		65	-5.401	2.814	-1.919	408	1.000
		70	-3.577	2.814	-1.271	408	1.000
		80	2.515	2.814	0.894	408	1.000
		85	-2.578	2.814	-0.916	408	1.000
		90	-1.835	2.814	-0.652	408	1.000
	80	60	-9.827	2.814	-3.492	408	0.011
		65	-7.916	2.814	-2.813	408	0.108
		70	-6.092	2.814	-2.165	408	0.651
		75	-2.515	2.814	-0.894	408	1.000
		85	-5.093	2.814	-1.810	408	1.000
		90	-4.350	2.814	-1.546	408	1.000
	85	60	-4.734	2.814	-1.682	408	1.000
		65	-2.823	2.814	-1.003	408	1.000
		70	-0.998	2.814	-0.355	408	1.000
		75	2.578	2.814	0.916	408	1.000
		80	5.093	2.814	1.810	408	1.000
		90	0.743	2.814	0.264	408	1.000
	90	60	-5.477	2.814	-1.946	408	1.000
		65	-3.566	2.814	-1.267	408	1.000
		70	-1.742	2.814	-0.619	408	1.000
		75	1.835	2.814	0.652	408	1.000
		80	4.350	2.814	1.546	408	1.000
		85	-0.743	2.814	-0.264	408	1.000
4	60	65	5.314	2.814	1.888	408	1.000
		70	9.299	2.814	3.304	408	0.022
		75	11.518	2.814	4.093	408	0.001
		80	12.358	2.814	4.391	408	<0.001
		85	6.203	2.814	2.204	408	0.589
		90	7.636	2.814	2.713	408	0.146
	65	60	-5.314	2.814	-1.888	408	1.000
		70	3.985	2.814	1.416	408	1.000
		75	6.205	2.814	2.205	408	0.588
		80	7.044	2.814	2.503	408	0.267
		85	0.890	2.814	0.316	408	1.000
		90	2.322	2.814	0.825	408	1.000
	70	60	-9.299	2.814	-3.304	408	0.022
		65	-3.985	2.814	-1.416	408	1.000
		75	2.220	2.814	0.789	408	1.000
		80	3.059	2.814	1.087	408	1.000
		85	-3.096	2.814	-1.100	408	1.000
		90	-1.663	2.814	-0.591	408	1.000
	75	60	-11.518	2.814	-4.093	408	0.001
		65	-6.205	2.814	-2.205	408	0.588
		70	-2.220	2.814	-0.789	408	1.000
		80	0.840	2.814	0.298	408	1.000
		85	-5.315	2.814	-1.889	408	1.000
		90	-3.882	2.814	-1.380	408	1.000

	80	60	-12.358	2.814	-4.391	408	<0.001
		65	-7.044	2.814	-2.503	408	0.267
		70	-3.059	2.814	-1.087	408	1.000
		75	-0.840	2.814	-0.298	408	1.000
		85	-6.155	2.814	-2.187	408	0.615
		90	-4.722	2.814	-1.678	408	1.000
	85	60	-6.203	2.814	-2.204	408	0.589
		65	-0.890	2.814	-0.316	408	1.000
		70	3.096	2.814	1.100	408	1.000
		75	5.315	2.814	1.889	408	1.000
		80	6.155	2.814	2.187	408	0.615
		90	1.433	2.814	0.509	408	1.000
	90	60	-7.636	2.814	-2.713	408	0.146
		65	-2.322	2.814	-0.825	408	1.000
		70	1.663	2.814	0.591	408	1.000
		75	3.882	2.814	1.380	408	1.000
		80	4.722	2.814	1.678	408	1.000
		85	-1.4 33	2.814	-0.509	408	1.000
5	60	65	3.484	2.814	1.238	408	1.000
		70	7.091	2.814	2.520	408	0.255
		75	7.577	2.814	2.693	408	0.155
		80	9.591	2.814	3.408	408	0.015
		85	4.001	2.814	1.422	408	1.000
		90	5.498	2.814	1.954	408	1.000
	65	60	-3.484	2.814	-1.238	408	1.000
		70	3.607	2.814	1.282	408	1.000
		75	4.094	2.814	1.455	408	1.000
		80	6.107	2.814	2.170	408	0.642
		85	0.517	2.814	0.184	408	1.000
		90	2.014	2.814	0.716	408	1.000
	70	60	-7.091	2.814	-2.520	408	0.255
		65	-3.607	2.814	-1.282	408	1.000
		75	0.486	2.814	0.173	408	1.000
		80	2.500	2.814	0.888	408	1.000
		85	-3.090	2.814	-1.098	408	1.000
		90	-1.593	2.814	-0.566	408	1.000
	75	60	-7.577	2.814	-2.693	408	0.155
		65	-4.094	2.814	-1.4 55	408	1.000
		70	-0.486	2.814	-0.173	408	1.000
		80	2.013	2.814	0.715	408	1.000
		85	-3.577	2.814	-1.271	408	1.000
		90	-2.079	2.814	-0.739	408	1.000
	80	60	-9.591	2.814	-3.408	408	0.015
		65	-6.107	2.814	-2.170	408	0.642
		70	-2.500	2.814	-0.888	408	1.000
		75	-2.013	2.814	-0.715	408	1.000
		85	-5.590	2.814	-1.986	408	1.000
		90	-4.093	2.814	-1.454	408	1.000
	85	60	-4.001	2.814	-1.422	408	1.000
		65	-0.517	2.814	-0.184	408	1.000
		70	3.090	2.814	1.098	408	1.000
		75	3.577	2.814	1.271	408	1.000

		80	5.590	2.814	1.986	408	1.000
		90	1.497	2.814	0.532	408	1.000
	90	60	-5.498	2.814	-1.954	408	1.000
		65	-2.014	2.814	-0.716	408	1.000
		70	1.593	2.814	0.566	408	1.000
		75	2.079	2.814	0.739	408	1.000
		80	4.093	2.814	1.454	408	1.000
		85	-1.497	2.814	-0.532	408	1.000

Based on estimated marginal means

a. Adjustment for multiple comparisons: Bonferroni
An estimate of the modified population marginal mean (I)

2.1.2 Angle at one level of group

Pairwise comparisons to compare angle while holding group (non-exercise) constant when ROI's are in a palmar position.

Dependent Variable: MEAN

(I) ANGLE	(J) ANGLE	Mean Difference (I-J)	Std. Error	T value	Degrees of freedom	Significance[a]
60	65	1.859	1.780	1.044	408	1.000
	70	5.340	1.780	3.000	408	0.060
	75	7.681	1.780	4.316	408	<0.001
	80	10.323	1.780	5.800	408	<0.001
	85	4.168	1.780	2.342	408	0.413
	90	5.125	1.780	2.879	408	0.088
65	60	-1.859	1.780	-1.044	408	1.000
	70	3.481	1.780	1.956	408	1.000
	75	5.822	1.780	3.271	408	0.024
	80	8.464	1.780	4.756	408	<0.001
	85	2.309	1.780	1.297	408	1.000
	90	3.266	1.780	1.835	408	1.000
70	60	-5.340	1.780	-3.000	408	0.060
	65	-3.481	1.780	-1.956	408	1.000
	75	2.341	1.780	1.316	408	1.000
	80	4.983	1.780	2.800	408	0.112
	85	-1.172	1.780	-0.658	408	1.000
	90	-0.215	1.780	-0.121	408	1.000
75	60	-7.681	1.780	-4.316	408	<0.001
	65	-5.822	1.780	-3.271	408	0.024
	70	-2.341	1.780	-1.316	408	1.000
	80	2.642	1.780	1.484	408	1.000
	85	-3.513	1.780	-1.974	408	1.000
	90	-2.556	1.780	-1.436	408	1.000
80	60	-10.323	1.780	-5.800	408	<0.001
	65	-8.464	1.780	-4.756	408	<0.001
	70	-4.983	1.780	-2.800	408	0.112
	75	-2.642	1.780	-1.484	408	1.000
	85	-6.155	1.780	-3.458	408	0.013
	90	-5.198	1.780	-2.921	408	0.077
85	60	-4.168	1.780	-2.342	408	0.413
	65	-2.309	1.780	-1.297	408	1.000
	70	1.172	1.780	0.658	408	1.000
	75	3.513	1.780	1.974	408	1.000
	80	6.155	1.780	3.458	408	0.013
	90	0.957	1.780	0.538	408	1.000
90	60	-5.125	1.780	-2.879	408	0.088
	65	-3.266	1.780	-1.835	408	1.000
	70	0.215	1.780	0.121	408	1.000
	75	2.556	1.780	1.436	408	1.000
	80	5.198	1.780	2.921	408	0.077
	85	-0.957	1.780	-0.538	408	1.000

Based on estimated marginal means

a. Adjustment for multiple comparisons: Bonferroni

An estimate of the modified population marginal mean (I)

Pairwise comparisons to compare angle while holding group (exercise) constant

Dependent Variable: MEAN

Angle (I)	Angle(J)	Mean difference (I-J)	Std Error	T Value	Degrees of freedom	Significance[a]
60	65	7.610	1.780	4.276	408	<0.001
	70	10.067	1.780	5.656	408	<0.001
	75	13.675	1.780	7.684	408	<0.001
	80	14.785	1.780	8.307	408	<0.001
	85	9.505	1.780	5.341	408	<0.001
	90	11.183	1.780	6.283	408	<0.001
65	60	-7.610	1.780	-4.276	408	<0.001
	70	2.457	1.780	1.380	408	1.000
	75	6.065	1.780	3.408	408	0.015
	80	7.175	1.780	4.031	408	0.001
	85	1.895	1.780	1.065	408	1.000
	90	3.573	1.780	2.007	408	0.953
70	60	-10.067	1.780	-5.656	408	<0.001
	65	-2.457	1.780	-1.380	408	1.000
	75	3.608	1.780	2.027	408	0.909
	80	4.718	1.780	2.651	408	0.175
	85	-0.562	1.780	-0.316	408	1.000
	90	1.116	1.780	0.627	408	1.000
75	60	-13.675	1.780	-7.684	408	<0.001
	65	-6.065	1.780	-3.408	408	0.015
	70	-3.608	1.780	-2.027	408	0.909
	80	1.110	1.780	0.624	408	1.000
	85	-4.170	1.780	-2.343	408	0.412
	90	-2.492	1.780	-1.400	408	1.000
80	60	-14.785	1.780	-8.307	408	<0.001
	65	-7.175	1.780	-4.031	408	0.001
	70	-4.718	1.780	-2.651	408	0.175
	75	-1.110	1.780	-0.624	408	1.000
	85	-5.280	1.780	-2.967	408	0.067
	90	-3.603	1.780	-2.024	408	0.916
85	60	-9.505	1.780	-5.341	408	<0.001
	65	-1.895	1.780	-1.065	408	1.000
	70	0.562	1.780	0.316	408	1.000
	75	4.170	1.780	2.343	408	0.412
	80	5.280	1.780	2.967	408	0.067
	90	1.678	1.780	0.943	408	1.000
90	60	-11.183	1.780	-6.283	408	<0.001
	65	-3.573	1.780	-2.007	408	0.953
	70	-1.116	1.780	-0.627	408	1.000
	75	2.492	1.780	1.400	408	1.000
	80	3.603	1.780	2.024	408	0.916
	85	-1.678	1.780	-0.943	408	1.000

2.2 Main effect of ROI

Pairwise comparisons to compare the main effect of ROI when ROI's are in a palmar position.

Dependent Variable:MEAN

ROI (I)	ROI(J)	Mean Difference (I-J)	Std error	Significance[a]
1	2	5.671*	1.064	<0.001
	3	9.101*	1.064	<0.001
	4	8.015*	1.064	<0.001
	5	5.433*	1.064	<0.001
2	1	5.671*	1.064	<0.001
	3	3.430*	1.064	0.001
	4	2.344*	1.064	0.028
	5	0.238[b]	1.064	0.823
3	1	-9.101*	1.064	<0.001
	2	-3.430*	1.064	0.01
	4	-1.085[b]	1.064	0.308
	5	-3.668*	1.064	0.001
4	1	-8.015*	1.064	<0.001
	2	-2.344*	1.064	0.028
	3	1.085[b]	1.064	0.308
	5	-2.583*	1.064	0.016
5	1	-5.433*	1.064	<0.001
	2	0.238[b]	1.064	0.823
	3	3.668*	1.064	0.001
	4	2.583*	1.064	0.016

Based on estimated marginal means

*. The mean difference is significant at the 0.5 level

a. Adjustment for multiple comparisons: Bonferroni

b. An estimate of the modified population marginal mean (1)

2.2.1 ROI at one level of group

Pairwise comparisons comparing ROI means, holding group (non-exercise) constant when ROI's are in a palmar position.

Dependent variable: MEAN

ROI (I)	ROI (j)	mean difference (I-J)	std err	t value	Degrees of freedom	Signifincance[a]
1	2	9.007	1.504	5.989	408	<0.001
	3	10.650	1.504	7.081	408	<0.001
	4	9.674	1.504	6.432	408	<0.001
	5	-0.545	1.504	-0.362	408	1.000
2	1	-9.007	1.504	-5.989	408	<0.001
	3	1.643	1.504	1.092	408	1.000
	4	0.667	1.504	0.443	408	1.000
	5	-9.552	1.504	-6.351	408	<0.001
3	1	-10.650	1.504	-7.081	408	<0.001
	2	-1.643	1.504	-1.092	408	1.000
	4	-0.976	1.504	-0.649	408	1.000
	5	-11.195	1.504	-7.443	408	<0.001
4	1	-9.674	1.504	-6.432	408	<0.001
	2	-0.667	1.504	-0.443	408	1.000
	3	0.976	1.504	0.649	408	1.000
	5	-10.219	1.504	-6.795	408	<0.001
5	1	0.545	1.504	0.362	408	1.000
	2	9.552	1.504	6.351	408	<0.001
	3	11.195	1.504	7.443	408	<0.001

Based on estimated marginal means

a. Adjustment for multiple comparisons: Bonferroni

2.2.1 Pairwise comparisons comparing ROI means, holding group (exercise) constant when ROI's are in a palmar position

Dependent variable: MEAN

ROI (I)	ROI (j)	mean difference (I-J)	std err	t value	Degrees of freedom	significance[a]
1	2	2.335	1.504	1.553	408	1.213
	3	7.552	1.504	5.021	408	<0.001
	4	6.357	1.504	4.227	408	<0.001
	5	11.411	1.504	7.587	408	<0.001
2	1	-2.335	1.504	-1.553	408	1.213
	3	5.217	1.504	3.469	408	0.006
	4	4.022	1.504	2.674	408	0.078
	5	9.075	1.504	6.034	408	<0.001
3	1	-7.552	1.504	-5.021	408	<0.001
	2	-5.217	1.504	-3.469	408	0.006
	4	-1.195	1.504	-0.795	408	4.273
	5	3.589	1.504	2.386	408	0.175
4	1	-6.357	1.504	-4.227	408	<0.001
	2	-4.022	1.504	-2.674	408	0.078
	3	1.195	1.504	0.795	408	4.273
	5	5.054	1.504	3.360	408	0.009
5	1	-11.411	1.504	-7.587	408	<0.001
	2	-9.075	1.504	-6.034	408	<0.001
	3	-3.859	1.504	-2.566	408	0.106
	4	-5.054	1.504	-3.360	408	0.009

Based on estimated marginal means

a. Adjustment for multiple comparisons: Bonferroni

2.2.2 ROI at one level of angle

Pairwise comparisons comparing ROI means, holding angle constant when ROI's are in a palmar position.

Dependent Variables:MEAN

ANGLE	(I) ROI	(J) ROI	Mean Difference (I-J)	Std. Error	T value	Degrees of freedom	Significance[a].
60	1	2	11.566	2.814	4.110	408	<0.001
		3	16.673	2.814	5.925	408	<0.001
		4	12.826	2.814	4.558	408	<0.001
		5	12.399	2.814	4.406	408	<0.001
	2	1	-11.566	2.814	-4.110	408	<0.001
		3	5.106	2.814	1.815	408	0.703
		4	1.260	2.814	0.448	408	1.000
		5	0.832	2.814	0.296	408	1.000
	3	1	-16.673	2.814	-5.925	408	<0.001
		2	-5.106	2.814	-1.815	408	0.703
		4	-3.847	2.814	-1.367	408	1.000
		5	-4.274	2.814	-1.519	408	1.000
	4	1	-12.826	2.814	-4.558	408	<0.001
		2	-1.260	2.814	-0.448	408	1.000
		3	3.847	2.814	1.367	408	1.000
		5	-0.427	2.814	-0.152	408	1.000
	5	1	-12.399	2.814	-4.406	408	<0.001
		2	-0.832	2.814	-0.296	408	1.000
		3	4.274	2.814	1.519	408	1.000
		4	0.427	2.814	0.152	408	1.000
65	1	2	9.992	2.814	3.551	408	0.004
		3	11.314	2.814	4.020	408	0.001
		4	10.870	2.814	3.863	408	0.001
		5	8.613	2.814	3.061	408	0.024
	2	1	-9.992	2.814	-3.551	408	0.004
		3	1.322	2.814	0.470	408	1.000
		4	0.878	2.814	0.312	408	1.000
		5	-1.379	2.814	-0.490	408	1.000
	3	1	-11.314	2.814	-4.020	408	0.001
		2	-1.322	2.814	-0.470	408	1.000
		4	-0.444	2.814	-0.158	408	1.000
		5	-2.701	2.814	-0.960	408	1.000
	4	1	-10.870	2.814	-3.863	408	0.001
		2	-0.878	2.814	-0.312	408	1.000
		3	0.444	2.814	0.158	408	1.000
		5	-2.257	2.814	-0.802	408	1.000
	5	1	-8.613	2.814	-3.061	408	0.024
		2	1.379	2.814	0.490	408	1.000
		3	2.701	2.814	0.960	408	1.000
		4	2.257	2.814	0.802	408	1.000
70	1	2	6.731	2.814	2.392	408	0.172
		3	8.795	2.814	3.125	408	0.019
		4	10.511	2.814	3.735	408	0.002
		5	7.876	2.814	2.799	408	0.054
	2	1	-6.731	2.814	-2.392	408	0.172

		3	2.064	2.814	0.733	408	1.000
		4	3.780	2.814	1.343	408	1.000
		5	1.145	2.814	0.407	408	1.000
	3	1	-8.795	2.814	-3.125	408	0.019
		2	-2.064	2.814	-0.733	408	1.000
		4	1.716	2.814	0.610	408	1.000
		5	-0.919	2.814	-0.327	408	1.000
	4	1	-10.511	2.814	-3.735	408	0.002
		2	-3.780	2.814	-1.343	408	1.000
		3	-1.716	2.814	-0.610	408	1.000
		5	-2.635	2.814	-0.936	408	1.000
	5	1	-7.876	2.814	-2.799	408	0.054
		2	-1.145	2.814	-0.407	408	1.000
		3	0.919	2.814	0.327	408	1.000
		4	2.635	2.814	0.936	408	1.000
75	1	2	5.192	2.814	1.845	408	0.658
		3	7.306	2.814	2.596	408	0.098
		4	7.665	2.814	2.724	408	0.067
		5	3.297	2.814	1.172	408	1.000
	2	1	-5.192	2.814	-1.845	408	0.658
		3	2.115	2.814	0.751	408	1.000
		4	2.474	2.814	0.879	408	1.000
		5	-1.895	2.814	-0.673	408	1.000
	3	1	-7.306	2.814	-2.596	408	0.098
		2	-2.115	2.814	-0.751	408	1.000
		4	0.359	2.814	0.128	408	1.000
		5	-4.009	2.814	-1.425	408	1.000
	4	1	-7.665	2.814	-2.724	408	0.067
		2	-2.474	2.814	-0.879	408	1.000
		3	-0.359	2.814	-0.128	408	1.000
		5	-4.368	2.814	-1.552	408	1.000
	5	1	-3.297	2.814	-1.172	408	1.000
		2	1.895	2.814	0.673	408	1.000
		3	4.009	2.814	1.425	408	1.000
		4	4.368	2.814	1.552	408	1.000
80	1	2	3.041	2.814	1.081	408	1.000
		3	6.740	2.814	2.395	408	0.171
		4	5.424	2.814	1.927	408	0.546
		5	2.229	2.814	0.792	408	1.000
	2	1	-3.041	2.814	-1.081	408	1.000
		3	3.699	2.814	1.314	408	1.000
		4	2.383	2.814	0.847	408	1.000
		5	-0.812	2.814	-0.289	408	1.000
	3	1	-6.740	2.814	-2.395	408	0.171
		2	-3.699	2.814	-1.314	408	1.000
		4	-1.316	2.814	-0.468	408	1.000
		5	-4.511	2.814	-1.603	408	1.000
	4	1	-5.424	2.814	-1.927	408	0.546
		2	-2.383	2.814	-0.847	408	1.000
		3	1.316	2.814	0.468	408	1.000
		5	-3.195	2.814	-1.135	408	1.000
	5	1	-2.229	2.814	-0.792	408	1.000

		2	0.812	2.814	0.289	408	1.000
		3	4.511	2.814	1.603	408	1.000
		4	3.195	2.814	1.135	408	1.000
85	1	2	2.100	2.814	0.746	408	1.000
		3	7.052	2.814	2.506	408	0.126
		4	4.674	2.814	1.661	408	0.975
		5	2.044	2.814	0.726	408	1.000
	2	1	-2.100	2.814	-0.746	408	1.000
		3	4.952	2.814	1.760	408	0.792
		4	2.574	2.814	0.915	408	1.000
		5	-0.056	2.814	-0.020	408	1.000
	3	1	-7.052	2.814	-2.506	408	0.126
		2	-4.952	2.814	-1.760	408	0.792
		4	-2.378	2.814	-0.845	408	1.000
		5	-5.008	2.814	-1.779	408	0.759
	4	1	-4.674	2.814	-1.661	408	0.975
		2	-2.574	2.814	-0.915	408	1.000
		3	2.378	2.814	0.845	408	1.000
		5	-2.630	2.814	-0.934	408	1.000
	5	1	-2.044	2.814	-0.726	408	1.000
		2	0.056	2.814	0.020	408	1.000
		3	5.008	2.814	1.779	408	0.759
		4	2.630	2.814	0.934	408	1.000
90	1	2	1.075	2.814	0.382	408	1.000
		3	5.826	2.814	2.070	408	0.391
		4	4.138	2.814	1.470	408	1.000
		5	1.572	2.814	0.559	408	1.000
	2	1	-1.075	2.814	-0.382	408	1.000
		3	4.751	2.814	1.688	408	0.922
		4	3.063	2.814	1.088	408	1.000
		5	0.497	2.814	0.177	408	1.000
	3	1	-5.826	2.814	-2.070	408	0.391
		2	-4.751	2.814	-1.688	408	0.922
		4	-1.688	2.814	-0.600	408	1.000
		5	-4.253	2.814	-1.511	408	1.000
	4	1	-4.138	2.814	-1.470	408	1.000
		2	-3.063	2.814	-1.088	408	1.000
		3	1.688	2.814	0.600	408	1.000
		5	-2.565	2.814	-0.912	408	1.000
	5	1	-1.572	2.814	-0.559	408	1.000
		2	-0.497	2.814	-0.177	408	1.000
		3	4.253	2.814	1.511	408	1.000
		4	2.565	2.814	0.912	408	1.000

Based on estimated marginal means

a. Adjustment for multiple comparisons: Bonferroni

2.3 Main effect of group

Pairwise comparison to compare groups when ROI is in palmar position.

position	Exercised (I)	Non-exercised (J)	Mean difference (I-J)	Std Error	Significance
palmar	138.38	120.10	18.28	0.476	<0.001

b. An estimate of the modified population marginal mean

2.3.1 Group at one level of angle

Pairwise comparisons of one group mean against another while holding angle constant.

Dependent Variable: MEAN

ANGLE	Mean Difference (I-J)	Std. Error	T VALUE	Degrees of freedom	significance
60	22.899	2.318	9.880	408	<0.001
65	17.148	2.318	7.399	408	<0.001
70	18.172	2.318	7.841	408	<0.001
75	16.905	2.318	7.294	408	<0.001
80	18.437	2.318	7.955	408	<0.001
85	17.562	2.318	7.578	408	<0.001
90	16.842	2.318	7.267	408	<0.001

I = exercised
J = non-exercised

2.3.2 Group at one level of ROI

Pairwise comparisons to compare group means. holding ROI constant when ROI's are in a palmar position.

Dependent Variable: MEAN

ROI	Mean Difference (I-J)	Std. Error	t value	Degrees of freedom	significance
1	-18.055	1.959	-9.218	62	<0.001
2	-24.726	1.959	-12.623	62	<0.001
3	-21.153	1.959	-10.799	62	<0.001
4	-21.372	1.959	-10.911	62	<0.001
5	-6.099	1.959	-3.114	62	0.003

I = exercised
J = nonexercised

3. ROI size analysis

Tabulated data prior to statistical analysis

Average of mean	angle	
radius	60	90
2.5mm	134.663	129.261
3mm	136.480	127.813
3.5mm	137.847	127.194

3.1 Main effect of radius size

There is no significant effect of diameter as determined by a p value of 0.819 from the analysis of variance performed by SPSS.

3.1.1 Angle at one level of radius

Pairwise comparisons to compare angle means while holding size of ROI constant.

Dependent variable: MEAN

Radius(mm)	Mean difference (60° - 90°)	Std error	T value	Significance[a]
2.5	5.401	1.275	4.236	0.000
3	8.667	1.275	6.7975	0.000
3.5	10.653	1.275	8.3555	0.000

3.1.2Radii size at one level of angle.

Pairwise comparison to compare ROI size holding angle constant.

Dependent variable: MEAN

angle	diameters	Mean difference	Std error	T value	Significance[a]
60	2.5vs3	1.817	1.275	1.425	0.931
	3vs3.5	1.368	1.275	1.073	1.000
	2.5vs3.5	3.184	1.275	2.497	0.078
90	2.5vs3	1.449	1.275	1.136	1.000
	3vs3.5	0.619	1.275	0.485	1.000
	2.5vs3.5	2.068	1.275	1.622	0.635

Based on estimated marginal means

a. Adjustment for multiple comparisons: Bonferroni